SURVIVAL PREDICTION IN GLIOBLASTOMA BRAIN TUMOR USING SEGMENTATION AND DETECTION WITH ADVANCE COMPUTATIONAL TECHNIQUES

A Thesis Submitted

IN PARTIAL FULFILLMENT OF THE REQUIREMENTS

FOR THE DEGREE OF

DOCTOR OF PHILOSOPHY

IN

COMPUTER SCIENCE AND ENGINEERING

By

DEEPENDRA RASTOGI

Regd. No. – 19SCSE3010013

Supervisor
Prof. Prashant Johri
Professor

Co Supervisor
Dr. Varun Tiwari
Assistant Professor

SCHOOL OF COMPUTING SCIENCE & ENGINEERING
GALGOTIAS UNIVERSITY
Plot No 2, Sector 17-A Yamuna Expressway
Greater Noida, Uttar Pradesh
INDIA

January 2024

APPROVAL SHEET

The Ph. D. thesis entitled "**Survival Prediction in Glioblastoma Brain Tumor using Segmentation and Detection with Advance Computational Techniques**" by **Deependra Rastogi** is approved for the degree of Doctor of Philosophy in Computer Science & Engineering.

Examiners

_____

Supervisor

Prof (Dr). Prashant Johri

Co Supervisor

Dr. Varun Tiwari

Chairman

_____

Date: _____

Place: _____

CANDIDATE'S DECLARATION

I hereby certify that the work which is being presented in the thesis, entitled — "**Survival Prediction in Glioblastoma Brain Tumor using Segmentation and Detection with Advance Computational Techniques**" in fulfilment of the requirements for the award of the degree of Doctor of Philosophy in Computer Science and Engineering, submitted in Galgotias University, Greater Noida is an authentic record of my own work carried out during a period from January 2020 –January 2024 under the supervision of Prof. Prashant Johri and co-supervision of Dr. Varun Tiwari.

The matter embodied in this thesis has not been submitted by me for the award of any other degree of this or any other University/Institute.

Deependra Rastogi

19SCSE3010013

This is to certify that the above statement made by the candidate is correct to the best of our knowledge.

Dr. Prashant Johri
Supervisor & Professor,
School of Computing Science & Engineering,
Galgotias University, Greater Noida
Uttar Pradesh, India

Dr. Varun Tiwari
Co-Supervisor & Assistant Professor,
Computer Science and Engineering
Manipal University Jaipur
Rajasthan, India

The Ph.D. Viva-Voice examination of Mr. Deependra Rastogi, Research Scholar, has been held on _____.

Sign. of Supervisor(s) Sign. of Co-Supervisor(s) Sign. of External Examiner

ABSTRACT

In recent times, a wealth of evidence has emerged, indicating a notable increase in brain tumor cases, solidifying its status as the 10th most prevalent type of tumor, affecting both children and adults. Glioma tumors, assessed pathologically, are divided into the formidable glioblastoma (GBM/HGG) and the less aggressive lower grade glioma (LGG). Glioblastoma, among various brain tumors, stands out as the most lethal and aggressive. Within gliomas, diverse histological subfields include peritumoral edema, a necrotic core, and enhancing/non-enhancing tumor cores. Radiology, specifically magnetic resonance imaging (MRI), plays a vital role in unraveling the phenotypic intricacies and intrinsic heterogeneity of gliomas. Utilizing multimodal MRI scans, such as T1-weighted, contrast-enhanced T1-weighted (T1GD), T2-weighted, and fluid attenuation inversion recovery (FLAIR) images, provides a holistic understanding of different glioma subfields. The need for precise predictions in overall survival, diagnosis, and treatment planning for glioma patients is met through automated algorithms embedded in a brain tumor segmentation and detection framework. These algorithms leverage fragmented tumor subfields and radiometric characteristics from multimodal MRI scans. The thesis introduces a model framework encompassing tumor classification, detection, and localization, integrating advanced Deep Learning algorithms as a foundational layer with localization techniques. The first method employs cutting-edge algorithms like Inception-V3, InceptionResNet-V2, MobileNet, NASNetMobile, ResNet-101, Xception, DenseNet, ResNet-50, and EfficientNetV7 for classification. This involves adding an extra layer of activation, normalization, and density. The power of repeated blocks is utilized in a multi-branch network topology, clearly defining the head (prediction), body (data processing), and stem (data intake). This design pattern, initiated with the first two or three convolutions processing the object in the stem, persists in contemporary deep networks. The second strategy applies the RESUNET model to segment and localize brain tumors, utilizing TCGA MRI data. This comprehensive approach delves into the intricate landscape of glioblastoma, merging advanced computational techniques with medical imaging to push the boundaries of survival prediction and treatment guidance. According to the BraTS

classification, a patient's survival outcome falls into three groups: short-term survivors, mid-term survivors, and long-term survivors. The thesis emphasizes effective feature selection from MRI images and advocates for the use of a deep learning-inspired replicator neural network for the task of Overall Survival prediction.

AKNOWLEDGEMENT

With profound appreciation, I extend my heartfelt thanks to the remarkable individuals who have contributed to the triumphant realization of my thesis, "Survival Prediction in Glioblastoma Brain Tumor through Segmentation and Detection using Cutting-edge Computational Techniques.". Foremost among them is Prof. Prashant Johri, my sagacious guide, whose unwavering support and illuminating feedback were indispensable throughout this research odyssey. Prof. Prashant Johri is expertise not only guided but also sculpted the trajectory of this study, making it a testament to collaborative brilliance. A special note of gratitude is reserved for my co-authors, with Dr. Varun Tiwari standing out for his substantial contributions to this doctoral endeavour. I owe a considerable debt of thanks to Dr. K. Mallikharjuna Babu, Hon'ble Vice-Chancellor, Dr. Avadhesh Kumar, the Pro Vice-Chancellor and Dr. Nitin Gaur, the Registrar of Galgotias University's, for his encouragement and benevolent blessings.

Recognition is also due to Galgotias University, Greater Noida, for providing the essential resources and an environment conducive to groundbreaking research. The accessibility to state-of-the-art computational facilities and databases significantly streamlined the implementation of advanced techniques in tumor segmentation and detection. Heartfelt appreciation extends to the medical professionals and researchers in the realm of oncology and my colleague, whose generous sharing of knowledge and insights during reviews and collaborative discussions elevated the clinical relevance of the computational models proposed.

Last but certainly not least, my heartfelt thanks go to my father, Shri Vijay Kumar Rastogi, my mother, Smt. Sushma Rastogi, and my wife, Swati Verma. Their steadfast support, understanding, and encouragement formed the foundation of this journey. Their enduring love and unshakable faith in my capabilities provided a consistent source of motivation. I extend my deep appreciation to my cherished children, Anirudh Rastogi and Arnika Rastogi, whose love, patience, and understanding have been the pillars of strength sustaining me throughout this academic pursuit.

I express my deepest gratitude to the Almighty of God, whose divine guidance has illuminated my path throughout this academic journey. In moments of challenge and uncertainty, His wisdom provided clarity, strength, and resilience.

Place: Deependra Rastogi
Date:

Table of Content

List of Figure

List of Table

LIST OF PUBLICATION

SCI

1. **Rastogi, D.**, Johri, P., Tiwari, V., & Elngar, A. A. (2024, February). Multi-class classification of brain tumour magnetic resonance images using multi-branch network with inception block and five-fold cross validation deep learning framework. *Biomedical Signal Processing and Control*, *88*, 105602. https://doi.org/10.1016/j.bspc.2023.105602

ESCI, SCOPUS

2. **Rastogi, D.**, Johri, P., & Tiwari, V. (2023). Brain Tumor Detection and Localization: An Inception V3 - Based Classification Followed By RESUNET-Based Segmentation Approach. *International Journal of Mathematical, Engineering and Management Sciences*, *8*(2), 336-352. https://doi.org/10.33889/IJMEMS.2023.8.2.020.

SCOPUS

3. **Rastogi, D.,** Johri, P., & Tiwari, V. (2023, May 30). Augmentation based detection model for brain tumor using VGG 19. International Journal of Computing and Digital Systems, 13(1), 1227–1237. https://doi.org/10.12785/ijcds/1301100

INTERNATIONAL CONFERENCE (SCOPUS INDEX)

4. **Deependra Rastogi**, Prashant Johri, "An Artificial Intelligence Algorithms Analysis for Brain Tumor Segmentation and Classification A Narrative Review" presented in International Conference on International Conference on

Communication, Security and Artificial Intelligence (ICCSAI-2023), Galgotias University, Greater Noida

5. **D. Rastogi**, P. Johri and V. Tiwari, "Brain Tumor Segmentation and Tumor Prediction Using 2D-VNet Deep Learning Architecture," *2021 10th International Conference on System Modeling & Advancement in Research Trends (SMART)*, 2021, pp. 723-732, doi: 10.1109/SMART52563.2021.9676317.
6. **Deependra Rastogi**, Prashant Johri, Varun Tiwari, "Brain Tumor Segmentation and Enhancing Prediction using UNet Deep Learning Model with Additive Skip Connection" presented in International Conference On Advance Computing And Ingenious Technology In Engineering Science organized by Galgotias College of Engineering and Technology, Greater Noida.

SUPPORTIVE INTERNATIONAL CONFERENCE PAPER (SCOPUS INDEX)

7. **Rastogi, D**., Johri, P., Gupta, M. & Prasad, S. K., (2021, December 17). Brain Tumor Classification using Advanced Computational Techniques. 2021 3rd International Conference on Advances in Computing, Communication Control and Networking (ICAC3N). https://doi.org/10.1109/icac3n53548.2021.9725405
8. **Rastogi, D.,** Johri, P., Yadav, S., & Gupta, R., (2022, August 26). Glioblastoma Brain Tumor Segmentation and Survival Prediction Using U Net. 2022 6th International Conference on Computing, Communication, Control and Automation (ICCUBEA. https://doi.org/10.1109/iccubea54992.2022.10010582

LIST OF ABREVIATION

Abbreviation	Notation
ABTA	American Brain Tumor Association
ANNS	American Association of Neurological Science
BFO	Bacteria Foraging Optimization
BRATS	Brain Tumor Segmentation
CAD	Computer-Aided Design
CBAM	Convolutional Block Attention Module
CCA	Connected Component Analysis
CCL	Connected Component Analysis
CNN	Convolutional Neural Network
CNS	Central Nervous System
CPTAC	Clinical Proteomic Tumor Analysis Consortium
CRF	Conditional Random Field
CT	Computed Tomography
DCSNN	Deep Convolutional Symmetric Neural Network
DNN	Deep Neural Network
DRLBP	Dominant Rotated Local Binary Patterns
DSC	Dice Similarity Coefficient
DTWT	Dual-Tree Wavelet Transform
DWT	Discrete Wavelet Transform
EBRT	External Beam Radiation Therapy
ECNN	Enhanced Convolutional Neural Network
EEG	Electroencephalography
ELM	Extreme Learning Machine
FA	Firefly Algorithm
FCM	Fuzzy C-Means
FCNN	Fully Convolutional Neural Network

Abbreviation	Notation
FFT	Fast Fourier Transform
FMRI	Functional Magnetic Resonance Imaging
GA-ANN	Genetic Algorithm with Artificial Neural Network
GAN	Generative Adversarial Network
GA-SVM	Genetic Algorithm with Support Vector Machine
GBM	Glioblastoma Multiforme
GCNN	Growing Convolutional Neural Network
GMM	Gaussian Mixture Model
GSWT	Growing Stationary Wavelet Transform
GTR	Gross Total Resection
HCS	Harmony Crow Search
HG	High-Grade
HGG	High-Grade Glioma
IBSR	Internet Brain Segmentation Repository
IRRC	International Association of Neurological Science
ISLES	Ischemic Stroke Lesion Segmentation
KNN	K-Nearest Neighbors
LG	Low-Grade
LGG	Low Grade Glioblastoma
LoG	Laplacian of Gaussian
LSTM	Long Short-Term Memory
MEG	Magnetoencephalogram
MFKM	Modified Fuzzy K-Means
MRI	Magnetic Resonance Imaging
MSE	Mean Square Error
NB	Naïve Bayes
NBTF	National Brain Tumor Foundation
NIRS	Near Infrared Spectroscopy
NLP	Natural Language Processing

Abbreviation	Notation
ONS	Oncology Nursing Society
PCA	Principal Component Analysis
PD	Proton Density
PET	Positron Emission Tomography
PGIMER	Postgraduate Institute of Medical Education and Research
PNN	Probabilistic Neural Network
PSNR	Peak Signal-to-noise ratio
PSO	Particle Swarm Optimization
RBF	Radial Basis Function
ReLU	Rectified Linear Unit
RESnet	Residual Neural Network
RNN	Recurrent Neural Networks
ROI	Region of Interest
RPN	Region Proposal Network
SEER	Surveillance, Epidemiology, and End Results
SSAE	Stacked Space Autoencoder
SSIM	Structural Index Similarity
STR	Sub Total Resection
SVM	Support Vector Machine
TCIA	The Cancer Imaging Archive
TRS	Tolerance Rough Set
VGG	Visual Geometry Group
WBA	World Brain Atlas
WHO	World Health Organization
ZFNet	Zeiler Furgus Net

CHAPTER 1

INTRODUCTION

1.1 Preamble

The utmost complex part in the body, the brain, is accountable for all of our thoughts and feelings, as well as our voluntary and involuntary actions and the regulation of our internal processes (Biswas-Diener, R., 2020). The nervous system, an intricate web of channels responsible for transmitting electrochemical signals, maintains the connection with each component of the body (Biswas-Diener, R., 2020). The brain is the greatest aspect of the nervous system that surrounds us, which may be seen by taking a close look at it. It assumes a paramount role in processing most of our sensations, perceptions, thoughts, awareness, emotions, and planning. Additionally, it exercises overall command over the entire nervous system, making it the core of this complex network. The human body comprises various types of cells, each with a specific function (Tiwari et al., 2020). These cells undergo a regulated process of growth and division, ensuring the body remains in a healthy physical state. However, certain cells lose their ability to control their growth and begin to proliferate in an abnormal manner, resulting in the formation of a mass of tissues known as a tumor (Tiwari et al., 2020). Brain tumors specifically refer to solid neoplasms that typically develop within the skull, either in the brain itself or in other locations such as lymphatic tissue, veins, cranial nerves, or the brain's protective membranes (Louis et al., 2016). Malignancies that start in further region of the human physique can metastasize to the intellect, causing tumours there:

(i). Multiple factors, together with the tumor's location in the brain, its malignant or benign nature, and the tissue from which it originated, allow for the categorization of brain tumours.

(ii). Malignant tumours are cancerous and have the potential to spread, while benign tumors are not cancerous.

Tumours that move to the brain from other organs usually start in the kidneys, lungs, breasts, or even skin melanomas.

1.2 Brain Anatomy

An understanding of the human brain's anatomy is necessary for delving into conversations about MR pictures and brain tumours [Fig 1]. The key elements of the human brain are presented in the following.

(i). **Brainstem:** The brainstem, a crucial physical component situated at the base of the nervous system, links the cervical vertebrae to the cerebral cortex, the higher brain structures. The functions encompassed by the brain include regulating involuntary processes such as respiration, cardiac rhythm, vascular tension, digestion, and circadian rhythms (Brain Anatomy and How the Brain Works, 2021). The midbrain, situated at the very top of the brainstem, is in charge of transmitting information about sensation and movement from the brain to the spinal cord. Additionally, it encompasses nuclei responsible for visual and auditory processing and aids in the control of eye movement. The pons is located beneath the midbrain and functions as a connector, linking several regions of the brain. The function of the structure is to facilitate the transmission of information between the cerebrum and the cerebellum, as well as to regulate facial movements, respiration, and sleep (Brain Anatomy and How the Brain Works, 2021, Brain Basics: Know Your Brain, n.d.). The medulla oblongata, situated at the lower region of the brainstem, plays a key role in essential processes such as controlling respiration, heart rate, blood pressure, and reflex actions such as coughing and swallowing. Additionally, the brainstem houses various nuclei that are responsible for cranial nerve functions, such as controlling facial expressions, chewing, hearing, and taste (Brain Basics: Know Your Brain, n.d.). Overall, the brainstem acts as a vital connector between the brain and the body, regulating essential functions necessary for our survival and coordinating sensory and motor information.

(ii). **Cerebellum:** Movement, particularly equilibrium and muscular interaction, are regulated by the cerebellum, (Brain Anatomy and How the Brain Works, 2021). Its structure appears distinct from the rest of the brain, as it is attached beneath the cerebral hemispheres. The cerebellum's outer layer, known as the cerebellar cortex, features closely spaced parallel grooves, which contrast with the broader and irregular folds of the cerebral cortex (Brain Anatomy and How the Brain Works, 2021). A thin, uninterrupted layer composed of tightly twisted tissue, like an accordion, makes up the cortex of the cerebellum, despite its outward appearance. There is a very regular arrangement of many kinds of neurons, including cells called Purkinje and granule cells, inside this very thin layer. This intricate neural organization enables the cerebellum to possess significant signal-processing capabilities. Nevertheless, a cluster of tiny deep nuclei embedded in the cerebellum's white matter receives the bulk of the cerebral cortex's output.

(iii). **Frontal Lobe:** Situated at the very front of the brain's outermost layer, the cerebral cortex, the frontal lobe is an important area. The brain plays a vital part in various intricate cognitive processes, the expression of personality, and the control of voluntary movements (Mark D'Esposito et. al., 2019). It allows us to anticipate outcomes, make reasoned judgments, and engage in strategic thinking (Mark D'Esposito et. al., 2019). The frontal lobe is also responsible for personality expression and social behavior. It contributes to the formation of our individuality, including our emotions, motivations, and social interactions. Damage or dysfunction in the frontal lobe can lead to alterations in personality, decision-making difficulties, impulse control problems, and changes in social behavior. The main motor cortex, situated in the frontal brain, is accountable for initiating and regulating deliberate motions across the entire body. According to Mark D'Esposito et. al. (2019), it collaborates with other motor-related regions to carry out accurate and synchronised movements. Furthermore, the frontal lobe plays a role in both the production and understanding of language, specifically in the left hemisphere for the

majority of people. It enables us to articulate and understand spoken and written language. The frontal lobe communicates with additional regions of the intelligence through neural networks, allowing for integrated processing and coordination of various cognitive functions. It interacts with the parietal lobe for spatial cognition, the temporal lobe for language processing, and the limbic system for emotional regulation.

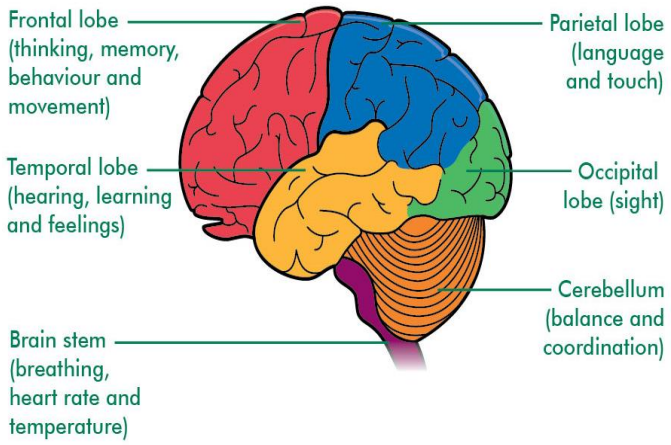

Fig 1.1 Brain Anatomy with various Function (Mark D'Esposito et. al., 2019)

(iv). **Occipital Lobe:** The occipital lobe, which is situated at the posterior of the brain, is in charge of deciphering visual data. It contains areas that aid in the recognition of shapes and colors, enabling us to accurately perceive and understand what our eyes are seeing (Rehman et. al. 2019). The occipital lobe plays a crucial role in quickly processing the rapid stream of visual information received by our eyes. The occipital lobe's role in understanding visual information is analogous to that of the temporal lobe's function in understanding auditory information (Rehman et. al. 2019). If the occipital lobe were impaired or injured, our ability to correctly process visual signals would be compromised, leading to visual confusion and difficulties in perception.

(v). **Parietal Lobe:** The parietal lobe is a cerebral cortex region situated in the superior and posterior part of the brain. When it comes to processing and making sense of data from several senses, the brain is indispensable, such as

tactile sensations, temperature, pain, and spatial perception (Loughan et al., 2022, Coslett & Schwartz, 2018). Perceiving and reacting to various textures, pressure, and vibrations are facilitated by the parietal lobe's processing and interpretation of tactile experiences. It also plays a role in proprioception, which is our sense of body position and movement. The parietal lobe helps us understand the location of our body parts in relation to each other and our surroundings (Coslett & Schwartz, 2018). Additionally, the parietal lobe is involved in spatial perception and awareness. It helps us navigate and orient ourselves in the environment, determine distances, and form mental maps. This region also contributes to our ability to perform mathematical calculations and manipulate numbers (Loughan et al., 2022). The parietal lobe works in close connection with other brain regions to integrate sensory information and facilitate higher-order cognitive processes. It interacts with the frontal lobe in planning and executing movements, as well as with the temporal lobe in language processing and spatial memory. When it comes to our sense of touch, our ability to navigate space, our knowledge of our own bodies, and our aptitude for mathematics, the parietal lobe is absolutely crucial. It integrates sensory inputs and contributes to our understanding of the world around us.

(vi). **Temporal Lobe:** The temporal lobe is a cerebral cortex area situated bilaterally above the ears. The brain employ a vital part in numerous essential tasks, such as processing auditory information, comprehending language, forming memories, and generating emotional reactions (Patel et. al., 2020). One of the primary functions of the temporal lobe is the processing of auditory information. It receives and interprets sound signals from the ears, allowing us to perceive and understand speech, music, and other auditory stimuli. The temporal lobe is involved in the analysis of sound patterns, distinguishing different frequencies and pitches, and recognizing and interpreting speech sounds. The temporal lobe also plays a significant role in language comprehension. It helps us understand and assign meaning to words,

sentences, and spoken or written language (Patel et. al., 2020). Damage to the temporal lobe can result in language impairments such as difficulties in understanding or producing speech. Memory formation and retrieval are other important functions associated with the temporal lobe. The creation of long-term impressions, especially those involving specific moments and occurrences (episodic memories), involves it. Retention of memories relies on the hippocampus, which is a system situated inside the temporal lobe (Patel et. al., 2020). Furthermore, the temporal lobe contributes to our emotional responses and the recognition of facial expressions. It helps us process and interpret emotional cues, allowing us to perceive and respond to different emotional states in ourselves and others. The temporal lobe works in conjunction with additional brain provinces, such as the parietal and frontal lobes, to integrate sensory information, facilitate language functions, and support memory processes. It plays a vital role in our perception of sound, language comprehension, memory formation, and emotional experiences.

1.3 Current Approaches and Prevailing Methods for the Diagnosis and Treatment of Brain Tumors

There have been tremendous advancements in the processing and interpretation of digital images in many fields, such as medical imaging, automation of processes in industry, and satellite imaging. Tissue categorization and analysis software has recently been developed for use in computers. Unfortunately, not a single one of these techniques provides reliable morphological data for malignant tumours in particular.

1.3.1 Detection of Brain Tumor

At this time, the identification of brain tumours using blood examinations or any other screening methods is not recommended by any authorities in the medical field. As a

consequence of this, the early analysis and dealing of brain tumours can dramatically progress a patient's chances of surviving their condition.

Following a thorough evaluation of the physical symptoms exhibited by a suspected brain tumor patient, the diagnosis typically entails a series of steps:

- Assessment of Neurological Function
- Brain Scan
- Biopsy

(i). **Assessment of Neurological Function:** The neurological examination serves as a valuable assessment method to evaluate a patient's neurological function. It offers several advantages as it aids in identifying the specific location of neurological disorders and assists in confirming or eliminating potential diagnoses. Neurological diseases can manifest in diverse ways, encompassing cognitive/behavioural, visual, motor, and sensory symptoms. Examining certain symptoms allows for the early diagnosis of serious neurological illnesses and the recognition of conditions that can greatly impact a person's standard of living (Shahrokhi, 2023).

(ii). **Techniques of Brain Scan:** Brain imaging provides a glimpse into the inner workings of the mind. Neuroimaging, also referred to as brain scanning, involves the utilization of different methods to imagine the construction, purpose, or pharmacology of the brain. This field is a relatively recent development within medicine, neuroscience, and psychology. Medical professionals specializing in performing and interpreting neuroimaging in clinical settings are recognized as neuroradiologists. Cognitive neuroscientists have access to a wide range of brain imaging tools (Xue et. al, 2010), which encompass various methods:

(a). **Positron Emission Tomography :** Positron Emission Tomography (PET) is a kind of imaging used in medicine that provides metabolic and functional information about organs and tissues, including the brain. It involves the use of a radioactive tracer, known as a

radiopharmaceutical, which emits positrons, or positively charged particles. During a PET scan, the patient is injected with the radiopharmaceutical, which travels to the targeted tissues or organs in the body. As the positrons emitted by the tracer encounter electrons in the body, they annihilate each other and produce gamma rays. A network of monitors encircling the patient picks up on these gamma rays (Berger, 2003). By analyzing the patterns of gamma ray emissions, a computer generates detailed three-dimensional images that illustrate the circulation and attentiveness of the radiopharmaceutical within the body. This information allows healthcare professionals to assess various physiological processes, such as blood flow, metabolism, oxygen utilization, and receptor binding. Among the many diseases that PET can help diagnose, stage, and monitor are those that impact the brain. Its capacity to provide insightful views into the molecular and functional aspects of the human body is the foundation upon which medical research and patient treatment are built.

(b). **Near Infrared Spectroscopy (NIRS):** One non-invasive optical method for monitoring and analysing brain hemodynamics and oxygenation in the blood changes is near-infrared spectroscopy (NIRS). It involves the detection of near-infrared light that can penetrate biological tissues to a certain depth (Pasquini, 2003). In NIRS, near-infrared light is emitted into the tissue and the reflected or transmitted light is measured. This light interacts with chromophores, such as oxyhemoglobin and deoxyhemoglobin, which have distinct absorption properties in the near-infrared range. By analysing the intensity of the detected light at different wavelengths, NIRS can provide information about the concentration changes of these chromophores. NIRS is particularly useful in monitoring brain activity and oxygenation levels in real-time. It is often used in studies related to

cognitive neuroscience, neuroimaging, and brain-computer interfaces [Ref 5]. NIRS is also employed in clinical settings to assess cerebral oxygenation and hemodynamics in patients with various neurological conditions, such as stroke, traumatic brain injury, and neurodevelopmental disorders. The advantage of NIRS is its portability, ease of use, and non-invasiveness, allowing for measurements to be taken even in naturalistic settings or during movement. However, its depth of penetration is limited compared to other imaging techniques like fMRI or PET.

(c). Magnetoencephalogram (MEG): Magnetoencephalography is a non-invasive neuroimaging method that uses the magnetic fields generated by the brain's electrical activity. It provides valuable information about the timing and location of neural activity with high temporal resolution. During an MEG procedure, the patient's head is placed inside a highly sensitive helmet-like device that contains an array of superconducting sensors (Pasquini, 2018). These sensors detect the extremely weak magnetic fields produced by the electrical currents in the neurons of the brain. Brain neurons generate little electric currents, which in turn generate magnetic fields, while they are actively firing. MEG measures these magnetic fields and creates a three-dimensional map of the brain's activity. By analysing the patterns and intensities of these magnetic fields, scientists and medical experts can identify specific brain areas linked to certain cognitive activities and processes. MEG has several advantages over other imaging techniques. It has exceptional temporal resolution, capturing the millisecond-scale changes in brain activity. This makes it particularly useful for studying fast cognitive processes, such as language processing, sensory perception, and motor control. MEG also has excellent spatial resolution, allowing for precise localization of brain activity (Pasquini, 2018).

(d). Electroencephalography (EEG): The noninvasive electroencephalography (EEG) technique measures and records the brain's electrical signals without penetrating the patient. The procedure comprises placing many electrodes on the top of the head in order to detect and amplify the extremely small electrical impulses generated by the brain's neurons. Electroencephalogram (EEG) procedures include the careful placement of electrodes on the scalp in order to capture electrical activity emanating from different regions of the brain (Soufineyestani et. al, 20200. These electrodes detect the electrical impulses produced by the synchronized firing of neurons, which reflect the ongoing brain activity. The recorded electrical signals are amplified and displayed as a series of waveforms known as an EEG recording or an EEG trace. EEG is particularly useful in studying brain function, diagnosing and monitoring epilepsy, assessing sleep disorders, and evaluating altered mental states (Read & Innis, 2017). It can provide insights into brain rhythms, arousal levels, cognitive processes, and the effects of different stimuli on brain activity.

(e). Functional Magnetic Resonance Imaging (fMRI): Neuroimaging is a way to determine how neurons are working by measuring changes in blood circulation to the brain and levels of oxygen. Functional magnetic resonance imaging (fMRI) takes precise images of the brain by using electromagnetic waves and a strong magnetic field. fMRI can indirectly identify brain regions that exhibit higher activity during specific tasks or cognitive processes by detecting alterations in blood oxygen levels (Scarapicchia et al., 2017). During a fMRI scan, the patient is usually asked to do certain things or engage in certain mental exercises while the scanner records their brain activity. The fMRI data is then analysed to identify brain regions that exhibit increased blood flow and oxygenation, indicating neural activity. fMRI is valuable in mapping brain functions related to sensory processing, motor control,

language, memory, and emotions. It helps researchers and healthcare professionals understand how different brain regions work together and how they are affected by various conditions and stimuli (Scarapicchia et al., 2017). One of the key advantages of fMRI is its high spatial resolution, which allows for precise localization of brain activity. It provides detailed maps of functional brain networks and can identify specific regions that are associated with certain cognitive functions or affected by neurological disorders.

(iii). **Biopsy:** A biopsy is a medical procedure performed to obtain a sample of tissue or cells from the body for further examination and analysis. It is commonly used to diagnose various medical conditions, including cancer and other diseases (Younger, 2023). During a biopsy, a healthcare professional, such as a surgeon or a specially trained physician, takes a small sample of tissue from the suspected area of abnormality. The procedure can be performed using various techniques depending on the location of the tissue being sampled (Younger, 2023).

There are different types of biopsies, including:

- Needle biopsy: This involves using a fine needle to extract a small sample of tissue or cells.
- Surgical biopsy: In some cases, a larger sample of tissue may be needed, and a surgical procedure is performed to remove the tissue. This may be done under general anaesthesia in an operating room.
- Endoscopic biopsy: This involves inserting a flexible tube with a camera (endoscope) into the body to visualize the suspected area and obtain tissue samples using special tools.

Although most biopsies pose no health hazards, some may be present depending on the tissue type and location of the biopsy. These risks can include bleeding, infection, bruising, and rare complications related to anaesthesia.

1.3.2 Post Biopsy Treatment of Brain Tumor

The post-biopsy treatment of a brain tumor refers to the therapeutic interventions and care provided to a patient after the biopsy procedure. After the biopsy, the collected tissue samples are analysed by pathologists to determine the nature of the tumor and its specific characteristics (Younger, 2023). Based on the biopsy results, a comprehensive treatment plan is developed to address the brain tumor.

The tumor's kind, grade, position, dimension, and the individual's general health are some of the variables that determine the precise post-biopsy therapy method. The primary objectives of post-biopsy care include symptom management, tumour expansion control, and catastrophe prevention.

The treatment options for brain tumors may include:

- **Surgery:** Occasionally, it may be advisable to undergo surgical excision of the tumour. The scope of the surgical procedure is contingent upon variables such as the dimensions, placement, and ease of access to the tumour. The surgical approach is intended to excise the tumour to the greatest extent feasible while safeguarding the adjacent healthy brain tissue.
- **Radiation therapy:** A medical practice known as radiation treatment or radiography uses radiation with high energies to destroy cells that are malignant in the body. Radiotherapy is a widely used and highly successful treatment method for several forms of cancer, such as brain tumours (Bradley et al., 2010). The objective of radiation therapy is to induce DNA damage in cancer cells, thereby inhibiting their capacity for cellular division and proliferation, ultimately leading to their demise. The administration of this therapy can be either external or internal, contingent upon the specific attributes of the tumour and the treatment strategy devised by the healthcare team (Bradley et al., 2010).
  - **(a). External Beam Radiation Therapy (EBRT):** External beam radiation therapy use a linear accelerator unit to administer radiation to the

tumour location externally. The radiation beams are meticulously moulded and aimed to precisely target the tumour while minimising the radiation dose to adjacent healthy tissues (Koka et al., 2022). The therapy is often delivered in numerous sessions, referred to as fractions, spanning several weeks. Every treatment is brief and painless, comparable to undergoing an X-ray procedure.

(b). **Internal Radiation Therapy (Brachytherapy):** For certain brain tumors, such as gliomas, brachytherapy may be used. The emitted radiation from the source is directed towards the tumor cells internally, providing a concentrated dose of radiation to the impacted region while preserving adjacent healthy tissues. Brachytherapy can be permanent or temporary, depending on the specific treatment plan (Skowronek, 2017).

(c). **Stereotactic Radiosurgery:** Stereotactic radiosurgery is a specialised technique in radiation therapy that administers a concentrated and accurate amount of radiation to a specific area in the brain. Contrary to its title, it does not entail conventional surgical procedures. Alternatively, the tumour is targeted by several radiation beams originating from various angles, precisely converging on the intended location. This allows for a large dose of radiation to reach the cancer with little collateral damage to healthy brain tissue. Stereotactic radiosurgery is usually conducted in a solitary or a small number of sessions, contingent upon the treatment strategy (Harris et. al, 2023).

(d). **Side Effects:** The potential for radiation-related adverse effects varies with each patient, treatment location, and dosage. Fatigue, alopecia (hair loss), skin changes, nausea, headaches, and cognitive impairments are common adverse effects of radiation treatment to the brain.

In the treatment of brain tumours, radiation therapy is an essential component. The specific approach and dose of radiation treatment are determined by a

variety of factors, such as the malignancy's features (type, size, location, and grade), the patient's overall health, and their tastes in treatment.

- **Chemotherapy:** One systemic method of treating malignancy is chemotherapy, which involves the administration of medications to specific cancer cells all over the body. It is a commonly employed treatment for various types of cancer, including brain tumors. Chemotherapy, in contrast to radiation or surgery, which aim their radiation beams at particular regions, travels through the circulatory system to kill cancer cells wherever they may be. The main objective of chemotherapy is to kill cancer cells or at least stop them from dividing. Chemotherapy drugs work by interfering with the cancer cells' DNA or other essential cellular processes, preventing them from multiplying and eventually leading to their death. Chemotherapy for brain tumors can be administered in different ways:

  (a). **Intravenous (IV) chemotherapy:** A needle or catheter is used to administer the medication straight into a vein. The medicine may then swiftly enter the circulation and reach all of the cancerous cells in the body.

  (b). **Oral chemotherapy:** Some chemotherapy drugs are available in pill or liquid form and can be taken orally. They are absorbed into the bloodstream through the digestive system and distributed throughout the body.

  Usually, chemotherapy is given in cycles, with certain treatment times and then rest intervals to give the body a chance to recuperate. How long each cycle is and how often they occur are both affected by the individual medications and the tumor's reaction to them.

  The medications used in chemotherapy might have side effects even on healthy cells in the body. Fatigue, dizziness, vomiting, baldness, lack of cravings, compromised immune functioning, elevated risk for infection, and alterations in the number of blood cells are among the most common adverse

effects. However, advances in supportive care medications and techniques have helped to manage and minimize these side effects.

The tumour type, stage, position, patient's general health, and personal preferences are among the many variables that influence the choice to administer chemotherapy, along with the precise medications and dose. The treatment is carefully monitored by an oncology team, and adjustments may be made based on the response to treatment and any side effects experienced.

The post-biopsy treatment of a brain tumor requires close monitoring by a multidisciplinary healthcare team, including oncologists, neurosurgeons, radiation oncologists, and other specialists.

1.4 Types of Brain Tumor

According to the World Health Organization (WHO), there are 120 different types of brain tumors. Brain tumors can be broadly considered into two types:

(i). **Primary Brain Tumor:** Based on their behaviour, brain tumours can be identified as either benign or malignant. The reference is from a learning directed by WAN et al. in 2016. Benign tumours are characterised by the absence of malignant development. According to the WHO classification, these tumours might be categorised as Low-Grade tumours or Grade I tumours. Benign tumours are non-metastatic and do not invade neighbouring cells or tissues, yet they have the potential to reach significant dimensions. When tumours develop in the brain and apply pressure on essential organs or block routes, they can cause problems. In contrast, malignant tumours are comprised of aberrant cells that undergo uncontrolled division and have the ability to infiltrate adjacent organs. The dissemination of these cells to other regions of the body occurs via the nervous system. Malignant tumours encompass various forms, including Carcinoma, Sarcoma, Leukaemia, and Lymphoma, among others.

(ii). **Secondary Brain Tumor:** This kind of tumour can spread from its original site in the brain to other areas of the body, a process called metastasis. Names for secondary brain tumours usually reflect the organ or place from which the tumour first disseminated. The distinction between malignant and benign tumours is illustrated in Figure 1.2.

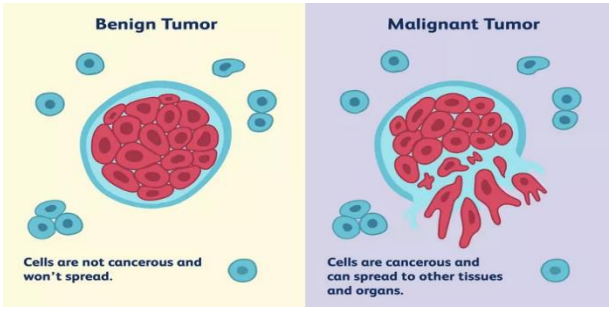

Fig 1.2 Difference between Benign Tumor and Malignant Tumor (Gupta & Khanna, 2017)

1.5 Brain Tumour Classification According to the Grade

Brain tumours are categorised based on their grade, which indicates the level of aggressiveness and malignancy of the tumour. Medical practitioners are better able to forecast the tumor's behaviour and prognosis and choose an appropriate treatment strategy with the use of the grading system. Tumours are categorised into four categories, from Grade I to Grade IV, according to a system established by the World Health Organisation (WHO). Figure 1.3 depicts the classification of brain tumour grades.

(i). **Grade I Tumor (Benign):** Grade I (Table 1.1) tumors are considered the least aggressive and are often referred to as benign tumors. These tumors grow slowly and are generally well-defined. They are not likely to metastasize (which is transmitted to other organs or regions of the body). Typically, grade I tumours are characterised by their generally normal-looking cells and clear boundaries. Pilocytic astrocytoma and meningioma are two types of Grade I brain tumours.

(ii). **Grade II Tumor (Low Grade):** Grade II (Table 1.2) tumors are still classified as relatively slow-growing and less aggressive compared to higher-grade tumors. They may have some characteristics of malignancy, such as an infiltrative growth pattern and abnormal-looking cells. These tumors have a higher chance of recurring and progressing to a higher grade over time. Examples of Grade II brain tumors include diffuse astrocytoma and oligodendroglioma. Fig 1.4 is the classification of brain tumor.

(iii). **Grade III Tumor (Anaplastic):** Grade III (Table 1.3) tumors are considered malignant or anaplastic tumors. These tumors are characterized by rapidly dividing cells and more aggressive growth. They tend to invade nearby tissues and have a higher likelihood of recurring after treatment. Grade III tumors often require more aggressive treatment approaches, such as surgery, radiation therapy, and chemotherapy. Examples of Grade III brain tumors include anaplastic astrocytoma and anaplastic oligodendroglioma.

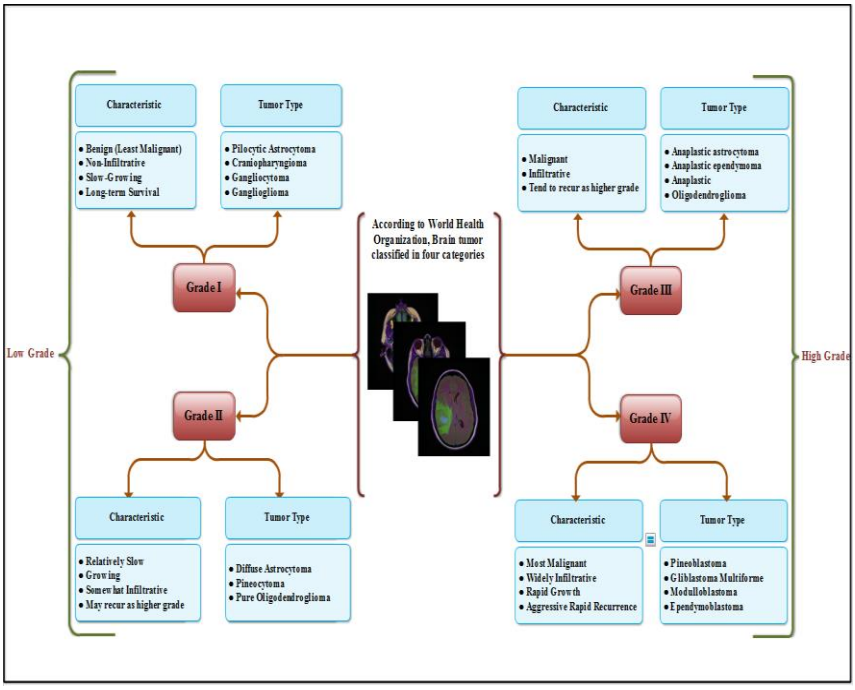

Fig 1.3 World Health Organization Brain Tumor Grade (Louis et al., 2016)

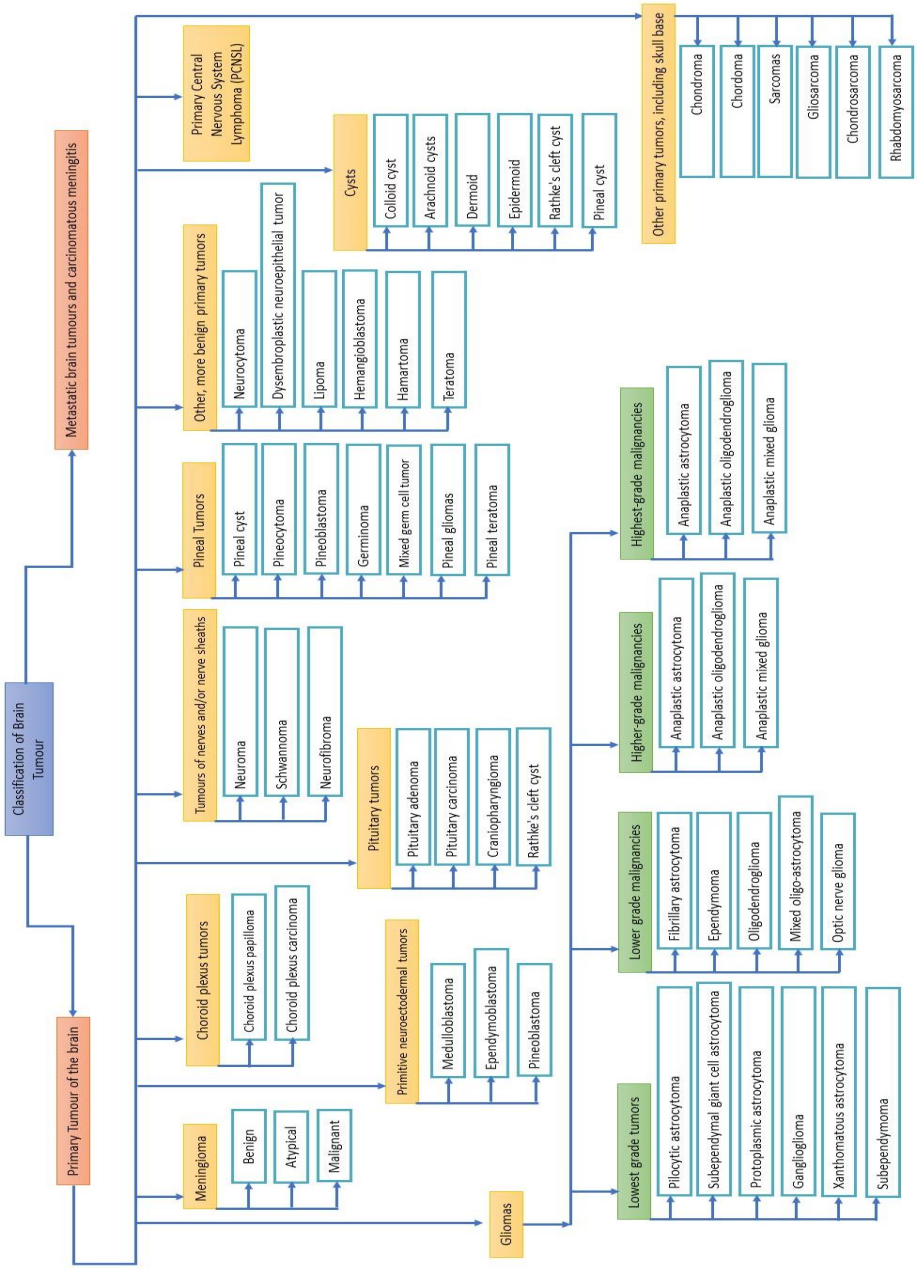

Fig 1.4 Brain Tumor Classification

(iv). Grade IV Tumor (Glioblastoma): Grade IV (Table 1.4) tumors are the most formidable and malignant form of brain neoplasms. Glioblastoma, or glioblastoma multiforme, is the predominant Grade IV. These tumours exhibit fast growth, infiltrate adjacent brain tissue, and have a pronounced propensity to reoccur after treatment. The management of Grade IV tumours often

necessitates a multimodal approach involving surgery, radiation therapy, and chemotherapy.

Table 1.1- Gliomas (Lowest Grade Tumors).

S No	Tumor Type	Tumor Grade	Location	Symptom	Treatment
1	Pilocytic astrocytoma	Grade-I	Cerebellum and chiasmatic / hypothalamic region, cerebral hemispheres, brainstem, and spinal cord	• Fatigue • Headache • Vomiting • Nausea	The initial treatment phase is surgery to eliminate as much of the tumor as possible without damaging any part of the brain. If the surgeon cannot remove the entire tumor, radiation may required after surgery. Chemotherapy is given regularly at the time of radiation because chemotherapy therapy destroys rapidly growing cells.
2	Subependymal giant cell astrocytoma	Grade-I	Aries in brain ventricle		Everolimus and Rapamycin, these mTOR inhibitor shown potential to reduce the volume of SEGA's in 35% to 45%.
3	Protoplasmic astrocytoma	Grade-II	Temporal Lobe, Frontal Lobe	• Seizure • Headaches • Hydrocephalus and focal neurological diseases including personality	Treatment be subject to on the clinical presentation, location and size of the tumor. • Radiotherapy • Recurrent tumor / differential tumor may have a role in

S No	Tumor Type	Tumor Grade	Location	Symptom	Treatment
				changes.	chemotherapy
4	Ganglioglioma	Grade-I	Temporal Lobe	• Increased Pressure inside the brain • Headache • Nausea • Vomiting • Fatigue	• Neurosurgery • Chemotherapy • Radiation Therapy Clinical trials and experimental treatments are also accessible to children who are not amenable to standard therapy with recurrent tumors
5	Xanthomatous astrocytoma	Grade-II	Temporal Lobe	• Seizure • Headache • Dizziness • Rarely Patient are asymptomatic	Radiation, radiotherapy, and reoperation may be options for recurrent tumors
6	Subependymoma	Grade-I	Lateral (30–40%) or Fourth (50–60%) ventricle; Though, sometimes it can also transpire in the third ventricle or septum pellucidum.(Gupta & Sasidhar,	• Headache • Confusion • Seizure • Nausea or vomiting • Weakness • Speech, vision, or memory problems. • Personality changes	Surgery and Radiation Therapy

S No	Tumor Type	Tumor Grade	Location	Symptom	Treatment
			2020)		

Table 1.2 -Gliomas (Higher-grade malignancies)

S No	Tumor Type	Tumor Grade	Location	Symptom	Treatment
1	Anaplastic astrocytoma	Grade-III	Location is cerebral hemispheres but can grow anywhere of the central nervous system	• Headache • Drowsiness or Lethargy • Vomiting or Nausea • Behavioural fluctuations • Memory loss • Seizures • Vision glitches, Coordination and balance complications	In most cases, the initial treatment is surgical excision and elimination of as many tumors as conceivable. Occasionally, only part of the tumor can be securely detached because malevolent cells can feast to the neighboring brain matter. Because surgery often cannot eliminate a tumor, chemotherapy is frequently used after surgery to endure treatment.
2	Anaplastic oligodendroglioma	Grade-III	Location is frontal lobe but can grow anywhere of the central nervous system.	• Focal Weakness • Headache • Cognitive deficits due to mass effect • vision changes	Maximum feasible solution is surgery, Radiation Therapy, Pharmacologic Treatment.
3	Anaplastic mixed	Grade-	Cerebrum	• Seizure	The initial treatment phase

S No	Tumor Type	Tumor Grade	Location	Symptom	Treatment
	glioma	III		• Headache • Changes in mood and personality	is surgery to eliminate as much of the tumor as conceivable without damaging any part of the brain. If the surgeon cannot remove the entire tumor, radiation may be required after surgery. Chemotherapy is assumed regularly at the time of radiation because chemotherapy treatment destroys rapidly growing cells.

Table 1.3 - Gliomas (Lower grade malignancies)

S No	Tumor Type	Tumor Grade	Location	Symptom	Treatment
1	Fibrillary astrocytoma	Grade-II	Cerebral Hemisphere	• Seizure • Headache • Frequent Mood Changes	• Surgery • Radiotherapy • Chemotherapy • Radiosurgery
2	Ependymoma	Grade-II	Common location is fourth ventricle	• Neck pain • Vision changes • Jerky eye movement • Difficulty in balance and walking • Nausea and	• Surgery • Radiotherapy • Chemotherapy • Radiosurgery

S No	Tumor Type	Tumor Grade	Location	Symptom	Treatment
				vomiting • Weakness in limbs	
3	Oligodendroglioma	Grade-II	Originate in cortex but can be anyplace in the Central Nervous System	• Headaches. • Seizures • Language difficulty. • Weakness on one side of the body • Balance and movement problems. • Behaviour and personality changes • Memory problems.	Maximum feasible solution take care by the surgeon to remove the tumor by surgery with the use of specialized surgical technique and if any tumor cells remaining after surgery, then additional treatment like Chemotherapy, Radiation Therapy as well as palliative care providing relief from pain.
4	Mixed oligo-astrocytoma	Grade-II	Cerebrum	• Seizures • Headaches • Change in personality	Dealing options consist of radiation and/or chemotherapy, surgery.
5	Optic nerve glioma	Grade-I	Found in optic chiasm	• Nausea and vomiting • Balance problems • Vision disturbances Headaches	Two possible ways to treat optic nerve glioma: Surgery and Radiation Therapy

Table 1.4 - Gliomas (Highest-grade malignancies)

S No	Tumor Type	Tumor Grade	Location	Symptom	Treatment
1	Anaplastic astrocytoma	Grade IV	Location is cerebral hemispheres but can grow anywhere of the central nervous system	• Headache • Drowsiness or Lethargy • Vomiting or Nausea • Behavioural fluctuations • Memory loss • Seizures • Vision glitches, Coordination and balance complications	In most cases, the initial treatment is surgical excision and elimination of as many tumors as conceivable. Occasionally, only part of the tumor can be securely detached because malevolent cells can feast to the neighbouring brain matter. For the reason that surgery often cannot eliminate a tumor completely, chemotherapy is frequently used after surgery to endure treatment.
2	Anaplastic oligodendroglioma	Grade IV	Location is frontal lobe but can grow anywhere of the central nervous system.	• Focal Weakness • Headache • Cognitive deficits due to mass effect • vision changes	Maximum feasible solution is surgery, Radiation Therapy, Pharmacologic Treatment
3	Anaplastic mixed glioma	Grade IV	Cerebrum	• Seizure • Headache • Changes in mood	The initial treatment phase is surgery to eliminate as much of

S No	Tumor Type	Tumor Grade	Location	Symptom	Treatment
				and personality	the tumor as conceivable without damaging any part of the brain. If the surgeon cannot remove the entire tumor, radiation may be required after surgery. Chemotherapy is assumed regularly at the time of radiation because chemotherapy treatment destroys rapidly growing cells.

1.6 Causes for Brain Tumor

According to the American Brain Tumor Association, the main factors associated with the development of brain tumors include:

- Exposure to medical radiation
- Cell phone usage
- Smoking and alcohol consumption
- Consumption of processed or cured foods
- Employment in synthetic rubber manufacturing or petroleum refining
- Genetic conditions
- Use of hair dye
- Utilization of medications such as birth control pills, sleeping pills, and headache remedies

- Exposure to air pollution
- Proximity to power lines
- Exposure to agricultural chemicals
- History of previous cancers

1.7 Symptom of Brain Tumor

The manifestation of brain tumours might differ according on the tumor's location, dimensions, and rate of expansion. Common indications of a brain tumour may include several symptoms.:

- Headaches: Persistent or severe headaches that may worsen over time or are different from usual headaches.
- Seizures: Sudden and uncontrolled movements or convulsions.
- Cognitive and memory problems: Difficulty concentrating, memory loss, confusion, and changes in thinking abilities.
- Visual disturbances: Blurred or double vision, loss of peripheral vision, or difficulty with coordination.
- Nausea and vomiting: Especially if they occur without any other apparent cause.
- Changes in speech or hearing: Difficulty speaking, slurred speech, or hearing problems.
- Weakness or paralysis: Weakness in the limbs, loss of coordination, or difficulty in performing tasks that require fine motor skills.
- Personality changes: Mood swings, irritability, depression, or personality changes.
- Balance and coordination issues: Trouble with balance, dizziness, or difficulty walking.
- Fatigue: Persistent tiredness and lack of energy.

1.8 Motivation

Primary brain or spinal cord tumours are defined by the scientific board at cancer.net as tumours that begin their malignant growth in these areas. Approximately 24,810 people in the US will receive a diagnosis of a brain or spinal cord tumour in 2023, with 14,280 men and 10,530 women affected. On average, fewer than one percent of people will have this cancer at some point in their lives. Approximately 85% to 90% of initial tumours in the CNS are neurologically derived malignancies. Primary brain or spinal cord tumours were estimated to have been newly detected in roughly 308,102 instances worldwide in 2020 (Brain Tumour - Statistics, 2023).

Brain and nervous system cancers are prominent contributors to global mortality, comprising 10% of total deaths across genders. According to current statistics, around 18,990 Americans (roughly 11,020 males and 7,970 females) would die from primary CNS tumours in the year 2023. The number of persons who died in 2020 from primary brain and CNS tumours was expected to be 251,329. Fig 1.5 shows the proportion of death due to cancer and other causes.

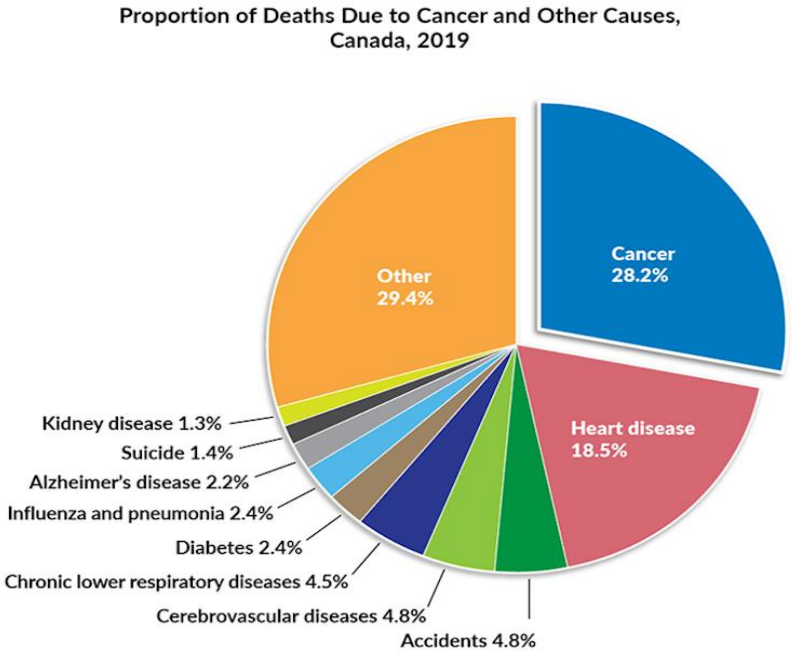

Fig 1.5 Percentage of death due to cancer and other ailments (Du Cancer, n.d.)

It was forecast that there will be 233,900 new-fangled instances of cancer in Canada in 2022, with 85,100 fatalities from the disease. (Non-melanoma skin cancer patients are excluded from the total number of new cases estimated.)

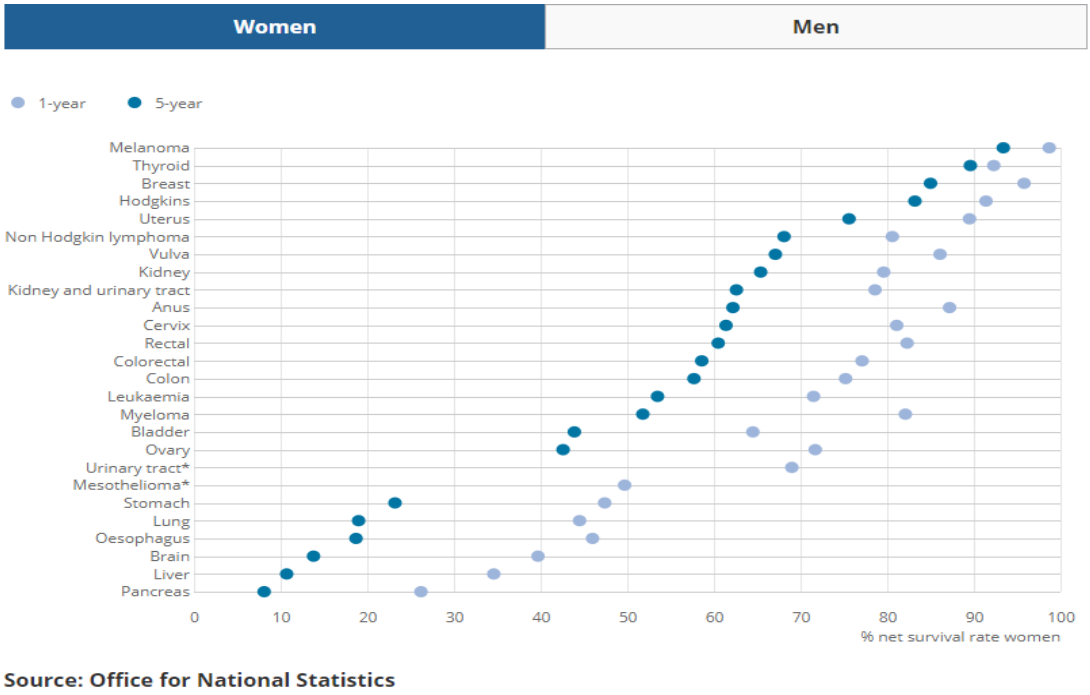

Fig 1.6 Cancer Survival in England five-year net survival guesstimates for adults (2013-2017) (Broggio, 2019)

Adults in England (15-99) diagnosed with one of the 29 most common malignancies between 2013 and 2017 and followed up to 2018 have their five-year net survival estimates reported in Fig 1.6 of Office for National Statistics, Cancer Survival in England.

1.9 Problem Statement

My problem statement is "**Survival Prediction in Glioblastoma Brain Tumor using Segmentation and Detection with Advance Computational Techniques**". Gliomas signify the most malignant form of brain tumors, and accurate predictions of overall survival, diagnosis, and treatment planning can greatly assist glioma patients. By employing automated algorithms, we aim to enhance prediction accuracy, robustness,

and mitigate overfitting issues. Furthermore, our goal is to identify a model that minimizes errors and provides valuable insights.

The problem can be formulated in the following manner:

- Explore innovative approaches for segmenting brain tumors.
- Develop a framework capable of distinguishing between tumor and non-tumor images.
- Conduct a comparative analysis of various techniques at each stage, from prototyping to final selection, to identify the most suitable approach for survival predictions.
- Evaluate different measurements such as specificity, sensitivity, accuracy, and DSC to enhance the model's performance at each level.

1.10 Organization of the Thesis

The thesis is organised in a manner that allows for a methodical investigation of the study subject. Chapter 1 functions as the introductory section, providing a thorough summary of the research background and clearly outlining the goals of the study. Chapter 2 undertakes a comprehensive examination of the current body of literature, encompassing both conventional and contemporary methodologies for the segmentation and categorization of brain tumours. Additionally, it includes an assessment of the technical inquiries conducted throughout the years. Subsequently, Chapter 3, named "Preliminaries," explores fundamental components essential for effectively carrying out the research. These components include pre-processing procedures, dataset preparation, tasks related to predicting overall survival, post-processing approaches, and evaluation measures. In Chapter 4, the "Model Framework for Detecting and Localising the Brain Tumour" is presented, establishing the fundamental concepts that will be built upon in the following chapters. Expanding on this structure, Chapter 5 concentrates on "MRI Based Brain Tumour Feature Extraction with Overall Survival Prediction Using Deep Learning Inspired Replicator Neural Network." It introduces the model and approach for extracting characteristics

from MRI data, with a particular emphasis on predicting overall survival. Chapter 6 concludes with an exploration of the "Future Scope and Conclusion." This chapter explores potential avenues for future research, offering valuable perspectives on the extension of the current study. The chapter finishes by providing a concise overview of the main discoveries, contributions, and the overall importance of the research. This organisation guarantees a coherent sequence of the many components of the study, starting with basic principles and progressing to the utilisation of sophisticated models, while also considering potential future directions for investigation.

CHAPTER 2

LITERATURE REVIEW

In the contemporary landscape of research, there has been a notable upswing in researchers favoring automated or semi-automated approaches for the segmentation of brain tumors. This is because these methods guarantee reproducibility while speeding up image interpretation. Researchers have been interested in brain tumour segmentation since the late 1990s. Various techniques, including both traditional and Fully Convolutional Neural Network approaches, have been developed throughout the years to accomplish this goal. This chapter's goal is to take a look at algorithms that are made to separate brain tumours and their surrounding tissues. The unexpected size, form, and location of tumours make automated brain tumour segmentation a tough task. This unpredictability is magnified when reference images from prior scans are unavailable. Traditional pattern recognition methods that are often employed to identify objects in different types of photos would not work in this particular case. A few pieces of information, though, such how a normal human brain is structured or how tumours appear in particular MR sequences, can be put to use. Because brain photos often have a more consistent colour palette and backdrop scene, this provides an advantage over object detection in other types of photographs (such as those of people or cars). A lot of computer vision research groups have been focusing on the automatic brain tumour segmentation problem, which has led to a general uptick in interest in creating such algorithms.

Most cutting-edge methods focus on the most common tumour types, including glioblastoma, because there are so many different kinds of brain tumours and how they look in MR images. On the other hand, a dedicated training database for particular tumour types is required by certain approaches.

This chapter provides a classification system for the many conventional methods of brain tumour segmentation according to the imaging data they use. Among these groups are:

- Threshold-based methods: These techniques segment brain tumours by comparing their intensities to those of the surrounding tissues.
- Region-based methods: They find groups of voxels that share characteristics and use them to segment data.
- Contour-based methods: These seek out the boundaries between brain tumours and their environs in order to segment them.
- Classification or clustering methods: They employ texture and intensity characteristics at the voxel level for segmentation.
- Atlas-based methods: These use what is already known about the normal brain to do the segmentation.

The boundary between these types of procedures is not always distinct, though, because many of the suggested solutions incorporate more than one strategy. Most cutting-edge methods in the last several years have relied on categorization and atlas guiding.

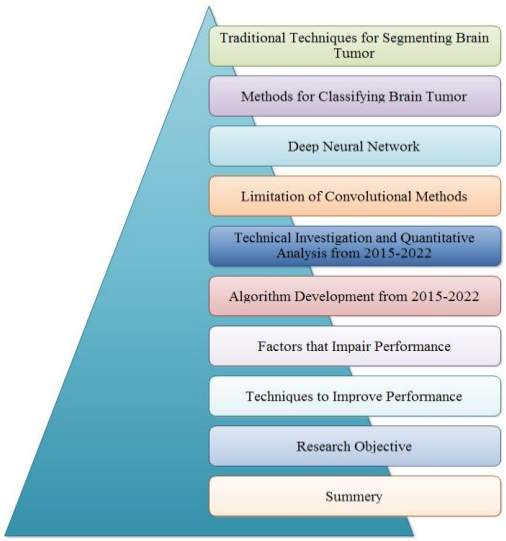

Fig 2.1 Outline for the Literature Review

Another way to classify brain tumour segmentation methods is by the degree to which they rely on human intervention. You can classify them as either fully-automatic or semi-automatic. Some semi-automatic processes, such as choosing seed sites or estimating initial border demarcation, necessitate human involvement. Fully automated procedures, on the other hand, do not require any kind of human involvement. This chapter, however, will make use of the division depending on the picture data utilised by specific algorithms. This literature review follows the format shown in Figure 2.1.

2.1 Traditional Techniques for Segmenting Brain Tumors

2.1.1 Thresholds Based Methods

Threshold-based methods (Fig 2.2 and Table 2.1) are a class of image processing techniques used in segmentation tasks, particularly for brain tumor segmentation. These methods rely on defining a threshold value to distinguish between different regions or objects in an image based on their intensity levels. In the context of brain tumor segmentation, threshold-based methods use intensity differences between brain tumors and surrounding tissues to identify the tumor region. The process involves selecting an appropriate threshold value that separates tumor pixels from non-tumor pixels in the image.

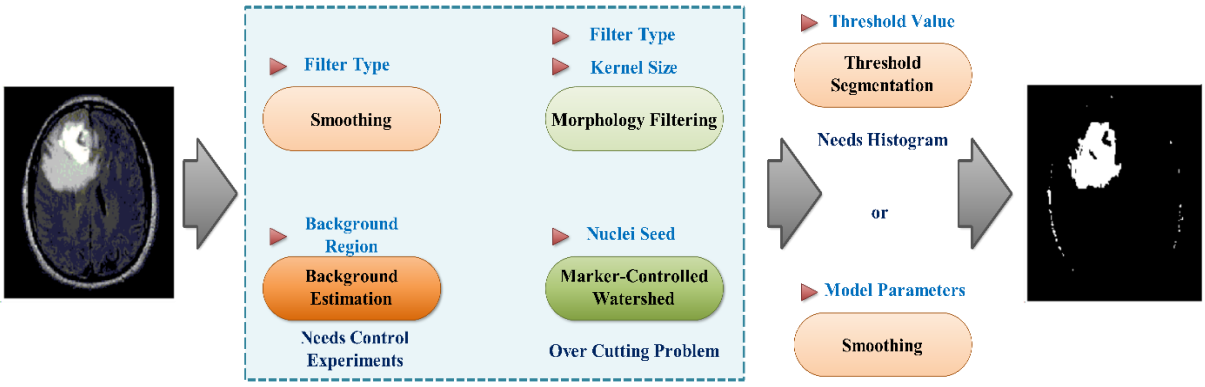

Fig 2.2 Thresholds Based Segmentation (Wu et al., 2021)

Typically, threshold-based methods work well when the intensity differences between the tumor and the surrounding tissues are distinct. However, they may have limitations when dealing with images that have varying intensity distributions or when there is overlap in the intensity levels between the tumor and normal tissues.

Thresholding is most effective when certain conditions are met:

- Minimal Noise: Thresholding performs optimally in scenarios with a low level of noise, as noise can interfere with the clear separation of pixels into different groups.
- Higher Intra-class Variance: When the intensity values of pixels within the same group (class) are more similar to each other than to pixels of other groups, thresholding yields better results.
- Homogeneous Lighting: Uniform lighting conditions contribute to better performance in thresholding, ensuring consistent intensity distributions.

Table 2.1 Thresholding Based Methods

S No	Proposed Technique	Remarks
1	Gaussian models and Threshold outlier detection (Domingues, et al., 2018)	• Secondary analysis on tumor area may be required after treatment of edema area. • Intensity features are another concept which is used in this technique. The concept of detecting technique is used to find the difference between normal and abnormal space.
2	Probability level set evolution (Deng et al., 2019)	A lower level of agreement compared with semi-automatic method.
3	Marker Controlled Watershed (Chattaraj	• To highpoint the mistrustful regions more

S No	Proposed Technique	Remarks
	et al., 2017)	noticeably. It is a morphological process on the basis of locating watershed outlines from a topographic demonstration of the participation image.
4	OTSUs threshold (Gupta & Khanna, 2017)	Otsu's thresholding technique is fragmented through multilevel optimization of non-homogeneous brain MR images.

2.1.2 Region Based Methods

Partitioning a picture into relevant or interesting sections according to predetermined criteria is the job of region-based approaches, a subset of image segmentation techniques. Clustering comparable pixels or voxels into consistent areas with similar features (such as intensity, texture, colour, etc.) is the objective of these methods. When it comes to segmenting brain tumours, region-based approaches look for groups of related pixels or voxels that stand in for the tumour and its environs. The goal of the method is to attain the necessary level of segmentation by repeatedly merging or separating regions according to predetermined criteria or rules.

Region-based methods typically involve the following steps:

- Initialization: The image is divided into small initial regions or super pixels using methods like graph-based segmentation or watershed transformation.
- Region Growing/Merging: To create bigger regions, adjacent areas with comparable characteristics are combined. This process continues iteratively until all pixels are assigned to meaningful regions.
- Region Splitting: In some cases, regions may be split if they contain mixed or heterogeneous information, allowing for more accurate segmentation.

- Feature Extraction: Feature extraction techniques are used to characterize the properties of each region. These features may include intensity histograms, texture features, or spatial attributes.
- Region Properties: The regions are evaluated based on their properties and compared with predefined criteria, such as size, shape, or intensity, to identify regions that represent the tumor and its surrounding tissues.

Region-based methods offer advantages in handling complex image structures and addressing intensity variations within the same object. They can effectively segment objects with irregular shapes and are less sensitive to noise compared to threshold-based methods. Table 2.2 provides the summery of region-based methods.

Table 2.2 Region Based Methods

S No	Proposed Technique	Remarks
1	Histogram analysis 2D region growing (Kumar et al., 2020)	2D histogram-based technology ignores evidence connected to boundaries and thinks only the background and contextual of objects. Non-local means constructed 2D histogram procedures are on condition that with improved post filter lucidity of images with improved consequences.
2	Texture Feature FCM (Vaibhavi & Rupal, 2018)	Upright results and also accomplished very precise outcomes of segmentation which efficiently extract the tumor region from brain MR images.
3	Seed-Based Region Growing (Vishnuvarthanan et al., 2017)	Here a judgement is made amid number of pixels of the underdone MRI brain images and Seed-Based Region Growing segmented abnormality area. As associated to the light MRI, it is realized that Seed-Based Region

S No	Proposed Technique	Remarks
		Growing achieved lesser in shady MRI segmentation

2.1.3 Edge Based Methods

Edge-based methods are a class of image segmentation techniques used to detect and locate edges or boundaries within an image. These methods aim to identify the abrupt changes in intensity, color, texture, or other image properties that correspond to object boundaries or regions of interest.

To segment brain tumours, edge-based approaches look for the boundaries that separate the tumour from the normal brain tissue. The first step is to locate the spots on the image where the intensity or other characteristics change noticeably; this will show you where the tumour is and where the healthy tissue is.

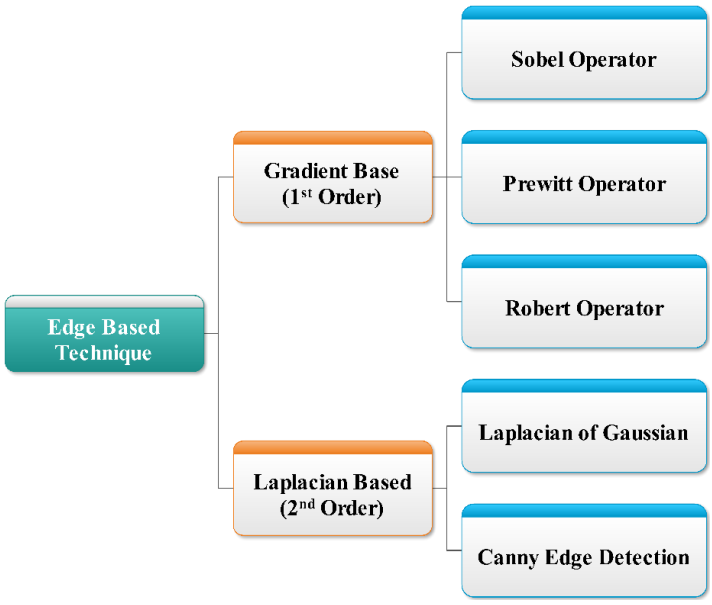

Fig 2.3 Edge Based Segmentation Techniques

Edge-based methods (Fig 2.3) are particularly effective in situations where objects have distinct and well-defined boundaries, making them suitable for segmenting

objects with sharp transitions in intensity or texture. They are robust to variations in lighting and contrast, which can be beneficial for brain tumor segmentation tasks.

This technique uses edge recognition operators to find image edges and then converts the original picture to edge pictures. Edges are formed by pixels located between the boundaries of two regions. The edge detection process typically involves three main steps: filtering, enhancement, and detection of edge points (Yogamangalam et. al., 2013, Lakshmi & Sankaranarayanan, 2010). Edges are crucial features in images, encompassing essential elements such as corners, lines, and curves (Kaur & Singh, 2016). According to Layaraja and Suganthi (2014) and Muthukrishnan and Radha (2011), edge detection is useful because it decreases the amount of data that has to be processed, removes unnecessary information, and keeps crucial structural features inside the image. Two popular approaches to edge identification are the first-order derivative, which is based on gradients (using operators such as Sobel, Prewitt, and Robert) and the second-order differential based on Laplacian (employing methods like Laplacian of Gaussian and Canny edge detection) (Kaur & Singh, 2016).

(i). Sobel Operator: One operator used in image processing to highlight edges is the Sobel operator, which is based on convolutional neural networks. It uses a convolution with two kernels—one for horizontal edge detection (Gx) and another for vertical edge detection (Gy)—to determine an image's gradient magnitude (Feature Detectors - Sobel Edge Detector, n.d.).

Mathematically, the Sobel operator is applied by convolving the image matrix (I) with the Gx and Gy kernels:

Horizontal Sobel Kernel (Gx):

$$\begin{bmatrix} -1 & 0 & 1 \\ -2 & 0 & 2 \\ -1 & 0 & 1 \end{bmatrix} \qquad [2.1]$$

Vertical Sobel Kernel (Gy):

$$\begin{bmatrix} -1 & -2 & -1 \\ 0 & 0 & 0 \\ 1 & 2 & 1 \end{bmatrix} \quad [2.2]$$

The convolution operation produces two new matrices, Gx and Gy, which represent the gradient values along the horizontal and vertical directions, respectively, at each pixel location.

The gradient magnitude (G) of the image can then be calculated using the following formula:

$$G = \sqrt{Gx^2 + G\,y^2} \quad [2.3]$$

The gradient direction (θ) can also be determined:

$$\theta = arctan(Gy \,/\, Gx) \quad [2.4]$$

The Sobel operator is applied by sliding the Gx and Gy kernels over the image matrix, computing the gradient values at each pixel. This process amplifies areas of rapid intensity change, effectively highlighting edges.

(ii). **Prewitt Operator:** When it comes to image processing, one such operator that uses convolution to find edges is the Prewitt operator. Just like the Sobel operator, the Prewitt operator uses a convolving operation with two kernels—one for horizontal edge detection and one for vertical edge detection—to determine the gradient magnitude.

Mathematically, the Prewitt operator is applied by convolving the image matrix (I) with the following kernels:

Horizontal Prewitt Kernel (Gx):

$$\begin{bmatrix} -1 & 0 & 1 \\ -1 & 0 & 1 \\ -1 & 0 & 1 \end{bmatrix} \quad [2.5]$$

Vertical Prewitt Kernel (Gy):

$$\begin{bmatrix} -1 & -1 & -1 \\ 0 & 0 & 0 \\ 1 & 1 & 1 \end{bmatrix} \quad [2.6]$$

The convolution operation generates two matrices, Gx and Gy, representing the gradient values along the vertical and horizontal directions at each pixel location.

The gradient magnitude (G) of the image can be computed using the subsequent formula:

$$G = \sqrt{Gx^2 + G\,y^2} \quad [2.7]$$

The gradient direction (θ) can also be calculated:

$$\theta = arctan(Gy\ /\ Gx) \quad [2.8]$$

The Prewitt operator is applied by sliding the Gx and Gy kernels over the image matrix, calculating the gradient values at each pixel. This process enhances areas of rapid intensity change, highlighting edges.

Similar to the Sobel operator, the Prewitt operator is sensitive to noise, and post-processing techniques like thresholding is often employed to improve the detected edges.

(iii). Robert Operator: For the purpose of image processing, the Robert operator is a straightforward edge detection operator. By using two 2x2 convolution kernels on the picture matrix, it determines the magnitude of the gradient.

Mathematically, the Robert operator is applied by convolving the image matrix (I) with the following kernels:

Horizontal Robert Kernel (Gx):

$$\begin{bmatrix} 1 & 0 \\ 0 & -1 \end{bmatrix} \quad [2.9]$$

Vertical Robert Kernel (Gy):

$$\begin{bmatrix} 0 & 1 \\ -1 & 0 \end{bmatrix} \quad [2.10]$$

The gradient magnitude (G) of the visuls can be computed using the subsequent formula:

$$G = \sqrt{Gx^2 + G\,y^2} \quad [2.11]$$

The gradient direction (θ) can also be calculated:

$$\theta = arctan(Gy\ /\ Gx) \quad [2.12]$$

In practice, the Robert operator is applied by sliding the Gx and Gy kernels over the image matrix, calculating the gradient values at each pixel. This process enhances areas of rapid intensity change, highlighting edges.

The Robert operator is a basic edge detection technique that is computationally efficient but can be sensitive to noise.

(iv). Laplacian of Gaussian: In the intricate domain of image processing and computer vision, the Laplacian of Gaussian (LoG) stands as a mathematical virtuoso, meticulously employed for feature detection, particularly in the intricate dance of edge detection. This technique is an alchemical fusion, birthing from the convolution of the additional derivative of a Gaussian function with an image. Described mathematically, the Laplacian of the Gaussian function intricately weaves its two-dimensional tapestry in the form of the function f(x, y).

$$LoG(x,y) = -\frac{1}{\pi\sigma^4}\left(1 - \frac{x^2+y^2}{2\sigma^2}\right) e^{-\frac{(x^2+y^2)}{2\sigma^2}} \quad [2.13]$$

- (x,y) represents the coordinates of the point in the image.
- This operation's scale is controlled by the standard nonconformity of the Gaussian function, denoted as σ.

For edge detection, the Laplacian of Gaussian is beneficial because it draws attention to regions of a picture where the intensity changes quickly. The

numerical result shows that the LoG reacts positively for edges where the intensity varies from dark to light, and adversely for edges where the intensity changes from light to dark.

(v). Canny Edge Detection: Using canny edge detection, one can greatly reduce the amount of data that requires processing while still extracting essential structural information from various visual objects. Many different kinds of computer vision systems have made extensive use of this method. Using edge detection to different vision systems has common requirements, as Canny noticed. Therefore, a versatile edge recognition method that encounters these necessities may be used to many situations (G et al., 2019). The fundamental criteria for successful edge detection encompass:

- Achieving accurate edge detection with minimal errors, ensuring that the algorithm captures as many edges as possible from the image.
- Precise localization of detected edge points at the center of the edges.
- Ensuring that each edge in the image is identified only once and, wherever feasible, avoiding false edge creation due to image noise.

As a mathematical tool for finding the optimal function for a specific functional, the calculus of variations was used by Canny to meet these requirements. The ideal function, which is the sum of four exponential terms, is represented in Canny's detector by a Gaussian first derivative estimation. The Canny edge detection technique is a well-defined method that provides reliable edge identification, setting it apart from other approaches that have been created thus far. Its superiority in meeting the three edge detection criteria, coupled with its straightforward implementation process, has contributed to its widespread popularity as an edge detection procedure.
The algorithm involves a sequence of five distinct stages:

(i). Employ a Gaussian filter to gently smoothen the image, aiming to eliminate any noise present.

(ii). Determine the intensity gradients across the image.

(iii). Employ thresholding based on gradient magnitude or suppress weaker responses to discard unintended edge detection outcomes.

(iv). Implement a double thresholding procedure to identify prospective edges.

(v). Utilize hysteresis for edge tracking: Conclude edge detection by suppressing weaker, unconnected edges, while emphasizing strong edges.

2.1.4 Atlas – Based Methods

Atlas-based methodologies, a cornerstone of medical image analysis, pertain to a category of techniques that harness pre-existing anatomical or spatial insights encapsulated in an "atlas" image to guide the analysis or processing of diverse images. These techniques unfold their brilliance when confronted with intricate or variable anatomical structures spanning different subjects.

sIn the realm of medical imaging, an atlas serves as a touchstone—a reference image or dataset embodying a prototypical or average anatomy. The orchestration of atlas-based methods involves the transference of information from this reference image onto a target image, lending a helping hand in a spectrum of tasks, including segmentation, registration, and feature extraction. Conceptually, these methods embody a form of image-centric knowledge transfer.

A prevalent example in brain tumor segmentation employs an atlas featuring a spatial probabilistic distribution of three normal brain tissues. This inter-patient atlas stands as a stalwart ally in this endeavor, as depicted in Fig 2.4. Approaches grounded in this atlas adeptly discern deviations from its representation, earmarking them as potential tumor regions (Fonov et al., 2011). Atlas-based methods weave their influence across diverse medical imaging applications, notably in brain MRI analysis, where individual

anatomies exhibit significant variability. By leveraging a shared reference (atlas), these methods play a pivotal role in elevating the precision, efficacy, and uniformity of image analysis tasks, solidifying their status as indispensable tools in the realm of medical image processing and research.

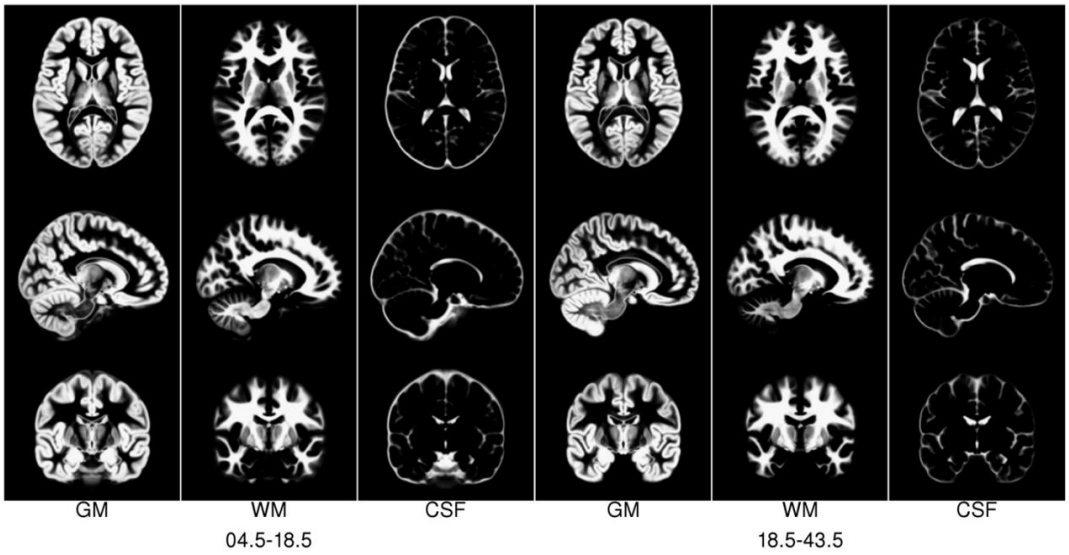

Fig 2.4 The GM, WM, and CSF brain tissue types in the ICBM 18.5-43.5 atlas are contrasted with those in the NIHPD 4.5-18.5 atlas (top three columns on the left). The highest-intensity voxels are very indicative of being part of that particular type of tissue. For the purpose of making comparisons, the contours of the skin and skull have been placed on each individual photograph. Research conducted by Fonov et al. in 2011.

2.2 Brain Tumor Machine Learning Based Classification Methods

These methods categorise each pixel or voxel by applying either supervised (classification) or unsupervised (clustering) techniques to assign labels. Classification methods are commonly used in several areas of medical image processing. A training dataset is required for the building of the model, which may subsequently be used on new, unfamiliar data. The training dataset consists of two crucial elements: the data's representation in a feature space (including attributes like as pixel intensities and local textures) and the accompanying labels (which include manually classifying the data).

Conversely, clustering approaches function independently of any requirement for training data or manually supplied labels. Instead, these algorithms independently detect fundamental structures and patterns within the data.

2.2.1 k-Nearest Neighbour (k-NN)

In the vast tapestry of machine learning techniques, the K-Nearest Neighbours (KNN) algorithm stands as a modest yet formidable artisan, proficient in the crafts of classification and regression. At its core lies the philosophy that kindred data points, like celestial siblings, share not just the same class but also a kinship in behavior. Embracing the ethos of instance-based learning, KNN carries the entire training dataset as its treasury, crafting predictions by orchestrating a symphony of similarities between newly encountered data points and their archived counterparts. It's a digital voyager navigating the cosmos of data, drawing upon the collective wisdom of its stored instances to illuminate the path of predictions in the ever-unfolding saga of information.

Here's how the KNN algorithm works:

Training Phase: Feature vectors and their associated class labels or goal values for extrapolation are stored in the learning dataset by the K-nearest neighbour’s approach. This is done throughout the learning stage of the algorithm.

Prediction Phase (Classification): The KNN algorithm embarks on a quest to unveil the "k" nearest companions within the training dataset when confronted with a novel and mysterious data point. It navigates this journey utilizing a distance metric, often the Euclidean distance, as its guiding compass. The class label bestowed upon the uncharted data point is a reflection of the prevailing class among its "k" closest comrades. In simpler terms, the new data point is adorned with the class that holds the highest prevalence within its intimate circle of neighbors.

Prediction Phase (Regression): By averaging (or weighting) the goal values of its "k" nearest neighbours, a new data point's projected target value in regression tasks is calculated.

Key concepts and considerations of KNN:

- **Distance Metric:** In the delicate choreography of uncovering the likeness between two data points, KNN navigates the intricate terrain using a distance metric, whether it be the brisk strides of Manhattan or the measured paces of Euclidean distances. The endeavor to fathom the distance of the nascent data point from each resident within the training dataset unfurls as a symphony of feature vectors, where the threads of each characteristic weave the narrative that binds the familiar and the enigmatic.
- **Choice of k:** The value of "k" is a hyperparameter that determines the number of neighbours considered for making predictions. A smaller "k" may lead to noisy predictions, while a larger "k" may introduce bias. The optimal value of "k" depends on the dataset and problem at hand.
- **Weighted Voting:** In some cases, a weighted voting scheme can be used, where closer neighbours have a higher influence on the prediction.
- Normalization: Features might have different scales, which can impact distance calculations. Normalizing features can help ensure that no single feature dominates the distance computation.
- **Computational Complexity:** Predicting the class or value of a new data point in KNN involves calculating distances to all training instances. This can become computationally intensive for large datasets.

However, it may not perform well on high-dimensional data or when the data is imbalanced. It's often used in combination with other methods or as part of more complex models.

2.2.2 Bayesian Approach

When it comes to predictive analytics, Bayesian machine learning is a top-tier modelling approach. Algorithms for machine learning are wed to probabilistic reasoning. The practical uses of Bayesian machine learning, including natural language processing (NLP) spam filtering and credit card fraud detection, have contributed to its rising popularity. In order to generate conclusions and forecasts that take uncertainty into consideration, Bayesian Machine Learning integrates machine learning with Bayesian statistics. To estimate posterior probabilities and make better judgements, it uses Bayes' theorem to update previous beliefs or probabilities based on observed facts. Applying Bayesian inference to real-world scenarios provides for more accurate predictions, as it is based on Bayes' theorem. (Fonov et al., 2011).

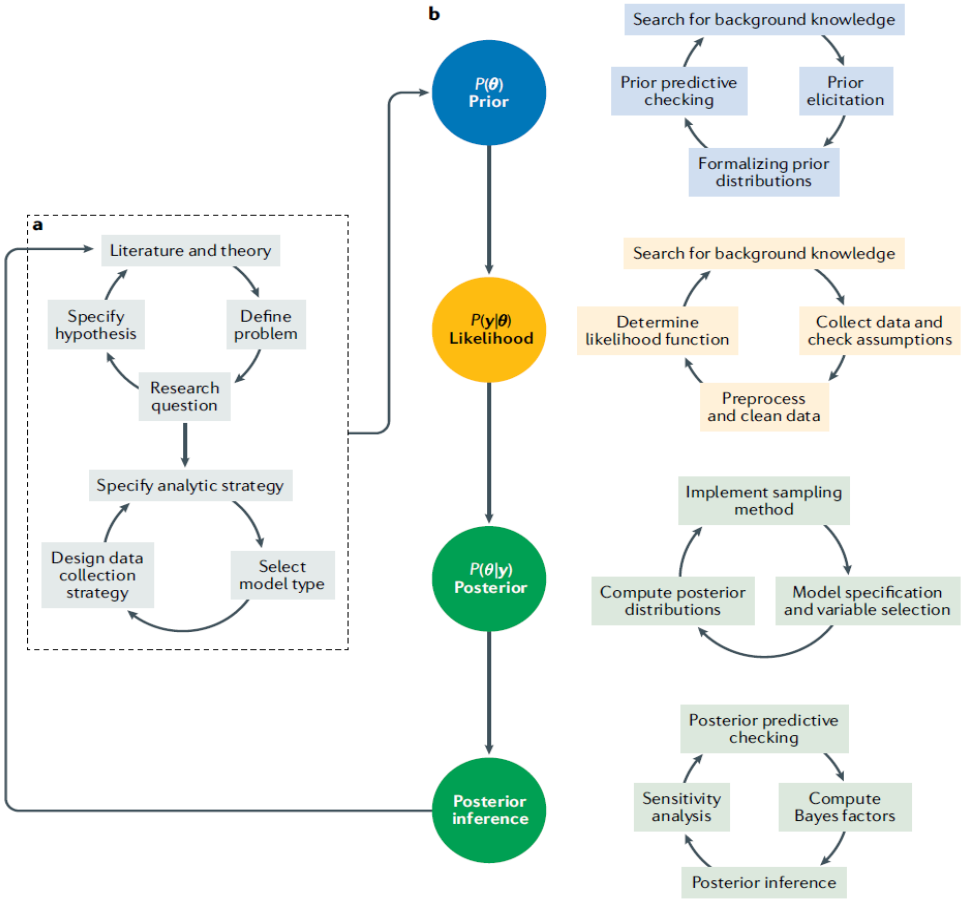

Fig 2.5 The Bayesian Research Cycle (Fonov et al., 2011)

The fundamental formula behind Bayesian Machine Learning is Bayes' theorem (Fig 2.5):

$$P(H|D) = (P(D|H) * P(H)) / P(D) \quad [2.14]$$

Where:

- P(H|D) is the posterior probability of hypothesis H given the observed data D.

- If hypothesis H is true, then the probability of data D is P(D|H).
- The prior probability of hypothesis H is denoted as P(H).
- The probability of the observed data D is denoted as P(D).

In Bayesian Machine Learning, this formula is used to update prior beliefs (P(H)) based on new evidence (P(D|H)) and calculate the posterior probabilities (P(H|D)).

The Bayesian approach plays a significant role in MRI (Magnetic Resonance Imaging) image processing, offering a principled and effective way to enhance, segment, and analyze medical images. This approach leverages probabilistic modelling to integrate prior knowledge, image data, and uncertainty, ultimately leading to more accurate and robust results.

Here's how the Bayesian approach is applied to MRI image processing (Fonov et al., 2011):

- **Prior Information**: In MRI image processing, prior information could include anatomical knowledge, tissue properties, or statistical distributions of intensities. This information is often incorporated into the Bayesian model as a prior probability distribution, representing our initial beliefs about the image properties.
- **Likelihood Model:** The likelihood model captures the relationship between the observed image data and the underlying image properties. It defines the conditional probability of observing the given data given the image properties.

In MRI, this could involve modelling noise characteristics and the expected signal behaviour for different tissues.

- **Posterior Probability:** By combining the prior distribution and the likelihood model using Bayes' theorem, the posterior probability distribution is computed. This distribution represents our updated beliefs about the image properties after observing the data.
- **Maximum A Posteriori (MAP) Estimation:** The Bayesian approach often seeks the most likely set of image properties given the observed data, which is known as the MAP estimation. This can be considered as finding the point estimate that maximizes the posterior probability.

2.2.3 Support Vector Machine

The Support Vector Machine is a multi-talented virtuoso in the field of supervised learning, deftly used to categorise and predict a wide variety of problems. Its influence stretches across domains as diverse as the intricate realm of signal processing, the nuanced landscapes of medical domains, the poetic realms of natural language processing, and the visual symphony of speech and image recognition.

At the core of the SVM algorithm lies the paramount goal of pinpointing an optimal hyperplane that adeptly partitions instances of one class from their counterparts in another class. This "optimal" hyperplane is characterized by the widest margin between the two classes, as depicted by the distinction between plus and minus in the diagram below. The margin corresponds to the maximal breadth of the space adjacent to the hyperplane that lacks interior data points. While the algorithm can indeed find such a hyperplane when the data is linearly separable, in practical scenarios, it typically maximizes a flexible margin to accommodate a limited number of classification errors.

Support vectors pertain to a subset of training observations that pinpoint the position of the dividing hyperplane. The typical SVM approach is framed for binary

classification tasks, and scenarios involving multiple classes are often converted into a series of binary ones.

Delving into the underlying mathematical intricacies, support vector machines (fig 2.6) belong to a category of machine learning algorithms termed kernel methods, in which features can undergo transformation through a kernel function. Kernel functions (Table 2.3) map the data onto an alternate space, often with higher dimensions, under the presumption that classes become easier to distinguish following this alteration. This may streamline intricate non-linear decision boundaries into linear ones within the augmented, mapped feature space. This entire procedure obviates the requirement for explicit data transformation, which would prove computationally intensive. This concept is commonly recognized as the "kernel trick."

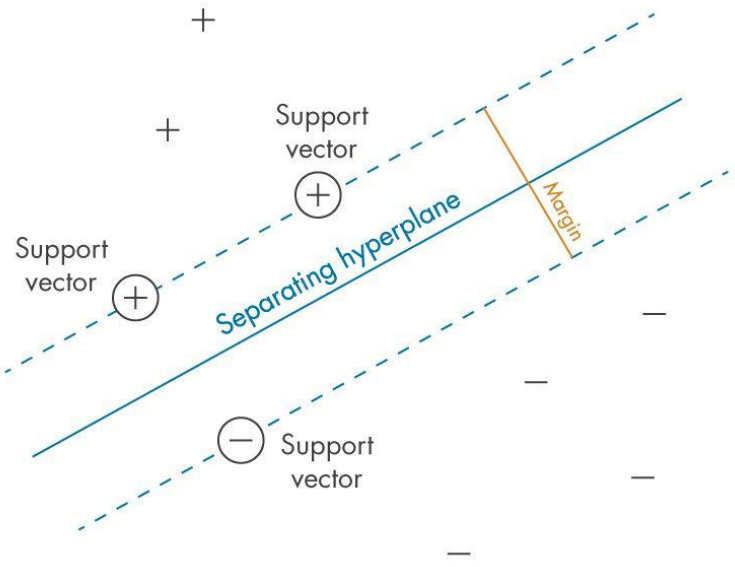

Fig 2.6 Defining the “Margin” Between Classes (Support Vector Machine (SVM) Explained. (n.d.)

Training a support vector machine involves addressing a quadratic optimization challenge to establish a hyperplane that fits snugly between classes while minimizing the soft margin. The quantity of transformed attributes aligns with the count of support vectors.

Table 2.3 Several Kernal Including in SVM

Type of Kernal	Mercer Kernal	Remarks
Gaussian or Radial Basis Function (RBF)	$K(x_1, x_2) = \exp\left(-\frac{\lvert x_1 - x_2\rvert^2}{2\sigma^2}\right)$	Single-class learning. The parameter σ signifies the kernel width.
Linear	$K(x_1, x_2) = x_1^T x_2$	Binary-class learning.
Polynomial	$K(x_1, x_2) = (x_1^T x_2 + 1)^\rho$	The parameter ρ represents the polynomial order.
Sigmoid	$K(x_1, x_2) = \tanh(\beta_0 x_1^T + \beta_1)$	This serves as a Mercer kernel solely for specific β0 and β1 values.

2.2.4 Random Forest

The Random Forest (RF) algorithm (Fig 2.7) falls within the category of supervised classification methods. RF relies on a collection of individual decision trees that collectively constitute a "Forest." The underlying concept of utilizing multiple decision trees (an ensemble) is to achieve a strong and resilient decision by amalgamating the outputs of many individual Decision Trees, as opposed to relying on a single one. Each decision tree in RF is self-learning, a process that involves automatically formulating rules at each node based on a training dataset containing known feature inputs and labels.

A strategy to determine the optimal partition, given a set of input features and training instances, is to minimize the heterogeneity (a mixture of classes) within the resulting subsets of data. The Gini impurity, originating from information theory's concept of entropy, is often employed as a measure of heterogeneity in decision tree learning. To identify the finest partition at each node, the Gini impurity index is computed for each potential data split, and the split that results in the least heterogeneity is chosen.

The term "Random" in Random Forest alludes to two significant layers of randomness within the learning process: First, RF employs a bootstrapped sample (random selection with replacement) of the original training dataset for the creation of each individual decision tree. Consequently, the training data for these trees typically differ from one another. While this may seem counterintuitive, it substantially decreases the correlation between trees and enhances the generalizability of predictions. The second element of randomness involves a random selection of features (e.g., spectral bands) considered at each tree node. As a result, the splits are determined based on varying features, aiding in reducing correlations between trees.

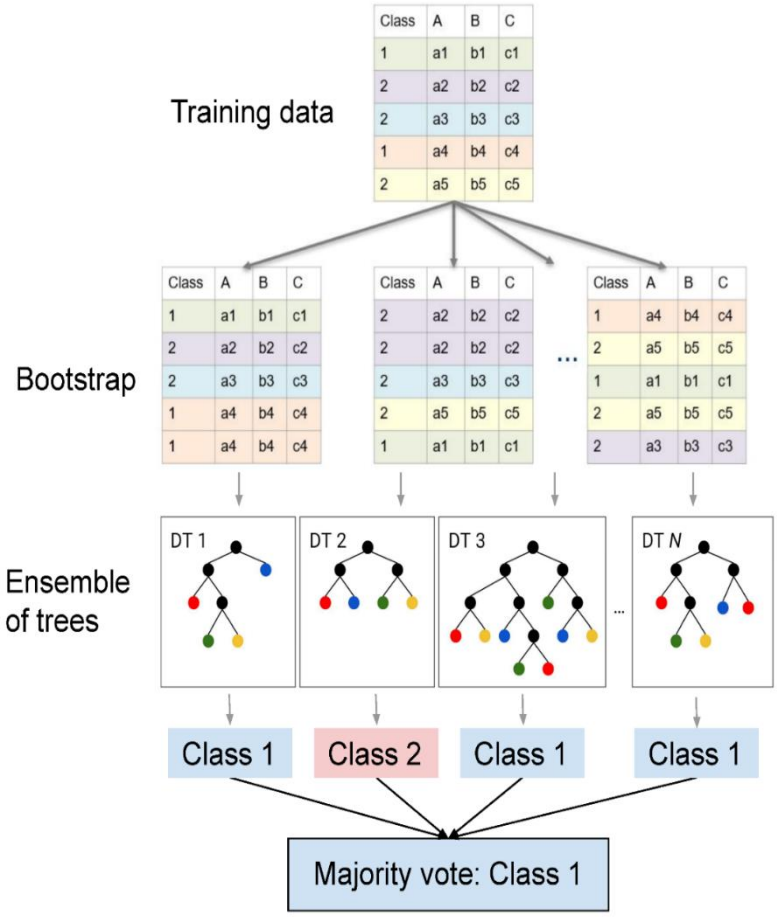

Fig 2.7 Schematic Structure of the RF Algorithm (Image classification - Random Forest. (n.d.).)

Multiple trees may generate diverse class labels for the same data point. The ultimate classification of each pixel in an image is determined by the majority consensus across all trees within the Random Forest ensemble.

2.2.5 Clustering

Clustering is a data analysis technique in which a set of objects or data points is grouped together based on their similarity or proximity to each other. Clustering seeks to discover underlying structures, connections, or trends in a collection without revealing these groups beforehand. It is a form of unsupervised learning where the algorithm autonomously discovers the clusters or groups within the data.

When data is clustered, it becomes clear that points within an identical cluster share more similarities than differences. The similarity between data points is typically defined using a distance or similarity metric, such as Euclidean distance or cosine similarity. By minimising intra-cluster distances and maximising inter-cluster distances, algorithms for clustering strive to optimise the organisation of points of data into the clusters.

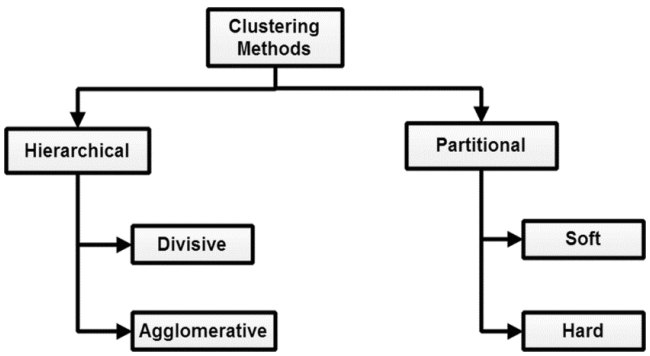

Fig 2.8 Classification of Clustering Based Image Segmentation Methods (Mittal et al., 2021)

Literature encompasses several clustering techniques designed for image segmentation. Nevertheless, a cluster lacks a specific definition, and several clustering

approaches have devised their own methodologies to categorise the data. Consequently, clustering approaches can be roughly categorised into two main groups based on the generation of clusters: hierarchical and partitional (Mittal et al., 2021). Figure 2.8 presents a taxonomy of the clustering approaches. The subsequent section delineates each classification of clustering in relation to picture segmentation.

- **Hierarchical clustering:** Data is grouped via a hierarchy of clustering based on their degree of similarity, as seen by a dendrogram, which is a structure that resembles a tree. Two main methods describe the procedure: divisive and agglomerative (Saxena et al., 2017).
- **Partitional Clustering:** Partitional clustering, notably favoured for larger datasets due to computational efficiency (Bouguettaya et al., 2015), utilizes similarity as a metric. It arranges data into clusters guided by an objective function, aiming for higher similarity within clusters. This involves comparing each data point's similarity with all clusters. The objective function generally aims to minimize within-cluster similarity, often employing Euclidean distance. It assesses cluster quality, yielding the best representation. Like hierarchical clustering, the number of clusters is predetermined. Partitional methods ensure data assignment, even if a data point is distant from the cluster centroid, potentially causing shape distortions or erroneous outcomes, particularly with noise or outliers.
- **Soft Clustering Methods:** Soft clustering assigns data to multiple clusters iteratively, with varying degrees of membership, portraying data association more reasonably. The degree of membership ranges from 0 to 1, based on an objective function, often minimizing the sum of squared Euclidean distances.
- **Hard Clustering Methods:** Hard clustering methodically separates data into distinct clusters based on an objective function. It assigns data solely to a single cluster, with a degree of membership as either 0 or 1. This approach is straightforward, computationally efficient, suitable for spherical, well-separated datasets, but suffers from drawbacks like suboptimal centroid

descriptions, sensitivity to initial parameters, and requiring prior knowledge of cluster count.

2.3 Limitation of Conventional Methods

Complexity of Tumor Patterns: Conventional methods struggle to accurately handle intricate tumor patterns, often leading to under-segmentation or over-segmentation due to limited ability to capture complex variations.

- **Manual Intervention:** Many conventional techniques require manual intervention, such as seed point selection or initial boundary delineation.
- **Limited Adaptability:** Traditional methods often lack adaptability to different tumor types, sizes, and locations, making them less effective in dealing with the diverse characteristics of brain tumors.
- **Dependency on Feature Engineering:** Conventional methods heavily rely on hand-crafted characteristics, which may not fully detention the rich information present in complex medical images, leading to suboptimal performance.
- **Inability to Handle Noise and Variability:** Brain images are inherently noisy and can vary significantly due to factors like imaging protocols and patient variability. Conventional techniques may struggle to cope with such noise and variability.
- **Limited Integration of Prior Knowledge:** Traditional methods might not effectively incorporate prior knowledge about brain anatomy, tissue properties, or tumor behavior, which could aid in improving segmentation accuracy.
- **Scalability:** Conventional techniques may face challenges in handling large-scale datasets efficiently, impacting both processing time and computational resources.
- **Difficulty with Non-linear Relationships:** Many brain tumor characteristics exhibit non-linear relationships, which conventional methods may not capture

well, resulting in suboptimal segmentation in regions with complex boundaries.

- **Lack of Robustness to Image Artifacts:** Conventional algorithms might be sensitive to artifacts introduced during image acquisition, leading to inaccurate segmentation results.
- **Challenging for Multi-modal Data:** Traditional methods struggle to effectively utilize multi-modal information from different imaging techniques, missing out on potentially valuable data for improved segmentation.
- **Generalization to New Data:** Conventional methods might not generalize well to unseen data or new datasets, limiting their applicability and requiring re-tuning or re-training for each specific scenario.
- **Inefficiency in Handling Large-Scale Data:** For datasets with a large number of images or high-resolution scans, conventional techniques may become computationally inefficient and impractical.

Overall, while traditional methods have paved the way for brain tumor analysis, their limitations highlight the need for more advanced and data-driven approaches.

2.4 Deep Neural Network

2.4.1 DNN Evolution

The evolution of deep neural networks has been marked by significant breakthroughs and innovations, fuelled by advancements in algorithms, hardware, and data availability. From the early days of single-layer perceptron’s to the current era of sophisticated architectures, deep learning continues to revolutionize various fields and shape. In the realm of medical image analysis, a frequent task is semantic segmentation, such as delineating organs or identifying lesions. The Convolutional Neural Network, a specialized form of Deep Neural Network architecture, rose to prominence around 1990 with LeNet's architectural design (Chavent et al., 2007). LeNet introduced a two-layer CNN architecture. Subsequently, about fifteen years later, the introduction of AlexNet (Kaya & Bilge, 2019) marked a significant

advancement, comprising five convolutional layers. The widespread availability of fast GPUs and improved computing resources contributed to the emergence of AlexNet and its subsequent impact. The Evolution of Deep Neural Networks (Kaya & Bilge, 2019):

- **Single-Layer Perceptrons (1950s-1960s):** The initial phase of neural network development saw the emergence of single-layer perceptrons, inspired by the functioning of biological neurons. However, their limitations in handling complex patterns and their restriction to linear separations hindered their practical applications.
- **Multilayer Perceptrons (1970s-1980s):** The introduction of the backpropagation algorithm in the 1970s marked a significant milestone. This breakthrough enabled the training of multilayer perceptrons (MLPs) with multiple interconnected layers. These networks could learn intricate features and patterns through the layers, paving the way for more complex tasks.
- **Limited Progress (1990s-2000s):** Despite early progress, neural networks faced challenges like vanishing gradients and computational constraints, leading to reduced interest and research during this period.
- **Rise of Convolutional Neural Networks (CNNs) (2010s):** The landscape shifted dramatically with the ascent of CNNs, particularly highlighted by the success of AlexNet in 2012. These networks demonstrated the potential of deep architectures by using convolutional layers to learn hierarchical features from raw data.
- **Advancements in Architectures (2010s):** Research into other designs grew in the wake of CNNs' success. These included RNNs for data that is sequential, LSTM networks that were optimised for better memory retention, and attention techniques for better feature extraction.
- **Deep Learning Revolution (2010s):** The synergy of ample datasets, powerful GPUs, and refined optimization techniques initiated a deep learning revolution. Neural networks achieved groundbreaking results in various

domains like speech recognition, natural language processing, image analysis, and autonomous systems.

- **Transfer Learning and Pre-trained Models (2010s):** pre-trained models like BERT and GPT leveraged vast data and transformed the landscape of transfer learning. Fine-tuning these models for specific tasks with limited data proved to be a game-changer.
- **Attention Mechanisms and Transformers (2010s):** Attention mechanisms, epitomized by the Transformer architecture, brought significant progress to language understanding, image captioning, and more. They enabled networks to focus on relevant information for improved performance.
- **Hybrid Approaches and Beyond (2020s):** Recent trends include hybrid models combining neural networks with symbolic reasoning and knowledge representation. Efforts are directed towards enhancing efficiency, interpretability, and robustness of deep learning models.

2.4.2 CNN for Deep Neural Network

Within the tapestry of artificial intelligence, convolutional neural networks emerge as intricate systems anchored in multi-layered neural networks, showcasing prowess in tasks ranging from object identification and recognition to classification, image object detection, and segmentation. ConvNets, a colloquial term for CNNs, stand as a prevalent framework in the deep learning landscape, excelling in discrimination tasks. A notable feature is their ability to autonomously glean insights from input data, eliminating the necessity for manual feature extraction (Thakur et al., 2019; Song et al., 2017).

2.4.2.1 CNN Fundamental

Acquiring a deep comprehension of the diverse elements comprising CNN components and their practical uses is crucial for unveiling the progressions in CNN architecture. In essence, a CNN comprises four discernible types of layers.

- Convolutional
- Pooling
- Function of Activation
- Fully Connected

(i). Convolutional Layer: The pivotal convolutional layer stands as a linchpin in the holistic architecture of a CNN. Comprising a suite of filters, often denoted as kernels, this layer orchestrates the processing of input data. These kernels, characterized by dimensions such as width, height, and weight, act as discerning agents, extracting unique features from the input data. Initially, the kernel weights embark on their journey with random assignments, gradually evolving as they glean more precise insights from the training data. Each numerical entry corresponds to a specific kernel weight reference, a starting point chosen through random selection and refined through various initialization procedures. This dynamic evolution of weights during training empowers the kernel to adeptly capture significant traits.

Operating within a high-dimensional, implicit feature space, the kernel performs computations without explicitly navigating data coordinates within that realm. It calculates the inner product of image representations across the myriad combinations of data pairs in the feature space. CNNs distinguish themselves from their conventional neural counterparts by their prowess in processing multi-channeled images, transcending the confines of vectorized data accepted by traditional neural networks. While RGB images boast three color channels, grayscale counterparts gracefully navigate with just a singular channel.

To demonstrate the application of convolutions, we will examine a grayscale image measuring 4 × 4 pixels. This image will be combined with a 2 x 2 kernel that has been initialised with random weights. This kernel does both

horizontal and vertical traversal throughout the full image. Simultaneously computing the dot product involves the synchronous multiplication of corresponding values from the input image and kernel, culminating in the summation of these products to yield a singular scalar value. This process continues in an iterative manner until it is no longer possible to slide any further (Thakur et al., 2019; Song et al., 2017).

The primary image denoted as (K) and the filter represented as (L).
The resulting matrix is derived using the formula

$$(K - L + 1) \qquad [2.15]$$

When applying the calculation (4-2+1), the outcome becomes 3, leading to a resulting matrix size of 3 x 3.

Indeed, the dot product values serve as indicators of the resulting feature map. Figure 3 visually illustrates the fundamental computations executed during each step. Within this diagram, the compact square (2 x 2) signifies the kernel, while the larger square (4 x 4) symbolizes the input image. Consequently, a numerical value emerges from the multiplication of both elements (Thakur et. al. 2019, Song et. al., 2017).

Nevertheless, in the prior instance, the kernel's stride is set at 1, while the input image remains unpadded. It's worth noting that you have the liberty to replace the stride value with an alternative if desired. Furthermore, elevating the stride value brings the added advantage of reducing the dimensionality of the resultant feature map. (Thakur et. al. 2019, Song et. al., 2017).

The dimensions of the provided image's border are significantly impacted by padding. Conversely, the characteristics of the border side undergo substantial alterations during this process. Padding results in an enlargement of the input

image, consequently leading to an increased size of the feature map. Each filter within the setup can represent a distinct feature. When a filter traverses an image without encountering a match, it remains inactive. CNN employs this strategy to identify the most efficient filters for describing objects. Fig 2.9 represents the primary calculation of convolutional layer.

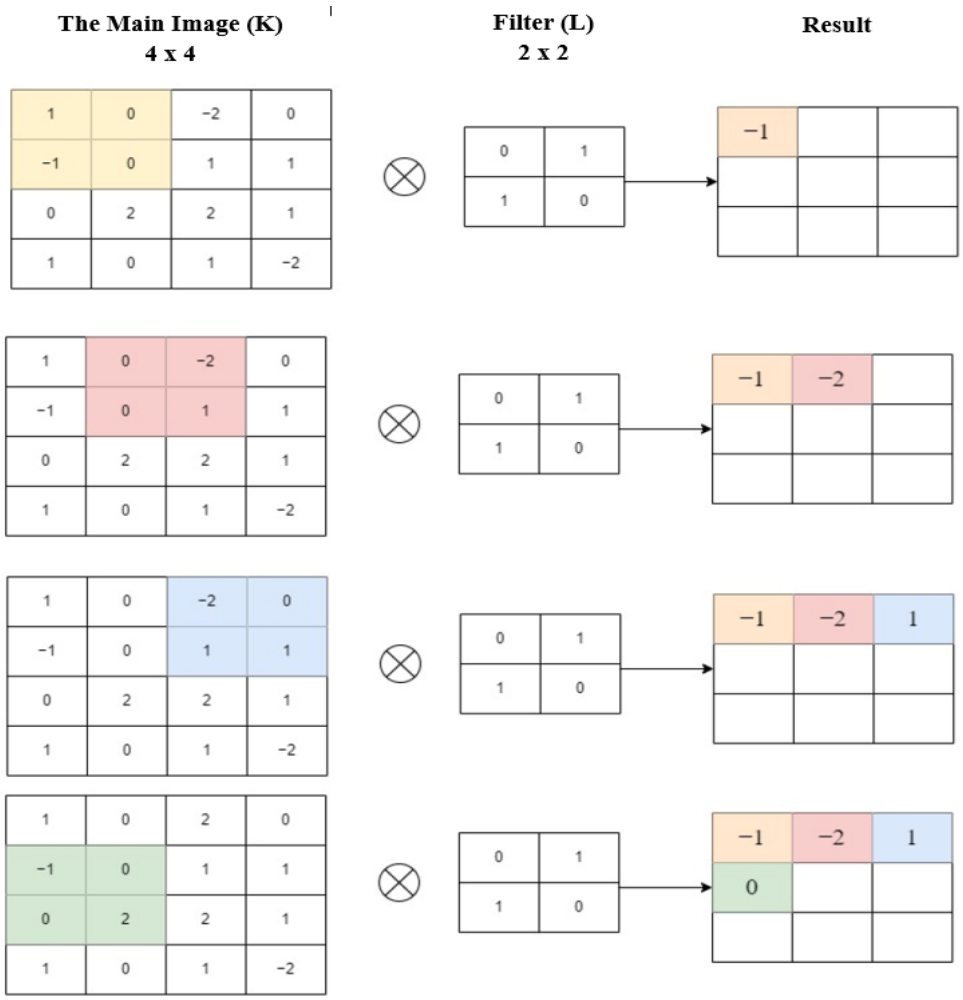

Fig 2.9 Primary Calculation of Convolutional Layer (Taye, 2023)

- **Weight Sharing:** Convolutional Neural Networks are a subset of deep learning architectures that are built to handle and analyse input that is grid-like, like photographs. One of its basic concepts is weight sharing.

In CNNs, weight sharing refers to the practice of using the same set of learnable parameters (weights) for multiple units within a specific layer of the network. Weight sharing helps CNNs capture local patterns and features present in various parts of the input, allowing them to learn hierarchical representations of increasing complexity. This concept has been crucial in the success of CNNs in tasks as it enables networks to efficiently learn and recognize features while leveraging spatial information effectively.

- **Stride:** The CNN stride is a parameter in Convolutional Neural Networks (CNNs) that specifies the distance at which a filter or kernel moves across the input data during the convolution operation. In the framework of Convolutional Neural Networks, the convolution process comprises methodically dragging a filter throughout the input information from an image like this, to obtain unique characteristics. The stride determines the amount of horizontal and vertical movement of the filter throughout the convolution process on the input.

  The term "stride" refers to the number of rows and columns covered with each sliding step. Thus far, we have consistently utilised a stride value of 1 for both the vertical and horizontal dimensions. Nevertheless, there are situations in which choosing a longer stride could be advantageous. A 2-dimensional cross-correlation process is illustrated in Figure 2.10 of the study. This process has a vertical stride of three and a horizontal stride of two. The shaded portions in the figure represent the output elements that are obtained as a result. These elements are computed using the input and kernel tensor components, taking into account the concepts of padding and stride. This information is sourced from the documentation titled "Padding and Stride — Dive into Deep Learning 1.0.3".

$$0 \times 0 + 0 \times 1 + 1 \times 2 + 2 \times 3 = 8$$

$$0 \times 0 + 6 \times 1 + 0 \times 2 + 0 \times 3 = 6$$

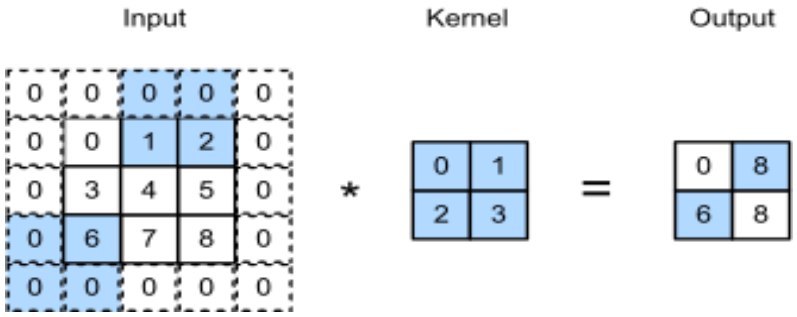

Fig 2.10 Cross-correlation is performed using vertical strides of 3 and horizontal strides of 2.[Padding and Stride — Dive into Deep Learning 1.0.3 documentation. (n.d.).]

The convolution window obviously descends three rows to accommodate the additional element in the primary column. The convolution window also moves a pair of columns to the right horizontally after producing the additional portion of the first row. In the subsequent steps, the input component is insufficient to fill the convergence window, therefore no output is generated when the window travels two columns to the correct position over the input. This constraint remains in effect unless an extra column of padding is added:

In a broader context, when the vertical stride is represented as s_h and the horizontal stride as s_w the resultant shape of the output is determined [Padding and Stride — Dive into Deep Learning 1.0.3 documentation. (n.d.).].

$$\lfloor (n_h - k_h + p_h + s_h)/s_h \rfloor \times \lfloor (n_w - k_w + p_w + s_w)/s_w \rfloor \quad [2.16]$$

- **Padding:** When implementing convolutional layers, a challenging aspect arises related to the potential loss of pixels along the image's

edges. Figure 2.11 shows the pixel use in relation to the size and location of the convolution kernel, which illustrates this problem. It should be noted that pixels located in the corners are not used very often.

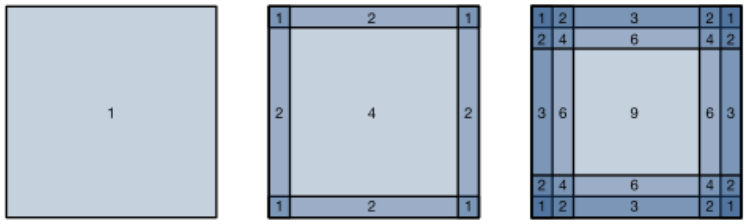

Fig 2.11 Utilization of pixels for convolutions with dimensions of 1 x 1, 2 x 2, and 3 x 3, respectively. [Padding and Stride — Dive into Deep Learning 1.0.3 documentation. (n.d.).]

Each convolution may only cause a little number of pixels to be lost because we frequently employ small kernels. However, this accumulation becomes meaningful as we employ numerous successive convolutional layers. An uncomplicated resolution to this problem entails augmenting the dimensions of the input image by incorporating supplementary pixels along its boundaries. Usually, these additional pixels are given a value of zero. Figure 2.12 demonstrates the addition of padding to a 3 x 3 input, which leads to an increased size of 5 x 5. As a result, the output is represented by a matrix with dimensions of 4 x 4. The input and kernel tensor components utilised to compute the output, together with the starting output element, are indicated by the shaded regions.

$$0 \times 0 + 0 \times 1 + 0 \times 2 + 0 \times 3 = 0$$

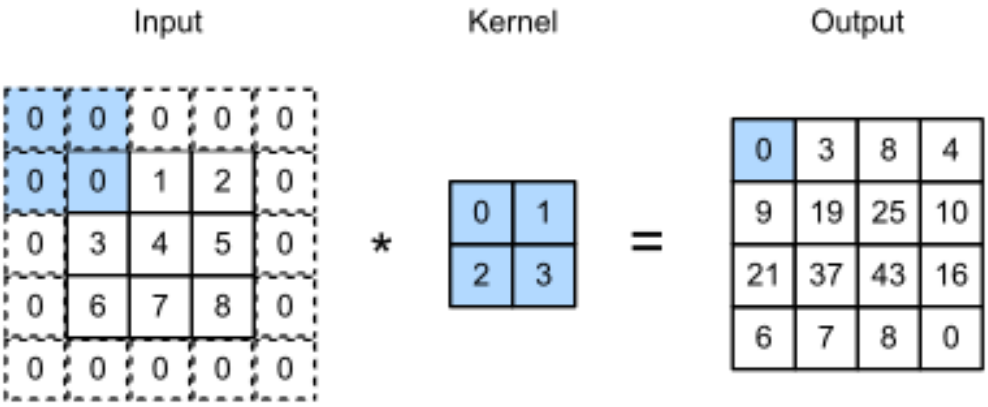

Fig 2.12 Two-dimensional cross-correlation with padding (Padding and Stride — Dive into Deep Learning 1.0.3 documentation. (n.d.)

In a general context, when we incorporate p_h rows of padding (approximately equally distributed between the top and bottom) along with p_w columns of padding (approximately equally distributed between the left and right), the resulting output shape will be:

$$(n_h - k_h + p_h + 1) \times (n_w - k_w + p_w + 1) \qquad [2.17]$$

Because of this, the output's height will grow by p_h and its width by p_w.

(ii). Pooling: For Convolutional Neural Networks, pooling—also called subsampling processes or down sampling—is an essential procedure for reducing the spatial dimensions of maps of features while keeping important information. The process entails dividing the input feature map into distinct or overlapping sections and subsequently consolidating the data within each section into a singular value (Taye, 2023).

The max pooling method is the most popular, and it works by taking the largest value from each region and using it as the output. The average pooling

is another kind; it averages the data in the area. Pooling helps achieve several benefits:

- **Dimensionality Reduction:** Pooling makes the network more efficient and less susceptible to overfitting by lowering the number of parameters and calculations by reducing the spatial dimensions of the feature maps.
- **Translation Invariance:** The network's pattern recognition capabilities can be improved by pooling, since it becomes less affected by little changes in the input data, such as translations or shifts.
- **Feature Hierarchy:** Pooling progressively reduces the spatial dimensions, allowing the network to capture high-level abstract features in deeper layers.

Pooling is usually applied independently to each channel or feature map, allowing CNNs to learn and detect patterns at multiple scales. It is typically performed after convolutional layers and activation functions, resulting in a smaller set of feature maps with reduced spatial dimensions. However, it's important to note that pooling can cause some loss of spatial information, which might not be desirable in certain tasks where precise spatial relationships matter, like segmentation.

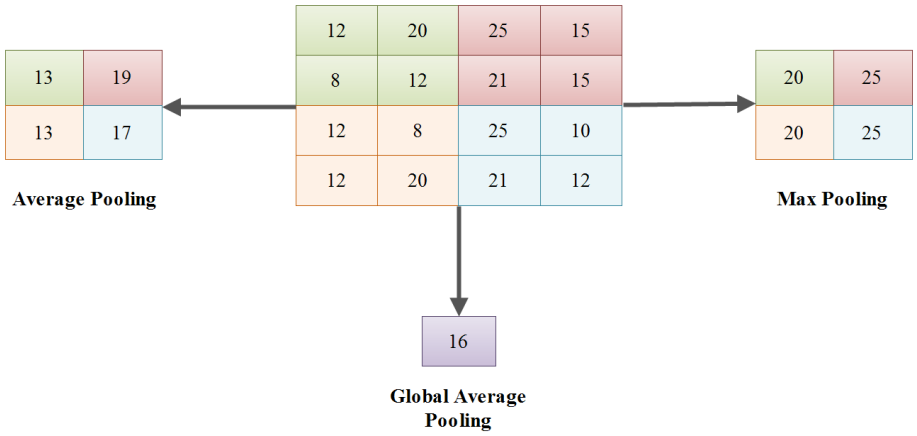

Fig 2.13 Pooling Layer (Taye, 2023)

As illustrated in Fig 2.13, upon applying pooling to the two-by-two blocks positioned in the upper-left corner, the emphasis transitions to the upper-right corner, resulting in a displacement of two steps. This leads to the utilization of a stride of 2 for pooling. Alternatively, a less common stride of 1 can be used to prevent down sampling. There are a number of different pooling levels that may be used. Among these techniques are gated pooling, global maximum pooling (GMP), average pooling, min pooling, and global average pooling (GAP). Figure 8 displays each of these methods. Pooling layers can't help convolutional neural networks (CNNs) determine whether a feature is present in an input picture, which is its main drawback; it mainly helps identify the feature's location [Alzubaidi et al., 2021, Du & Swamy, 2019]. Consequently, there are instances where the overall performance of the CNN model might suffer a decline. Nonetheless, such instances lead to the omission of essential information by the CNN model.

(iii). Function of Activation: An essential part of every Convolutional Neural Network (CNN) is the activation function, which makes the network's computations non-linear. In Convolutional Neural Networks (CNNs), every neuron inside a layer calculates a weighted sum of its input values, which is subsequently processed by the activation function. Activation functions process the aggregated input to a neuron and determine whether the neuron should be activated or not. A neuron activates and sends its output to the next layer when its function of activation output surpasses a certain threshold.

Different activation functions offer varying degrees of complexity and behaviour, influencing how the network learns and converges during training.

- **Rectified Linear Unit (ReLU):** A function of activation commonly used by CNNs and other neural networks is the Rectified Linear Unit. Its ability to introduce non-linearity to the calculations of the network

is well-known, and it is also noted for being simple, making it a fundamental building block of deep learning architectures. Fig 2.14 represent ReLU Activation Function.

The ReLU activation function operates as follows:

For any given input x:

- The output is x if and only if x is non-zero.
- The result is 0 if x is a negative integer.

Mathematically, the ReLU function can be represented as:

$$f(x) = max(0, x) \qquad [2.18]$$

Here, Considering an input x, the outcome of the ReLU algorithm is denoted as f(x).

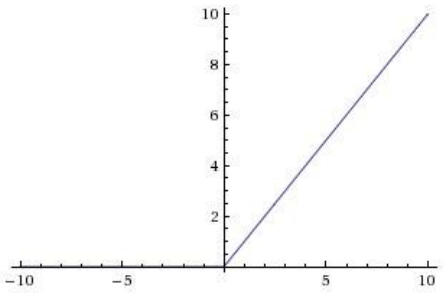

Fig 2.14 Graphically representation of ReLU Activation Function

- **Sigmoid:** Neural networks and artificial intelligence models often use the sigmoid function, often called the logistic function, which serves as a function of activation. It may compress the outcome into a range of 0 to 1 and introduce non-linearity into calculations, which is its main function. Because of this quality, it may be used effectively in functions of activation and for binary tasks such as classification. Fig 2.15 represents the Sigmoid Activation Function.

The sigmoid function operates as follows:

Given an input x, the sigmoid function computes the output y using the following formula:

$$y = \frac{1}{1 + e^{-x}} \quad [2.19]$$

The input value x is used in conjunction with the base of the natural logarithm, denoted as e. For each given input value, the sigmoid function returns a value between zero and one.

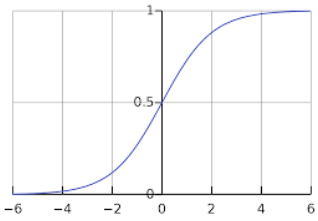

Fig 2.15 Graphically representation of Sigmoid Activation Function

- **Hyperbolic Tangent (tanh):** One activation function utilised in neural networks and ML models is the tangent hyperbolic operate or tanh function. It shares similarities with the sigmoid function but has an output range between -1 and 1, making it suitable for a wider range of tasks that require both positive and negative values. Fig 2.16 represents of Hyperbolic Tangent Activation Function

  The tanh function operates as follows:

  Given an input x, the tanh function computes the output y using the following formula:

$$y = \frac{e^{x} - e^{-x}}{e^{x} + e^{-x}} \quad [2.20]$$

  Here, e represents the base of the natural logarithm.

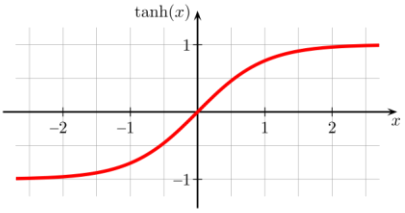

Fig 2.16 Graphically representation of Hyperbolic Tangent Activation Function

(iv). Fully Connected Layer: An integral part of neural networks, including CNN and other deep learning architectures, is a Fully Connected Layer, often called a dense layer. To make definitive recommendations or classifications, the previously described layer is crucial for collecting complex data relationships.

A totally Connected Layer is characterised by the fact that each neuron is related to every single neuron in the preceding layer, which is why it is referred to as "fully connected." The weight of each connection is linked to it, and the outcome of each neuron is evaluated by adding all the weighted inputs from the preceding layer and applying an activation function.

The process within a Fully Connected Layer (Fig 2.17) involves the following steps:

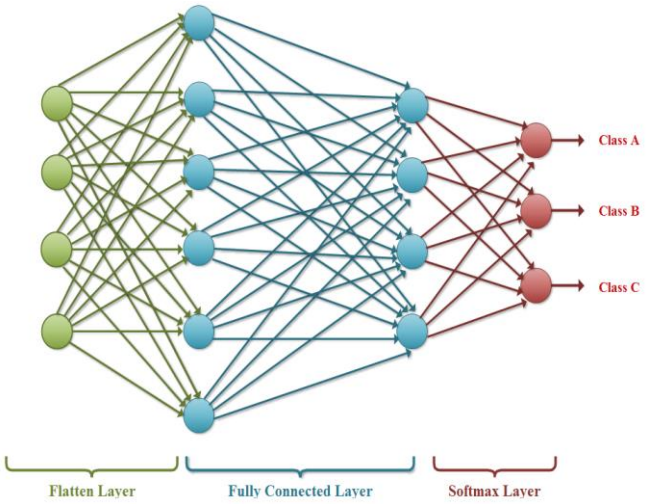

Fig 2.17 Fully Connected Layer

(i). The inputs from the previous layer are multiplied by their corresponding weights and then added together in a weighted sum.

(ii). The weighted sum is then adjusted by adding a bias term. Important to the model's performance is the bias term's ability to change the activation function.

(iii). By feeding the final tally into an activation function, we may make the model non-linear. Rectified Linear Unit, the sigmoid operation, and hyperbolic tangent are three famous functions for activation.

(iv). A neuron's output in the Fully Connected Layer feeds into the next layer's input, and so on.

At the very end of most neural network topologies you'll see Fully Connected Layers, where all of the collected properties are combined to make final predictions. As an example, in picture categorization tasks, the convolutional and pooling layers first extract useful characteristics from the image, which are subsequently flattened and used by a Fully Connected Layer to forecast the input image's class.

The main limitation of a fully connected layer is the extensive set of parameters, which requires intensive computations during training on data samples. Hence, there's an effort to reduce the count of connections and nodes.

2.4.2.2 Comparison of Common CNN Architecture

Deep learning proves its potency through the utilization of Artificial Neural Networks (ANNs) featuring an extensive array of processing layers, surpassing conventional Neural Network methodologies (Zhang et al., 2019). Among the premier selections in deep learning, Convolutional Neural Networks (CNNs) stand out. This technique adeptly assimilates significant features from unprocessed data. Within this architecture, the extraction of image attributes, encompassing color and texture intricacies, is undertaken to discern and categorize images effectively. LeNet, one of

the early CNNs, has a relatively simple structure and is primarily suitable for handwritten digit recognition. On the other hand, AlexNet introduced deeper architectures with multiple convolutional layers, making it adept at handling more complex tasks like image classification (Du & Swamy, 2019).

VGG16 and VGG19, while even deeper than AlexNet, stand out due to their uniformity in layer architecture, using only 3x3 convolutional filters. This consistent structure simplifies network design and optimization, but comes at the cost of increased computational requirements (Simonyan et. al. 2014).

GoogLeNet (Inception) innovatively employs inception modules, featuring multiple filter sizes within a single layer. This architecture facilitates the capture of multi-scale features, but its complexity can lead to computation challenges (Szegedy et al., 2015).

ResNet's groundbreaking residual connections enable training of extremely deep networks without degradation in performance. This architecture's skip connections aid gradient flow, preventing the vanishing gradient problem (Zagoruyko et. al., 2016). DenseNet introduces dense connectivity, connecting every layer to every other layer in a feedforward fashion. This design promotes feature reuse and enhances gradient flow, making it efficient for training (Huang et al., 2017).

Table 2.4 Comparison of Common CNN Architecture

Ref No	Architecture	Year	Layer	Parameter	Highlights
El-Sawy et al., 2016	LeNet	1998	3 Convolutional Layer + 2 Subsampling Layer + 2 Fully Connected Layer	60 k Parameters	Key highlights include: • Early CNN: One of the first successful CNNs for image analysis. • Handwritten Digits: Achieved high accuracy in handwritten digit recognition, setting the stage

Ref No	Architecture	Year	Layer	Parameter	Highlights
					for modern image classification. • Hierarchical Features: Introduced the concept of hierarchical feature learning through convolutional layers. • Inspiration: Inspired subsequent deep learning advancements and remains historically significant in AI and computer vision
Krizhevsky et al., 2017	AlexNet	2012	5 Convolutional + 3 Fully Connected Layer	62.3 million	Key highlights include: • Deep CNN: One of the first deep CNN architectures with eight layers, effectively addressing image classification tasks. • ReLU Activation: Originally the use of the activation of the ReLU function, greatly improved training speed. • Dropout Regularization: Introduced dropout regularization to mitigate overfitting, improving generalization. • GPU Acceleration: Utilized GPU acceleration for faster training, making deep learning practical at scale.

Ref No	Architecture	Year	Layer	Parameter	Highlights
					• Deep Learning Renaissance: Marked the beginning of a deep learning renaissance, leading to a surge in research and applications in computer vision and beyond.
Shi et al., 2020	ZFNet	2013	5 Convolutional + 1 Max-Pooling Layers + 1 Fully Connected Layer + 1 Output Layer	60 million	Key highlights include: • Improved ImageNet Performance: Demonstrating the promise of deep learning for picture categorization jobs, ZFNet performed well in the ImageNet Large Scale Visual Identification Challenge. • Visualization Techniques: Introduced visualization techniques to better understand neural network activations and feature hierarchies. • Architectural Evolution: Served as an architectural evolution between earlier CNNs like AlexNet and later networks like VGGNet. • Convolutional Visualization: Zeiler and Fergus demonstrated the importance of convolutional visualization techniques to interpret and improve deep

Ref No	Architecture	Year	Layer	Parameter	Highlights
					neural network performance.
Simonyan et. al. 2014	VGGNet	2014	13 or 16 Convolutional Layer + 3 Fully Connected Layer	138 million	Key highlights include: • Deep Architecture: VGGNet is characterized by its deep architecture, featuring 16 or 19 weight layers (16-layer and 19-layer versions), which increased model depth for improved feature learning. • Consistency in Convolution: It maintained a consistent 3x3 convolutional filter size throughout the network, emphasizing smaller filter sizes as building blocks. • Simplicity and Elegance: Known for its simplicity and elegance in design, VGGNet's uniform architecture made it easier to understand and replicate. • Impact on Deep Learning: VGGNet's design principles influenced subsequent CNN architectures, serving as a benchmark for deep learning model design.
Szegedy et al., 2015	GoogLeNet	2014	22 Convolutional Layer + 9 Pooling Layer	4 million	Key highlights include: • Inception Module: Presented the Inception module, a new

Ref No	Architecture	Year	Layer	Parameter	Highlights
					idea in architecture that enables the network to efficiently collect characteristics at many scales by using several filter sizes (1x1, 3x3, 5x5) within a single layer. • GoogLeNet's Architectural Depth: GoogLeNet utilized a deep network with 22 layers but fewer parameters than other deep networks of the time, making it more computationally efficient. • Reduction in Dimensionality: Employed dimensionality reduction techniques, such as 1x1 convolutions, to reduce the computational cost of convolutional layers. • Impact on CNN Design: Inspired the development of efficient and scalable CNN architectures, emphasizing both performance and computational efficiency. • Advancements in Deep Learning: GoogleNet contributed to the broader adoption of deep learning and the exploration of model architectures beyond

Ref No	Architecture	Year	Layer	Parameter	Highlights
					traditional designs.
Szegedy et al., 2016	Inception V3	2015	48 Layer in Deep	25 million	Key highlights include: • GoogLeNet's Successor: Building upon the success of the original GoogLeNet (Inception V1), Inception V3 improved both performance and computational efficiency. • Factorization: Introduced factorization into the Inception module, splitting 5x5 convolutions into two 3x3 convolutions, which enhanced learning while reducing parameters. • Batch Normalization: Incorporated batch normalization, improving convergence speed and overall network stability during training. • Fine-Grained Feature Extraction: Enabled fine-grained feature extraction, making it suitable for tasks that require detailed feature analysis. • Transfer Learning: Facilitated transfer learning and fine-tuning, making it a popular choice for reusing

Ref No	Architecture	Year	Layer	Parameter	Highlights
					pretrained models on various datasets. • Impact on Computer Vision: Inception V3 contributed to advancements in computer vision by pushing the boundaries of model accuracy while maintaining computational efficiency.
Shafiq & Gu, 2022	ResNet	2015	50-layer CNN in ResNet-50	23 million	Notable points comprise: • Innovative Deep Architecture: ResNet models can include hundreds of layers, making it famous for its great depth. Training extremely deep neural networks was proven to be feasible. • Residual Blocks or Skip Connections: These were introduced to make gradient flow easier during training. As a result, deep network training is possible and the vanishing gradient problem is reduced • ResNet enhanced accuracy with fewer parameters compared to shallower networks, despite its depth. This is due to parameter efficiency. • The usage of ResNet models

Ref No	Architecture	Year	Layer	Parameter	Highlights
					that have been pretrained on big datasets for transfer learning has grown in recent years. • Converging Use: ResNet-50 and ResNet-101, two of ResNet's architectures, are now de facto options for many computer vision jobs.
Iandola et al., 2016	Squeeze Net	2016	18 Layer in deep	50 times fewer parameter then AlexNet	Key highlights include: • Fire Module: Introduces the "fire module," a unique building block that combines convolutional layers with both 1x1 and 3x3 filters to maximize feature extraction while minimizing computational cost. • Efficiency: Demonstrates remarkable computational efficiency by reducing model size and computational requirements without sacrificing performance. • Transfer Learning: SqueezeNet models pretrained on large datasets are valuable for transfer learning across various applications.
Szegedy	Inception	2017	The exact	43 million	Key highlights include:

Ref No	Architecture	Year	Layer	Parameter	Highlights
et al., 2017	V4		number of layers in Inception-v4 depending on the specific implementation and variations, but it typically consists of hundreds of layers.		• Architecture Evolution: Inception V4 builds upon the success of earlier Inception models, refining architectural components for improved accuracy. • Stem Block: Introduced a novel stem block at the network's entrance to enhance feature extraction from input images. • Inception Blocks: Employed carefully designed Inception blocks, including various convolutional filter sizes and efficient factorization techniques. • Scalability: Achieved scalability by using multiple versions of Inception modules with varying depths, allowing users to choose the trade-off between model size and performance. • Reduction Blocks: Included reduction blocks to reduce spatial dimensions and computational cost. • Transfer Learning: Pretrained Inception V4 models are commonly used for transfer learning in

Ref No	Architecture	Year	Layer	Parameter	Highlights
					various image-related tasks.
Huang et al., 2017	DenseNet	2017	DenseNet-121 has 121 layers. DenseNet-169 has 169 layers. DenseNet-201 has 201 layers. DenseNet-264 has 264 layers.	DenseNet-201 (20 million)	Key highlights include: . • Parameter Efficiency: Achieves high accuracy with fewer parameters compared to traditional deep networks, thanks to feature reuse and skip connections. • Gradient Flow: Addresses the vanishing gradient problem by enabling gradient information to flow directly through the network, making training deep networks easier. • Bottleneck Layers: Reduces the network's parameter count without sacrificing expressive capability by using bottleneck layers, which are 1x1 convolutions. • Impact on Deep Learning: Inspired further research into densely connected networks and influenced the design of subsequent CNN architectures.
Howard et. al., 2017	MobileNets	2017	27 CNN Layer	13 million	Key highlights include: • Efficiency: MobileNet models are specifically designed to be

Ref No	Architecture	Year	Layer	Parameter	Highlights
					computationally efficient and lightweight, making them suitable for deployment on resource-constrained devices. • Parameter Efficiency: Achieves a balance between model size and accuracy, making it suitable for scenarios with limited computational resources. • Transfer Learning: Pretrained MobileNet models are commonly used for transfer learning and fine-tuning in mobile and edge device applications. • Model Compression: MobileNet's design principles have influenced research on model compression and efficient neural network architectures.
Chollet, 2017	Xception	2017	71 Layers in Deep	22.8 million	Key highlights include: • Extreme Depth and Efficiency: Xception achieves both high accuracy and computational efficiency by utilizing an extremely deep architecture while reducing computational complexity.

Ref No	Architecture	Year	Layer	Parameter	Highlights
					• Transfer Learning: Pretrained Xception models have been widely used for transfer learning in various computer vision applications. • Compact Architecture: Despite its depth, Xception maintains a relatively compact architecture, which makes it suitable for real-time and embedded applications. • Inception Influence: Xception is influenced by the Inception architecture, refining its ideas and pushing the boundaries of efficiency.
Tan et. al., 2019	Efficient Net	2019	342 Layer	11 million	Key highlights include: • Efficiency-Accuracy Trade-off: Offers a range of models (e.g., B0, B1, B2, ..., B7) with varying depths and computational requirements, allowing users to choose the model that suits their specific computational constraints and accuracy needs. • State-of-the-Art Performance: EfficientNet models consistently achieve

Ref No	Architecture	Year	Layer	Parameter	Highlights
					top performance in various computer vision tasks, including image classification and object detection, on benchmark datasets like ImageNet. • Transfer Learning: Pretrained EfficientNet models have become popular for transfer learning, enabling rapid development of computer vision applications with limited data. • Architectural Advancements: EfficientNet incorporates architectural innovations, including a novel compound scaling rule and efficient building blocks, to maximize model efficiency.

2.5 Existing Methodology for Segmentation and Classification

To classify and segment, brain MRI metaphors, current practices follow a set of pre-defined procedures. The phases for classifying and detecting non-tumour and tumor matters in brain MRI images are depicted in the fig 2.18. The following is a basic explanation of the possible stages and methods:

- Input Images: Most input pictures are magnetic resonance imaging (MRI) brain scans. A two- or three-dimensional input is possible, depending on the design and available memory.
- Pre-processing: For normalization of images, it is one of the most significant processes that has been extensively described in the literature. Because of its ability to dramatically improve the input images, it has proven to be as vital as any other phase.
- Segmentation: The input image is divided into similar segments according on a set of criteria, allowing only the most significant information to be recovered and the remainder to be discarded. When studying tumours, some researchers choose to isolate them from the surrounding tissue, while others prefer to use a hybrid approach. You have a lot of choices.
- Classification: The primary goal is to sort the entering data into several groups based on their commonalities in conduct.

Multimodality, Because of its comprehensive capabilities, in almost all of the research included in this article, Magnetic Resonance Imaging has been universally acknowledged as a routine medical imaging method for detecting brain tumours. Pre-processing the medical images for noise reduction and enhancement is done by around 70% of the researchers. To expand the dataset, some authors use pre-processing and data augmentation. They then used any of the image processing procedures available to separate the tumour area. The segmented extent is then utilised to train a learning system after segmentation. Another frequent method is to send pre-processed photographs directly to the learning system without segmentation. Segmentation is infrequently utilised in classification problems because it is not a necessary component of classification. The model undergoes a learning phase where it assimilates and trains on the distinctive features within the input image. Following this, the model's competency is evaluated in a testing scenario to ascertain its accuracy in correctly classifying items.

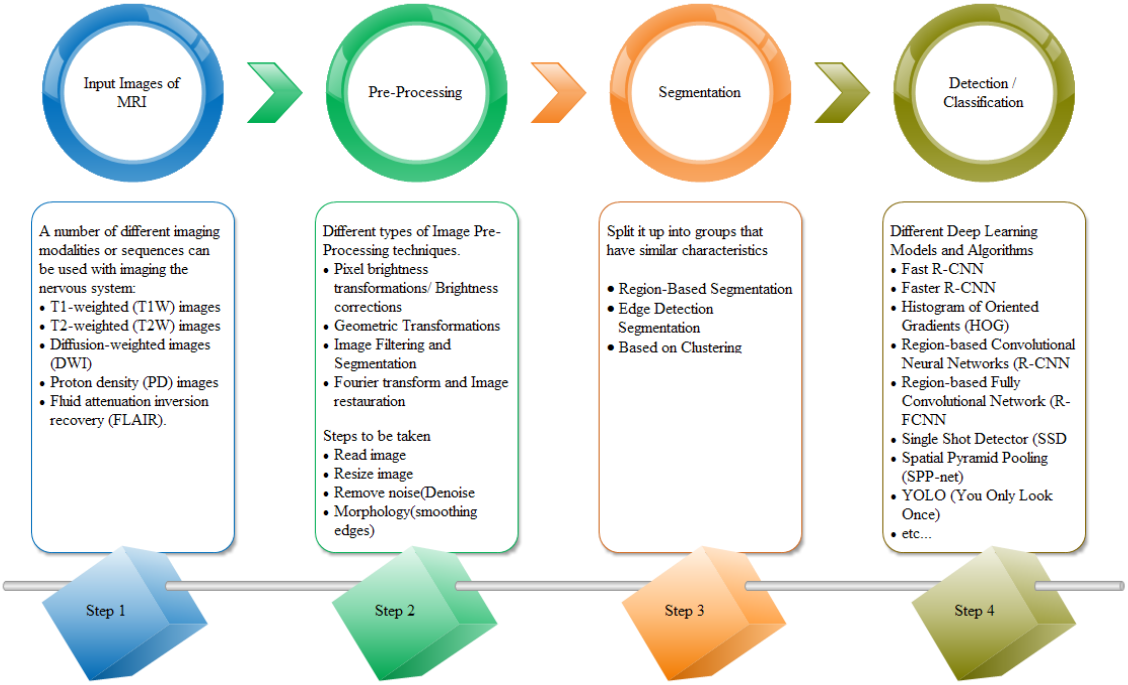

Fig 2.18 Existing Methodology for Segmentation, classification and Detection

2.6 Datasets used in Segmentation and Classification

Several datasets that the researchers utilised to evaluate the suggested methodologies are publicly available. This section discusses several important and difficult datasets (Table 2.5). The BRATS datasets are the most difficult MRI datasets.

Table 2.5 - List of publicly available datasets used in different papers

S No	Database Name	References
1	BRAINWEB	Vishnuvarthanan, et. al.,2017
2	BRANIX	Mittal, et. al.,2019
3	BRATS 2012	Raju, et. al.,2018; Fernandes, et. al.,2019; Amin, et. al.,2020; Abd El Kader I, et. al.,2021
4	BRATS 2013	Sharif, et. al.,2020; Zhao, et. al.,2018; Kalaiselvi, et. al.,2020; Amin, et. al.,2020; Sharif, et. al.,2020; Amin, et. al.,2019 ; Shehab LH, et. al.,2021

S No	Database Name	References
5	BRATS 2014	Sharif, et. al.,2020; Amin, et. al.,2020; Amin, et. al.,2019; Abd El Kader I, et. al.,2021
6	BRATS 2015	Siva Raja, et. al.,2020; Shehab, et. al.,2020; Chen, et. al.,2020; Thaha, et. al.,2019; Kamnitsas, et. al.,2017; Zhao, et. al.,2018; Amin, et. al.,2020; Amin, et. al.,2019; H. Mohsen, et. al.,2018; Abd El Kader I, et. al.,2021
7	BRATS 2016	Zhao, et. al.,2018; Han, et. al.,2020; Amin, et. al.,2019
8	BRATS 2017	Sharif, et. al.,2020; Huang Z, et. al.,2021
9	BRATS 2018	Sharif, et. al.,2020; Chen, et. al.,2020; Ben naceur, et. al.,2020; Amin, et. al.,2020; Huang Z, et. al.,2021; Zhang Y, et. al.,2021; Wang J, et. al.,2021; Wang YL, et. al.,2021; Zhou X, et. al.,2021; Zhang Y, et. al.,2021; Ranjbarzadeh R, et. al.,2021; Bidkar PS, et. al.,2022; Neelima G, et. al.,2022; Ahuja S, et. al.,2022; Chen W, et. al.,2022; Sasank VVS, et. al.,2022; Akbar AS, et. al.,2022; Giammarco M Di, et. al.,2022
10	BRATS 2019	Wang J, et. al.,2021; Ravikumar M, et. al.,2021; Wang Y, et. al.,2022; Li P, et. al.,2022; Sasank VVS, et. al.,2022; Akbar AS, et. al.,2022; Maji D, et. al.,2022; AboElenein NM, et. al.,2022
11	BRATS 2020	Karayegen G, et. al.,2021; Liew A, et. al.,2021; Ramya P, et. al.,2021; Bidkar PS, et. al.,2022; Sasank VVS, et. al.,2022; Sahayam S, et. al.,2022; Akbar AS, et. al.,2022; Gull S, et. al.,2022
12	BRATS 2021	Akbar AS, et. al.,2022
10	ISLES 2015	Akbar AS, et. al.,2022; Abd El Kader I, et. al.,2021
11	HARVARD	Amin, et. al.,2017; Talo, et. al.,2019; M. Kachwalla, et. al.,2017
12	FIGSHARE	Deepak, et. al.,2019; Kurup, et. al.,2020; Ghassemi, et. al.,2020; Yiming, et. al.,2019; Maharjan, et. al.,2020; Zhou, et. al.,2019
13	RIDER	Amin, et. al.,2017
14	IBSR	Ito, et. al.,2019
15	KAGGLE	Çinar, et. al.,2020; Toğaçar, et. al.,2020; Díaz-Pernas FJ, et. al.,2021; Rai HM, et. al.,2021; Badža MM, et. al.,2021; Waghmare VK, et.

S No	Database Name	References
		al.,2021; Al-Saffar ZA, et. al.,2021; Khairandish MO, et. al.,2022; Sunsuhi GS, et. al.,2022; Alnowami M, et. al.,2022; Kapila D, et. al.,2022
16	MD-1, MD-2	Nayak, et. al.,2020
17	REMRANDT	Nair, et. al.,2020
18	PGIMER	Sachdeva, et. al.,2016
19	TCIA	Naser, et. al.,2020; Boustani, et. al.,2019; Ghosh S, et. al.,2021
20	CPTAC	Boustani, et. al.,2019

2.7 Performance Measure

In the literature review studies, it analysed that the research uses various methods and techniques to validate and evaluate the results as well as the performance. The following table 2.6 presents a list of performance parameters.

Table 2.6 - Performance Matrices

S No	Performance Metric	Formula	Definition / Functionality
1	True Positive (TP)	$\frac{No\ of\ resulted\ images\ having\ brain\ tumor}{total\ No\ of\ images}$	The model is considered to have achieved a true positive when it successfully predicts the positive class, proving that it is adept at recognising the desired category.
2	True Negative (TN)	$\frac{No\ o\ images\ that\ haven't\ tumor}{total\ No\ of\ images}$	When the algorithm accurately forecasts the negative category, we say that it is a true negative.
3	False Positive (FP)	$\frac{No\ of\ images\ that\ haven't\ tumor\ and\ detectd\ positive}{total\ No\ of\ images}$	When the model predicts the class of positives incorrectly, it is called a

S No	Performance Metric	Formula	Definition / Functionality
			false positive.
4	False Negative (FN)	$\frac{No\ of\ images\ have\ tumor\ and\ not\ detected}{total\ No\ of\ images}$	A false negative occurs when the model predicts the negative class inaccurately.
5	Accuracy (ACC)	$\frac{TP+TN}{TP+TN+FP+FN}$	The degree of accuracy should be considered while assessing the performance of categorization models. In a nutshell, accuracy is the percentage of right predictions made by our model. The number of correct answers can also be expressed as a percentage when using binary classification.
6	Area Under Curve (AUC)	$\int_{\infty}^{-\infty} TPR\ (T)FPR\ (T)dT$	The area under a curve between two points is found out by doing a definite integral between the two points.
7	Sensitivity or Recall	$\frac{TP}{TP+FN}$	One measure of sensitivity is the True Positive Rate. It is also known as recall. It basically shows us what percentage of real positive examples our algorithm got right.
8	Specificity	$\frac{TN}{TN+FP}$	Specificity is the percentage of expected negative results that really occurred as negative results.
9	Precision	$\frac{TP}{TP+FP}$	A computer model's accuracy in making a positive prediction is known as its precision. The ratio of true positives to the overall number of positive predictions is the definition of

S No	Performance Metric	Formula	Definition / Functionality
			precision.
10	False Positive Rate	$1 - Specificity$	The false positive rat is a statistic used to assess the accuracy of a test, whether it's a medical screening procedure, a machine multilayer perceptron, or something else. In technical terms, the false positive rate refers to the chance of mistakenly rejecting the null hypothesis.
11	False Negative Rate	$1 - Sensitivity$	In contrast to a false positive, a false negative occurs when a test result wrongly suggests the absence of a condition when it is actually present.
12	F - Score or Similarity Index	$\frac{2\,TP}{2\,TP + FP + FN}$	The reliability of a test can be expressed as an F-score or F-measure. The test's precision and recall are used to calculate it.
13	Dice Coefficient	$2\frac{\lvert G_a \cap S_a \rvert}{\lvert G_a \rvert + \lvert S_a \rvert}$	A statistical instrument known as the dice coefficient is used to quantify the degree of resemblance between two datasets.
14	Noise Ratio of Peak Signal	$PSNR = 20 \times Log_{10}\left(\frac{255}{RMSE}\right)$	A signal's performance about the quantity of noise that might damage the representation is measured by the peak signal-to-noise ratio, typically abbreviated as PSNR.
15	Root Mean Square Error	$\sqrt{\frac{\sum_{i=1}^{M}\sum_{j=1}^{N}(I(i,j) - Seg(i,j))^2}{M \times N}}$	The Root Mean Square Error (RMSE) represents the inflation factor of the variance caused by prediction errors.

S No	Performance Metric	Formula	Definition / Functionality
			The residuals serve as a quantification of the degree to which the observed values deviate from the regression line, while the RMSE provides a measure of the extent to which the residuals are spread out. Essentially, it offers insights into the level of compactness of the data points around the line that represents the most accurate fit. Root mean square error is commonly employed to assess experimental findings in climatology, prediction, and regression analysis.
16	Jaccard Index	$J\ (G,K) = \frac{\lvert G \cap K \rvert}{\lvert G \cup K \rvert}$	A statistic for assessing sample set resemblance and diversity is the Jaccard indices, sometimes referred to as the Jaccard similarity coefficient.

2.8 Related Work Based on Machine Learning and Deep Learning Model

Since the emergence of Deep Learning techniques, a number of research articles have surfaced. Deep neural networks have facilitated feature extraction and selection by virtue of their capacity for self-learning. A variety of Deep Learning models, spanning from rudimentary to intricate, have progressed over time and exhibited exceptional accomplishments in the realm of medical imaging.

Almost 64 research papers are analysed in this study to determine the effectiveness of learning in intracranial tumour segmentation and classification using medical

imaging. Since last year, utilisation of Deep Learning set of rules for tumour segmentation and classification has increased.

2.8.1 Technical Investigation Carried Out in 2022

This study (Bidkar PS, et. al.,2022) introduces a unique method for classifying brain tumours using a Deep Belief Network with Salp Water Optimization (SWO-based DBN). The input image is initially pre-processed to remove any artefacts that may be there. SegNet, which was trained using the suggested SWO, performs segmentation after pre-processing. Additionally, the features are mined using CNN) features for later processing. Finally, the newly developed SWO-based DBN approach successfully classifies the brain tumour according to the collected attributes.

Through MRI-based categorization, this work (Dang K, et. al.,2022) seeks to overcome this problem and provide an appropriate prediction for glioma. Here, they used a pipelined deep learning framework that included these three crucial steps: To differentiate between high-grade tumours of the brain and low-grade tumours, MRI images were initially segmented using preprocessing approaches and the UNet framework. Subsequently, the brain tumour areas were extracted by segmentation.

This research (Neelima G, et. al.,2022) develops a system that can automatically catalogue tumours using MRI. Pre-processing is referred to as the first step in normalising intensity. Here, min-max normalisation is used for pre-processing. With the help of the newly developed Political Optimizer based on selfish (SPO) algorithm, the segmentation is carried out utilising the Optimal DeepMRSeg technique. The optimization algorithm based on selfish (SOA) and political optimizer are combined to create the suggested SPO (PO). Following the extraction of the CNN features, augmentation of data is carried out. CNN is used for data augmentation such as left or right switching, brightness, orientation, or contrast change.

In this study (Deepa G, et. al.,2022), delineation with ensemble classification using modified particle swarm optimization (MPSO) is suggested as a method for detecting

brain tumours. Initially, a wiener filter is used to reduce picture noise. Haralick features are then used in the feature extraction procedure.

This research (Rasool Reddy K, et. al.,2022) presents a novel methodology that utilizes local texture features and adaptive techniques. Here, we primarily use a median filter to filter out noise from MRI scans of the brain. Then, in order to get meaningful sub-images, we use adaptive decomposition techniques as modified sort of pseudo variational mode decomposition (MQBVMD) and two - dimensional empirical mode decomposition (BEMD). After that, we classify brain MRI pictures as either low-grade or high-grade using a support vector machine, and we use an ELDP feature descriptor to extract hidden texture information from the sub-images. Finally, we localise the glioma's affected region by employing morphological techniques and adaptive K-means clustering.

The suggested study (Ahuja S, et. al.,2022) aims to utilise T1W-CE MRI data for the identification, categorization, localization, and segmentation of brain tumours. The training data is enhanced with a 2-level discrete wavelet transform and topological approaches to mitigate the challenges of overfitting, such as scaling, rotation, and translation. In this study, we assess the efficacy of two trained beforehand DarkNet models—DarkNet-19 and DarkNet-53—in the context of malignancy localization and classification according to multiple classes. The previous DarkNet model achieved an accuracy of 98.81% during validation and 99.60% during training, making it the top performer. The T1W-CE MRI sample demonstrates that the evaluation metrics effectively support the positive benefits of the recommended methodology over the current state-of-the-art.

In this study (Khairandish MO, et. al.,2022), the classification of brain MRI images using CNN's superior performance on a publicly available dataset to identify benign and malignant tumours will be done. Image classification is one area where deep learning approaches have shown to be effective in recent years. Over time, Convolution Neural Networks can increase their classification performance by

extracting features utilising a number of ways that do not include bespoke models. Support vector machines were utilised for detection in the suggested hybrid method, while threshold-based classifiers were employed for classification.

The recommended work (Vankdothu R, et. al.,2022) differs from previous works in that it has the most extreme execution for evaluating tumour image segmentation. According to the result, when compared to other individual algorithms, the hybrid approach (SSO-GA) achieves the maximum accuracy of 99.24%.

This study (Walsh J, et. al.,2022) suggests a simplified U-Net architecture. U-Net with minimalist architecture is proposed, which not only offers real-time categorization of MRI images but also does not require a considerable number of learned data. In addition, there is no requirement for any additional data augmentation phase. Lightweight U-Net outperforms conventional benchmark methods on the BITE dataset, with an average intersection-over-union (IoU) of 89%. Additionally, this study shows how the three viewpoint planes may be used well for streamlined brain tumour segmentation in place of the underlying three-dimensional volumetric data.

In this study (Wang Y, et. al.,2022), the three-dimensional U-Net framework for segmenting brain tumours was subjected to an augmentation technique termed TensorMixup. The basic concepts were as follows: first, two image regions of 128 x 128 x 128 voxels were chosen based on ground truth labelling for gliomas from the data of magnetic resonance imaging that presenting using the same modality. After that, the picture patches were mixed using a tensor whose components were all individually selected from the beta distribution.

Scientists employed the dataset sourced from the Brain Tumour Segmentation Challenge 2019 (Li P, et al., 2022) to train 3D U-Net and 3D U-Net++ networks with the goal of autonomously detecting brain cancers in magnetic resonance imaging from the BRATS 2019 dataset. In the first step of the process, the brain tumour is segmented into three distinct parts: the entire tumour (WT), the tumour core (TC), and the improved tumour (ET). After that, the models are trained with images that are

taken in the axial, coronal, and sagittal planes. The next step is to combine the information from all three perspectives in order to arrive at the ultimate segmentation result. The enhanced tumour is specifically segmented using U-Net++ because to its more intricate structure as contrasted to other sub-regions.

The primary objective of this research piece is to identify and categorise cancers that are present in the human brain.According to Sunsuhi GS et al. (2022). There are three fundamental processes, which are pre-processing, segmenting, and categorising. Phases one and two include detecting boundary boxes using a binary approach and an asymmetrical diffusion filter. We use the suggested Adaptive Eroded Deep Convolutional Neural Network for the new segmentation process. It enables us to distinguish between meningiomas, gliomas, and the pituitary brain region. Then, as a state-of-the-art classification method for brain images, Inception resnetV2 is recommended as the stage of segmentation. The division of the tumour cell area is the first step in the separation process. The degree of spatial membership is decided using the method AEDCNNS.

This paper (Sunsuhi GS, et. al.,2022) proposes a novel multi-threading 3D dilated convolutional infrastructure (MTDC-Net) for autonomously segmenting brain tumours. The encoder component initially presents a multi-threading distorted convolution (MTDC) technique that efficiently extracting and include the low-dimensional spatial essential characteristics.

To assess the diagnostic accuracy of fully automated radiomics-based methods (Joo B, et. al.,2022) in identifying several types of brain tumours, including developing tumours, malignant tumours, central nervous system lymphoma, and metastatic tumours. The effectiveness was achieved when the LASSO was employed as an attribute selection approach.

In this study (Sahayam S, et. al.,2022), multi-resolution, deep supervisory, residual, and dual attention blocks have been examined in addition to the basic U-Net model. Residual blocks attempt to successfully feature extraction in order to close the

expectation relations between slightly elevated features from hidden neurons and low-level properties from the decoded. The addition of the multiple resolution blocks allows for the feature extraction and scale-dependent tumour analysis. To draw attention to tumour representations and lessen over-segmentation, the dual attention method has been included. To get the goal segmentation, deep supervision blocks have been introduced to use features from different decoder levels.

The Multipath Residual Attention Block, which we propose in this paper (Akbar AS, et. al.,2022), substitutes the computing block with two arous convolution processes connected to the concentration of the unknown and one residual route, and adds attentiveness in the skip connection (MRAB).

In this study (Sun Y, et. al.,2022), a trustworthy and effective Convolutional Neural Network (CNN) method for segmenting brain tumours is suggested. It is made up of a segmentation-CNN, a condition characterized block, and a refinements block. The special CNN is specifically created to conduct pixel categorization, tumour localization, and mono- and cross-modality feature extractions while adhering to the suggested ASCNN (Application Specific CNN) paradigm. High-pass filtering convolution layers can use as few as half as many kernels thanks to the suggested activation function Full-ReLU, without sacrificing processing effectiveness. The frequency of kernels within every layer is set adequate for its objective rather than continuously extending across the layers in order to increase spreadsheet or database in data channels and decrease unpredictability in network training.

The design proposed by Maji D. et al. (2022) can actively guide the learning process of each decoder layer. By keeping tabs on its learning process, the decoder layers are able to generate more accurate feature maps. Instead of letting everything go through the Res-UNet's skip connections, attention-grabbing barriers in the generators concentrate on encouraging useful information.

Chawla R. et al. (2022) suggested a technique to identify brain cancers in MRI images using a Convolutional neural network and the Bat algorithm. Data is a component that

helps to eliminate background noise. If you have an MRI of your brain, you can use the 2-D Gabor filter to pull out certain details. To choose features with higher precision, the network models are employed. The data utilised in this investigation were supplied by Nanfang Hospital and the Community Hospital of Tianjing Medical University. When compared to the current system, the proposed BCNN approach achieves an overall accuracy of 99.5%.

Giammarco M Di, et. al.,2022 provide a method for brain segmentation utilizing MRI in this work. Approach builds upon a redesigned iteration of a convolutional neural system akin to the U-Net model, forming the basis for our technique. The efficiency of the suggested method for segmenting high grade brain cancer is shown by investigations on high grade bowel cancer MRI.

This article (AboElenein NM, et. al.,2022) presented the Multi Inception Residual Attention U-Net (MIRAU-Net), an unique encoder-decoder framework. It adds the residual transformation approach with attention barriers into U-Net to significantly increase the segmentation's efficacy for brain tumours.

2.8.1.1 Quantitative Analysis of 2022 Model and Algorithm

Unlike prior years, a significant amount of effort was put on identifying and categorising brain tumours in MRI scans in 2022. Researchers moved their focus back to image improvement approaches by applying several pre-processing techniques to the input brain MRI datasets as well as feature extraction, classification and segmentation to find the localization of the tumor and prediction for that. They began by combining several machine and deep learning approaches to create hybrid models (Fig 2.19, 2.20, 2.21, 2.22).

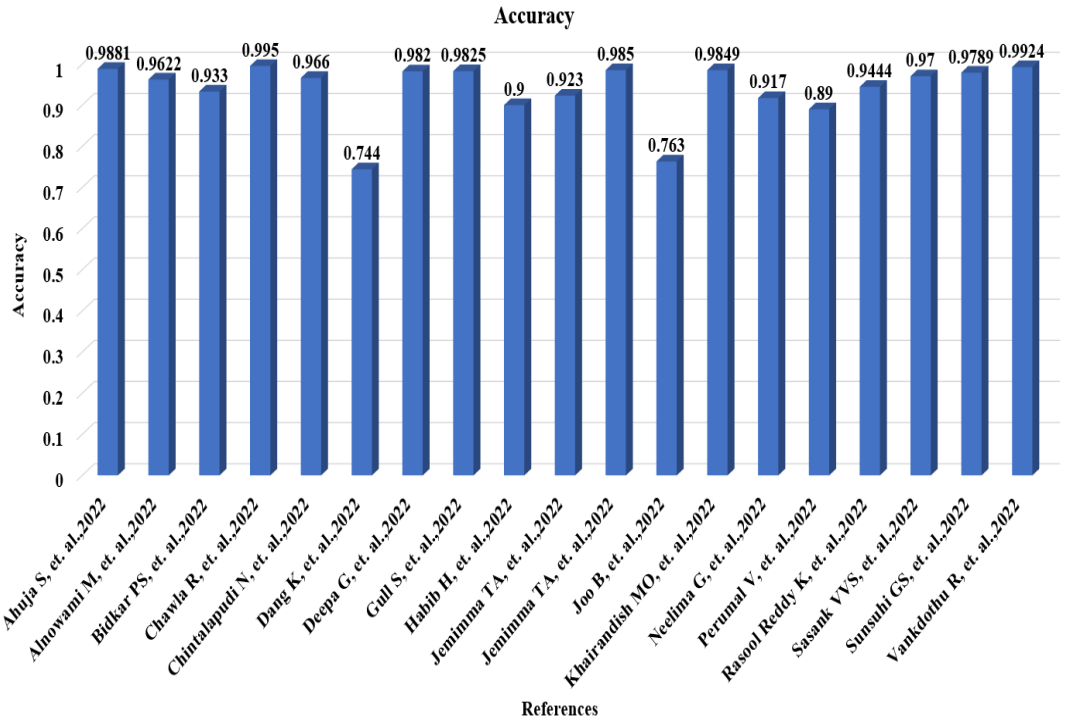

Fig 2.19 Analysis of Accuracy for 2022 Model and Algorithm carried in studies

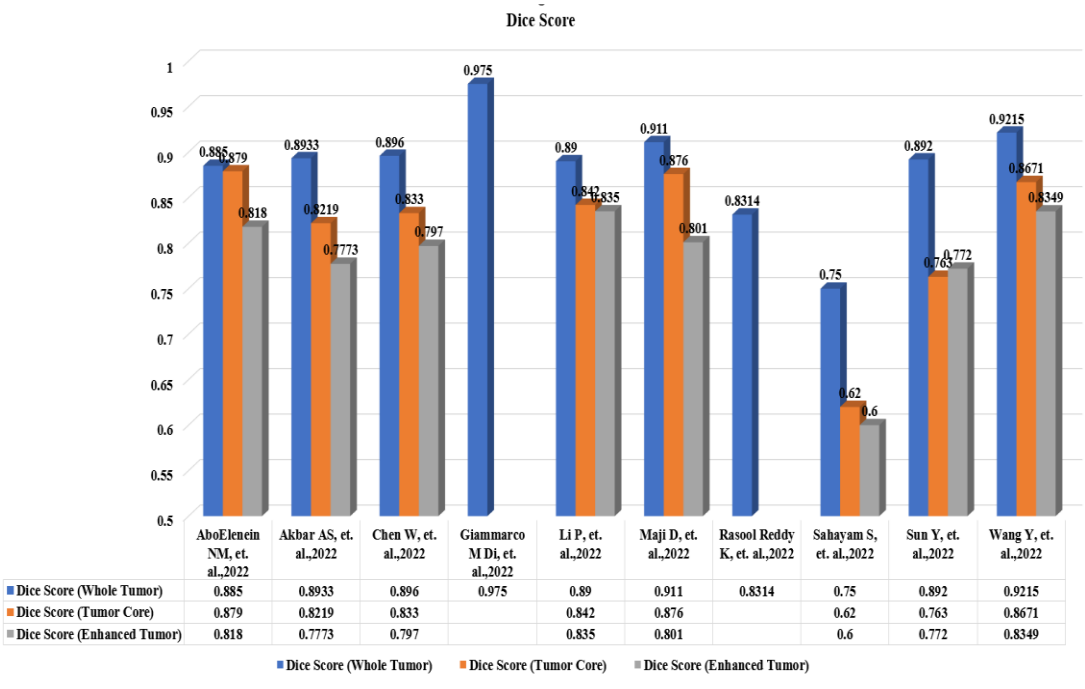

	AboElenein NM, et. al.,2022	Akbar AS, et. al.,2022	Chen W, et. al.,2022	Giammarco M Di, et. al.,2022	Li P, et. al.,2022	Maji D, et. al.,2022	Rasool Reddy K, et. al.,2022	Sahayam S, et. al.,2022	Sun Y, et. al.,2022	Wang Y, et. al.,2022
Dice Score (Whole Tumor)	0.885	0.8933	0.896	0.975	0.89	0.911	0.8314	0.75	0.892	0.9215
Dice Score (Tumor Core)	0.879	0.8219	0.833		0.842	0.876		0.62	0.763	0.8671
Dice Score (Enhanced Tumor)	0.818	0.7773	0.797		0.835	0.801		0.6	0.772	0.8349

Fig 2.20 Analysis of Dice Score for 2022 Model and Algorithm carried in studies

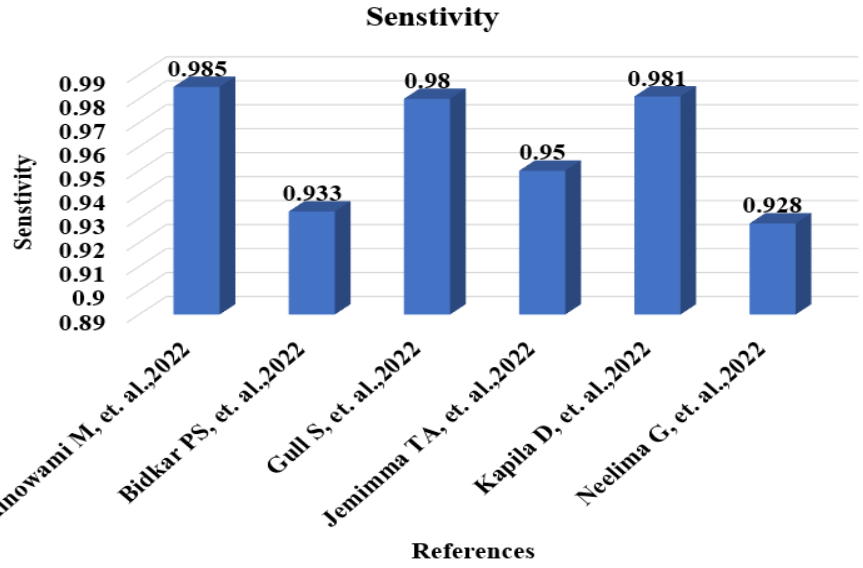

Fig 2.21 Analysis of Sensitivity for 2022 Model and Algorithm carried in studies

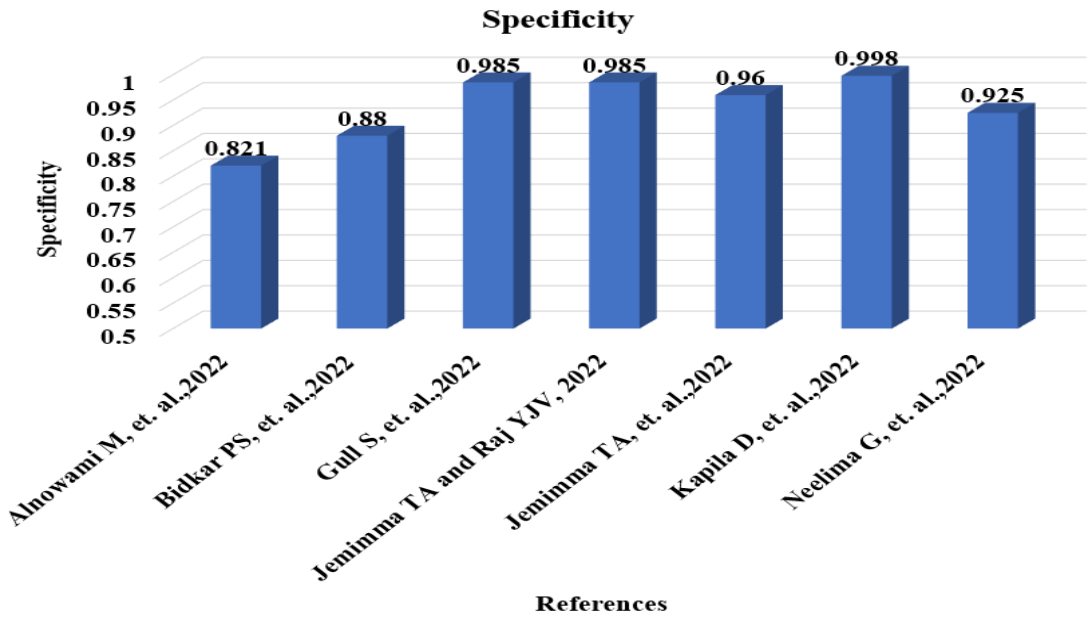

Figu 2.22 Analysis of Specificity for 2022 Model and Algorithm carried in studies

2.8.2 Technical investigation carried out in 2021

To improve brain tumour the process of segmentation this work (Huang Z, et. al., 2021) demonstrates how attention residual UNet with group cross-channel can make full advantage of the low-level fine characteristics of cancer locations. The disruptions

caused by background and light changes are first removed using iterative background removal and picture normalising. After that, GCAUNet is built to segment brain tumours. The detail recovery (DR) path, a concurrent network channel, is developed to recover the detailed properties of brain tumours. From multiscale low-level feature maps, it extracts specific sets of characteristics. The GCA procedure, a transceiver for coarse-to-fine cross-channel attention, is also supplied to highlight the important feature clusters and routes. To collect multiscale context data, GCAUNet is given a second multiscale input (MI) pathAccording to the experimental findings, GCAUNet's average dices for the whole tumour (WT), enhancing tumour (ET), and tumour core (TC), respectively, on BraTS 2017 and BraTS 2018, are 87.2%, 78.1%, and 79.6%.

This study (Karayegen G, et. al.,2021) uses convolutional neural networks to provide a technique for automatically segmenting brain tumours on 3D BraTS sets of image data comprised of four different imaging techniques. Our work also compares predicted labels in 3D to ground truth labels using whole-brain 3D imaging. This method was effectively used, and images were shown in sagittal, coronal, and axial planes to obtain the precise tumour location and parameters such as height, width, and depth. Deep learning network-based semantic segmentation evaluation results are quite encouraging in terms of tumour prediction. The calculated average prediction ratio was 91.718. The average average BF scores and intersection over union (IoU) were found to be, respectively, 92.938% and 86.946%.

In this study, the authors establish a channel and radially wise asymmetric attention (CASPIAN), which they use to detect prominent areas in tumours (Liew A, et. al.,2021). In order to demonstrate the usefulness of the layer, it should be included into a well-known CNN framework in order to get better Dice scores while utilising fewer resources of GPU. They also research the addition of supplementary multiplanar and multiscale attention divisions to enhance the spatial background necessary in semantic segmentation. The new CASPIANET++, the resultant

construction, obtains Dice Scores of 87.6%,91.19%, and 81.03% for the tumour core, the whole tumour and the enhancing tumour, correspondingly.

A novel multi-scale mesh aggregation network (MSMANet) for brain tumour segmentation is suggested in this study (Zhang Y, et. al., 2021). First, an improved Inception module is used to extract and integrate efficient information from different receptive fields, so replacing the standard encoder convolution. Step two involves suggesting a novel mesh aggregation method to progressively enhance the shallow features and significantly reduce the semantic gap. This strategy makes the most of the aggregation of multi-level traits at different sizes and reaps the benefits of qualities that complement each other. Finally, using deep supervision and attention mechanisms improves the capacity for network identification and convergence. On BraTS2018, experiments were run to assess the suggested network.

The network (Wang J, et. al.,2021) is composed of a spatial DFP-ResUNet module, a residual constituent, an encrypting and deciphering structure, and a U-Net. We initially recommend using a spatial DFP component made up of many parallel dilated convolution operations to replicate the multiscale visual properties. The spatial DFP architecture enhances the neural network's capacity to recognize and take use of its multiscale sensory features. The network architecture is then furthered using the surviving module. To further mitigate the impact of unbalanced data on the segmentation of brain tumours, we advise using a multiclass Dice loss function.

To fully utilise multi-scale features, (Wang YL, et. al.,2021) suggest a novel U-shaped network which is linked by cross-level (CLCU-Net) that connects the features of various scales. In addition, suggested a general attention component (Segmented Attention Module, SAM) for arbitrarily aggregating observations on the connections of various scale features.

A less computationally expensive and GPU memory-intensive neural network with 3D residual operation (ERV-Net) was suggested for splitting brain tumours in this study (Zhou X, et. al., 2021). The 3D ShuffleNetV2 computation-efficient network

was initially used as an encoder in ERV-Net to free up GPU resources and improve ERV efficiency. Net's The next step is to incorporate a decoder that stores residual blocks (Res-decoder) in order to stop degradation. Also, a loss function of fusion is developed that combines cross-entropy loss with dice loss to solve the problems of transitory network and data imbalance. We also propose a quick and effective post-processing method to enhance the segmentation output of the ERV-coarse Net.

A fully automated model for multiscale brain tumour classification and segmentation based on Deep Convolutional Neural Networks (CNN) is provided in the study (Díaz-Pernas FJ, et. al., 2021). In contrast to previous attempts, the input images in the proposed concept undergo processing at three separate spatial scales using a variety of processing pathways. No prior processing of input images is necessary for the proposed neural model to eliminate parts of the vertebral column or skull. The MRI images with pituitary tumours, gliomas, and meningiomas can be deciphered from axial, sagittal, and coronal views.

Authors have suggested utilising the DWT-RBFNN classifier to automatically segment and categorise tumours from brain MR images (Rai HM, et. al.,2021). Segmentation and classification are the two sections of the project. Prior to performing segmentation and classification, MR images are first pre-processed. Images are scaled and denoised using the hybrid approach DWT-ICA during the pre-processing step. These segmented pictures are utilised for the categorization of brain tumours after being segmented using a hybrid Ostu-canny edge approach. Following segmentation, 13 different types of features—including the standard deviation (SD), variance, median, mean, smoothness, RMS (root mean square), energy, correlation, entropy, skewness, homogeneity, power spectral density, and contrast, —are retrieved using multiresolution DWT. The feature-extracted and segmentation images of the brain tumour are classified into three classifications using the RBNN classification model: normal, benign, and malignant. Seven different assessment measures are utilised to measure the effectiveness of the classifier: F1-score, recall, precision, classification error rate, specificity, and total accuracy. The effectiveness of the

suggested classifier was also evaluated in comparison to classifiers using feed-forward neural networks and back-propagation neural networks.

This study (Chahal PK, et. al.,2021) recommends a fuzzy k-means using hybrid weight brain tumour segmentation approach using medical images in order to identify relevant clusters. To address problems with numerous pixel subscriptions and exponentially increasing cycle counts, it is based on a weighted fuzzy learning method that influences the spatial representation and the lighting penalise membership approach. After picture segmentation, support vector machines are used to classify tumour types as benign or malignant.

The tumour area of the brain MRI image is segmented in this article (Ramya P, et. al.,2021) using the ensemble approach of background subtraction. In order to prepare the images for segmentation, the Laplacian cellular automata filtering method is employed. This method is one of several clustering techniques that are considered, including fuzzy based clustering, K-means, self-organization map, and an ensemble of Gaussian mixture models. This composite cluster tag is utilised to classify the aberrations using deep super learning and is taken into consideration as the segmentation output.

This paper (Chen B, et. al., 2020) built a Support Vector Machine (SVM) employing an Extended Kalman Filter, an SVM-based image processing step, to automatically identify brain tumours. The five main parts of a machine learning algorithm are as follows. The first step is to standardise the graphic representation of all the objects. Following that, a non-local means filter is employed to remove the noise, and improved dynamic histogram equalisation is employed to enhance the contrast. The second step is to use a gray-level co-occurrence vector to gather visual features. Thirdly, an EKF is utilised to categorise brain cancers in the brain MRIs after the retrieved characteristics are supplied through an SVM to classify the MRI first. Fourth, cross-validation is employed to check the classifier's accuracy. Finally, a brain

tumour detection technique based on artificial segmentation that combines area growth and k-means clustering is employed.

In this study (Badža MM, et. al.,2021), a novel convolutional neural autoencoder for semantic segmentation-based segmentation of brain tumours is presented. The largest internet photo resource is utilised to assess the compactly planned architecture. 30,64 MRI scans on file Included in the collection are T1-weighted contrast-enhanced images. To put the suggested architecture to the test, we combine two separate data division approaches, two separate assessment methodologies, and train the model with both the existing and augmented datasets. Using one of these data division strategies, we also looked at the network's ability to generalise in terms of medical diagnosis. The optimal approach was the performance data division technique, which utilised the supplied dataset for network training.

In order to overcome the gradient problem of DNN, presented paper (Shehab LH, et. al.,2021) describe in this research an autonomous method for segmenting brain tumours that relies on Deep Residual Learning Network (ResNet). ResNets are more accurate than their counterpart DNN and can speed up the training process. ResNets add a shortcut skip link parallel to the convolutional neural network stages to accomplish this improvement.

Ghosh S, et. al.,2021, suggest an enhanced VGG16 using U-Net in this study to partition, images of brain MRI and determine tumor cell for region-of-interest. By evaluating the dataset of 3929 images of TCGA-LGG from the TCI repository, Author’s compared the outcomes of enhanced U-Net with a custom-designed U-Net construction and obtain pixel accuracies of 0.9975 and 0.994 from improved U-Net and basic U-Net designs, correspondingly.

In this study (Ranjbarzadeh R, et. al.,2021), will begin by proposing a pre-processing technique for building a versatile and efficient brain tumour segmentation system. This strategy will focus on a tiny portion of the image instead of the complete thing. This methodology not only resolves overfitting concerns within a Cascade Deep

Learning model but also optimizes computational efficiency, resulting in a more streamlined and effective solution. For the second step, it is advised to use a quick and Convolutional Neural Network with effective cascade, as we are only interested in one specific dimension of each brain part. This C-CNN model employs two distinct strategies to take use of both local and global characteristics. As an added bonus, study improve upon state-of-the-art models' segmentation accuracy of brain tumours using a new Distance-Wise Attention (DWA) method. The DWA method accounts for the brain and tumor's central location within the prototype.

Because CNN is able to perform the task of image classification, encompassing image identification, positioning, segmentation, normalization, and detection, automatic classification of brain tumours is predicted with their assistance in this study (Waghmare VK, et. al.,2021). As segmentation divides the picture into several parts based on certain similarity criteria, we are able to abstract various information from the images.

Several methods have been investigated in this work (Al-Saffar ZA, et. al., 2021) with the aim of improving the outcomes and reducing the challenges of medical image analysis. Some of these methods include an SVD-based reduction of dimensionality approach, a method for dividing tumours in the brain using regional variations in intensity-means, a method for brain tumour classification using both Support Vector Machine and Multi-Layer Perceptron, and a method for feature extraction using Mutual Information.s.

Using a deep wavelet autoencoder, or "DWAE model," to categorise input data slices as having tumours or not was recommended in this study (Abd El Kader I, et. al., 2021). The heterogeneity of the MRI pictures and their incorporation with the image features were demonstrated in this paper using a high pass filter.

For the purpose of segmenting brain tumours from MR images, researchers have introduced notch transformation function (Ravikumar M, et. al.,2021) to improve and a deep learning-based hybrid SegX-Net technique.

In this study (Rajasree R, et. al.,2021), a 3 x 3 kernel-sized semantic-based U-NET convolutional neural network is suggested. Compact kernels only give a lesser number of parameters in this structure and have an impact against generalisation in the deeper construction. For several dimensions of magnetic resonance images, a multiscale multimodal convolutional neural network (MSMCNN) with an LSTM-based deep learning semantic segmentation strategy is employed (MRI). By scrutinising each pixel in the picture, the suggested approach seeks to recognise and categorise the various types of tumours.

Researchers suggest (Zhang D, et. al.,2021) a convolutional neural network-based 2D-UNET model (CNN).

2.8.2.1 Quantitative Analysis of 2021 Model and Algorithm

Fig 2.23, 2.24, and 2.25 shows that during 2021, individuals employed CNN the most, despite the fact that more projecting and efficient designs exist in the review of WT, TC and ET. This is due to CNN's great generalizability, consistency, and accuracy rate.

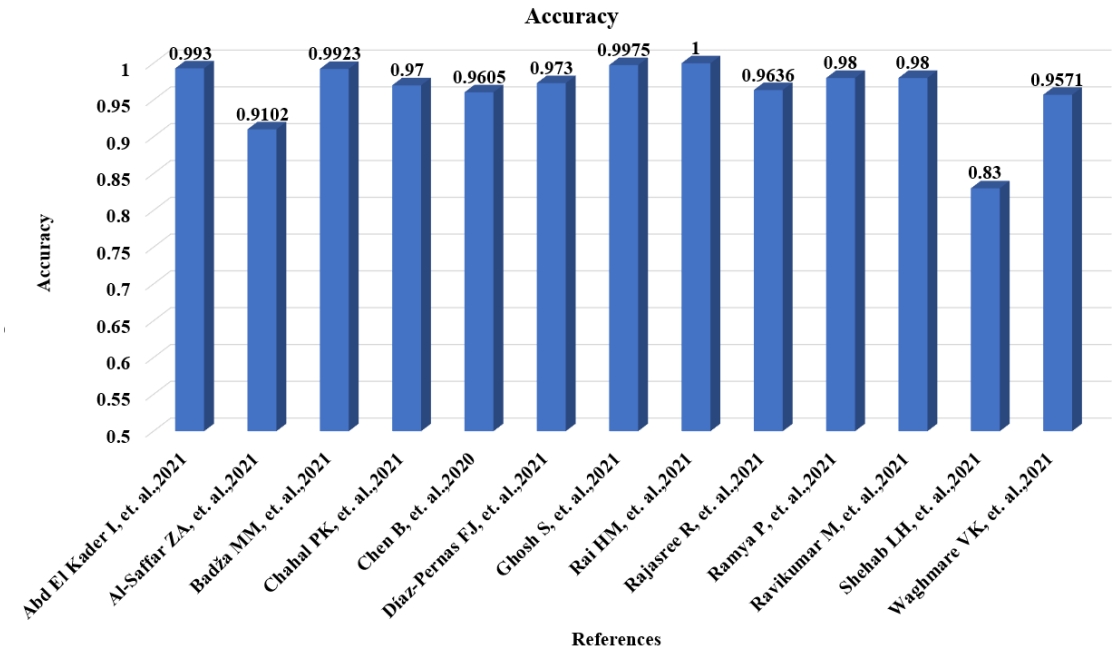

Fig 2.23 Analysis of Accuracy for 2021 Model and Algorithm carried in studies

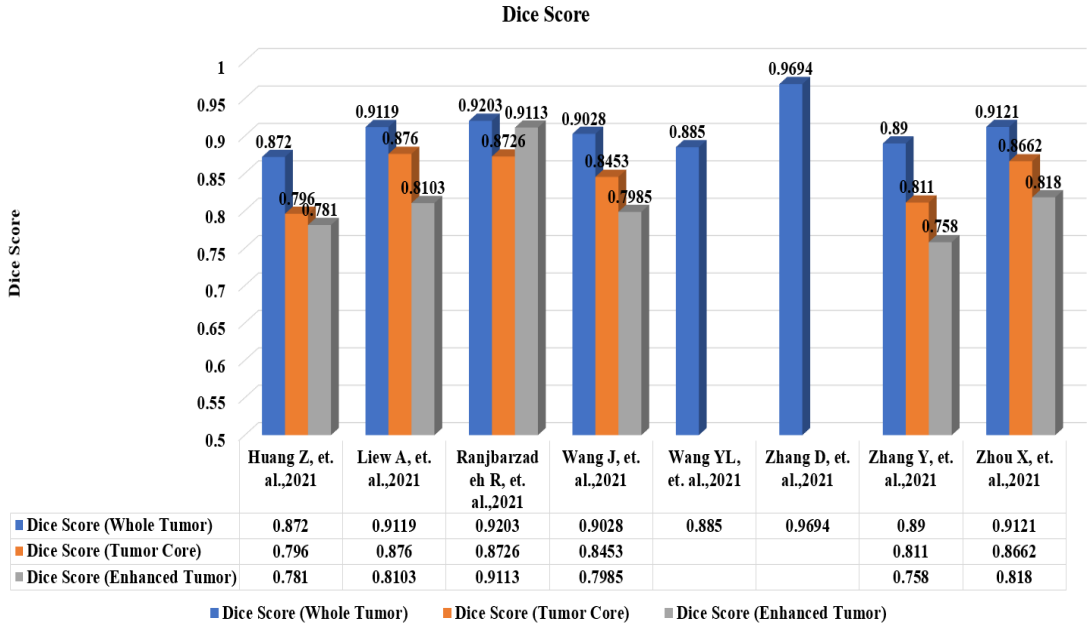

Fig 2.24 Analysis of Dice Score for 2021 Model and Algorithm carried in studies

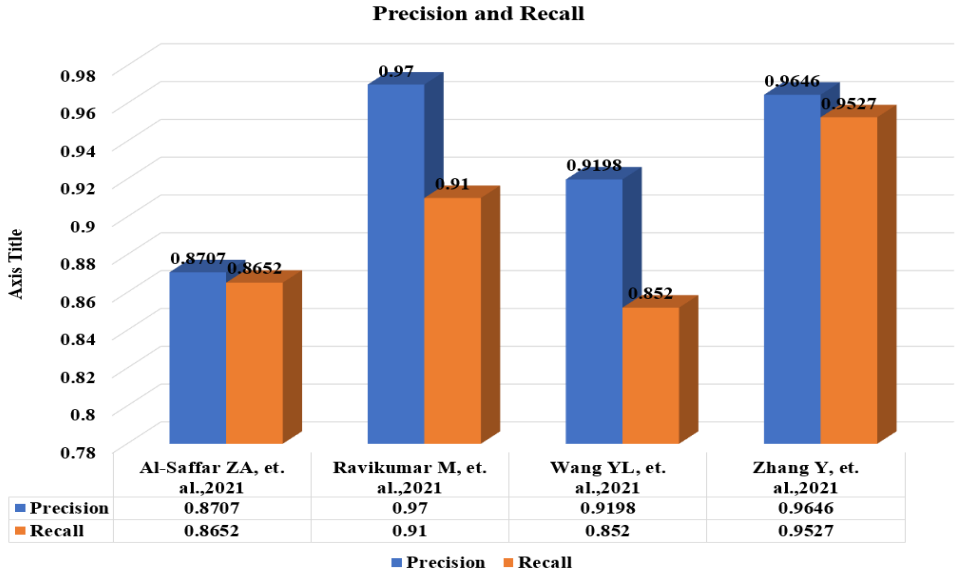

Fig 2.25 Analysis of Precision and Recall for 2021 Model and Algorithm carried in studies

2.8.3 Technical investigations carried out in 2020

This paper's objective is to demonstrate how to categorise malignancies in the brain using Bayesian fuzzy clustering-based segmentation with the assistance of a hybrid

deep autoencoder, as stated in (Siva Raja, et. al., 2020). The non-local mean filter was used in the first stage to denoise the reality of this approach. The segmentation of brain tumours was then done using the Bayesian-fuzzy clustering method. The authors used the Tsallis entropy, measures, and scattering change, a fictional statistics wavelet packet, to extract characteristics following segmentation. Lastly, for brain tumour categorization, they employed a hybrid structure of the Jaya optimisation problem based on a deep autoencoder and a softmax regression. This approach used the BRATS 2015 database, which proves the classification accuracy of 98.5 % when likened to other methods.

The exhibit provided in (Naser et al., 2020) shows how an in-depth learning approach to MRI images can be used to potentially make one-to-one tools available for automatic and simultaneous tumour segmentation, grading, and detection of LGGs for medical purposes. The authors' primary focus in this draft is the categorization and division of gliomas, which are brain tumours. For tumour segmentation, they have combined transfer learning methods based on an already-learned Vgg16 convolution-base with deep learning approaches founded on convolutional neural networks anchored on U-net. The model presented for LGG grade-II and grade-III classification has a 0.98 accuracy rate, 0.92 specificity, 0.87 sensitivity, and patient-specific MRI picture phases of 0.95, 0.97, and 0.98.

In (Chen, et. al.,2020), the author's much attention to contribute an outline for automatic brain lesion segmentation. To classify the segmentation of brain lesions, they proposed and regulated a two-stage supervised learning approach. The authors have prioritised using intensity-based statistical operations, GMM-based matter probabilities maps, and template-based asymmetric characteristics as their preferred strategy to train the classifier based on random forests in the initial stage. The next step is to optimise the possibility maps from the basic random forest classification algorithm of a densely confined random field, with full tumour areas referred to as regions of focus. In phase two, we use enhanced probability maps, expert randomly generated forests, template-based asymmetrical features, and intensity-based

statistical characteristics to classify vowels inside the ROI. In addition to training an iterative flood of random forests with the completed possibilities maps, the compressed conditional random grounds will be used to improve them. In order to get the best possible segmentation result, the output probability maps are improved layer by layer. Multimodal global and local presence statistics are combined with detailed information because they are the cause of ranked learning of dense conditional random fields and random cascade forests. The authors employed the proposed method and investigated the brain tumor datasets of BRATS2015, BRATS2018, and ISLES2015 (ischemic stroke dataset).

In order to obtain the features of various entropies like estimated entropy, Shannon entropy, and specimen entropy, as well as the Nave Bayes (NB) classifier used for the classification result, a method for cataloguing a brain image from the magnetic resonance imaging (MRI) is mentioned in (Aljunid, et. al.,2019). To extract the aforementioned entropy properties, DTWT principally disintegrates the aberrant and normal categories of MRI brain pictures.

In (Arunkumar, et. al.,2020), In this study, the authors projected a new dissection method using MR images for brain matters. The proposed segmentation approach comprises three computer vision fiction policies, segmenting images, enhancing images, clarifying out non-region of attention grounded on the HOG features and texture. Authors developed a copiously automated model-based train classification and segmentation method for MRI brain lumps that use artificial neural networks to identify ROI. To choose the accurate object in brain MRI, filtering out non-ROI is the next step in the presented methodology, and for this purpose, they have used histogram investigation. In this paper, 200 MRI images have used to prove the comparison between the automated and manual segmentation processes. The analysis of the results then asks whether the automatic model-based train segmentation manual method and brain recognition ROI design fully utilize the features. The chronicled identification correctness is 92.14%, with 94 specificities and 89 sensitivities.

In Nayak, et. al.,2020, this paper states that an approach grounded on an intensive deep convolutional neural network (CNN) has designed to diagnose multi-level brain abnormalities. Five layers of parameters included giving the proposed CNN model potential and making it learnable: four layers of convolutional (Conv-I to Conv-IV) and individual fully interconnected layers. Through an order of concealed layers, this prototypical learns to get hierarchical topographies automatically. This model has four BN, RealU, and maximum-pooling layers and the five layers (pool I to pool IV). A custom deep network determines to work out the number of parameters and achieve maximum classification performance. The proposed model has evaluated on the MD-1 and MD-2 multi-class brain MRI datasets. Authors applied the MD1, and MD2 datasets to SAE (Hinton and Salakhutdinov, 2006), SDAE (Vincent et al., 2008), ML-ELM (Kasun et al., 2013) and from that find the accuracy, for MD1 (90.00, 93.33, 93.33) and MD2 (60.45, 90.00, 9,125) respectively. The duets measured on their proposed model and made an accuracy find, which was MD1 (100%) and MD2 (79.50), respectively. Hence comparative analysis shows the superiority of the projected method.

The Deep Conventional Neural Network (CNNs) solution (Ben naceur, et. al.,2020) is entirely devoted to a high and low-grade division of glioblastoma brain tumors. The proposed CNN prototypical is fully stimulated by the occipital-Temporal pathway, emphasizing selective attention whose job is to locate critical objects in the successive layers of a scene using different receptive field sizes. The proposed system also concentrates on two more issues: the relationship between image patches and class-imbalance. For the first issue, the authors supposed two steps: Equal sampling and experimental analysis for weight cross-entropy loss function in terms of the segmentation consequences, furthermore, to overwhelmed the second problem, the result of overlying patches studied in contradiction of adjacent spots, where overlying pieces show improved segmentation consequences due to the local characteristics of the image patches. BRATS-2018 dataset model used for the experimental result.

To express the breadth of the advances in deep learning (Toğaçar, et. al.,2020), Hyperloom technology, recursive feature elimination, combining Alexnet and VGG-16 networks, and support vector machines (SVM) and in keeping with recent advances, authors have introduced a novel Confidential Neural Network (CNN) model. With the assistance of the hyperloom method, the proposed model can hold local discriminatory features mined from layers situated at dissimilar stages of the deep architecture and projected prototypical exploits their normalization capabilities by fusing fully interconnected elements of VGG-16 networks and AlexNet. The use of RFE in the proposed prototype to bring out the most potent in-depth features enhances its discriminative capability. As a result, the projected prototypical achieved 96.77% accuracy without using a handcrafted feature engine.

T. Kalaiselvi and S. T. Padmapriya recently published a paper in which they built six CNN models for brain tumour categorization (Kalaiselvi, et. al.,2020). The number of layers in each of the six CNN models differs primarily. Two CNN models use a drop out layer for regularisation, and two others use stopping batch and criteria normalisation in accumulation to the drop out layer. Without these layers, the other two approaches are employed. The training is carried out using the BRATS 2013 Dataset, whereas the testing is carried out using the World Brain Atlas (WBA).

In a different study, preliminary data processing is used to enhance the CNN architectural performance for brain tumour identification (Kurup, et. al.,2020). To enlarge the dataset, two key pre-processing techniques, patch extraction and rotation, are used as standard approaches of data augmentation and pragmatic to the dataset of 3064 medical images. The photos are then scaled to 28 x 28 to simplify the prototypical. Lastly, capsule-net is employee to test usefulness of augmentation as well as to categorize three different types of brain tumour image: pituitary, meningioma, and glioma tumour. Findings suggest that pre-processing has a significant impact on performance.

The relevance of segmentation and pre-processing of medical MRI medical images beforehand feeding them into a deep learning algorithm was highlighted by the

authors in (Amin, et. al.,2020). Their plan is to improve the medical images before applying median filtering to smooth out the noise. After that, a fine-tuned stacked sparse autoencoder (SSAE) model is used to segment the tumour area utilising region growth. On the BRATS dataset for 2012, 2013, 2014, and 2015, the model was trained and tested. The proposed technique's accuracy and sensitivity have improved as a result of the findings.

In their study, Çinar, et. al.,2020, provide an upgraded version of RESnet50 that demonstrates enhanced performance in classifying brain MRI medical images into tumour and non-tumor categories. RESnet 50's fundamental structure was augmented by an additional 8 layers and subsequently trained using the Kaggle MRI dataset. The outcomes are compared to established CNN architectures such as Googlenet, Alexnet, and DENSEnet, among others. The proposed method exhibits a 97% enhancement in accuracy when compared to the current Deep Learning models.

Toğaçar, et. al.,2020, built and discussed a unique BrainMRNET convolutional neural network. The model is made up of three primary components. The Convolution Block Attention Module (CBAM) is the first portion, which allows the network to spatial information and learn channel. The residual block is used in the second stage to help the network learn more salient characteristics, and the hyper Column method is used before the completely connected layer. For higher generalizability and classification efficiency. The BrainMRNet model had a classification success rate of 96.05 %.

The influence of pre-processing of data on prediction performance as well as margin of error was exploited by the authors of (Abdelaziz Ismael, et. al.,2020). To increase generalizability and lessen the challenge of gradient vanishing, the solutions mostly rely on data augmentation. The facts is initially reaped from the centre to minimise the inclusion of contextual statistics, as they impede the classification process. Subsequently, seven augmentation techniques were employed to expand the dataset. Lastly, the expanded dataset of images is inputted into the Resnet50 framework, which is utilised for both training and testing purposes. The precision of the outcomes is 98%.

Using dwt technology, the authors of (Amin, et. al.,2020) offer a novel technique for fusing four MRI modalities into a single MRI image. For each patient, the approach creates a single fused MRI sequence. The results suggest that the accuracy of fused images has improved.

Ghassemi, et. al.,2020 proposes a unique Generative Adversarial Networks that is based on deep learning architecture. Their plan was to pre-train CNN as a GAN discriminator utilising the two sets of data. In order to generate more precise pictures of the brain MRI scans, data augmentation was used by GAN's generating part. When training a GAN for classification, the last CNN discriminator layer is substituted with SoftMax. The rate of correctness is 88%.

To optimise the categorization process, the data is initially trimmed from the centre to reduce the inclusion of background statistics, which can hinder the process. Afterwards, seven augmentation approaches were used to increase the dataset in order to reduce overfitting. Ultimately, the enlarged collection of MRI images is fed into the Resnet50 framework, which is employed for both training and testing. The accuracy of the results is 98%.

The work emphases on multi-level segmentation for successful classification and abstraction of features of neurological disorders from MRI data (Islam, et. al.,2020). The authors employed thresholding, watershed technique, and morphological operation to segment the MRI images data after pre-processing them. The pictures of tumours were categorised as tumorous or non-tumorous using K-SVM after features were extracted using CNN. Overall, the suggested method is accurate to 87.4 %.

The authors of (Sharif, et. al.,2020) offer a classification method that relies on multiple feature engineering. The researchers have developed designs architecture with two level of network: one for separation and another for classifying. The inception V3 pre-trained prototypical was adjusted using the BRATS input vector. Dominant Rotated Local Binary Patterns and Deep features were integrated via fundamental array-based splicing (DRLBP). The characteristics are subsequently reduced using Particle Swarm Optimization. Outcomes on the dataset show a 92 percent accuracy. The characteristics are subsequently concentrated using Particle

Swarm Optimization. Measurements on the BRATS sample show a 92 overall accuracy.

2.8.3.1 Quantitative Analysis of 2020 Model and Algorithm

Figure 2.26 shows that during 2020, individuals employed CNN the most, despite the fact that more projecting and efficient designs exist in the review. This is due to CNN's great generalizability, consistency, and accuracy rate.

2.8.4 Technical investigations carried out in 2019

In Deepak, et. al.,2019, the authors of this research paper focus on 3 class classification problems distinguished among pituitary, glioma, and meningioma tumors. The cataloguing of brain tumors is challenging research in itself, and the classification of its subtypes is even more difficult. These encounters accredited to the subsequent factors: Brain tumors parade high variability due to their intensity and size; tumors with different pathological types can show similar looks. Remove the obstruction and overcome; the author's methodology made some contribution in this area. The algorithm proposed by the Authors is modified to study features of tumor brain MRI images and uses GoogLeNet. The authors emphasized this and stated that the model learned transfer has a softmax classifier layer that classifies the image into three tumor classes and takes the image's data from it in a figshare. When excellent CNN facilities are on condition that to well-established pattern classifiers, better performance expected. In work authored by Authors, features verified on two cliques of classifier replicas other than softmax classifiers within deep learning. These classifiers are SVM and K-Nearest Neighbor (KNN). In this work, the performance criteria was observed in such manner. The deep transferable learnt (standalone) prototypical's classification accuracy is 92.30.7%, and it is even more efficient when using SVM on in-depth Feature extraction (97.80.2%) and KNN on in-depth CNN spotlights (98.00.4%).

The purpose of this study is to examine a deep learning method that has been advertised for use in brain cancer picture segmentation (Mittal, et. al., 2019). The two most well-known and widely used approaches are GCNN and SWT, or Growing

Stationary Wavelet Transform. Raising the correctness of the standard scheme is the primary objective of this effort. The author took into account and evaluated related studies using Support Vector Machine (SVM) and Convolution Neural Network (CNN) to define the surface of this work in order to characterise the methodological scope of the investigation. The researcher who conducted this work used MRI scans to segment brain tumours. This paper accomplished to achieve multiple automatic

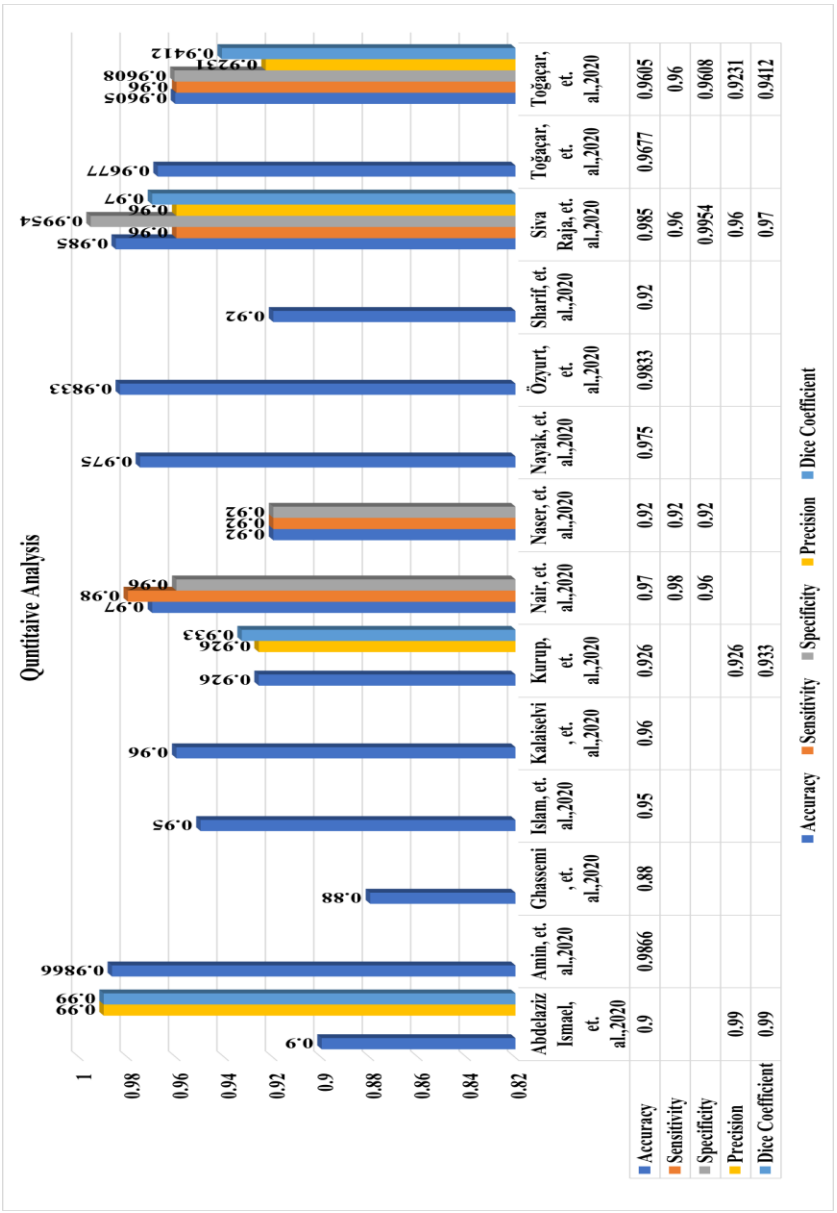

Fig 2.26 Quantitative Analysis for 2020 Model and Algorithm carried in studies

procedures such as feature extraction, segmentation, and presented technique illustrate large datasets and complex structure. Author's proposed methodology performed the following steps to materialized and simulated the result of accuracy: Execute skull stripping technique (initialise the media technologies if the first pixel is prominent pixel, then add label curblab) after pre-processing (normalise the MRI à undertake filtering using Weiner filter à Register to other input pictures). After locating the area of interest, third phase extracted features is carried out with the aid of SWT. Pop out an element, add à increment Curlab by 1, and then, if a neighbour is a forefront pixel, pop out that element.After completed this phase, GCNN is used to classify and train the abnormal and standard data. This paper provides a performance metric of comparison based on MSE, PSNR, SSIM parameter, and check the accuracy among the KNN, SOM, SVM, Genetic algorithm, CNN, and CNN.

In Sharif, et. al.,2020, the main highlights of the paper are that the proposed Pixel Growth along with Limit based augmentation method, segmentation of tumor carried out through saliency-based deep learning, Active feature selection (based on PSO optimization), comparison of features. In this paper, the author concentrates on the high-grade glioma tumor and suggests a deep learning-based feature selection method. The primary step is contrasting enhancement and provided to SbDL for construction of the saliency map and applying simple thresholding to analyze in the form of binarized. In the phase of classification, the Inception V3 pre-trained CNN model administered for the mining of the in-depth feature. For better texture analysis, dominant rotated LBP concatenated with the resulted features. After that, the led vector is concentrated and optimized with the help of a particle swarm optimization technique. Using a softmax classifier classifies the optimized result presented experiment framed in two phases. In the first stage, BRATS-2017 and BRATS-2018 datasets used to validate the SbDL approach and the dice score for the dataset of BRATS 2017 is 83.73% (Core tumor) for the entire and enhanced tumor is respectively 93.7% and 79.94%. The dice score obtained for the BRATS 2018 is 88.34% for Core, 91.2% for the whole, and 81.84% for enhanced. In the new stage,

authors applied the classification approach on BRATS-2013, BRATS-2014, BRATS-2017, BRATS-2018, and find out the average accuracy as a result is more than 92%.

In Aljunid, et. al.,2019, The methodology employed in this research study is based on the utilisation of Naïve Bayes classification, clustering, and morphological scanning. This process involves analysing the input image using clustering and morphological scanning techniques to identify distinct and related clusters within the image. The Naïve Bayes classifier method was employed to address the issue of tumour detection. In this article, the authors examined the outcome based on the following parameters: Peak Signal-to-Noise Ratio, MSE, calculation of overlapping area, and defect detection. The advanced technique is utilised to verify the accuracy of the analysis in relation to the provided parameters. This proposed method achieved high precision, with a remarkable 86% accuracy in detecting cells.

In Talo, et. al.,2019, the study of this paper focuses on presenting an approach that automatically classifies normal and abnormal brain MRI with the use of deep transfer learning. A foundational component of the deep learning system, ResNet34 is a convolutional neural network. To complete the assignment, the writers relied on deep learning techniques. The authors anticipated a 5-fold classification method to authenticate the accuracy. This paper evolved three stages (Stage1, Stage 2, and Stage 3), divided by the epochs in increasing order and finding the accuracy value for each stage in terms of training loss and validation loss. During 5-fold training, broach overlapping results of a confusion matrix for each stage and examined all stages in abnormal and normal classes. The sensitivity, average precision, validation accuracy, and F1-Score used to fix the trueness of the presented model. For stage 1 abnormal class (Precision – 98.16%, Sensitivity - 99.65%, F1-Score – 98.90%) , normal class (Precision – 71,66%, Sensitivity – 56.00%, F1-Score – 61.51%) and overall accuracy 97.86 ±1.24, For stage 2 abnormal class (Precision – 97.84%, Sensitivity - 100%, F1-Score – 98.90%) , normal class (Precision – 80.00%, Sensitivity – 48.00%, F1-Score-57.85%) and overall accuracy 97.86 ±1.48, For stage 3 abnormal class (

Precision-100%, Sensitivity 100%, F1-Score 100%) , normal class (Precision 100%, Sensitivity 100%, F1-Score 100%) and overall accuracy 100%.

In contrast to Deep Convolutional Neural Network (Chen, et. al.,2020), the author proposed a Deep Convolutional Symmetric Neural Network (DCSNN) that automatically segments the brain tissues. The proposed methodology was validated and analyzed in the BRATS2015 dataset and given some baselines for that. The projected technique attained an average DSC of 0.852. The proposed method does not produce the best result in the BRATS2014 dataset, but this method gives on other DCNN-based ways.

This article (Thaha, et. al., 2019) suggested an Enhanced Convolutional Neural Networks with the loss function optimised using the BAT method to address the issue of manually segmenting data. Creating an optimized image segmentation is the primary objective in this proposed methodology for understanding and optimizing MRI image segmentation. For the pre-processing operations, image enhancement algorithms and skull stripping used and experimental results of the projected practise show better performance associated to existing methods.

The authors of one of the types of research in (Alagarsamy, et. al.,2019) used the proficiency of compression methods to improve the execution time and accuracy of CNN in brain MRI categorization. Before categorization, authors introduced a unique stage of pre-processing. The approach first uses a Probabilistic Neural Network (PNN) for the process of segmentation the Region of Interest (ROI) (mostly brain tissue region), and then uses two layers for the Back Propagation Neural Networks to compress the ROI (BPNN). Last but not least, the compressed pictures are sent into CNN for classification. The findings were collected for three distinct kinds of optimizers for the determination of comparison and showed accuracy rates of more than 90%.

Another research Kaur, et. al.,2019 exploits the effectiveness of the newly created Capsule network. Convcaps is the term given to a new Capsulenet model created by

the authors. They fed the network two inputs: a tumour picture and a segmented tumour area. In addition, a novel loss function is added to optimise the model in all ways. As per the assessment with other approaches, six various types of tests were carried out by modifying the input, and the findings reveal that the optimised method provides the maximum accuracy of 93 %.

Narayanan, et. al.,2019 assesses the density of the RESNET34 architecture's efficient usability. For demonstrating and creation of a novel algorithm G-RESNET, the authors used the fundamental deep RESNET34 method. In this new method, the flattening layer is replaced by a max pooling layer, and implemented of a novel loss function. Different versions of the reduction function and the universal max pooling layer were tested independently to determine their impact on the precision of classification. Lastly, an experiment employs fusion of feature for high-level and low-level traits. According to the findings, the newly projected G-RESnet with feature fusion feature fusion and enhanced loss function enhanced loss function achieves 95 percent accuracy.

Another study's authors (Mekhmoukh, et. al., 2019) also presented a novel approach to cancer detection and classification. The proposed technique leverages score side by side fusion of the outcome routes from pre-trained Googlenet and Alexnet. Their approach uses linear and log transformations to pre-process the raw MRI pictures the tumour is then segmented using morphological and thresholding processes, and the segmented region is then used with the BRATS dataset to categorise the tumour as high or low grade. The recommended methodologies' accuracy has improved as a result of the findings. The training duration and loss curve were also compared to state-of-the-art methods by the authors.

A modified version of the model developed by Ari and Hanbay (Fernandes, et. al.,2019) is presented in Elazab, et. al.,2019. The suggested approach alters the prior model's pre-processing and classification stages. Because median filtering keeps the edges while reducing noise, the system employs it for pre-processing. Second,

because the function sigmoid is incompetent for classes of multiple images classification difficulties, the model utilises a modified SoftMax function in the convolution network. The last step uses the watershed algorithm and morphological procedures to segment the tumour. Finally, the findings were presented, 97 % rate of accuracy and half in processing time.

In order to determine if brain MRI pictures show tumours or non-tumors, the researchers in (Wong, et. al.,2019) used an 8-layer traditional Convolutional Neural Network (CNN) trained on a proprietary dataset. At first, the application sorts the photos according to the suggested Convolutional Neural Network (CNN). The next step, after cancer detection in the picture, is to segment it. The first step is to use a global thresholding approach to convert the picture to binary representation. Afterwards, morphological procedures and a watershed algorithm are used to isolate the cancer. The final step is to determine the tumor's dimensions. The results show that the suggested method is 98% accurate.

The requirement for a labelled dataset is one of CNN's limitations. The researcher missions in (Zhou, et. al.,2019) addressed this issue. This research revolves around a fundamental idea: representing 3D magnetic resonance image scans by breaking them down into 2-dimensional slices to be utilized as input arrays. The DENSEnet-LSTM, DENSEnet-DENSEnet, and DENSEnet-RNN models were developed using deep learning and compared. The first model uses DENSEnet to extract features, and the second model uses a Recurrent Neural Network (RNN) to classify data. The DENSEnet learning algorithm was used in the model overview, and the Long Short-Term Memory (LSTM) technique of classification algorithm was applied. Accuracy rates of 87%, 92%, and 91% were found in the three methods, according to the testing data.

2.8.4.1 Quantitative Analysis of 2019 Model and Algorithm

Unlike prior years, a significant amount of effort was put on identifying and categorising brain tumours in MRI scans in 2019. Researchers moved their focus back

to image improvement approaches by applying several pre-processing techniques to the input brain MRI datasets. They began by combining several machine and deep learning approaches to create hybrid models. Fig 2.27 shows the analysis for 2019 algorithm.

2.8.5 Technical investigations carried out in 2018

In Raju, et. al.,2018, the author of this paper strong imposes that segmentation of brain tumor is a noteworthy job in processing of medical image as well as also state that MRI is not adequate for diagnosing and identifying the intracranial tumor, but This needs detailed classification based on segmentation of brain tumor MRI images and segmentation technique. Authors offered research papers that summarized those non-tumorous tissues and tumorous tissues cubicle in the brain are exciting areas for segmentation and classifying brain tumors and to overwhelmed the challenges tackled by traditional methods. For the subdivision operation of the brain tumor, this paper used the baysian fuzzy clustering technique. The classification of this proposed method regulates brain tumors' neck and neck with the help of Bayesian fuzzy clustering using the basis features set on it. The BRATS database used to authenticate the effectiveness of the projected method and to test the efficiency of the technique using it. The expected HCS-based tumor classification and segmentation accomplishes a classification accuracy of 0.93 and improves comprehensive segmentation approaches.

This paper Zhao, et. al.,2018 proposed a unified framework that obtains the result of segmentation in terms of appearance and spatial consistency. Authors have used Conditional Random Fields with Fully Convolutional Neural Networks. They have trained this segmentation model in the following steps: First, to teach FCNNs using image patches; Second, Image parts were used with FCNNs parameters to train CRF as a Recurrent Neural Network (CRF-RNN); and Third, fine-tuning the CRF-RNN and the FCNNs using image slices. The authors presented the method that performed the segmentation operation slice by slice. Authors used BRATS-2016, BRATS-2015, and BRATS-2013 datasets for evaluation of the given model.

Interval Type-1 Fuzzy C-Means (IT2FCM) segmentation, which is centered on BAT, has been created as a better-quality brain image segmentation technique in (Kaur, et. al.,2018). In order to reduce the computing complexity of the IT2FCM process, the BAT technique aids in locating the ideal cluster placement.

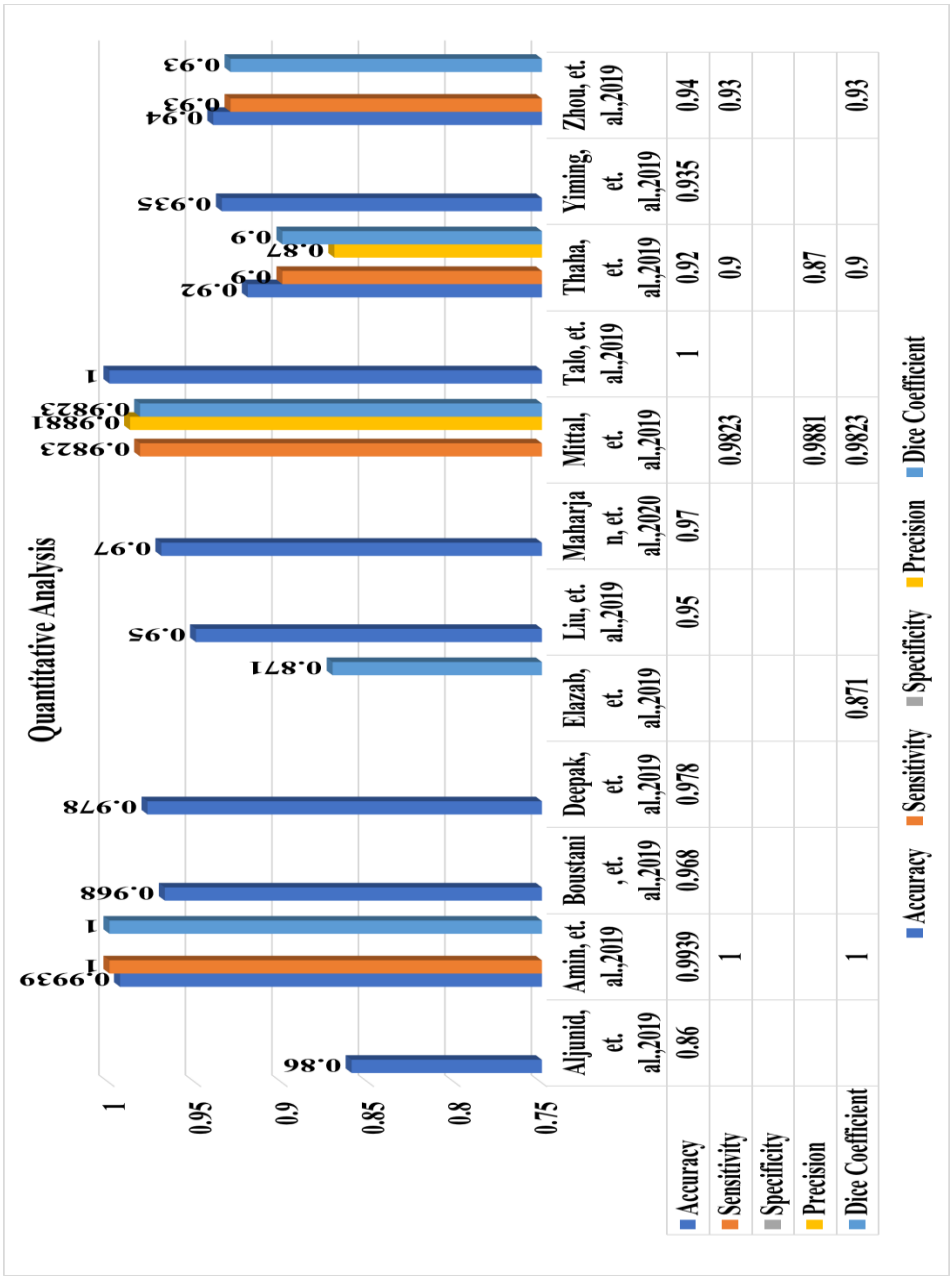

Fig 2.27 Analysis for 2019 Model and Algorithm carried in studies

In [64], the authors used CNN to categorise tumour and non-tumor pictures from the radiopedia datasets and BRATS 2015. The plan was to train only the last coating of the CNN prototypical and then use the ImageNet features retrieved. Back propagation was calculated using the gradient decent approach. The accuracy was only discovered by the authors, who then compared it against DNN and SVM. Their projected method has a 97 % accuracy rate.

2.8.5.1 Quantitative Analysis of 2018 Model and Algorithm

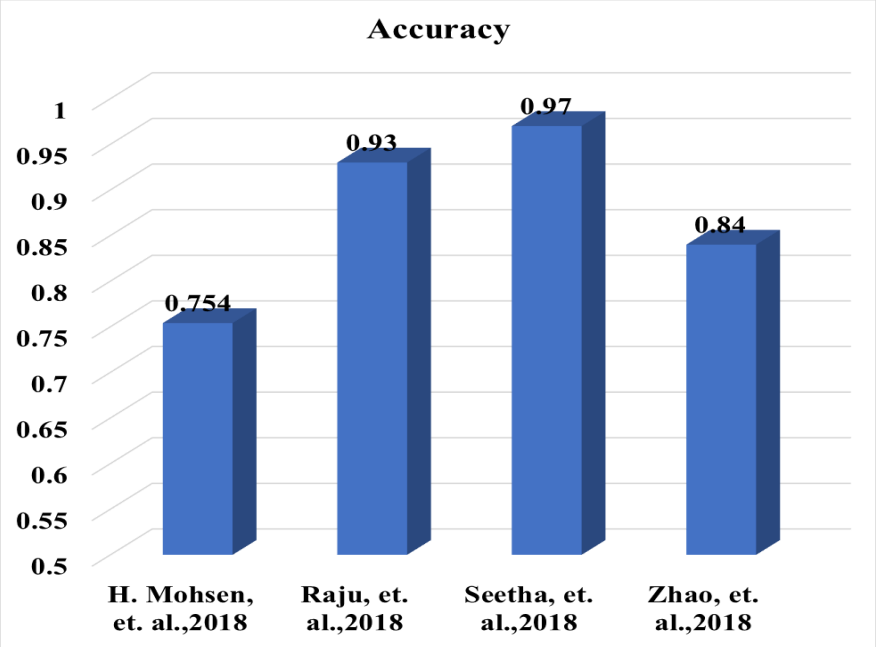

Fig 2.28 Analysis of Accuracy for 2018 Model and Algorithm carried in studies

2.8.6 Technical investigations carried out in 2017 and 2016

In Amin, et. al.,2017, Muhammad Sharif, Javeria Amin, Mussarat Yasmin, and Stephen Lawrance Fernandes have proposed a methodology validated on three benchmarks dataset: Harvard, Rider, and Local. The author's main contribution to this research is that the paper proposed an automatic method that detects and classifies the

intracranial tumor at the level of image and lesion. By this automated methodology, it quickly distinguished between brain tumor and non-tumorous MRI. In this automated proposed methodology exist several stages: pre-processing, classification, and feature extraction. In the author's methodology, the first stage is to segment the candidate lesion and apply various methods on that segment. In the next step, for each candidate wound, they have involved shape, texture, and intensity-based feature sets. Finally, several tests completed on the designated feature extract set to select a more suitable classification strategy. The author's proposed methodology achieved performance in terms of the multiple parameters Like average 0.98 area under the curve, 97.1% accuracy, 91.9% sensitivity, and 98.0%.

In Sachdeva, et. al.,2016, the mainstay of the experimented research paper is to propose a communicating CAD framework for multiclass brain tumor classification. To achieve the targets, authors used the first dataset of Astrocytoma, childhood tumor-Medulloblastoma, Meningioma, and Glioblastoma Multiforme along with subordinate tumor-Metastatic. In subsequent dataset mostly focus on Low-Grade Meningioma, Astrocytoma, and Glioblastoma. To mark the tumor segment region, the author used the active contour model and saved it as a segment region of interest. After applying this methodology, 71 texture and intensity feature set has extracted. Genetic algorithms impose on this input set and select the optimal feature set from that. This paper investigates and proposes two hybrid frameworks for machine learning that are applied by means of the Genetic Algorithm with substantiation of artificial neural network and support vector machine. Testing results from the first dataset showed that the Genetic Algorithm optimization approach amplified the overall accuracy of SVM (79.3% to 91.7%) and ANN (75.6% to 94.9%). The accuracy result of individual class which is delivered by Genetic Algorithm–Support Vector Machine in different parameter like that GBM (83.3%), AS (89.8%), MEN(91.8%), MED (95.6%) and MET(97.1%) and carried by Genetic Algorithm–Artificial Neural Network classifier on the following parameter: GBM (86.6%), MED(93.3%), AS(96.6%), MET (100%)

and MEN(96%). Comparable individual results found from the second dataset. Accuracy of Support Vector Machine has improved result 80.8% to 89%, and for Artificial Neural Network has exceeded as of 77.5% to 94.1%. Separate class accuracies of Genetic Algorithm and Support Vector Machine in term of the following parameter like that AS (83.3%), LGL (88.8%), MEN (93%) and for Genetic Algorithm-Artificial Neural Network classifier has proved the accuracy result like that AS(92.6%), LGL(94.4%), MED(95.3%). Hence experiment results have shown that the Genetic Algorithm-Artificial Neural Network classifier has indicated better outcomes than Genetic Algorithm-Support Vector Machine.

With the use of a framework developed in (Alfonse, et. al.,2016) for the categorization and segmentation of brain tumours from MR images. After using the Fast Fourier Transform (FFT) feature to extract the models, the adaptive threshold technique was used to segment the models. Next, the element was selected using the Minimal Redundancy Maximal Relevance Techniques, and then the normality and abnormality of the intracranial images were catalogued. The suggested method has a classification accuracy of 98.9%.

Tolerance Rough Set Firefly based Quick Reduct (G., et. al.,2016), a novel procedure has projected in this paper. This hybrid-based intelligent algorithm is a feature selection for MRI brain image that emphasizes the advantages and characteristics of basic models and their limitations. Features mined from segmented MRI metaphors based on strength, size, and texture. This paper hybridizes the Firefly Algorithm (FA) and Tolerance Rough Set (TRS) to select the brain tumor's experimental features to generate an intellectual system that can moderate the characteristics and limitations of basic models.

2.8.6.1 Quantitative Analysis of 2017 and 2016 Model and Algorithm

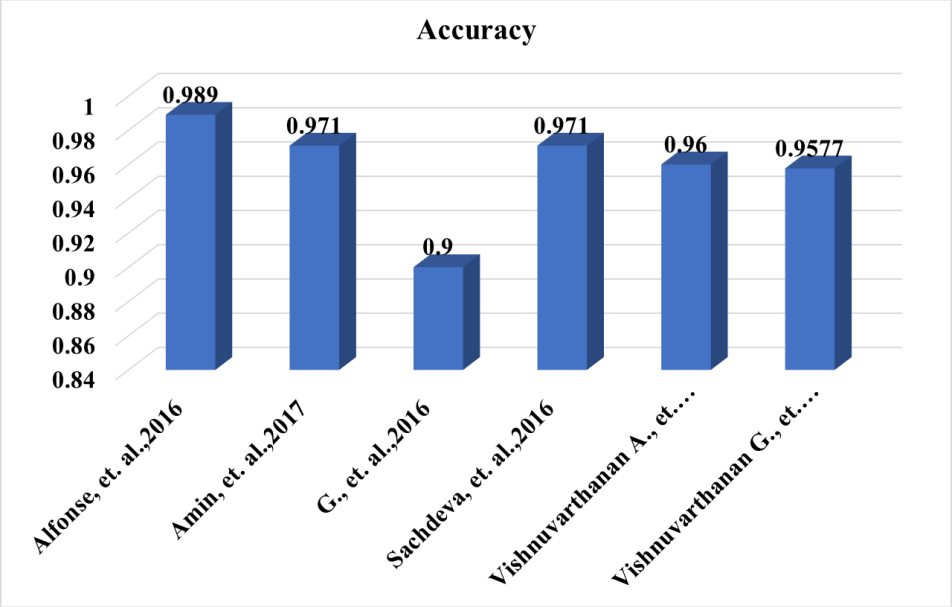

Figure 2.29 Analysis of Accuracy for 2017 and 2016 Model and Algorithm carried in studies

2.9 Algorithmic Development from 2015-2022

Deep learning methods are utilised for the categorization and detection of MRI images, as well as for the pre-processing and segmentation. As in Fig 2.30, 2015 was the weakest year for deep learning progress. Deep learning elicited a tepid reception from the general public. They were acquainted with machine learning techniques and didn't want to devote any time on deep learning. From mid-2017 to mid-2019, a lot of effort on algorithm development was done. In the meanwhile, others experimented with various algorithms. The pre-processing of MRI images became the focus of study in 2019, which prompted the creation of new algorithms using deep learning for this use. Data augmentation caused the paradigm to shift from manual to automated. The whole focus of the year 2020 was on testing various data augmentation, feature extraction, and pre-processing techniques and algorithms. Algorithmic progress was modest, and there were no significant architectural advancements during this time. During the year 2022, conventional or current models were used with little revisions.

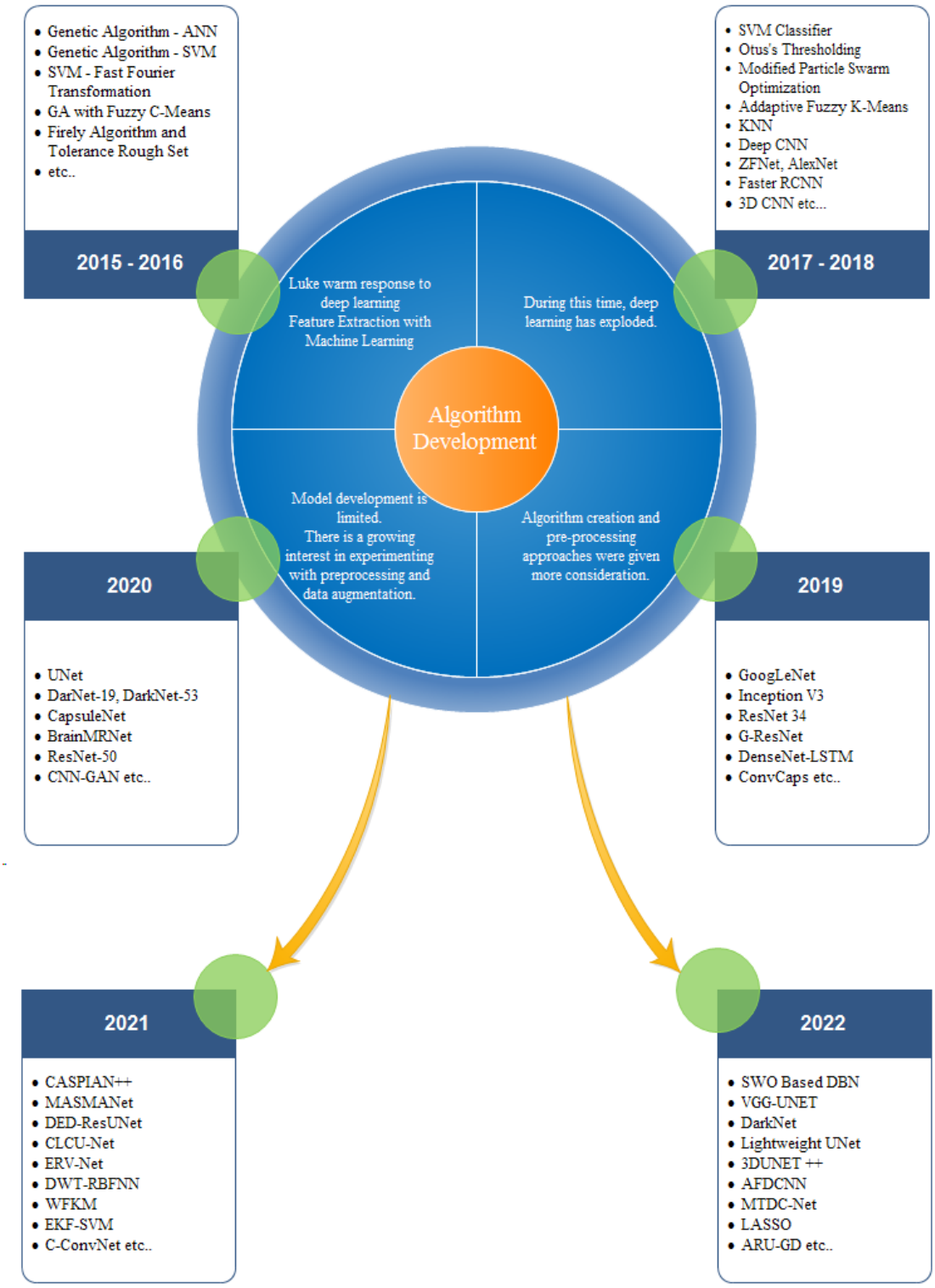

Fig 2.30 Algorithmic Development

2.10 Factors that Impair Performance

The in-depth examination of current methodologies aided us in compiling a list of critical components that affect the CAD system's performance directly or indirectly. The performance of a given Deep Learning algorithm developed for classification is harmed by a number of things. These variables have an equivalent impact on other tasks. Fig 2.31 shows how they can be classified.

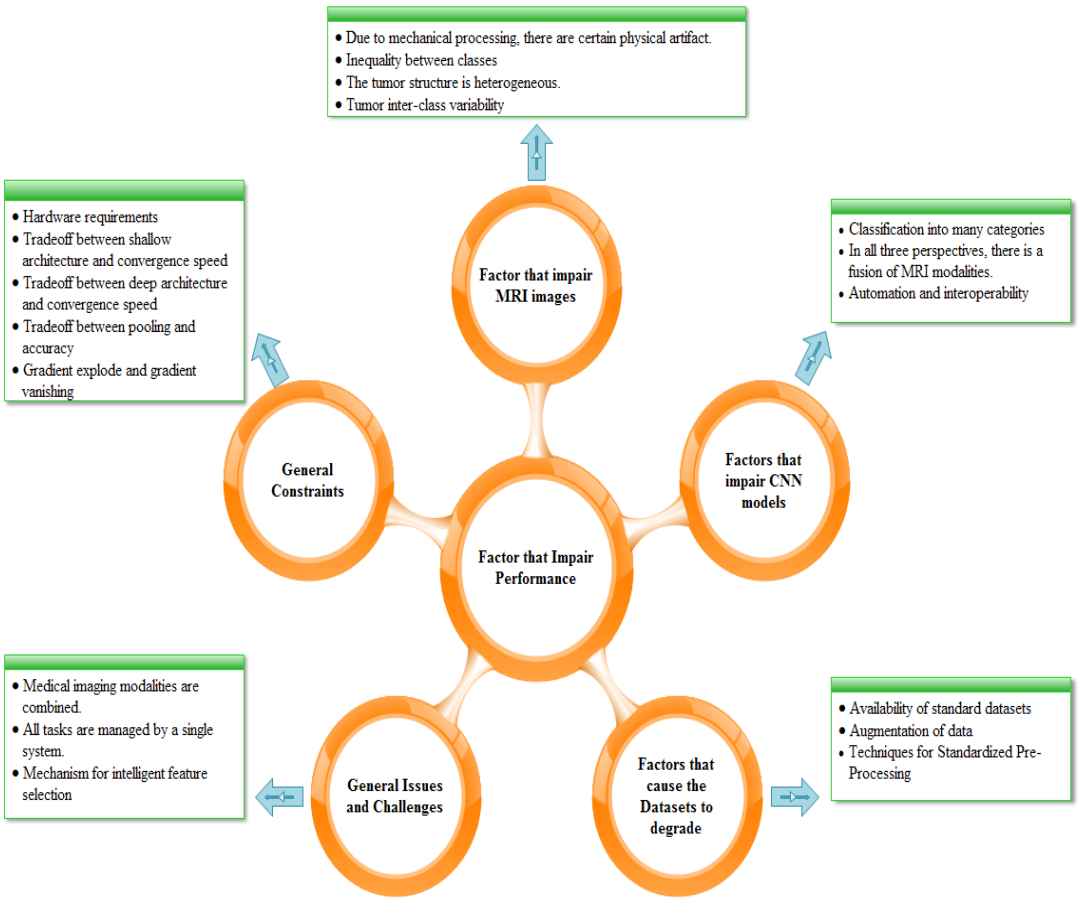

Figure 2.31 Factor that impairs performance (Nazir M, et. al.,2021)

2.11 Techniques for Improved Performance

Based on the thorough critical analysis shown above, certain performance enhancement strategies are offered, and some studies have supported them as important components for good performance (Fig 2.32). This component was

developed to make it possible for academics and scientists working on this topic to combine all of the scattered solutions offered in all of the studies to build effective, durable CAD systems.

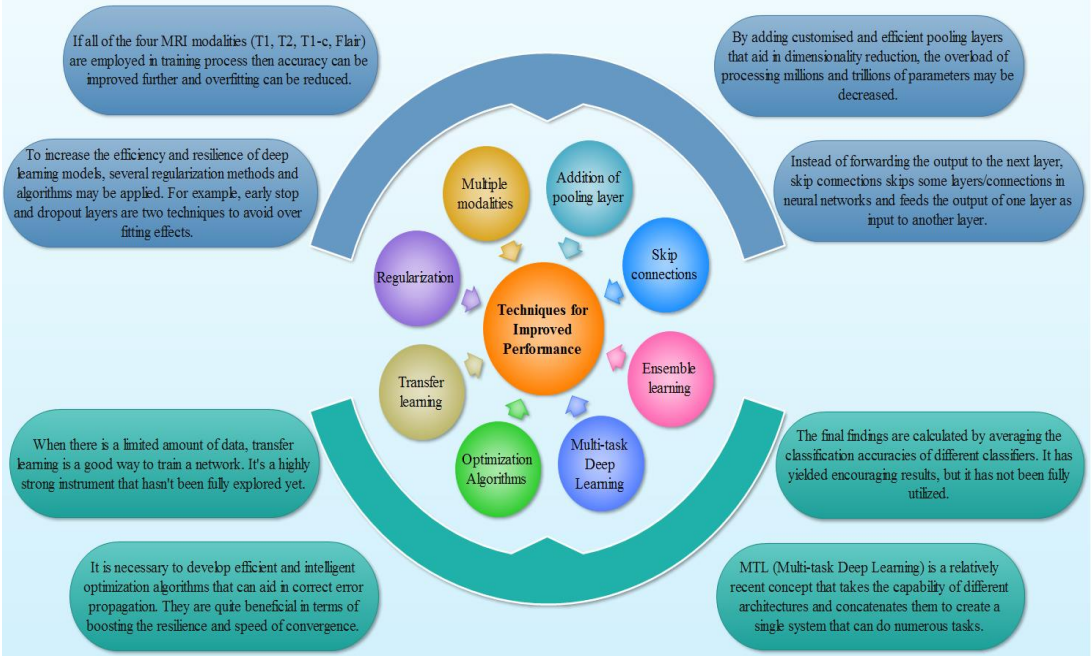

Fige 2.32 Techniques for Improved Performance (Nazir M, et. al.,2021)

2.12 Research Gap and Objective

The prediction of brain tumors and assessing their likelihood in patients pose ongoing challenges for researchers. The use of MRI scans has opened up new avenues of research in the field of brain tumors, including tasks like classification, prediction, and segmentation. Researchers investigate various aspects of tumor characteristics, including their location, shape, deep features, and intensity. To improve regression-based approaches, there's a growing need for more extensive exercise data. Furthermore, the duration of tumor persistence varies among high-grade glioma patients, spanning long-term, short-term, and mid-term cases.

Several key challenges and research gaps exist in the domain of tumor recognition:

(i). Gliomas, the predominant forms of primary brain tumors, exhibit diverse levels of aggressiveness, distinct prognoses, and variable histological subregions. Consequently, the utilization of advanced monitoring algorithms becomes crucial for classifying tumor survival durations into long-term, short-term, and midterm categories.

(ii). Concerning the segmentation task, current consensus seems to favor a cascaded or hierarchical approach. This involves initially distinguishing between normal and abnormal/tumorous tissue and subsequently proceeding with the segmentation of tumor subregions.

(iii). The interplay between Deep Learning and traditional Machine Learning methods is a significant area of focus, particularly for addressing clinically relevant challenges like predicting clinical outcomes, such as overall survival. This becomes particularly challenging when dealing with smaller training datasets.

(iv). To improve survival prediction for long-term, mid-term, and short-term survivors, it is required to optimise feature selection approaches and use different network designs and training procedures.

(v). To create additional examples of brain tumour lesions, data augmentation methods including scaling and rotation are used. Nevertheless, problems with class imbalance may be introduced by these methods.

(vi). It's worth mentioning that the majority of deep learning methods used for brain tumour analysis are still struggling with reinforcement categorization, which leaves the network unsure of the exact location of the patch.

The objective is to enhance model performance in terms of prediction accuracy, robustness, and the mitigation of overfitting, as well as reducing error-related indications. Therefore, the problem can be formulated as follows:

(i). Explore novel approaches for brain tumor segmentation.

(ii). Develop a framework capable of distinguishing between tumor and non-tumor images.

(iii). Conduct a comparative analysis of methods at each stage of the model and select the most suitable one for survival predictions.

(iv). Model framework for detection and localization the brain tumor

(v). Compute various metrics such as accuracy, sensitivity, specificity, DSC, etc., to bolster the model's effectiveness at each level.

Thus, the aim of this problem statement is to introduce a computational model for Glioblastoma Brain tumor. This model encompasses network architecture, feature extraction and selection, segmentation, and detection, all geared towards predicting brain tumor survival.

2.13 Conclusion

This chapter has thoroughly examined the scope of brain tumour segmentation and classification, encompassing a range of conventional and contemporary approaches. The investigation of conventional techniques, such as threshold-based methods, region-based methods, edge-based methods, and atlas-based methods, offers understanding into the historical development of segmentation procedures. The discourse surrounding machine learning-based classification techniques, including k-Nearest Neighbour, Bayesian approach, Support Vector Machine, Random Forest, and clustering, demonstrates the advancement of computer technologies for brain tumour analysis. The constraints of traditional methods emphasise the necessity for sophisticated methodologies, leading to the investigation of deep neural networks (DNN), specifically convolutional neural networks (CNN). An analysis of current approaches for segmentation and classification, the datasets employed, and the metrics used to evaluate performance offers a thorough comprehension of the cutting-edge advancements in this domain. The comprehensive analysis of prior research conducted between 2015 and 2022 demonstrates the evolution of studies throughout the years, providing quantitative evaluations of models and algorithms for each year

under investigation. The process of identifying variables that hinder performance and implementing ways to enhance performance lays the foundation for identifying research gaps and objectives. This chapter establishes a strong basis for the proposed research by integrating information from earlier studies. It directs the reader towards the distinctive contributions and breakthroughs that the current study seeks to accomplish in the ever-changing field of brain tumour segmentation and classification.

CHAPTER 3
PRELIMINARIES

The focus of this chapter is on investigating the techniques used for MRI image pre- and post-processing. Further investigation into standardised datasets for comparison and assessment criteria is also included.

3.1 Techniques for Pre-processing

The goal of pre-processing methods applied to MRI images is to enhance the foundational data with the aim of optimizing the image for segmentation. These approaches encompass the removal of unwanted components from the input, enhancing images using noise, and aligning or resampling them with a reference image. This alignment enables the extraction of features from corresponding positions across several images.

Pre-processing often encompasses various essential stages, such as bias field correction, image registration or resampling, skull stripping or, brain extraction and intensity normalisation. When working with publicly available datasets that might have undergone partial pre-processing, additional pre-processing steps are selectively applied as needed, based on specific requirements.

3.1.1 Image Registration and Sampling

Image registration involves the resampling and alignment of an image to a common image space, ensuring the extraction of features from corresponding locations across different images. There are two primary situations where image registration is necessary:

1. When there is variation in the orientation of the input images.
2. When handling many modalities of a single input picture, each with its own orientation.s

In the initial scenario, all input images undergo resampling in order to align with a reference anatomical template. Figure 3.1 demonstrates manually outlining tumours and pre-operative alignment for malignant and lower-grade tumours in the left hemisphere. The tumour is manually delineated inside the patient's coordinate system, shown by the colour blue, while the matching estimated volume of the target is shown in green within the anatomical reference coordinate system. The tumour segmentation following the linear transformation is depicted in the colour orange, whereas the tumour segmentation following the non-linear transformation is illustrated in the colour red.

The image's upper row captures the radiographic profile of a patient grappling with glioblastoma, juxtaposed with the lower row portraying the imaging specifics of a patient contending with a lower-grade glioma. The photos illustrate a progression from left to right:

(A) Patient-centric domain,

(B) Anatomical reference framework,

(C) Linear conversion of the patient's spatial coordinates to the anatomical reference space,

(D) Non-linear transformation of the patient's spatial coordinates to align with the anatomical reference space.

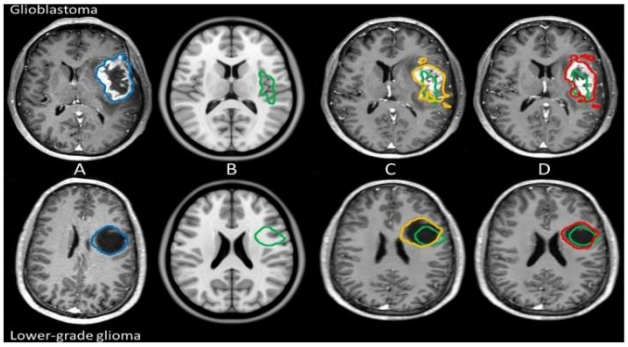

Fig 3.1 Pre-Processing: Image Registration (Visser et. al, 2020)

3.1.2 Skull-Striping

Skull-stripping, a pivotal facet in neuroimaging and medical image processing, serves to meticulously eliminate non-brain elements from an image. This intricate method isolates the brain region by adeptly identifying and segregating the intricate structures while delicately excluding surrounding elements like the scalp, skull, and meninges. (Thakur et. al. 2019).

Skull removal serves as a critical step to heighten the precision and efficiency of subsequent image processing tasks like brain segmentation, registration, and feature extraction. By meticulously isolating the brain, researchers gain the ability to delve into the analysis and comprehension of brain structures and functions without interference from extraneous non-brain tissues. This undertaking is particularly pivotal in studies exploring brain abnormalities, aiding in disease diagnosis and intricate brain mapping endeavors, where precise and reliable delineation of brain regions holds utmost importance (Dandil et al., 2014). Figure 3.2 visually contrasts a brain image with and without the removed skull, exemplifying the significance of this process.

3.1.3 Correction for Bias Field

The bias field manifests as a gradual and low-frequency strength shift crossways the image, introducing variations in tissue appearance at different locations. Rooted in imperfections during image capture and anatomical disparities related to a patient's morphology, posture, alignment, and magnetic permeability, the bias field arises from dual sources (Song et al., 2017).

Typically expected to be multiplicative or cumulative, the cumulative form in MRI results from magnetic field amalgamation, while the multiplicative form is contingent on receiving coil sensitivity (Lefkovits et al., 2015).

Enter the N3 bias field correction, employing an iterative B-spline least-squares fitting procedure. An evolution of this method, the N4 bias field correction by Tustison et al. (2010), refines the process by determining residual bias fields rather than total bias fields. Adopting a multiresolution approximation approach, the N4 bias field correction enhances efficiency and reduces execution times. Visualized in Figure 3.3, the implementation of N4ITK bias field correction on a FLAIR image vividly demonstrates the resulting extracted additive bias field.

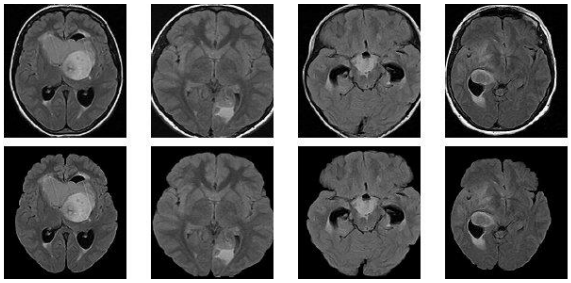

Fig 3.2 Pre-processing: Skull Stripping Process (Dandil et. al., 2014)

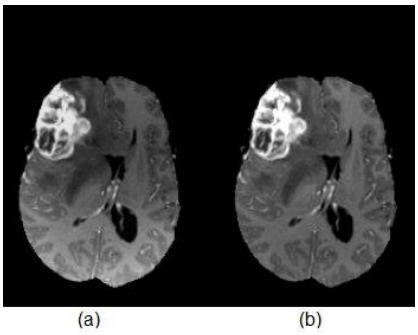

Fig 3.3 MRI scan (a) before (b) after N4ITK bias field correction.

3.1.4 Intensity Normalization

In the intricate realm of image analysis, intensity normalization emerges as a pivotal pre-processing technique, orchestrating the harmonization of intensity values within an image or image set onto a uniform scale. The essence of this normalization lies in transcending the challenges posed by intensity fluctuations, fostering not only comparability but also precision in analyses and insightful comparisons (Alnowami et al., 2022).

Within the domain of medical imaging, intensity normalization takes center stage, acting as a virtuoso conductor orchestrating the alignment of intensity distributions across images sourced from varied patients, scanners, or imaging protocols. This orchestration becomes crucial due to the inherent variability in intensity values attributable to diverse factors like imaging settings, acquisition parameters, or individual patient characteristics. The normalization process is a meticulous dance, a rescaling of intensity values with a commitment to preserving their intrinsic relationships. The several methods that make up this symphony include min-max scaling, z-score normalisation, histogram equalisation, and linear scaling.

By weaving the magic of intensity normalization into the fabric of image analysis, researchers and practitioners not only diminish the impact of intensity variations but also elevate the performance of algorithms and models. The outcome is a dataset finely tuned for quantitative analysis and comparison, a transformative resonance particularly resonant in the realms of image registration, segmentation, and classification within the realms of medical imaging and computer vision applications (Pereira et al., 2016).

3.2 Dataset

In the vast landscape of segmentation methodologies, a multitude of approaches have been presented in the literature, each vouching for its effectiveness and contribution across various dimensions. Initially, these techniques found application in images sourced from private hospitals or radiology laboratories, rendering them inaccessible for comparative assessments among different methods. This inherent limitation posed a barrier, hindering researchers from conducting comprehensive evaluations.

To surmount this challenge, the research community responded by constructing publicly accessible datasets and evaluation frameworks. These initiatives aimed to facilitate the comparison and assessment of different segmentation methods through standardized metrics. An illustrious example in this domain is the Multimodal segmentation challenge dataset, commonly referred to as BraTS (Pereira et al., 2016;

Bakas et al., 2017). Serving as a cornerstone resource for addressing issues related to brain tumors, the BraTS dataset is widely employed for both segmentation tasks and prognostic predictions.

Comprising images associated with both High-Grade Glioma and Low-Grade Glioma, the BraTS presents a comprehensive and diverse collection of brain tumor cases. The public availability and well-defined characteristics of this dataset empower researchers to confidently leverage it for their experiments, fostering a collaborative environment for advancements in segmentation research.

- The dataset is composed of multi-parametric MRI images, encompassing volumes in T1c, T1, T2-FLAIR, and T2 modalities.
- The images in the dataset are sourced from a diverse array of institutions, utilizing various 2D or 3D clinical protocols and scanners with magnetic strengths ranging from 1.5T to 3T.
- To ensure coherence and enable effective comparisons, the dataset underwent meticulous pre-processing procedures, focusing on harmonization and standardization. These techniques are intricately designed to preserve the informational essence of the images while maintaining the distinct characteristics.
- Each individual scan has undergone alignment with a T1 reference anatomical template, followed by interpolation, guaranteeing consistent and equal resolution in all directions. Additionally, the implementation of skull-stripping techniques enhances the precision and accuracy of the dataset.

3.3 Overall Survival Prediction Task

The BraTS 2017 competition introduced an intriguing facet by incorporating an additional task, specifically honing in on the prediction of Overall Survival (OS) for individuals grappling with High-Grade Glioma (HGG). Beyond the wealth of imaging data, this dataset enriches the information pool with crucial details encompassing age, survival days, and resection status (Subtotal Resection – STR or Gross Total

Resection - GTR) for HGG patients. The primary objective of this challenge transcends mere classification; it seeks to stratify patients into three distinctive categories based on their survival timelines: those who endure mid-term survivors (OS days between 10 to 15 months), long-term (OS days > 15 months), and short-term survivors (OS days < 10 months). Illustrated in Figure 3.5 is an elaborate exploration of the OS-related data, providing an insightful panorama into the intricate dynamics of patient survival predictions that has been available since the BraTS 2017 competition.

Table 3.1 BRATS Dataset

Year	Total Images	Training Images	Validation Images	Testing Images	Tasks
2012	Clinical: 45 Instances Synthetic: 65 Instances	Clinical data: 30 instances (20 High-Grade Glioma + 10 Low-Grade Glioma) Synthetic data: 50 instances (25 High-Grade Glioma + 25 Low-Grade Glioma)	N/A	15 instances for Clinical Data 15 instances for Synthetic Data	Segmentation
2013	65 Instances	HGG: 51; LGG: 14	N/A	N/A	Segmentation, Disease Progression
2014	238 Instances	200	N/A	38	Segmentation, Disease Progression
2015	384 Instances	HGG: 220; LGG: 54	N/A	110	Segmentation, Disease Progression
2016	465 Instances	HGG: 220; LGG: 54	N/A	191	Segmentation, Disease Progression
2017	477 Instances	HGG: 210; LGG: 75	46	146	Segmentation, Survival Prediction
2018	542 Instances	HGG: 210; LGG: 75	66	191	Segmentation, Survival Prediction
2019	626 Instances	HGG: 259; LGG: 76	125	166	Segmentation, Survival Prediction
2020	660 Instances	HGG: 293; LGG: 76	125	166	Segmentation, Survival Prediction
2021	2000 Instances				Segmentation on sub-regions, Survival Prediction

In addition to BRATS Dataset (Table 3.1), there are other datasets available for research and experiments, which are listed in the fig 3.4.

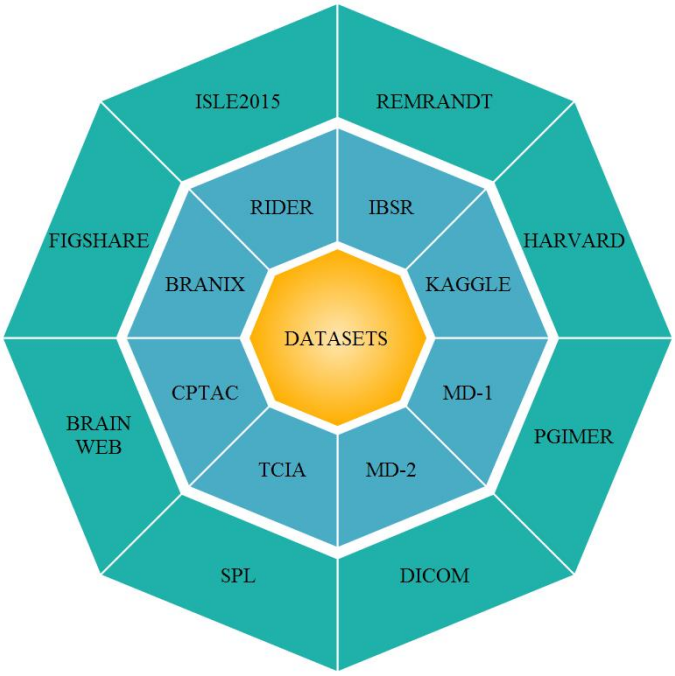

Fig 3.4 Dataset available for research and experiments.

3.4 Post-processing Technique

Post-processing techniques refer to a set of methods and operations applied to data or results after the primary processing stage. These techniques aim to refine, enhance, or extract additional information from the processed data to improve its quality, utility, or interpretability. Computer-assisted methods for segmentation may produce inaccurate segmentations in the image owing to inappropriate feature selection. However, post-processing techniques can enhance the segmentation by employing the following methods:

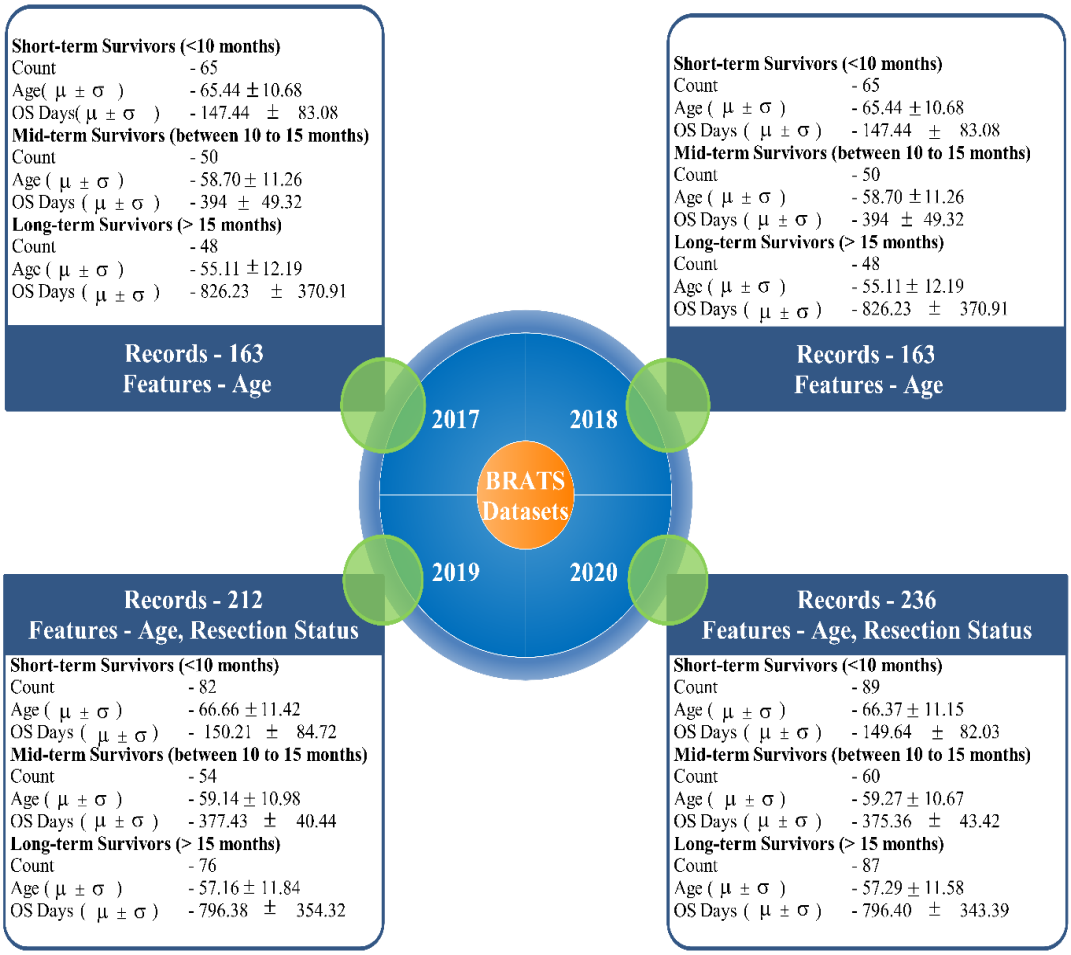

Fig 3.5 The arrangement of features from the BRATS dataset across survival classes.

2.4.1 Connected Component Analysis: Analysis of Connected Component, also known as Connected Component Labelling (CCL), is a fundamental image processing technique used to identify and label separate related areas or elements within a binary or segmented picture. In a binary image, pixels or voxels are classified as either foreground (typically represented by white) or background (typically represented by black). The CCA algorithm analyzes the binary image and groups adjacent foreground pixels into distinct connected components based on their spatial proximity. A connected component is a set of foreground pixels that are contiguous,

meaning they are connected through either thei r edges or corners. The primary goal of CCA is to label each connected component with a unique identifier or label so that further analysis or processing can be performed on individual regions separately.

2.4.2 Conditional Random Field: In the intricate realm of machine learning and the nuanced landscape of computer vision tasks, a Conditional Random Field (CRF) serves as a refined statistical model meticulously crafted to elegantly capture the complexities inherent in structured data representations. Conditional Random Fields (CRFs) are a specific kind of graphical model that may effectively represent intricate relationships and interconnections between variables in structured data. Conditional Random Fields (CRFs) utilise a graphical structure to organise data, with nodes representing random variables and edges representing the conditional connections between these variables. CRFs aim to represent the conditional distribution of the output variables (such as labels or states) based on the input variables (such as features or observations).

2.4.3 Morphological Operations: Morphological operations stand out as advanced techniques in image processing, intricately designed to scrutinize and reshape the contours and structure of entities within digital images. These operations find their roots in the principles of mathematical morphology, an intricately woven tapestry of mathematical set theory and geometry. In the realm of visual data transformation, these operations carve a distinctive path, offering precision and innovation. Morphological operations are primarily applied to binary images, where each pixel can have one of two values, typically representing foreground (object) or background. The operations involve the use of a small, predefined pattern called a structuring element or kernel. The structuring element moves over the image, and for each position, it is compared with the corresponding neighbourhood of pixels.

3.5 Evaluation Metrics

Embedded within the fabric of predetermined evaluation for tumor segmentation and the foresight of overall survival lies an intricate array of subsequent metrics.

I. **Dice Similarity Coefficient (DSC):** The Dice Similarity Coefficient, affectionately termed the Dice Index, unfolds as a nuanced quantitative measure navigating the terrain of binary images. It measures the degree to which systematically projected and true truth segmentations are in concord, serving as a discernible compass in the complex world of picture segmentation. The formula for calculating the Dice Similarity Coefficient is as follows:

$$DSC = (2 * |A \cap B|) / (|A| + |B|) \quad [3.1]$$

where:

- The symbol $|A \cap B|$ denotes the cardinality, or the number of items, in the intersection of sets A and B, which refers to the region where the two sets overlap.
- The sign $|A|$ represents the cardinality of collection A, which is the total number of items in the expected segmentation.
- The sign $|B|$ represents the cardinality of collection B, which corresponds to the overall number of items in the basic truth segmentation.

II. **Sensitivity:** Sensitivity, often hailed as the true affirmative prowess or recall prowess, emerges as a distinctive performance gauge in the realm of binary classification models. The level of accuracy with which the model identifies instances of positive within a dataset is finely measured by this parameter. In the context of binary classification, there are four possible outcomes for a model's predictions:

- True Positives: The methodology correctly classified instances as positive.
- True Negatives: Signifies cases where the model properly determined that the data was negative.
- False Positives: These occur when the algorithm incorrectly labels negative situations as positive.
- False Negatives: Eventualities that the model incorrectly interpreted as negative, even though they were actually positive.

Things that happened that the model assumed were unacceptable but out beneficial:

$$\text{Sensitivity (Recall)} = \text{TP} / (\text{TP} + \text{FN}) \quad [3.2]$$

Sensitivity serves as the litmus test for the model's prowess in pinpointing positive instances amid the vast landscape of actual favorable occurrences within the dataset. A robust sensitivity score signifies the model's prowess in unearthing positive cases, while a subdued sensitivity hints at the framework's challenge in navigating the realm of positive instance recognition.

III. **Specificity:** Among all the actual instances of negativity in a dataset, specificity measures how well a model using binary classification identifies negative situations. The determination of specificity involves the division of the true negative projections by the summation of actual rejections and false positives in the calculation process:

$$\text{Specificity} = \text{TN} / (\text{TN} + \text{FP}) \quad [3.3]$$

An apex of specificity underscores the model's finesse in astutely discerning negative cases, while a nadir in specificity unveils the model's inclination to misstep, mistakenly labeling negative instances within the positive realm.

IV. **Accuracy:** Accuracy, a linchpin metric in the evaluation realm, scrutinizes the efficiency of a classification model, whether navigating the landscapes of traditional learning or immersed in the complexities of deep learning tasks. This metric delves into the model's artistry, discerning its adeptness in accurately categorizing cases relative to the dataset's entirety.

$$\text{Accuracy} = (\text{TN} + \text{TP}) / (\text{TN} + \text{TP} + \text{FN} + \text{FP}) \quad [3.4]$$

A pinnacle in accuracy unveils the model's prowess in orchestrating a symphony of precise forecasts, while a dip in accuracy hints at the model's inclination to compose a melody marked by a higher frequency of imprecise predictions.

V. **Precision:** In the realm of binary classification models, precision emerges as a discerning metric, especially when the goal revolves around mitigating false positives (FP). This statistic unfurls as a poetic measure, quantifying the harmony between accurate positive predictions and every positive forecast crafted by the model, offering a nuanced symphony of accuracy assessment.

$$\text{Precision} = \text{TP} / (\text{FP} + \text{TP}) \quad [3.5]$$

VI. **F1-Score:** Embedded within the neural network architecture, Fully Connected Layers, also known as the dense layers, stand as the backbone of not only Convolutional Neural Networks (CNNs) but also various intricate blueprints in the expansive landscape of deep learning. These layers play a pivotal role, intricately weaving together complex data connections to birth conclusive classifications or informed suggestions. What sets them apart is their knack for harmonizing precision and recall, sculpting a singular statistic that judiciously appraises the classifier's prowess. Precision, a distinguished metric in this assessment, unfurls its tapestry by calculating the ratio of spot-on positive

predictions (true positives) to the entirety of positive forecasts (encompassing both authentic positives and deceptive positives). This metric not only scrutinizes the classifier's aptitude in accurately identifying negative occurrences as negative but also dances delicately, avoiding the misstep of erroneously categorizing them as positive.

$$\mathrm{F1-score} = 2 * (\mathrm{recall} \times \mathrm{precision}) / (\mathrm{recall} + \mathrm{precision}) \quad [3.6]$$

The F1-score can be anywhere from 0 to 1, with 0 indicating inadequate performance and 1 suggesting excellent recall and precision.

VII. **Loss:** In the expansive landscape of deep learning, loss, a multifaceted entity also recognized as cost or objective function, emerges as the alchemist measuring the intricate dance between the model's predictions and the elusive true target values. This enigmatic function, akin to a masterful conductor, orchestrates the symphony of the model's performance, delving into the nuances of precision woven into its forecasts during the intricate ballet of training.

Throughout the training process, the model endeavours to minimise the loss by modifying its parameters, including weights and biases, utilising optimisation procedures such as gradient descent. The goal is to identify the most favourable combination of parameters that leads to the minimal loss, hence enhancing the model's performance.

VIII. **Tversky Loss:** In the intricate realm of image segmentation tasks, particularly within the intricate tapestry of medical image analysis, the Tversky loss unfurls as a subtle yet potent arbiter, delicately measuring the likeness between the predicted partition and the tangible segments. This avant-garde approach, akin to a bespoke rendition of the Dice Similarity Coefficient (DSC), gracefully steps into the limelight with a unique prowess tailored for the idiosyncrasies of unbalanced datasets. These datasets, marked by a

pronounced asymmetry in instance numbers across classes, find refuge in the specialized artistry of this method.

The Tversky loss is mathematically defined using the following formula:

$$\text{Tversky Loss} = 1 - (\text{Tversky Index}) \quad [3.7]$$

where:

$$\text{Tversky Index} = (\text{TP}) / (\text{TP} + \alpha * \text{FP} + \beta * \text{FN}) \quad [3.8]$$

TP: "True Positives" refers to the quantity of voxels or pixels that were accurately identified as positive.

FP: "False positives" refer to the amount of pixels or voxels that were incorrectly identified as positive.

FN refers to the count of incorrectly classified negative pixels or voxels, also known as false negatives.

The values of the parameters α and β are used as weights to modify the ratio of false positives to false negatives.

The Tversky Index is a generalized form of the Dice Similarity Coefficient (DSC), where the parameters α and β allow for fine-tuning the loss to emphasize either false positives ($\alpha > \beta$) or false negatives ($\alpha < \beta$).

By using the Tversky loss as an optimization objective during training, the model can effectively handle class imbalance and provide better segmentation results, particularly when the dataset contains a disproportionate number of pixels or voxels belonging to one class compared to the other.

IX. **MeanIOU:** When evaluating semantic segmentation models, one frequent measure to utilise is Mean Intersection over Union, often known as mIOU. When used to a segmentation problem, it calculates the mean intersection over union of all classes. The purpose of semantic segmentation is to label each area or pixel in a picture with a unique class. For every dataset class, the Mean

IOU determines the degree to which the anticipated and ground truth segmentations match.

$$\text{IOU (Class\_i)} = \text{(Intersection (Class\_i) / Union (Class\_i))} \quad [3.9]$$

where:

Intersection (Class_i): The count of pixels accurately identified as Class_i by both the anticipated segmentation and the actual truth segmentation.

Union (Class_i): The cumulative count of pixels categorised as Class_i in either the anticipated segmentation or the ground truth segmentation.

The Mean IOU is then calculated as the average of the IOU scores across all classes:

$$\text{Mean IOU} = \frac{\left(\text{IOU (Class}_1\text{)} + \text{IOU (Class}_2\text{)} + \ldots + \text{IOU (Class}_n\text{)}\right)}{\text{Number of Classes}} \quad [3.10]$$

The Mean IOU serves as a comprehensive metric, offering insights into the model's segmentation accuracy across all classes. A heightened Mean IOU signifies superior performance, where a perfect segmentation alignment is denoted by a value of 1.0, while lower values indicate less precise segmentations. Widely employed in image segmentation tasks, particularly in domains like object detection, scene understanding, and medical image analysis, Mean IOU is a crucial measure for assessing the precision and quality of a model's predictions.

3.6 Conclusion

This chapter offers an in-depth exploration of the foundational steps crucial for the effective execution of the envisioned research. The pre-processing manoeuvres, encompassing facets like bias field correction, sampling, skull-stripping, image registration and intensity normalization, not only form the bedrock but also elevate the caliber and uniformity of medical imaging data. The meticulous curation and

priming of the dataset, as deliberated upon, stand as linchpins in guaranteeing the pertinence and dependability of the study. Furthermore, the delineation of the overarching task involving overall survival prediction serves as the focal point, accentuating the pragmatic application of the proposed methodologies within a clinical ambit. Post-processing strides, play a pivotal role in refining segmentation outcomes and amplifying the precision of overall survival predictions. The introduction of evaluation metrics crafts a robust framework for scrutinizing the model's prognostic capacities. The integration of post-processing phase not only fortifies the resilience of segmentation results but also augments the trustworthiness of overall survival predictions. In essence, this comprehensive exploration spanning pre-processing, dataset preparation, task delineation, post-processing, and evaluation metrics lays a sturdy groundwork for ensuing chapters, setting the stage for an intricate exploration of proposed methodologies and their resonance in steering the research towards triumph.

CHAPTER 4

MODEL FRAMEWORK FOR DETECTING AND LOCALIZING THE BRAIN TUMOR

The chapter begins with the model outline of the classification, identification, and localization of tumours. It suggests an advanced algorithm as a foundational layer, along with localization strategies. The classification approach utilises advanced deep learning algorithms such as Inception-V3, InceptionResNet-V2, MobileNet, NASNetMobile, ResNet-101, Xception, DenseNet, ResNet-50, and EfficientNetV7 as the base layer. In addition, a further layer of activation, normalisation, and denseness is added to the structure. Within the framework of a multi-branch network design, the robustness of recurrent segments was implemented in conjunction with a diversified collection of convolutional kernels. It is essential to make a distinct distinction between the head, which predicts, the body, which processes data, and the stem, which processes data intake. Deep neural networks have consistently made use of this design outline over the course of the years that have followed. In this architecture, the number of convolutions responsible for processing the item at the outset determines the stem. They obtain the essential object and are able to deduce fundamental information from it. After this, the technique incorporates a sequence of convolutional frames. The next step, which might include an identification and localization issue, is for the brain to make a link between the recognised attributes and the relevant classification. The RESUNET paradigm is employed in the second technique for the goal of partitioning and localising brain tumours by making use about MRI scans acquired through the TCGA.

First and foremost, this chapter adds the following:

- Employing a data generator that scales data from 0 to 1 and performs a 0.1 validation to facilitate the categorization process.

- Presenting a system that uses Deep Learning to detect and categorise brain tumours automatically.
- Evaluating the effectiveness of the proposed classification model in comparison to previously published deep learning models.
- To develop and trained a model of localization with the help of REEUNET in order to precisely pinpoint the location of the tumour.

Deep learning is a research field that models its methods after how the human brain works. The field's overarching objective is to model its operations after how people normally collect, process, and understand data. Both Kumar and L. (2018) and Srinivas et al. (2022) agree that it is crucial to data science since it speeds up and improves data processing and generates patterns that inform decision-making. The training of networks of neurons that are capable of acquiring knowledge on their own through the use of both labelled and unlabeled input is essential to the process of deep learning. Learning with supervision algorithms requires considerable feature extraction, which is a precondition for deep learning techniques. Deep learning techniques considerably reduce the requirement for considerable feature extraction. According to Muniasamy and Alasiry's research from 2020, this is achieved by the technique of data compression, the transformation of images into fundamental structures, and the building of network architectures that effectively eliminate repetition. The Convolutional Neural Network technique and architecture are well-known in the field of supervised neural network training. Big datasets are utilised for learning convolutional deep neural networks. These networks possess the capability to independently retrieve feature representations through the execution of convolutional operations. This eliminates the need for human feature extraction, which was previously necessary. The convolutional neural network construction consists of three separate layers of data: input, outcome, and hidden. The hidden layers consist of convolutional layers, layers that use Rectified Linear Unit algorithm, layers that use max pooling, and layers that are completely linked. Convolutional neural networks

are widely employed in deep learning for tasks such as voice, text, and picture identification as well as classification (LeCun et al., 2015, Ker et al., 2018).

4.1 Visualization and Dataset Analysis

The TCGA-GBM dataset, a component of a broader initiative, aims to foster a scientific community dedicated to establishing connections between cancer characteristics and genetic factors. It accomplishes this by providing patient images associated with individuals from the TCGA. In this context, one of the datasets that has been supplied by TCGA is comprised of 3929 MRI scans and the masks that correlate to them. In Figures 4.1 and 4.2, the fundamental and advanced visualisations of this customised dataset and distribution graph for tumour and no tumour are displayed. These figures also show the distribution graph for the tumour.

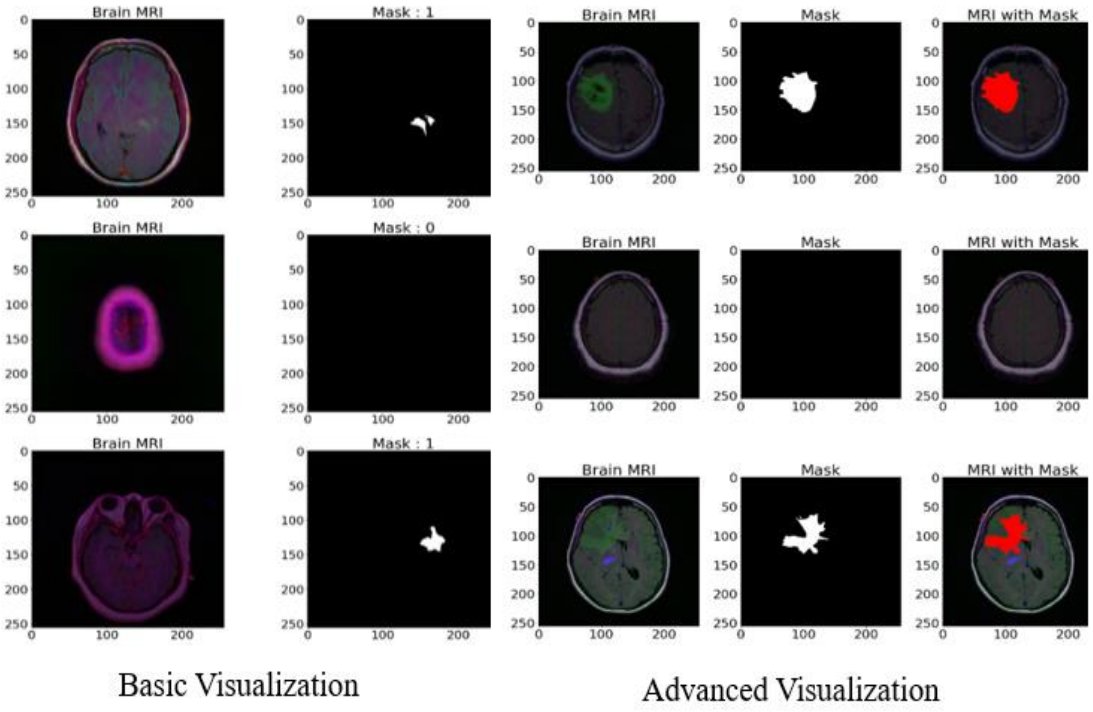

Fig 4.1 Imaging of the TCGA MRI Scan Visualisation

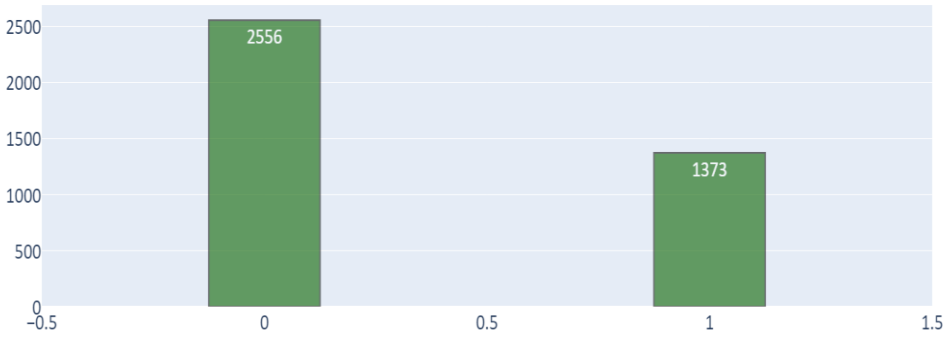

Fig 4.2 Distribution of Tumours (1) and the Absence of Tumours (0)

4.2 Pre-processing

During the first stage of processing, improving the level of contrast in MR images is the main goal, along with improving image quality and optimising the data. The first step in the process of aligning the dataset with the customised dataset is to remove any unnecessary data columns from the dataset completely. As a subsequent step, the information contained in the mask column is converted into a string format so that it can be utilised for categorization purposes. The data is subsequently divided into three sets: the one used for the training set, the set for validation, and the set being tested. This process is illustrated in Table 4.1 and Figure 4.2.

A data generator is created throughout the categorization step for use in the validation, testing, and training phases. The data generator in question employs a 256 × 256 target size, a batch size of 16, and a mode for classifying classes. This file must be created in order to fulfil the aims.

Table 4.1 Distribution the Dataset

S No.	Data	No of Images (Tumor and No-Tumor)
1	Train	2829
2	Test	786
3	Validate	314

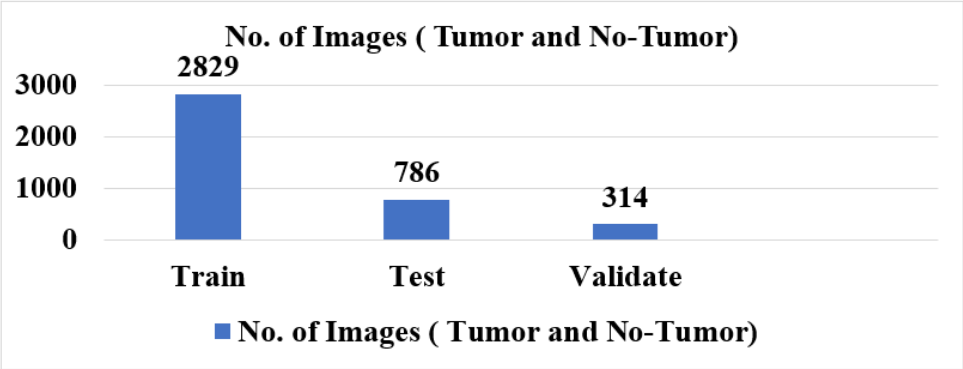

Fig 4.3 Split Data according to Train, Test and Validate

4.3 Adapted Techniques for classification as a Base Model

4.3.1 Inception V3

Inception V3, the latest iteration of the Inception framework introduced by Fettah et al. in 2022, stands out due to its incorporation of additional factorization principles. The Inception V3 model for image recognition utilizes batch normalization for input activation and employs Softmax for loss computation. It is made up of fully-connected layers, concatenation processes, convolutional layers, average and max pools, dropouts, and them.

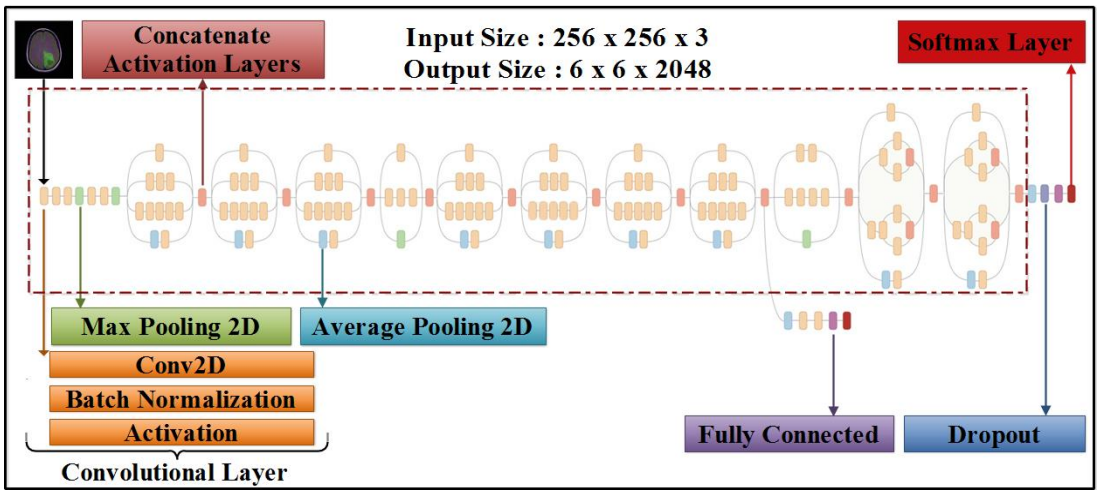

Fig 4.4. Inception V3 Model

With 42 strata and a rate of error that is lower than the earlier versions, the model of Inception V3 is shown in Figure 4.4. The following are the most noteworthy changes:

(i). **Factorized Convolutions:** While simultaneously monitoring the effectiveness of the network, the complexity of the algorithm is increased as the amount of constituents in a network is narrowed down.

(ii). **Smaller Convolutions:** Using smaller convolutions rather than larger ones speeds up the training process. This is because smaller convolutions are applied. When compared to the use of two 3x3 filters, which only require 18 variables (3x3 + 3x3), a 5x5 convolution with 25 components is more complicated than the latter. This is demonstrated in figure 4.5.

(iii). **Asymmetric Convolutional Spatial Factorization:** Instead of utilising a 3x3 convolution, you have the option to use a blend of 1x3 and 3x1 convolutions. It is crucial to acknowledge that this method would lead to significantly greater computational complexity when compared to the asymmetric convolution, as depicted in figure 4.6.

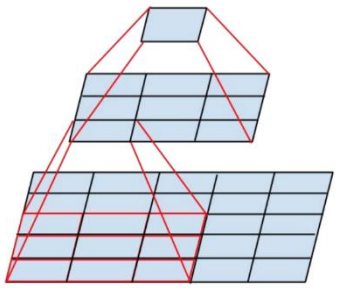

Fig 4.5. Smaller convolution

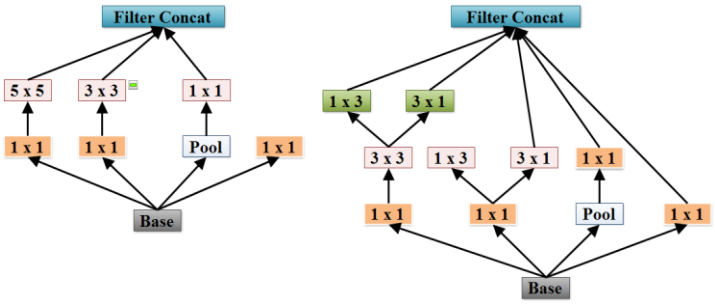

Fig 4.6. The process of factorising spatial data into asymmetric convolutions

(iv). **Incorporate Auxiliary Classifiers:** In order to incorporate an intermediate categorization into the learning process, a condensed Convolutional Neural Network (CNN) is utilised. Any errors that the CNN encounters are blended with the loss that the complete network experiences. While auxiliary categories were utilised to enhance the architectural complexity of GoogleNet,

they served as a structural element in guiding Inception V3. This is illustrated in figure 4.7.

(v). **Efficient Grid Size Reduction:** Grid size reduction is often achieved through pooling methods. Additionally, a more efficient approach is presented to address the inefficiencies in computational complexity, as illustrated in fig 4.8.

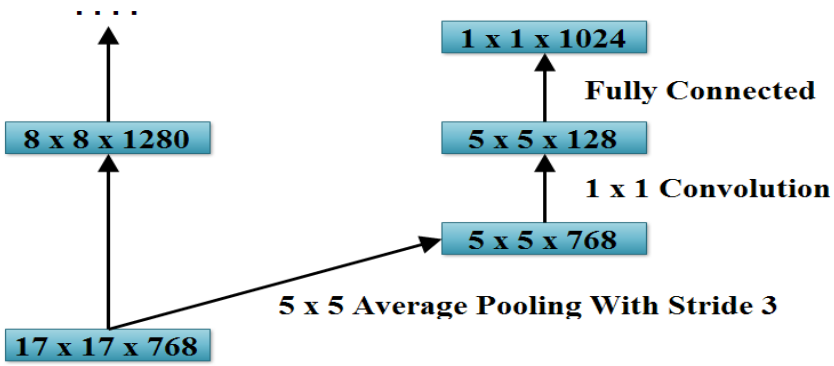

Figure 4.7 Auxiliary Classifier

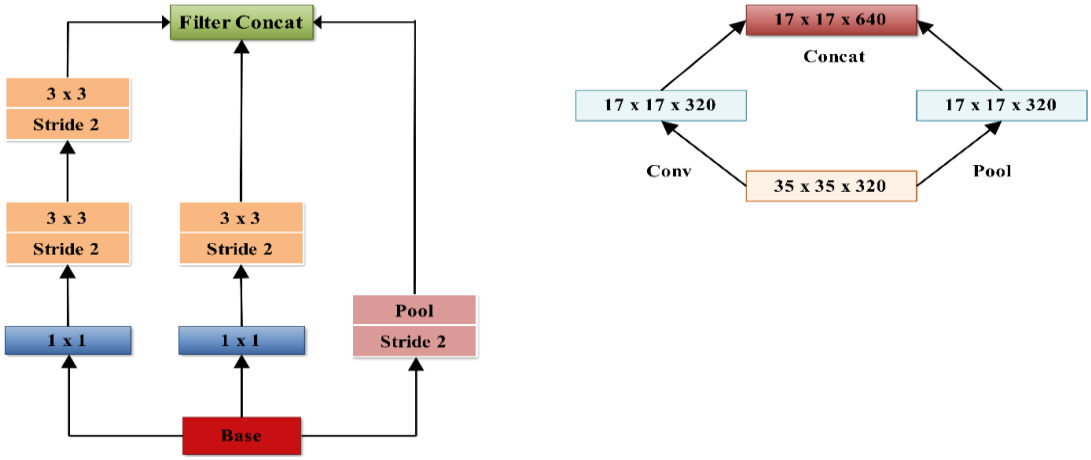

Figure 4.8 Grid Size Reduction

A convolutional neural network architecture, is quite complex due to its deep and intricate design. It's difficult to represent the entire architecture in a single equation, as

it involves many layers and parameters. However, I can provide a simplified representation of the forward pass through a single Inception module, which is one of the building blocks in InceptionV3. This will give you a sense of how the operations are structured within an Inception module. The Inception module is a key component of InceptionV3 and is represented as follows in mathematical notation:

Given an input tensor X, an Inception module performs the following operations:

Step 1. *1x1 Convolution:*

- ***i.*** *Apply a 1x1 convolution with N_1 filters and ReLU activation.*
- ***ii.*** *Denote the output as X_{1x1}.*

Step 2. *1x1 Convolution followed by 3x3 Convolution:*

- ***i.*** *Apply a 1x1 convolution with N_2 filter and ReLU activation to X.*
- ***ii.*** *Then, apply a 3x3 convolution with N_3 filter and ReLU activation to the result.*
- ***iii.*** *Denote the output as X_{3x3}.*

Step 3. *1x1 Convolution followed by 5x5 Convolution:*

- ***i.*** *Apply a 1x1 convolution with N_4 filter and ReLU activation to X.*
- ***ii.*** *Then, apply a 5x5 convolution with N_5 filter and ReLU activation to the result.*
- ***iii.*** *Denote the output as X_{5x5}.*

Step 4. *3x3 Max-Pooling followed by 1x1 Convolution:*

- ***i.*** *Apply 3x3 max-pooling to X with a stride and padding such that it retains the spatial dimensions.*
- ***ii.*** *Then, apply a 1x1 convolution with N_6 filters and ReLU activation to the result.*
- ***iii.*** *Denote the output as X_{pool}.*

Step 5. *Concatenation:*

i. *Concatenate the outputs X_{1x1}, X_{3x3}, X_{5x5} and X_{pool} along the depth axis to produce the modules final output.*

Mathematically, the concatenation operation is represented as:

$$output = concatenate\left(\left[X_{1\times1}, X_{3\times3}, X_{5\times5}, X_{pool}\right], axis = -1\right)$$

Each N_i represents the number of filters used in the corresponding convolutional layers, and you would have specific values for these parameters in the InceptionV3 architecture.

4.3.2 InceptionResNetV2

The complex convolutional neural network (CNN) architecture known as Inception-ResNetV2 (figure 4.9) was developed specifically for the purpose of performing computer vision and image classification tasks. It represents a fusion of two influential CNN architectures: Inception, known for its efficient feature extraction, and ResNet, renowned for mitigating training issues in deep networks. Inception-ResNetV2 combines the best of both worlds by incorporating Inception modules for feature extraction and ResNet's residual connections, which ease the training of very deep networks. Its architecture includes stem and grid components, with the stem handling initial image processing and the grid containing stacked Inception-ResNet modules.

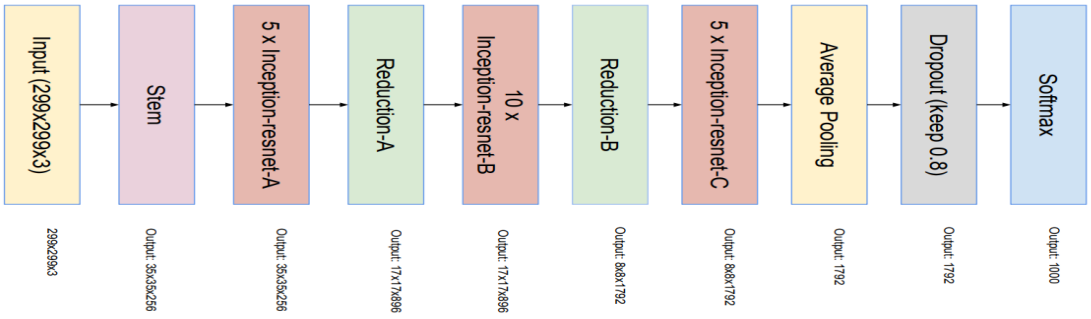

Fig 4.9 InceptionResNetV2 Overall Architecture (Inception V4 and Inception ResNets, 2022)

Combining concepts from both the Inception and ResNet architectures, Inception-ResNetV2 is a convolutional neural network with a deep design. Computer vision tasks such as object recognition and picture categorization are its intended use. Below is a detailed overview of the architecture (fig 4.10):

Stem Architecture:

- Input: Inception-ResNetV2 typically takes a 299x299 pixel RGB image as input.
- Convolutional Layers: In the first few layers of Inception-ResNetV2, a sequence of two-dimensional convolutional layers, batch normalisation, and ReLU activations are applied.
- Stem Max-Pooling: Max-pooling is a technique that is utilised to minimise the spatial dimensions while maintaining the essential characteristics.

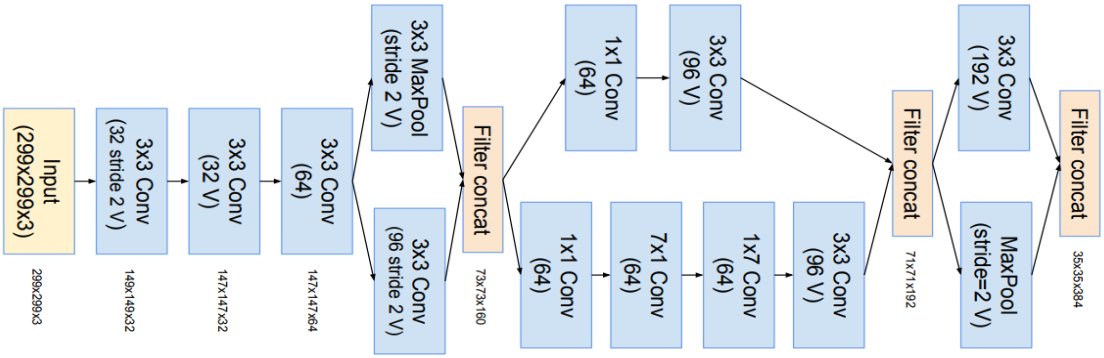

Fig 4.10 Stem Architecture (Inception V4 and Inception ResNets, 2022)

Inception-ResNet Blocks:

The core building blocks of Inception-ResNetV2 are Inception-ResNet modules. Each module combines the power of the Inception architecture and ResNet's residual connections.

- Inception-ResNet Module:
  - The process involves the input being guided via a sequence of parallel convolutional paths.

- The first path consists of 1x1 convolutions.
- The second path includes 1x1 convolutions followed by 3x3 convolutions.
- The third path includes 1x1 convolutions followed by 5x5 convolutions.
- The fourth path involves 3x3 max-pooling followed by 1x1 convolutions.
- The outputs of all paths are concatenated.
- A residual connection (shortcut) allows the gradient to flow directly through this module, improving training.

Grid Architecture:

Inception-ResNetV2 (fig 4.11 and fig 4.12) is organized into a grid structure that stacks multiple Inception-ResNet modules.

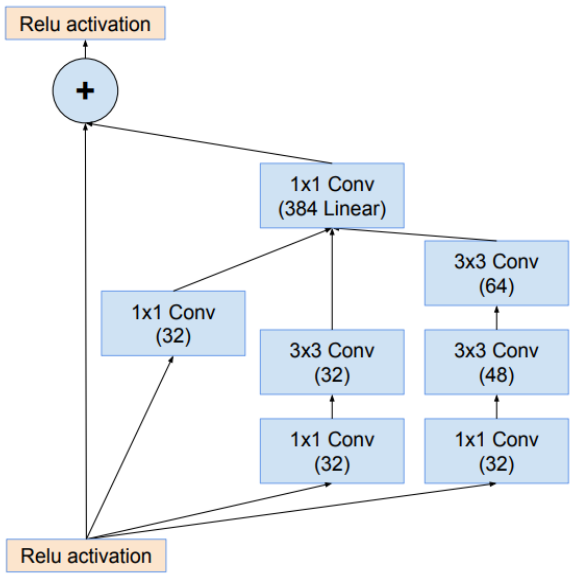

Fig 4.11 The schema represents the module of the Inception-ResNet-v2 network known as Inception-ResNet-A, which consists of a 35 x 35 grid.

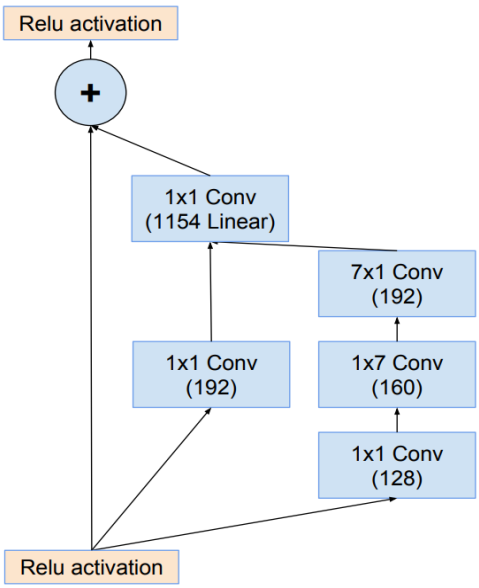

Fig 4.12 The schema represents the module of the Inception-ResNet-v2 network, namely the 17 x 17 grid (Inception-ResNet-B).

Reduction Blocks:

Throughout the architecture, there are also reduction blocks that are used to reduce the spatial dimensions while increasing the depth (fig 4.13 and fig 4.14).

- Reduction Blocks:
  - These blocks typically involve max-pooling and convolutions to reduce spatial dimensions and increase the number of filters in the feature maps.

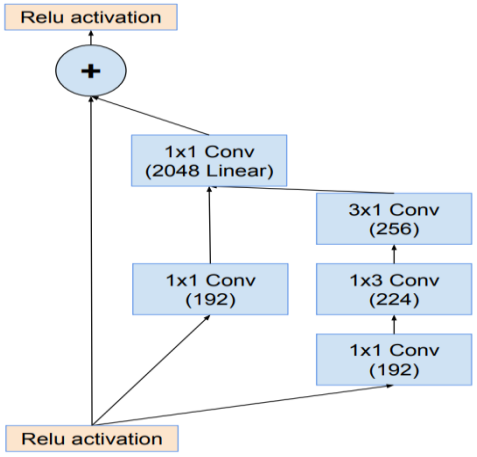

Fig 4.13 The schema for 8×8 grid (Inception-ResNet-C) module of the Inception-ResNet-v2 network.

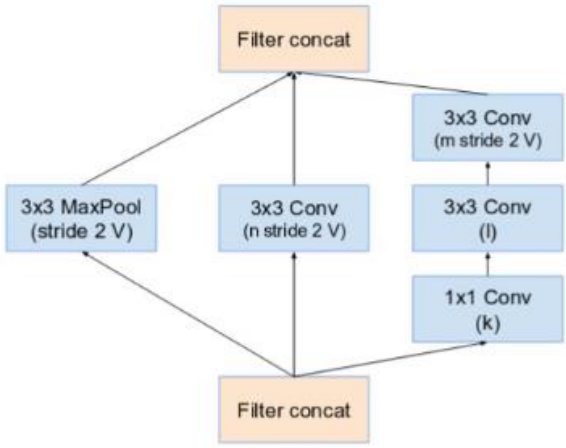

Figure 4.14 Reduction Block A (Inception V4 and Inception ResNets, 2022)

Fully Connected Layer:

- Global Average Pooling:
  - Instead of the traditional fully connected layers, Inception-ResNetV2 often uses global average pooling.
  - In order to reduce parameters and avoid overfitting, the Global Average Pooling method computes the mean of feature maps over all of their spatial dimensions.

Output Layer:

- Output Layer:
  - Class probabilities are generated by the learnt features in the last layer, which is a softmax layer.

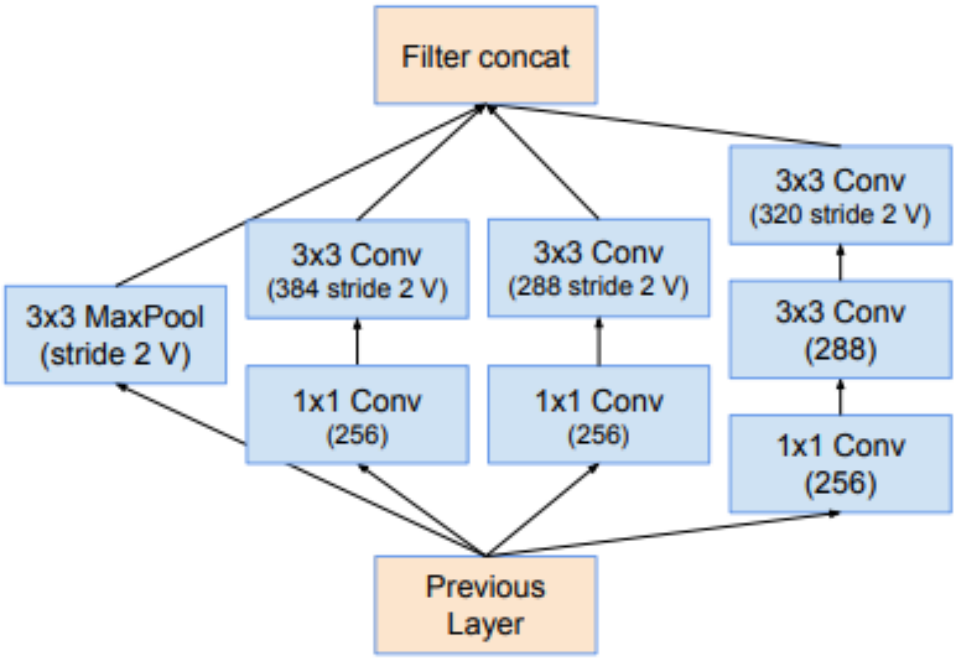

Fig 4.15 Reduction Block B (Inception V4 and Inception ResNets, 2022)

Inception-ResNetV2, like many complex neural network architectures, cannot be represented by a single mathematical equation due to its intricate design, multiple layers, and numerous parameters.

Let's denote the input tensor as X.

Step 1. ***1x1 Convolution Path:***

- ***i.*** *Apply a 1x1 convolution to X with N_1 filters and ReLU activation.*
- ***ii.*** *Denote the output as X_{1x1}.*

Step 2. ***1x1 Convolution followed by 3x3 Convolution Path:***

- ***i.*** *Apply a 1x1 convolution to X with N_2 filter and ReLU activation to X.*
- ***ii.*** *Then, apply a 3x3 convolution with N_3 filter and ReLU activation to the result.*
- ***iii.*** *Denote the output as X_{3x3}.*

Step 3. ***1x1 Convolution followed by 5x5 Convolution Path:***

- ***i.*** *Apply a 1x1 convolution to X with N_4 filter and ReLU activation to X.*
- ***ii.*** *Then, apply a 5x5 convolution with N_5 filter and ReLU activation to the result.*
- ***iii.*** *Denote the output as X_{5x5}.*

Step 4. ***3x3 Max-Pooling followed by 1x1 Convolution Path:***

- ***i.*** *Apply 3x3 max-pooling to X with appropriate stride and padding such that it retains the spatial dimensions.*
- ***ii.*** *Then, apply a 1x1 convolution to the pooled with N_6 filters and ReLU activation to the result.*
- ***iii.*** *Denote the output as X_{pool}.*

Step 5. ***Concatenation:***

- ***i.*** *Concatenate the outputs X_{1x1}, X_{3x3}, X_{5x5} and X_{pool} along the depth axis to produce the modules final output.*

Mathematically, the concatenation operation is represented as:

$$output = concatenate\left(\left[X_{1\times1}, X_{3\times3}, X_{5\times5}, X_{pool}\right], axis = -1\right)$$

The number of adjustments in the various layers of convolution is represented by Ni. This is just a simplified representation of a single module within Inception-ResNetV2. The complete architecture includes multiple such modules, fully connected layers, auxiliary classifiers, and other components.

4.3.3 MobileNet

For efficient and rapid image processing on low-resource devices like embedded systems and cellphones, MobileNet compiles many small deeply convolutional neural network architectures. MobileNet utilises depth-wise separable convolutions, which is a crucial advancement in contrast to conventional deep networks. This new development successfully reduces the complexity of computation and the number of variables without sacrificing accuracy. This architecture is highly optimized for mobile applications, enabling real-time object recognition, image classification, and more without requiring massive computational power or extensive memory.

MobileNet is a model that applies convolutional operations similar to those in traditional CNNs but employs a distinctive approach. It introduces the concept of depth convolution and point convolution, which differs from the standard convolution utilized in conventional CNNs. These novel techniques enhance the efficiency of CNNs in image prediction, allowing them to be effective in mobile systems. Because these convolution methods notably decrease comparison and recognition time, they yield rapid and accurate responses, making them our preferred choice for image recognition models.

(i). Depth-wise Convolution: Depth-wise convolutions involve the application of a single filter to each input channel, which distinguishes them from regular convolutions where filters are applied across all input channels simultaneously.

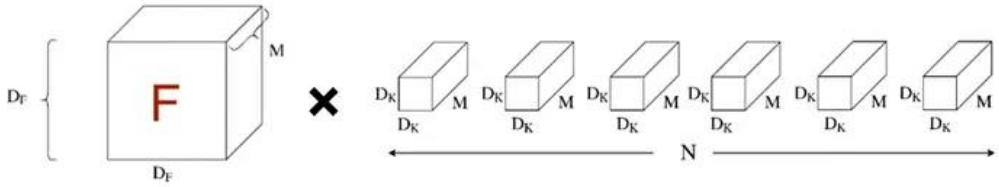

Fig 4.16 Standard Convolution (Pa, 2021)

Based on the image (fig 4.16) shown above, we can compute the computational expense as follows:

$$D_k . D_k . M . N . D_F . D_F$$

Here, DF stands for the input characteristic map's individual dimensions and DK for the convolution kernel's diameter. The amounts of the input channels are M and the amount of the outcome channels are N. The outcome and input channel, as well as the spatial metrics of the feature map of the input and convolution kernel, determine the computing effort and, consequently, the cost for a standard convolution.

In the scenario of depth-wise convolution, as depicted in the image below, there is an input feature map with dimensions D_F*D_F and M individual kernels, each having a channel size of 1.

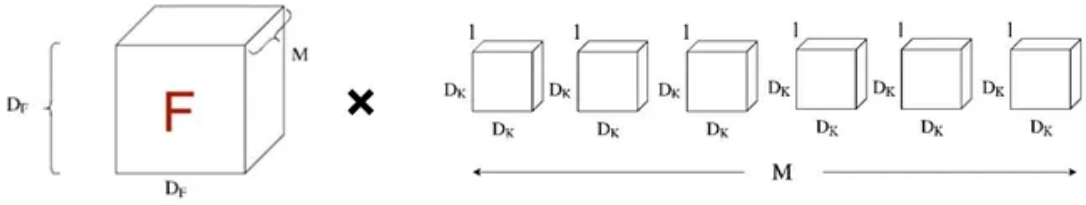

Fig 4.17 Depth-wise Convolutional (Pa, 2021)

Referring to the image (fig 4.17) provided above, it's evident that we can calculate the overall computational expenditure as follows:

$$D_k . D_k . M . D_F . D_F$$

(ii). Point-wise Convolution: Because the depth-wise convolution solely filters the input channels without merging them to create fresh features, an extra layer known as the pointwise convolution layer is introduced. Using a 1 × 1 convolution, the aforementioned layer calculates a linear combination of the outcome of the depth-wise convolution.

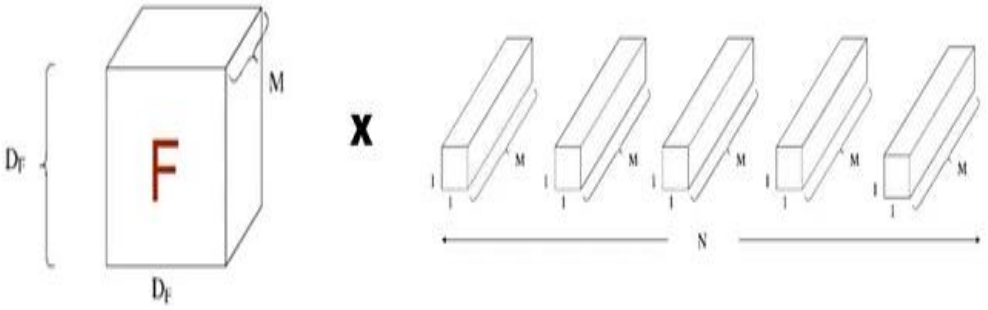

Fig 4.18 Point-wise Convolution (Pa, 2021)

Referring to the image (fig 4.18), let's once more determine the computational expense:

$$M.N.D_F.D_F$$

Therefore, we can compute the overall computational expenditure of Depth-wise separable convolutions as follows:

$$D_k.D_k.M.N.D_F.D_F + M.N.D_F.D_F$$

However, these technologies [figure 4.19] demand a powerful GPU to enhance the speed of comparisons among vast amounts of data, a capability not currently available on any mobile device.

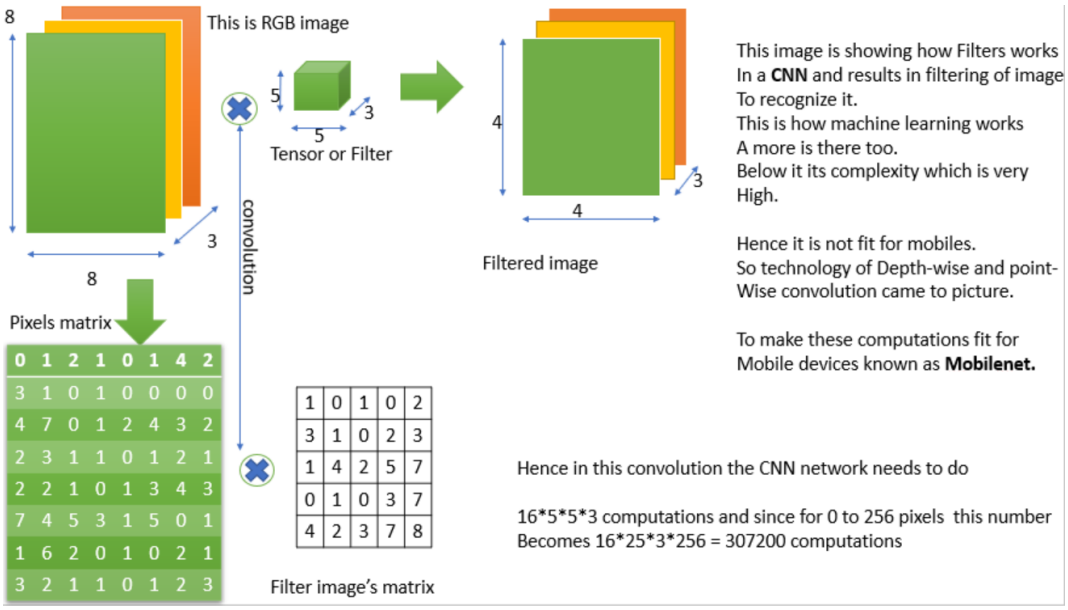

Fig 4.19 Convolutional Neural Network Working (Image Recognition With Mobilenet, 2022)

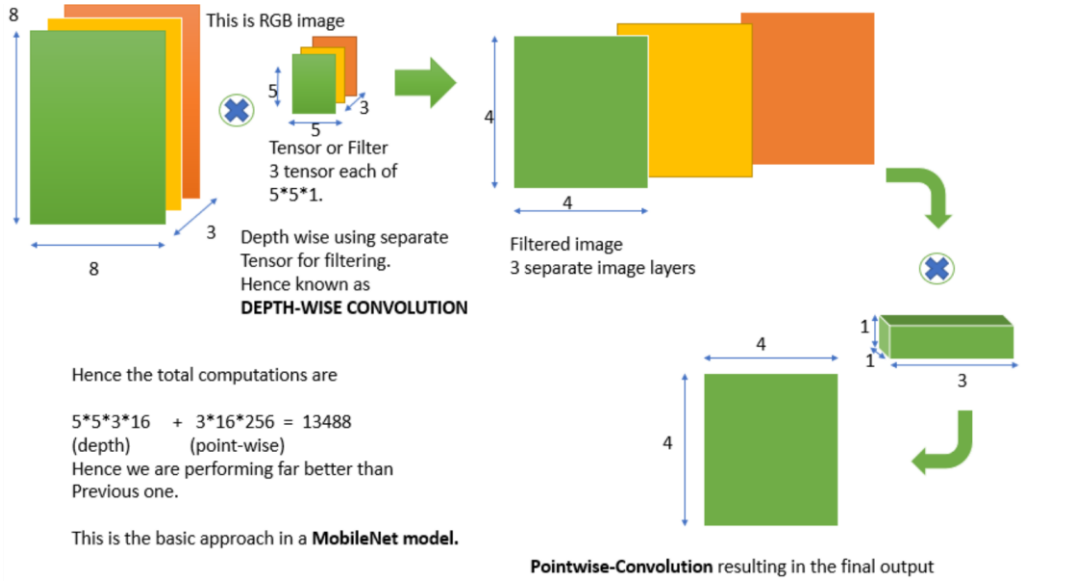

Fig 4.20 MobileNet Working Approach (Image Recognition With Mobilenet, 2022)

4.3.4 NASNetMobile

NASNetMobile is an architecture for convolutional neural networks that has been fine-tuned for mobile devices to reduce the amount of computation required and increase the speed of processing. Convolutional layer blocks facilitate parallel processing (Reda et al., 2022). As a successor to MobileNetV2, it is considered an improvement that preserves accuracy while boosting the speed of model processing. This is accomplished by transitioning from the traditional sequential processing method to a technique that simultaneously processes numerous layers, employing a system of blocks and strides. Blocks are pre-established network layers that serve as the overarching structure, whereas strides are subdivisions within each block, consisting of one to two layers (Reda et al., 2022). The stride-based design's key advantage is that it uses a search algorithm to divide layers and execute skips throughout the network. More accurate predictions are the outcome of this optimised performance, which improves layer processing (Reda et al., 2022).

With an input layer, 188 activation layers, 371 convolutional layers, and 144 reduction layers, the algorithm has a total of 769 buildup layers. In addition, the model incorporates global average pooling layers and batch normalisation techniques as described by Reda et al. (2022). This model stands out because to its utilisation of various kernel sizes, such as 3 × 3 and 5 × 5 kernels, within its blocks. This unorthodox methodology distinguishes it from other models and enhances the variety of layers, thus accelerating the search procedure. For a graphic depiction of NASNetMobile's architecture, please consult Figure 4.21.

4.3.5 ResNet101

ResNet-101 is a convolutional neural network architecture that is highly regarded for its extensive depth and exceptional performance in applications related to image classification and computer vision. A modified version of the original ResNet, it utilises a sophisticated technique known as residual connections, which enable the training of highly deep networks without encountering issues with the vanishing

gradient problem. ResNet-101 is constructed from a set of fundamental components, each with multiple convolutional layers and skip connections. These skip connections enable the network to learn both the identity mapping and residual features simultaneously, leading to faster and more stable convergence during training. With its 101 layers, ResNet-101 excels in capturing intricate image features, making it one of the go-to choices for image recognition tasks, including object detection and segmentation. Its success has solidified its place as a cornerstone in the field of deep learning, often serving as a benchmark for other architectures.

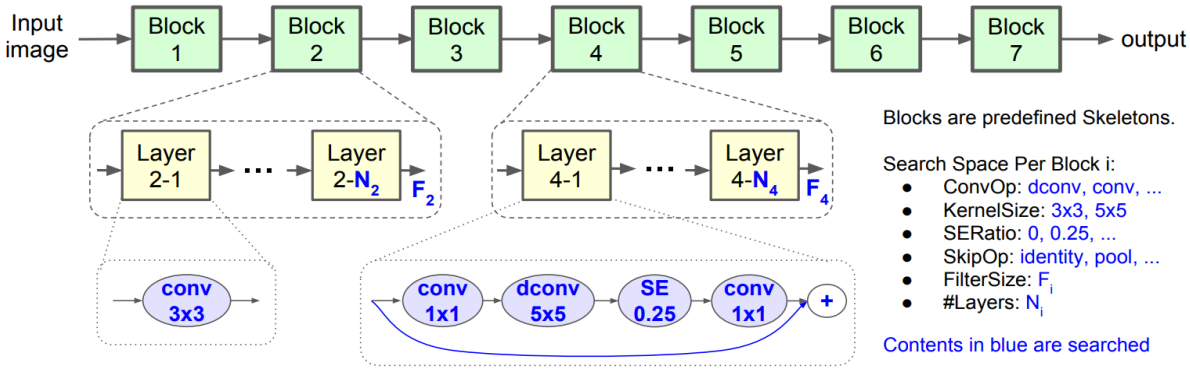

Fig 4.21 Visual Overview of NASNetMobile Architecture (Reda et al., 2022)

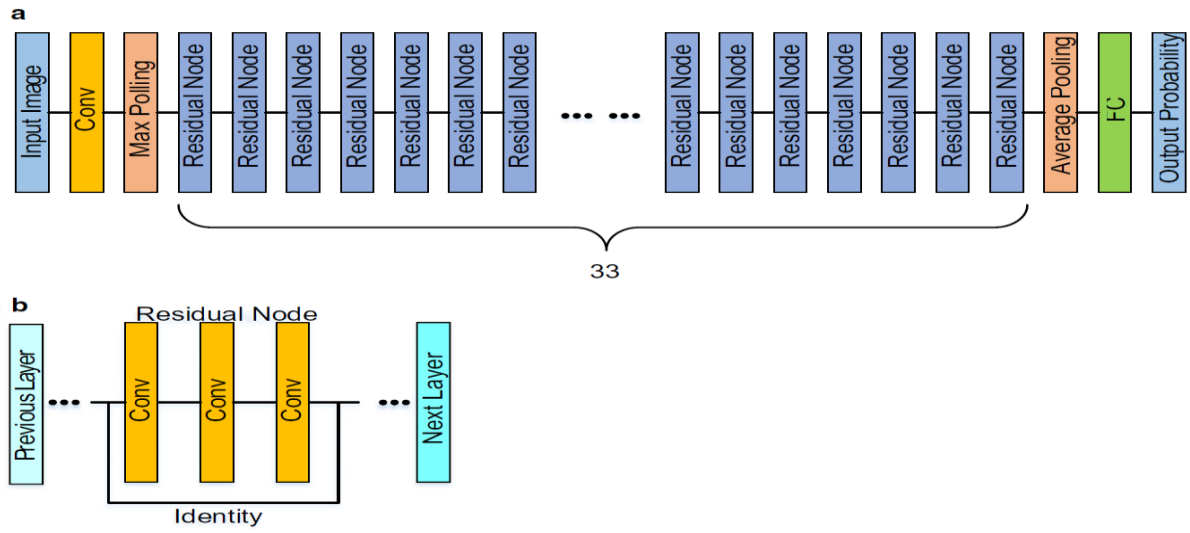

Fig 4.22 a) Schematics of the ResNet101 architecture, which included 33 residual nodes in total. b) The residual node served as building block for the ResNet101 architecture.

ResNet101 = deep residual neural network;

Conv = convolutional;

FC = fully connected

The main components of the ResNet101 architecture that we are examining are fully connected layers, convolutional layers, and pooling layers. By adjusting the initial pixel values of the input picture, convolutional layers progressively extract information. In order to reduce the dimensionality of the recovered features, pooling layers like max pooling and average pooling merge data with similar significance (Paoletti et al., 2018). Subsequently, the fully linked layers amalgamate these features to generate classifications at the image level. More complex and detailed visual features may be learned by deeper convolutional neural networks (CNNs), according to recent studies. However, they often run into problems related to gradient divergence and vanishing gradients, which prevent information from being transmitted from lower to higher layers. ResNet101 gets around these issues by learning deep networks using connections that are shortcuts that skip a level or two (as shown in Figure 4.22). The relevant shortcut relationships accomplish the mapping of identities with no extra variables or computational overhead added. This simplifies the optimisation of the deep network and ensures that information is effectively transferred between layers during training (Medeiros et al., 2019). As a result, ResNet101 achieves higher accuracy with considerably deeper networks in image classification tasks compared to shallower networks.

4.3.6 Xception

Xception is an advanced neural network structure that utilises deep convolutional layers and incorporates Depthwise Separable Convolutions. The creation of this was undertaken by researchers affiliated with Google. Google has created a concept in convolutional neural networks called Inception modules. These modules act as an intermediate step, connecting normal convolution with the depthwise separable convolution operation. The separable convolution with depth method consists of a

convolution in depth and a pointwise convolution. Looking at a convolution that is separable by depth through this lens could make us picture an Inception component with several towers. Their research led them to suggest a new design for deep convolutional neural networks, drawing inspiration from the Inception model but using depthwise separable convolutions instead of the Inception modules.

After the data has gone through the eight iterations of the middle flow, which is where it is processed, it is eventually sent out through the exit flow. It is of the utmost importance to highlight that batch normalisation is carried out after each layer of Convolution and SeparableConvolution. Figure 4.23 displays the sequence of Xception, which demonstrates the succession of phases that comprise the entire procedure.

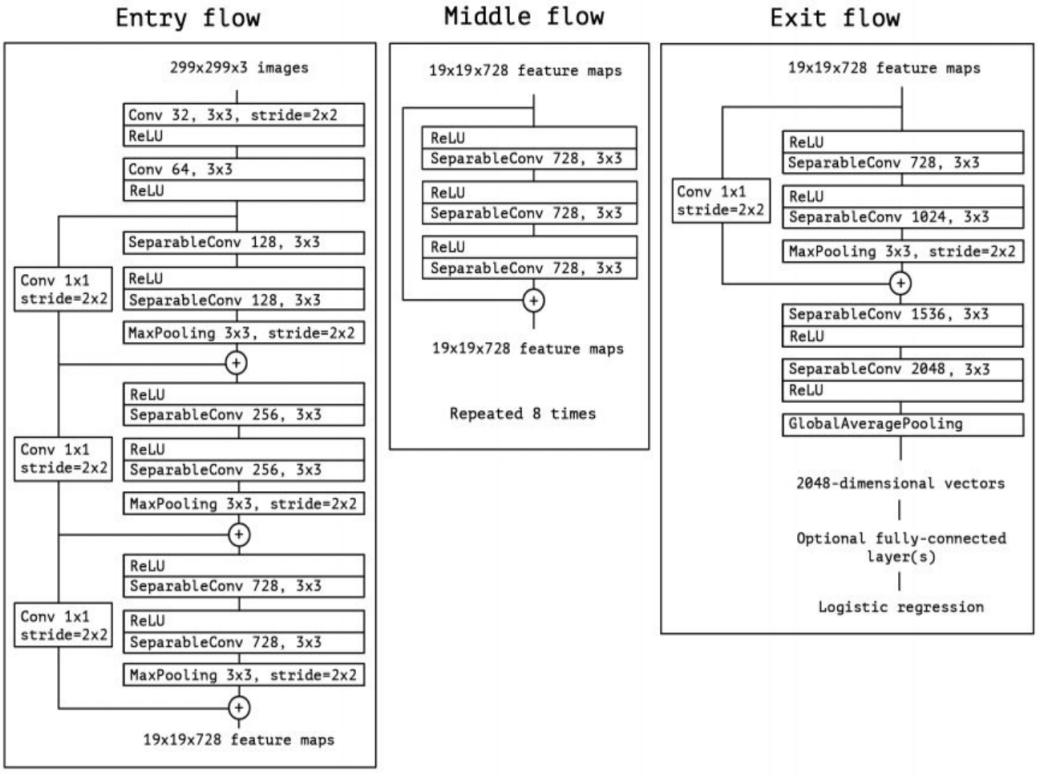

Fig 4.23 Flow for Xception Architecture (XCeption Model and Depthwise Separable Convolutions, 2019)

Xception is a streamlined architecture built on two primary principles:

- **Depthwise Separable Convolution** are considered as substitutes for traditional convolutions, with the promise of significantly improved computational efficiency. To begin, let's examine convolutions.

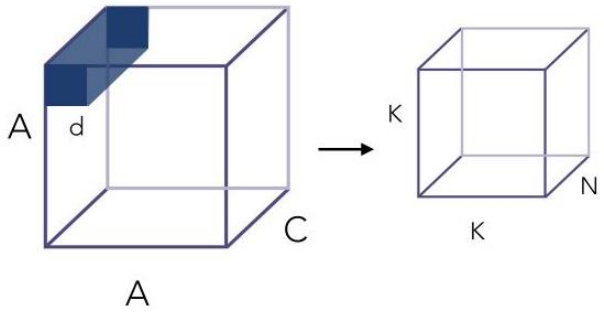

Fig 4.24 Convolutional Operation (XCeption Model and Depthwise Separable Convolutions, 2019)

The input image possesses a specific number of channels, for instance, 3 in the case of a color image, and it also has a particular size, let's say 100 by 100 pixels. We then apply a convolution filter with dimensions d by d, such as 3 by 3. The convolution process is depicted as follows:

Well, for 1 Kernel, that is:

$$K^2 \times d^2 \times C$$

The value of K, which represents the resulting dimension after convolution, is contingent upon the applied padding. For instance, if "same" padding is used, it implies that A will be equal to K.

Therefore, for N Kernels (depth of the convolution) :

$$K^2 \times d^2 \times C \times N$$

In order to address the computational expense associated with these operations, depthwise separable convolutions were introduced. They can be broken down into two key steps:

- **Depth-wise Convolutional:** In the initial step, Depthwise Convolution replaces the conventional convolution of size d×d×C with a d×d×1 convolution. In simpler terms, it means that the convolution operation is performed individually for each channel, one at a time, rather than across all channels simultaneously. Fig 4.25 shows convolutional process.

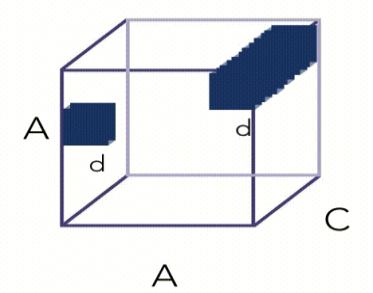

Fig 4.25 Convolutional Process (XCeption Model and Depthwise Separable Convolutions, 2019)

This results in an initial volume with dimensions K×K×C, as opposed to the previous K×K×N. To clarify, we have only performed the convolution operation for one kernel or filter, not for all N of them. This transition brings us to our next step.

- **Point wise Convolutional:** Pointwise convolution conducts a standard convolution with dimensions 1×1×N across the K×K×C volume. This enables the formation of a volume with the K×K×N dimensions. Here is a visual representation of Pointwise Convolution (fig 4.26):

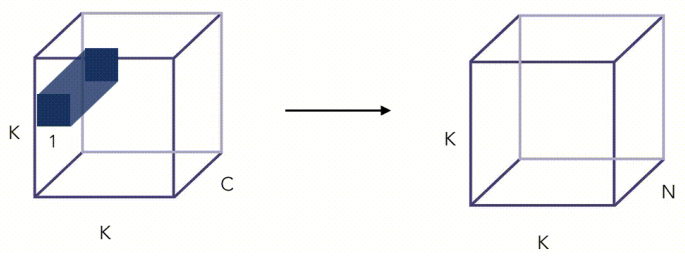

Figure 4.26 Pointwise Convolutional (XCeption Model and Depthwise Separable Convolutions, 2019)

What sets XCeption apart is that it reverses the order of operations compared to the conventional approach. In XCeption, Depthwise Convolution is succeeded by Pointwise Convolution (fig 4.27), as demonstrated in this example:

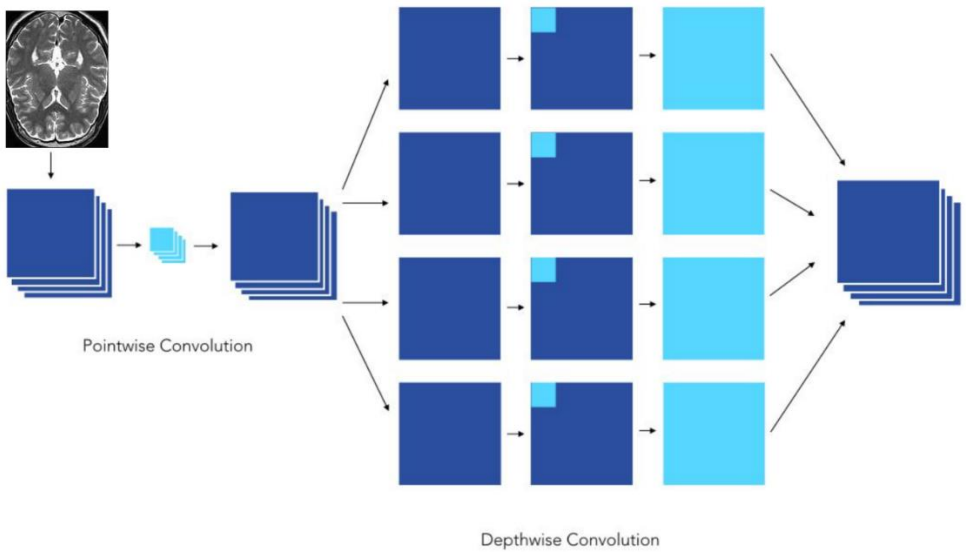

Fig 4.27 Demonstration the order of Depthwise and Pointwise Convolutional (XCeption Model and Depthwise Separable Convolutions, 2019)

4.3.7 DenseNet201

DenseNet, also known as Densely Connected Convolutional Networks, is a type of convolutional neural network (CNN) that utilises a highly linked structure across

layers. This architecture facilitates efficient sharing and propagation of features and gradients throughout the network.

Two well-known versions of this architecture include DenseNet121 and DenseNet201, which are highly efficient for image classification tasks. Initially, these models were designed for image sizes of up to 224 x 224 pixels with precisely 3 channels in the input. However, certain adaptations and implementations of the architecture allow for larger input sizes. It's worth noting that some other variants may support even larger input sizes, but it's essential to consider that expanding the input size can result in increased model memory requirements and computational expenses. Hence, the choice of the input size for DenseNets should be determined based on the specific requirements of the application and the available hardware resources.

DenseNet has demonstrated notable effectiveness in tasks that involve abundant data resources, including:

- **Image Classification:** DenseNet is frequently applied to image classification assignments, including tasks like image object recognition, facial identification, and the classification of various animal or plant species.
- **Object Detection:** DenseNet is applicable to object detection assignments as well, which encompass the task of pinpointing the positions of objects within images and outlining bounding boxes around them.
- **Medical Image Analysis:** DenseNet121 has found application in medical image analysis endeavors, including tasks like the identification of cancerous cells in mammograms or the detection of irregularities in brain scans.
- **Natural Language Processing:** While initially designed for computer vision tasks, specifically image classification, the fundamental concept of DenseNet, which involves dense interconnections between all network layers, holds the potential for application in natural language processing (NLP). However, it's important to acknowledge that the standard DenseNet architecture may require

adjustments to be directly relevant to NLP tasks, potentially involving adaptations to handle sequential data.

Architecture

DenseNet has dense blocks with several convolutional layers. Each dense block uses the outputs from all previous blocks as input. This interconnects all network levels, allowing information to flow effectively.

DenseNet is based on the fundamental premise of combining the feature maps that are generated by each layer in order to provide the input for the subsequent layer. To a large extent, the outcome of each layer serves as the contribution for all levels that come after it. A transition layer within DenseNet effectively handles the management of both spatial dimensionality and the quantity of feature mappings. Positioned between each dense block, this layer plays a crucial role in regulating these aspects within the architecture. The batch normalisation layer, the 1x1 convolutional layer, and the pooling layer are the components that make up the transition layer.

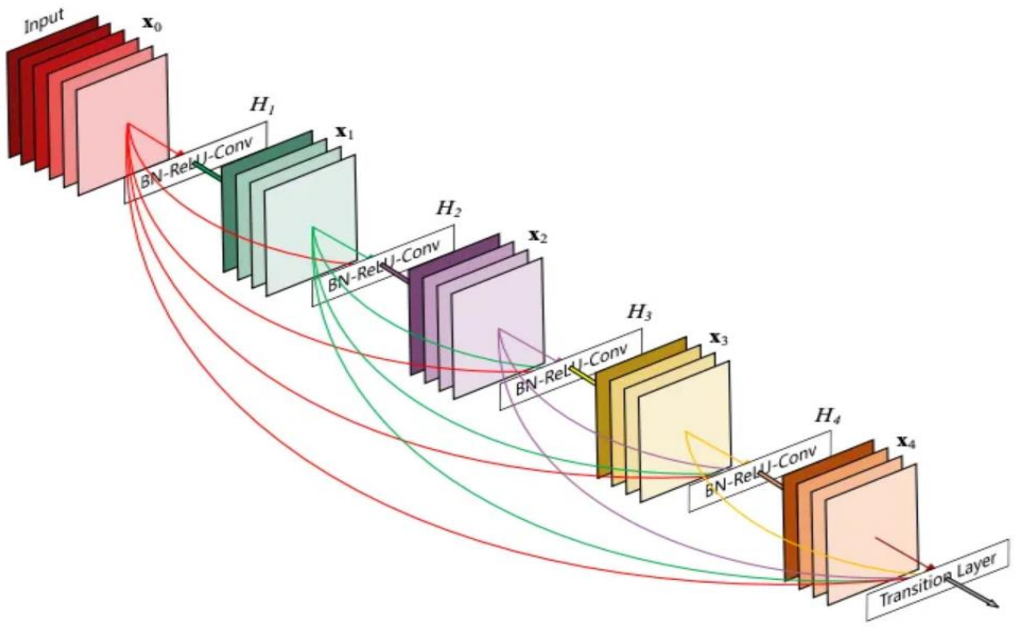

Fig 4.28 DenseNet Working Architecture (Huang et al., 2017)

DenseNet201 is a larger model with a significantly greater parameter count compared to DenseNet121, nearly doubling the parameters, rendering it a more intricate architecture. Due to its increased number of layers, DenseNet201 demands a higher level of computational resources during both training and inference, making it computationally more intensive than DenseNet121.

In a DenseNet, the output of each layer is formed by concatenating the feature maps from all previous layers within the same dense block. Mathematically, this can be expressed as:

$$Y_i = H([X_0, X_1, X_2, X_3, X_4, \dots\dots, X_{i-1}])$$

Where:

- Y_i is the outcome of the ith level.
- H stands for the combined map of features composite function.
- X_0, X_1, X_2, …. , X_{i-1} are the feature maps from the preceding layers within the same dense block, all concatenated together.

This equation illustrates the concept of densely connecting feature maps from previous layers to produce the output of the current layer, allowing for effective feature reuse and facilitating the flow of information throughout the network. Here's an overview of the working architecture of DenseNet-201:

- **Input Layer:** A network's initialization process begins with an input layer that receives the original picture data.
- **Initial Convolution:** The input image passes through an initial convolutional layer to extract basic features.
- **Dense Blocks:** DenseNet-201 is distinguished by its inclusion of many dense blocks. To extract characteristics, each compressed block employs a succession of layers of convolution. The primary concept in these blocks is merging the feature maps from all previous levels and using them as the input for the current layer. The intricate network of connections facilitates efficient

utilisation of features and smooth propagation of gradients, hence enhancing the network's efficacy.

- **Transition Layers:** Transition layers can be seen in between successive thick blocks. Batch normalisation, 1x1 convolutional layers, and average pooling are the main components that make up these layers. Transition layers are utilised in order to lower the spatial dimension as well as the amount of feature maps, all while preserving the dense connectedness.
- **Global Average Pooling (GAP):** Using a layer of global average pooling after processing the last dense block reduces the characteristic maps' spatial dimensions to 1x1.
- **Fully Connected Layer:** The framework's final predicted classes are generated by integrating either an entirely connected layer or a softmax layer. An estimate of the likelihood that each category appears in the picture categorization is the output of this layer.

Layers	Output Size	DenseNet-121	DenseNet-169	DenseNet-201	DenseNet-264
Convolution	112 × 112	7 × 7 conv, stride 2			
Pooling	56 × 56	3 × 3 max pool, stride 2			
Dense Block (1)	56 × 56	[1 × 1 conv, 3 × 3 conv] × 6	[1 × 1 conv, 3 × 3 conv] × 6	[1 × 1 conv, 3 × 3 conv] × 6	[1 × 1 conv, 3 × 3 conv] × 6
Transition Layer (1)	56 × 56	1 × 1 conv			
	28 × 28	2 × 2 average pool, stride 2			
Dense Block (2)	28 × 28	[1 × 1 conv, 3 × 3 conv] × 12	[1 × 1 conv, 3 × 3 conv] × 12	[1 × 1 conv, 3 × 3 conv] × 12	[1 × 1 conv, 3 × 3 conv] × 12
Transition Layer (2)	28 × 28	1 × 1 conv			
	14 × 14	2 × 2 average pool, stride 2			
Dense Block (3)	14 × 14	[1 × 1 conv, 3 × 3 conv] × 24	[1 × 1 conv, 3 × 3 conv] × 32	[1 × 1 conv, 3 × 3 conv] × 48	[1 × 1 conv, 3 × 3 conv] × 64
Transition Layer (3)	14 × 14	1 × 1 conv			
	7 × 7	2 × 2 average pool, stride 2			
Dense Block (4)	7 × 7	[1 × 1 conv, 3 × 3 conv] × 16	[1 × 1 conv, 3 × 3 conv] × 32	[1 × 1 conv, 3 × 3 conv] × 32	[1 × 1 conv, 3 × 3 conv] × 48
Classification Layer	1 × 1	7 × 7 global average pool			
		1000D fully-connected, softmax			

Fig 4.29 DenseNet Architecture (Huang et al., 2017)

4.3.8 ResNet50

ResNet-50, belonging to the ResNet (Residual Network) family, is a robust deep neural network structure generally employed for tasks related to image classification and computer vision. Its effectiveness in training deep networks with 50 layers is widely recognised. The architectural design commences with an initial convolutional layer that extracts fundamental information from the input pictures, subsequently followed by max-pooling to diminish the spatial dimensions. The most important innovation that ResNet-50 brings to the table is its residual blocks. These blocks are where skip connections make it possible for gradients to flow directly through the network. Each residual block utilizes a bottleneck architecture, which includes 1x1, 3x3, and 1x1 convolutions, making the network computationally efficient. Multiple stages, each housing a sequence of residual blocks, capture features at different levels of abstraction. After the final stage, global average pooling reduces the feature maps to 1x1 dimensions, and a fully connected layer produces class predictions. ResNet-50's exceptional depth, skip connections, and efficient design have made it a benchmark model for various computer vision tasks, consistently delivering state-of-the-art performance (fig 4.30).

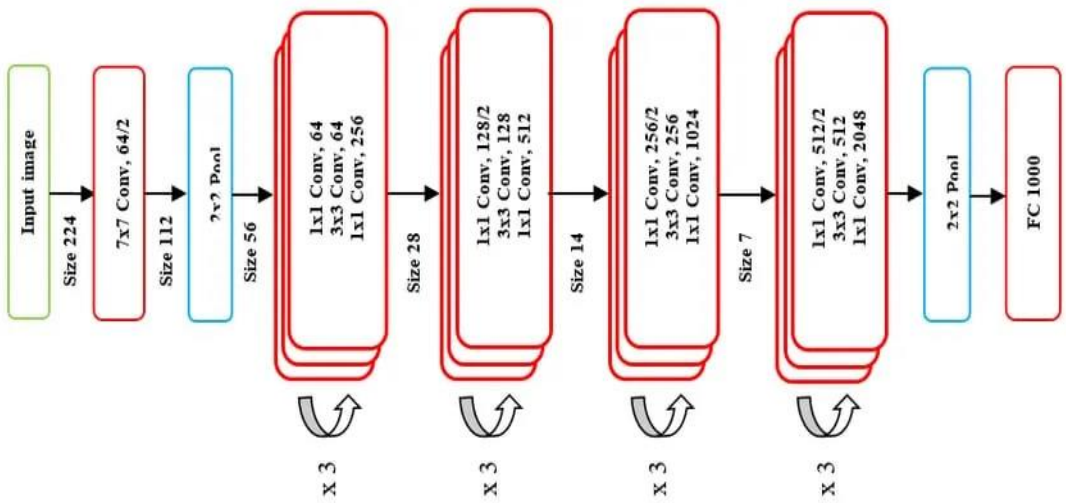

Fig 4.30 ResNet-50 Architecture (He et al., 2016)

Skip connections, also mentioned to as identity connections, play a key role in ResNet-50. They enable the retention of information from previous layers, enhancing the network's capacity to acquire more effective data representations. These connections are established by summing the outcome of a prior level with the output of a subsequent level.

In particular, they make it possible for the layers to modify a residual mapping, abbreviated as H(x), and for the nonlinear layers to accept a second mapping, F(x) = H(x) - x. This results in the original mapping being expressed as H(x) = F(x) + x, as illustrated in Figure 4.31.

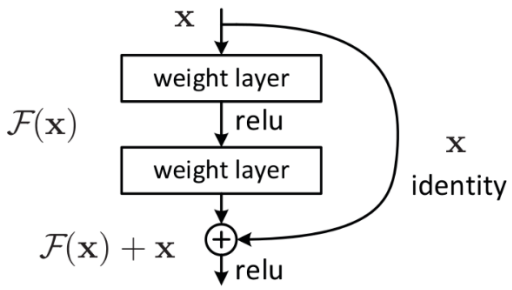

Fig 4.31 Skip Connection (He et al., 2016)

As seen in figure 4.32 below, the subsequent components make up the 50-layer ResNet construction:

- Using a stride of 2 and an extra 64 kernels, a 7x7 kernel convolution is employed.
- Layer 2 of maximum pooling with a stride of 2.
- Subsequently, there are 9 more layers, which consist of a 3x3 convolution with 64 kernels, another convolution with 1x1 dimensions and 64 kernels, and a third convolution with 1x1 dimensions and 256 kernels. The three layers are replicated thrice.

- 12 additional layers proceed, with 1x1 convolutions using 128 kernels, 3x3 convolutions using 128 kernels, and 1x1 convolutions using 512 kernels as the last layer. Iterating four times, this sequence is maintained.
- Then, 18 more layers are added, including 1x1 convolutions using 256 kernels, 3x3 convolutions using 256 kernels, and 1x1 convolutions using 1024 kernels each. Six times this pattern is repeated.
- Then, there are nine more layers, with 512-kernel 1x1 convolutions, 3x3 convolutions, and 2048-kernel 1x1 convolutions making up the layers in that order. This pattern is repeated three times. The network now consists of fifty tiers.
- Lastly, there is a fully connected layer with 1000 nodes that use the softmax activation function. This is followed by an average pooling layer.

layer name	output size	18-layer	34-layer	50-layer	101-layer	152-layer
conv1	112×112	7×7, 64, stride 2				
conv2_x	56×56	3×3 max pool, stride 2				
		$\begin{bmatrix} 3\times3, 64 \\ 3\times3, 64 \end{bmatrix}\times2$	$\begin{bmatrix} 3\times3, 64 \\ 3\times3, 64 \end{bmatrix}\times3$	$\begin{bmatrix} 1\times1, 64 \\ 3\times3, 64 \\ 1\times1, 256 \end{bmatrix}\times3$	$\begin{bmatrix} 1\times1, 64 \\ 3\times3, 64 \\ 1\times1, 256 \end{bmatrix}\times3$	$\begin{bmatrix} 1\times1, 64 \\ 3\times3, 64 \\ 1\times1, 256 \end{bmatrix}\times3$
conv3_x	28×28	$\begin{bmatrix} 3\times3, 128 \\ 3\times3, 128 \end{bmatrix}\times2$	$\begin{bmatrix} 3\times3, 128 \\ 3\times3, 128 \end{bmatrix}\times4$	$\begin{bmatrix} 1\times1, 128 \\ 3\times3, 128 \\ 1\times1, 512 \end{bmatrix}\times4$	$\begin{bmatrix} 1\times1, 128 \\ 3\times3, 128 \\ 1\times1, 512 \end{bmatrix}\times4$	$\begin{bmatrix} 1\times1, 128 \\ 3\times3, 128 \\ 1\times1, 512 \end{bmatrix}\times8$
conv4_x	14×14	$\begin{bmatrix} 3\times3, 256 \\ 3\times3, 256 \end{bmatrix}\times2$	$\begin{bmatrix} 3\times3, 256 \\ 3\times3, 256 \end{bmatrix}\times6$	$\begin{bmatrix} 1\times1, 256 \\ 3\times3, 256 \\ 1\times1, 1024 \end{bmatrix}\times6$	$\begin{bmatrix} 1\times1, 256 \\ 3\times3, 256 \\ 1\times1, 1024 \end{bmatrix}\times23$	$\begin{bmatrix} 1\times1, 256 \\ 3\times3, 256 \\ 1\times1, 1024 \end{bmatrix}\times36$
conv5_x	7×7	$\begin{bmatrix} 3\times3, 512 \\ 3\times3, 512 \end{bmatrix}\times2$	$\begin{bmatrix} 3\times3, 512 \\ 3\times3, 512 \end{bmatrix}\times3$	$\begin{bmatrix} 1\times1, 512 \\ 3\times3, 512 \\ 1\times1, 2048 \end{bmatrix}\times3$	$\begin{bmatrix} 1\times1, 512 \\ 3\times3, 512 \\ 1\times1, 2048 \end{bmatrix}\times3$	$\begin{bmatrix} 1\times1, 512 \\ 3\times3, 512 \\ 1\times1, 2048 \end{bmatrix}\times3$
	1×1	average pool, 1000-d fc, softmax				
FLOPs		1.8×10^9	3.6×10^9	3.8×10^9	7.6×10^9	11.3×10^9

Fig 4.32 Layered Architecture of ResNet Varient (He et al., 2016)

4.3.9 EfficientNetB7

EfficientNetB7 is a model specifically developed for various computer vision applications, with a special emphasis on picture categorization. It is a associate of the EfficientNet family, prominent for its exceptional efficiency in terms of both accuracy

and processing resources. EfficientNetB7 is the most extensive and potent iteration within this series.

At its core, EfficientNetB7 leverages a compound scaling method, which optimizes model depth, width, and resolution. It combines deep layers, a large number of filters, and higher image resolutions, resulting in a network that can capture intricate features from images. Compared to conventional deep networks, this method uses a smaller number of parameters and less processing resources without sacrificing state-of-the-art performance.

EfficientNetB7's architecture includes various building blocks, such as convolutional layers, normalization layers, and nonlinear activations, all structured to efficiently process image data. It also employs techniques like dropout and batch normalization for regularization and stability during training.

One notable feature of EfficientNetB7 is its adaptability to different input image sizes. This flexibility allows it to handle a variety of image resolutions while maintaining high accuracy, making it suitable for tasks that involve images of varying sizes.

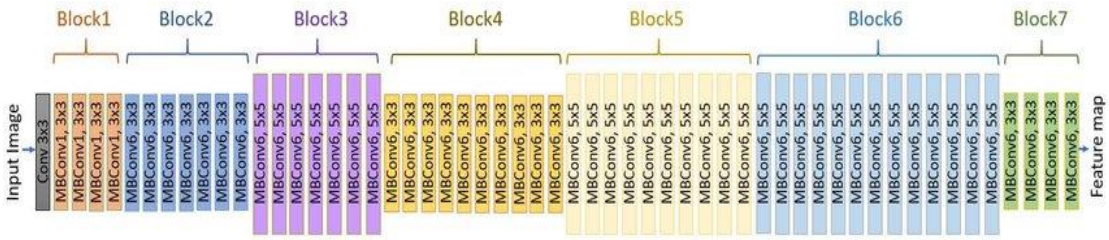

Fig 4.33 EfficientNetB7 Architecture (Baheti et al., 2020)

Below is a detailed description of the EfficientNetB7 architecture (Fig 4.33):

- **Input Layer:** The network starts with an input layer, accepting images of varying resolutions. This adaptability to input size is a key feature of EfficientNet.

- **Convolutional Layers:** The architecture includes a series of convolutional layers, organized into blocks. These layers perform feature extraction and are responsible for capturing hierarchical features in the input images.
- **Width and Depth Scaling:** EfficientNetB7 uses a compound scaling method that adjusts the number of filters (width) and the depth of the network. This scaling is based on a compound coefficient, allowing the model to find a balance between complexity and efficiency.
- **Resolution Variability:** Another unique aspect is that EfficientNet can handle images of different resolutions. It uses different resolutions for different variants, with EfficientNetB7 accommodating higher resolutions.
- **Normalization Layers:** Batch normalization layers are integrated into the architecture, enhancing training stability and accelerating convergence.
- **Activation Functions:** Non-linear functions for activation, such as the ReLU (Rectified Linear Unit), are utilised following convolutional processes to include non-linearity into the network.
- **Dropout:** Dropout layers are used for regularization, preventing overfitting during training.
- **Global Average Pooling (GAP):** To bring the maps of features down to 1x1 spatial dimensions, a global average pooling layer is applied following the layers of convolution. Characteristics are concisely represented in this stage.
- **Fully Connected Layer:** The last layer is a fully connected one, and its node count is equal to the entire amount of classes used for classification. To calculate the probability for every category, the softmax activation function is used.

4.4 RESUNET for Segmentation and Localization with added layers

The convolutional linguistic segmentation technique known as RESUNET was introduced by Zhang and his colleagues in the year 2018. RESUNET was initially developed for the purpose of extracting roads from high-resolution aerial photos in

remote sensing applications. It provides improved performance with its simplified architecture and fully convolutional neural network. This provides a significant improvement over the current UNET architecture by using the capabilities of Deep Residual Learning with the UNET framework, as seen in Figure 4.34.

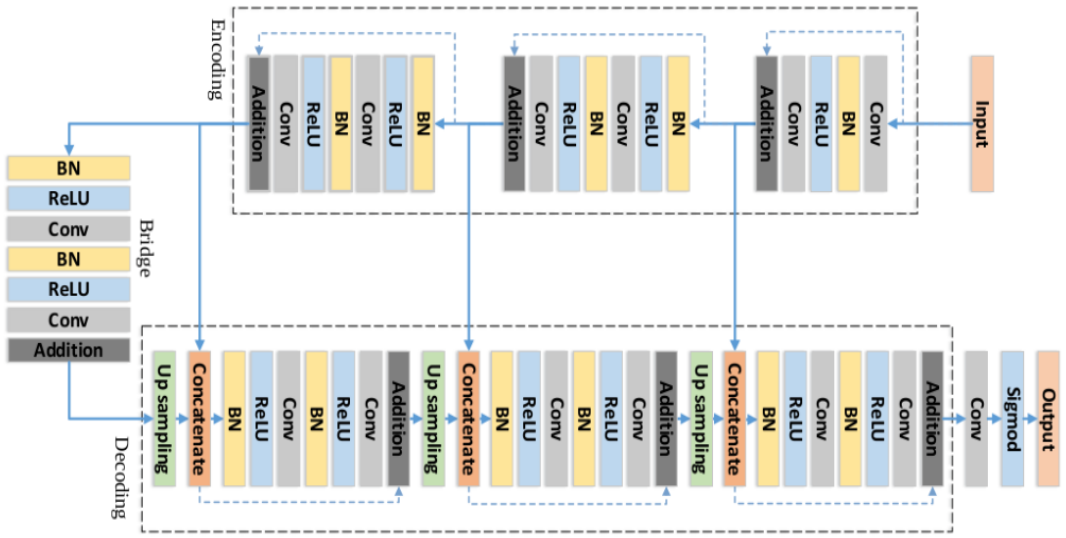

Fig 4.34 RESUNET Architecture Walkthrough

The graphic shows how the investigation framework identifies and localises brain tumours. The first step in using category mode is to prepare the pictures of the TCGS MRI scan. This can only be achieved once the dataset has been cleaned up by removing unnecessary columns, transforming the data in the mask column into a usable format, and then separating the sample into validation, testing, and training sets. Afterwards, for each set, a data generator is built using 16 batches, a category-based class mode, and an aim of a 256 × 256 picture size.

To complete the classification task, the fundamental models are supplemented with a classification head that includes features such as average pooling, flattening, a thick layer with activation functions ReLU and SoftMax, and dropout. In order to train the algorithm, the optimizer of Adam and the categories cross-entropy loss function are employed.

In the second stage, the main goal is to construct and train a segmentation model that can detect and localise tumours correctly by utilising the RESUNET architecture. The initial stage of this design entails extracting the MRI data frames that are accompanied by masks. The data is partitioned into separate training and testing sets. Additionally, utility files are generated, which include code for bespoke loss functions and custom data generators. Afterwards, the RESUNET segmentation model is trained, and ultimately, tumour prediction and localization are performed.

The subsequent layers have been incorporated into the classification model:

Flatten Layer: A Flatten layer is a fundamental component in many neural network constructions, especially in convolutional neural networks. Its purpose is to reshape or flatten the multidimensional input data into a one-dimensional vector. The extraction of features from the layers of a neural network must undergo this procedure before they can join the fully linked layers.

Here's how a Flatten layer works:

- **Input Data:** The input to a Flatten layer is typically a multidimensional array or tensor. In the context of a CNN, this input often consists of feature maps or activations from convolutional and pooling layers.
- **Reshaping:** All the Flatten layer does is restructure the incoming data. Although it arranges the input items in a single line, it keeps all of them. The Flatten layer will create a 1D vector with the dimensions (height * width * channels) from a 3D tensor with the input (height, width, channels, for instance).
- **Output:** The Flatten layer produces this one-dimensional vector as its output; subsequent processing is carried out by one or more fully linked layers. The flattened data may be learned by these fully linked layers in a complex web of links and patterns.

The Flatten layer is crucial because it bridges the gap between the feature extraction layers, which work with spatial information in multidimensional data, and the fully connected layers, which require a one-dimensional input. It allows neural networks to leverage the hierarchical features learned in earlier layers to make predictions or classifications in the final layers.

In this study, a Flatten operation is used to aggregate the output of the convolutional layers into a single prolonged representation of features. The final classification model, called a fully-connected layer, is then linked to this altered data.

Dense Layer: Most neural network designs, such as feedforward neural networks and deep learning models, begin with a dense layer, which is also called a fully connected neural network or simply a fully connected layer. For the purpose of discovering intricate connections and patterns in data, it is indispensable. Here's an explanation of a Dense layer:

- **Neurons/Units:** A thick layer always has the same amount of neurons or units. The term "fully connected" is used to describe a network in which every neuron has connections to all inputs and outputs from every previous layer. The interconnectedness of dense layers allows them to comprehend complex, nonlinear relationships within the data.
- **Weighted Sum:** A Dense layer assigns a weight to each input-neuron link. Considered together, the inputs to a neuron—which may comprise values from a prior layer or input features—are multiplied by a weight to get the neuron's output.
- **Bias:** In addition to the weighted sum, a bias term is added to the neuron's input. The bias is a learnable parameter that allows the network to model offsets or biases in the data.
- **Activation Function:** The result is derived by applying a function of activation to the weighted total, which includes the bias. The network is

capable to acquire complex patterns because the activation function has non-linear properties.

- **Output:** Every neuron in the Dense layer produces its final output when the activation function is applied to the weighted aggregate plus bias.

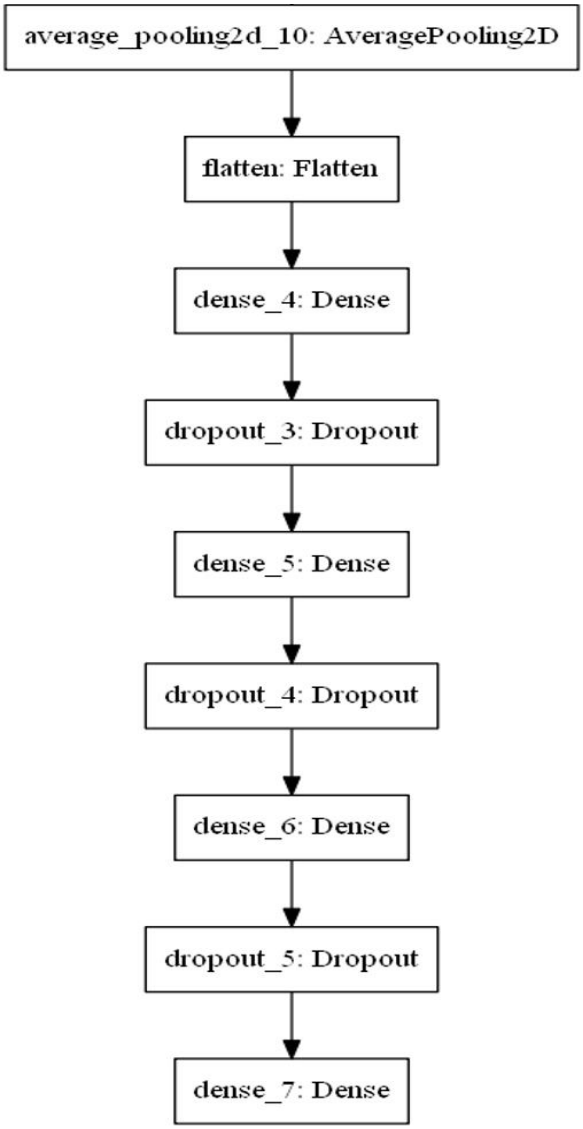

Fig 4.35 Added Subsequent Layer

Dense layers are typically used for higher-level feature learning and complex data representations. In deep neural networks, multiple Dense layers are often stacked

together to form the so-called hidden layers. The network's ability to learn and generalise from data is affected by several architectural decisions, such as the amount of hidden layers, the activation function chosen, and the density layer's neuron count.

Activation Layer: The activation mechanism in a network of neurons can be built up and placed either at the beginning of the network or inside its layers. These functions ascertain whether a neuron will become activated or remain inactive. The activation function modifies the input signal in a non-linear manner.

Drop out Layer: In neural networks, the dropout layer is a regularisation approach that helps avoid overfitting. During training, this method operates by randomly deactivating a designated proportion of neurons (nodes), therefore enhancing the network's resilience and reducing its dependence on individual neurons. This hinders the network from excessively conforming to the training data and encourages improved generalisation to novel, unobserved input.

In the process of adding a Dense Layer, Flatten Layer, Dropout Layer, and Activation Layer to a classification base model, there are a number of substantial advantages that may be gained. The flattened layer is crucial in transforming multidimensional feature maps into vectors with a single dimension. This facilitates the efficient processing of data and makes it simpler for following layers to extract and learn complicated patterns. The network's irregularities is introduced via the Activation Layer. Essential for accurately collecting complex properties, this allows the network to capture complex and non-linear relationships within the data. The Dense Layer, characterised by complete connectivity, possesses the capacity to acquire complex patterns and interdependencies, rendering it a good layer for extracting information and facilitating learning. As an additional function, the Dropout Layer functions as a regularisation strategy, which prevents overfitting by randomly deactivating neurons while the training is being performed. Because of this, the network may be generalised and do well on data it has never seen before. The combination of these layers not only

improves the categorization model's performance as a whole, but it also makes it more resilient and versatile for use in other areas of machine learning.

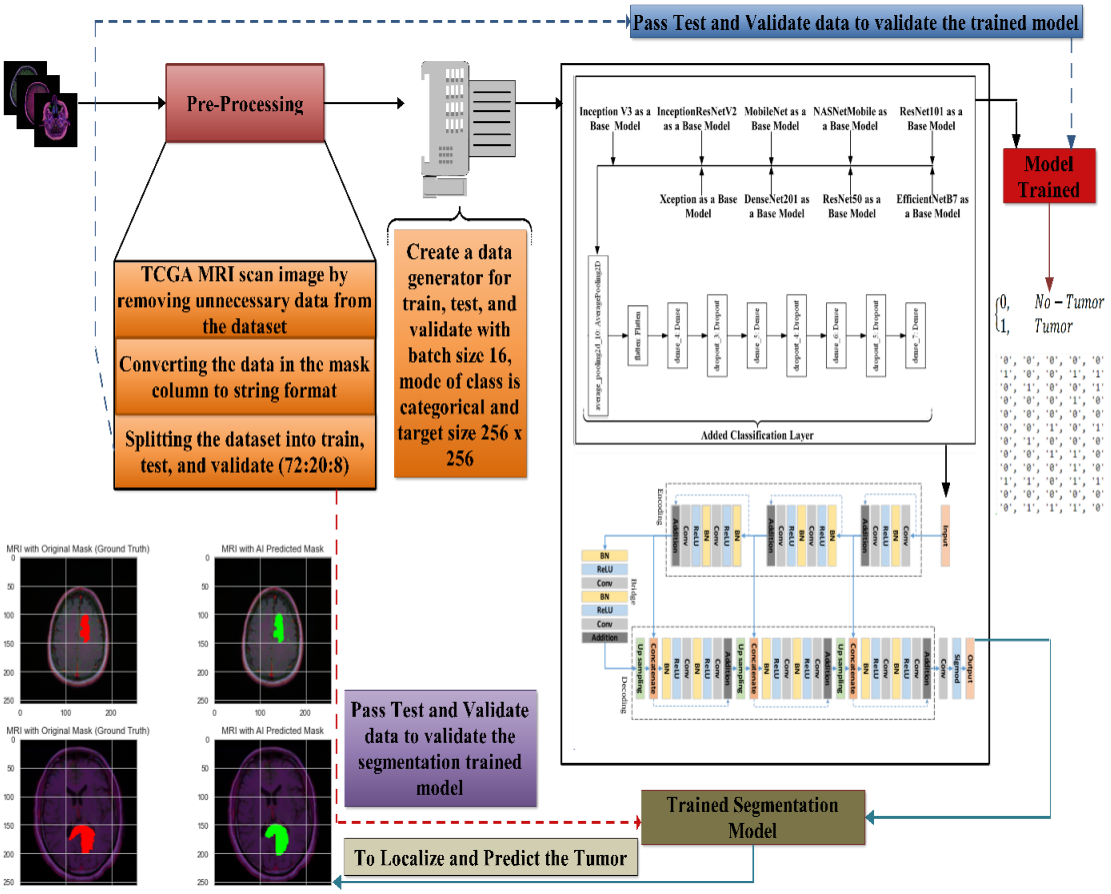

Fig 4.36 Proposed Model

4.5 Model Performance Measuring Parameter

Accuracy: The accuracy of a model is determined by its ability to effectively recognize patterns and relationships among the variables in the dataset when trained with the input data.

$$Accuracy = \frac{TP + TN}{TP + TN + FP + FN} \quad [4.1]$$

Precision: It is a performance measure in the fields of deep learning and statistics that measures the precision of positive predictions produced by a model, specifically in issues involving binary classification. Precision is a quantification of the accuracy of positive predictions. An alternative name for this metric is the "proportion of accurately produced positive forecasts," and it is simply the proportion of the algorithm's actual positive forecasts to its overall number of positive predictions. The preciseness of positive predictions, or more precisely, the proportion of truly positive occurrences predicted, is the primary focus of precision.

$$Precision = \frac{TP}{TP + FP} \quad [4.2]$$

Here's what precision represents:

- **True Positives (TP):** The count of accurately forecasted of positive occurrences.
- **False Positives (FP):** The total number of cases when the projected outcome was negative.

F1-Score: When it comes to binary categorization tasks, the F1-score is an efficiency metric that is heavily used in analytics and deep learning. It is a single numerical value that measures both precision and recall, combined to give a complete assessment of the efficacy of a model. When dealing with unevenly distributed samples or when trying to strike a balance between recall and accuracy, the F1-score comes in quite handy.

The F1-score is calculated using the following formula:

$$F1 - Score = 2 \times \frac{Precision \times Recall}{Precision + Recall} \quad [4.3]$$

When accuracy and recall are combined in the F1-score, a harmonic mean is produced, which means that both measures are given equal weight in the overall result. Obtaining a high F1-score requires good memory in addition to accurate

results. This indicates that such a score is reached. In situations in which the outcomes of false positives and false negatives are considerably different from one another, the F1-score is a very helpful tool.

Recall: For tasks involving binary classification in particular, recall is a useful performance measure in learning as well as statistics areas. The term "sensitivity" can be used interchangeably with "true positive rate" in different contexts. Precision measures how well a model can identify all occurrences of a given class, also called the positive class. Basically, recall is a way to quantify how many real positive examples the model accurately identifies as positive.

The recall formula is as follows:

$$Recall = \frac{TP}{TP + FN} \quad [4.4]$$

Recall is particularly important in scenarios where the cost of false negatives (missing relevant instances) is high, and there is a need to ensure that as many true positives as possible are correctly identified. This is common in applications were failing to detect positive instances can have significant consequences, such as in medical diagnoses, fraud detection, or security-related tasks.

Key points about recall:

- It measures the model's ability to capture all relevant positive instances.
- It ranges from 0 to 1, with a higher value indicating better recall.
- It is a critical metric when minimizing false negatives is a primary concern.

Loss: To quantify the degree to which a strategy predicted values diverge from the actual values in the dataset—also called the ground truth—the idea of "loss" or "loss function" is fundamental in deep learning. The loss function quantifies the degree of success or failure of the model in performing its designated task. Throughout the

training phase, the aim is to minimise this loss to indicate that the model is more matched with the data.

Tversky Loss: The Tversky loss is a loss function employed in the realm of deep learning, specifically in tasks pertaining to picture segmentation, object recognition, and other scenarios necessitating the equitable consideration of various error kinds. It is an extension of the Dice loss and is named after Amos Tversky, a cognitive psychologist.

The Tversky loss is designed to handle imbalanced data and to provide more control over the balance between unreliable results and inaccurate results. It allows you to assign different weights to these types of errors, making it a versatile choice for tasks where one type of error is more costly or significant than the other.

The Tversky loss is demarcated by the subsequent formula:

$$Tversky\ Loss = \frac{|X \cap Y|}{|X \cap Y| + \alpha|X \backslash Y| + \beta\,|Y \backslash X|} \quad [4.5]$$

- |X∩Y| represents the intersection of sets X and Y, which corresponds to the true positives.
- |X\Y| represents the elements in set X that are not in set Y, corresponding to false positives.
- |Y\X| represents the elements in set Y that are not in set X, corresponding to false negatives.
- α and β are hyperparameters that control the weight assigned to false positives and false negatives, respectively. The values of α and β determine the trade-off between these two types of errors.

4.6 Results and Evaluation Graph

The table displays the classification model's level of accuracy.

Table 4.2 Average Accuracy performance matrices for classification model.

S. No	Deep Learning Model with added Layer	Average Accuracy
1	InceptionV3 + Added Layer	0.9681
2	InceptionResNetV2 + Added Layer	0.9600
3	MobileNet + Added Layer	0.9600
4	NASNetMobile + Added Layer	0.9700
5	ResNet101 + Added Layer	0.9500
6	Xception + Added Layer	0.9700
7	DenseNet201 + Added Layer	0.9600
8	ResNet50 + Added Layer	0.9630
9	EfficientNetB7 + Added Layer	0.9800

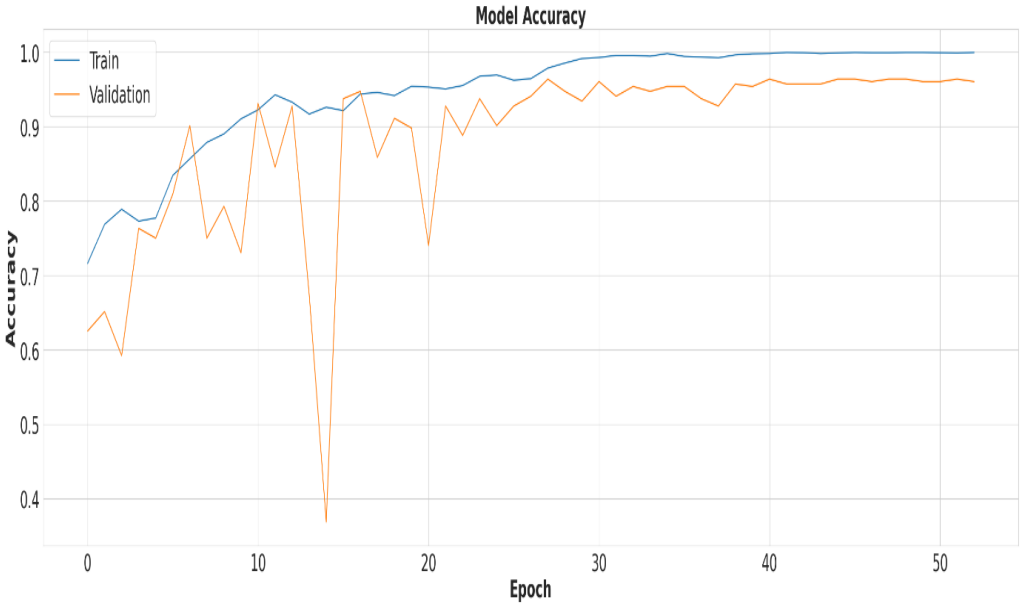

Fig 4.37 Accuracy Performance Graph of InceptionV3 + Added Layer

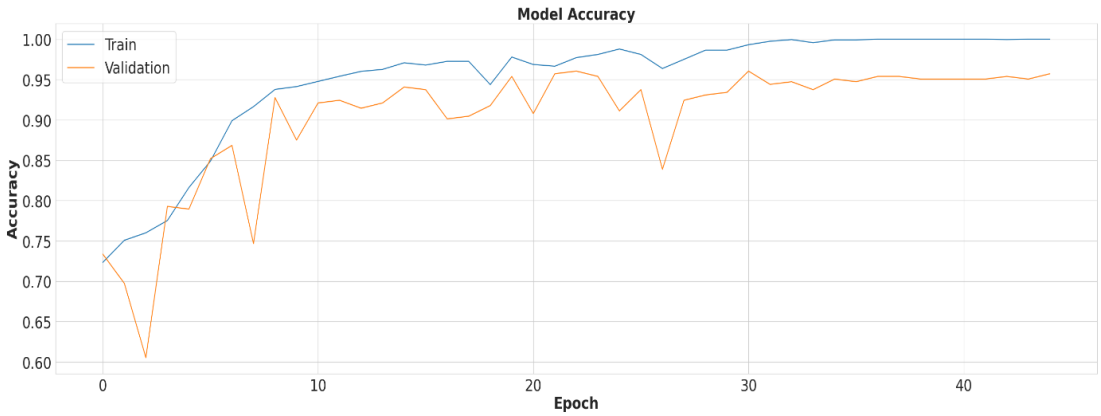

Fig 4.38 Accuracy Performance Graph of InceptionResNetV2 + Added Layer

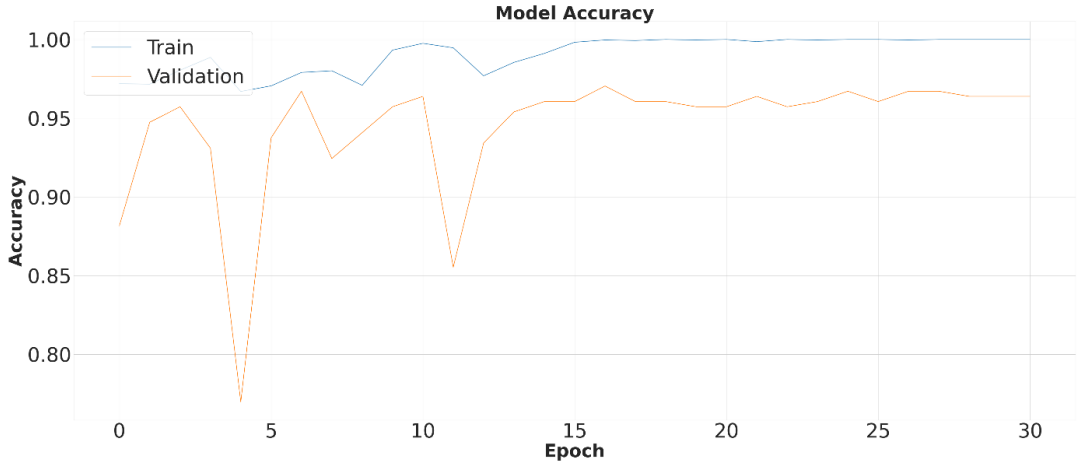

Fig 4.39 Accuracy Performance Graph of MobileNet + Added Layer

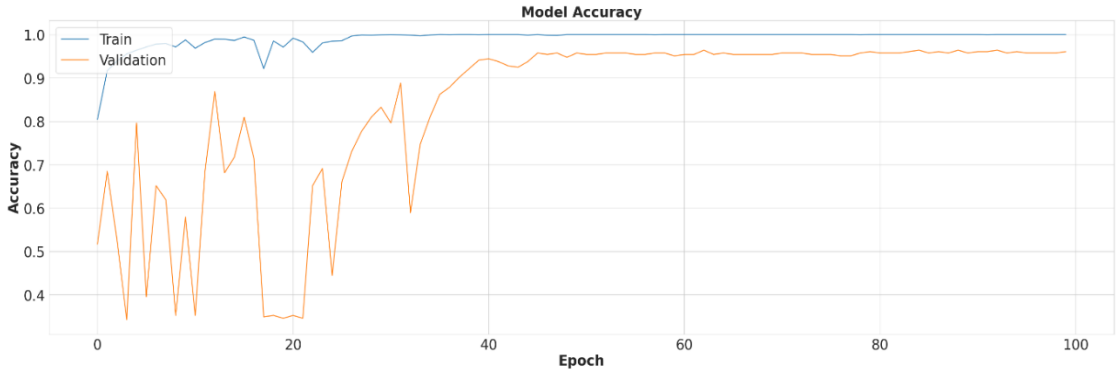

Fig 4.40 Accuracy Performance Graph of NASNetMobile + Added Layer

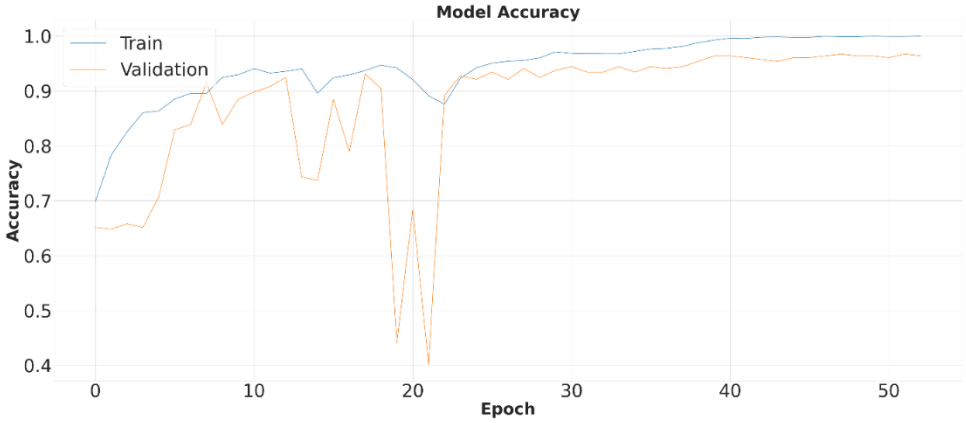

Fig 4.41 Accuracy Performance Graph of ResNet101 + Added Layer

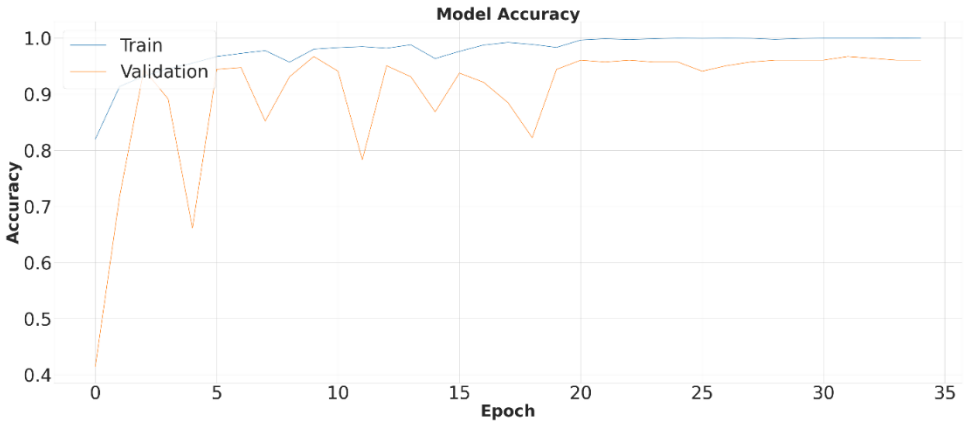

Fig 4.42 Accuracy Performance Graph of Xception + Added Layer

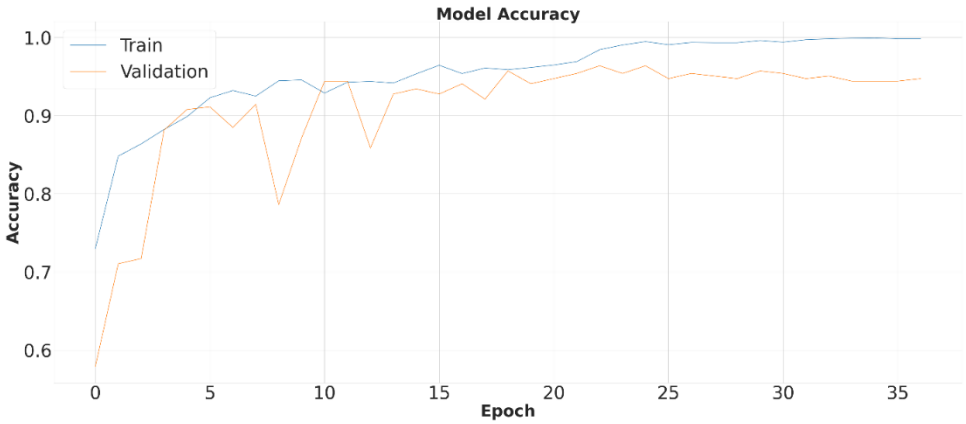

Fig 4.43 Accuracy Performance Graph of DenseNet201 + Added Layer

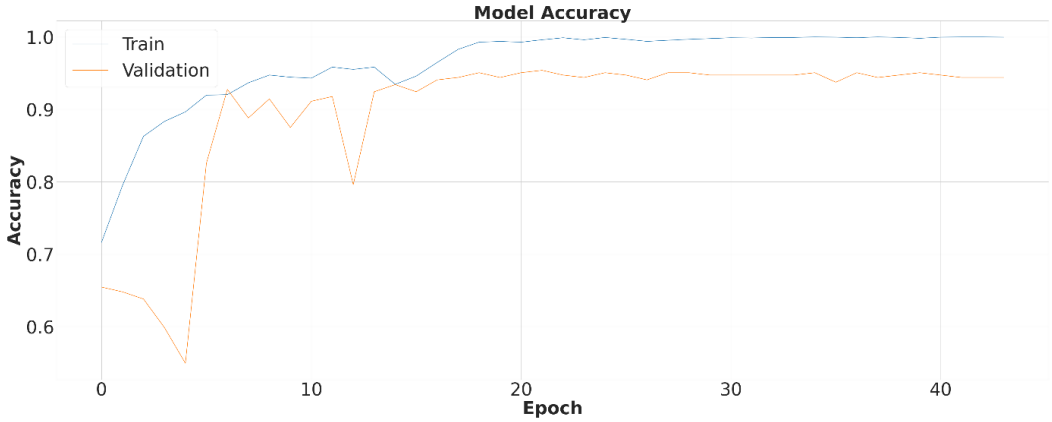

Fig 4.44 Accuracy Performance Graph of ResNet50 + Added Layer

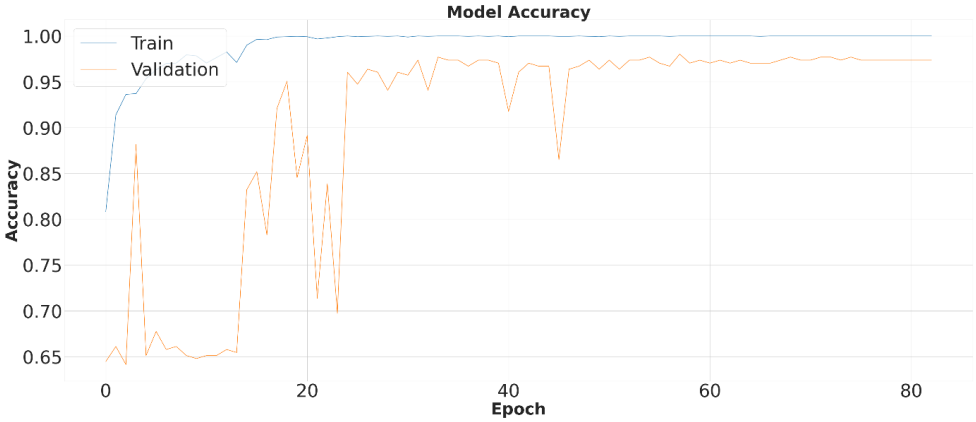

Fig 4.45 Accuracy Performance Graph of EfficientNetB7 + Added Layer

Table 4.3 Classification Report

S No	Deep Learning Model with added Layer	Parameter	Precision	Recall	F1 Score
1	InceptionV3 + Added Layer	0	0.96	1.00	0.98
		1	0.99	0.94	0.96
		Accuracy	0.97	0.97	0.97
		Micro Average	0.98	0.98	0.97
		weighted Average	0.98	0.97	0.97

S No	Deep Learning Model with added Layer	Parameter	Precision	Recall	F1 Score
2	InceptionResNetV2 + Added Layer	0	0.96	0.97	0.97
		1	0.95	0.93	0.94
		Accuracy	0.96	0.96	0.96
		Micro Average	0.96	0.96	0.96
		weighted Average	0.96	0.96	0.96
3	MobileNet + Added Layer	0	0.95	0.99	0.97
		1	0.98	0.92	0.95
		Accuracy	0.96	0.96	0.96
		Micro Average	0.97	0.95	0.96
		weighted Average	0.96	0.96	0.96
4	NASNetMobilev + Added Layer	0	0.96	0.99	0.98
		1	0.99	0.93	0.96
		Accuracy	0.97	0.97	0.97
		Micro Average	0.97	0.96	0.97
		weighted Average	0.97	0.97	0.97
5	ResNet101 + Added Layer	0	0.97	0.96	0.96
		1	0.93	0.94	0.94
		Accuracy	0.95	0.95	0.95
		Micro Average	0.95	0.95	0.95
		weighted Average	0.95	0.95	0.95
6	Xception + Added Layer	0	0.96	0.99	0.97
		1	0.99	0.92	0.95
		Accuracy	0.97	0.97	0.97
		Micro Average	0.97	0.96	0.96
		weighted Average	0.97	0.97	0.97
7	DenseNet201 + Added Layer	0	0.95	0.99	0.97
		1	0.99	0.92	0.95

S No	Deep Learning Model with added Layer	Parameter	Precision	Recall	F1 Score
		Accuracy	0.96	0.96	0.96
		Micro Average	0.97	0.95	0.96
		weighted Average	0.97	0.96	0.96
8	ResNet50 + Added Layer	0	0.97	0.98	0.97
		1	0.96	0.94	0.95
		Accuracy	0.96	0.96	0.96
		Micro Average	0.96	0.96	0.96
		weighted Average	0.96	0.96	0.96
9	EfficientNetB7 + Added Layer	0	0.97	0.99	0.98
		1	0.98	0.95	0..97
		Accuracy	0.98	0.98	0.98
		Micro Average	0.98	0.97	0.97
		weighted Average	0..98	0.98	0.98

Table 4.4 Loss performance matrices for classification model.

S. No	Deep Learning Model with added Layer	Loss	Tversky Loss
1	InceptionV3 + Added Layer	0.1658	0.9086
2	InceptionResNetV2 + Added Layer	0.1567	0.9152
3	MobileNet + Added Layer	0.1556	0.9161
4	NASNetMobile + Added Layer	0.1580	0.9142
5	ResNet101 + Added Layer	0.1659	0.9085
6	Xception + Added Layer	0.1651	0.9089
7	DenseNet201 + Added Layer	0.1767	0.9001
8	ResNet50 + Added Layer	0.1742	0.9024
9	EfficientNetB7 + Added Layer	0.1614	0.9116

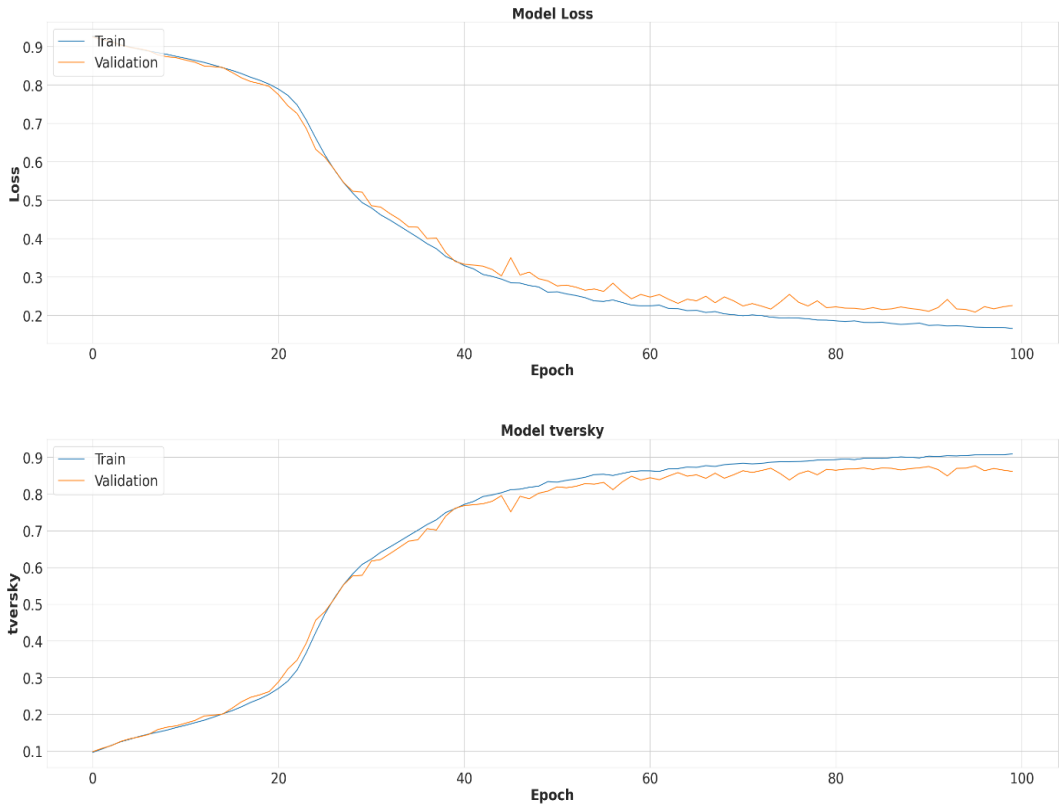

Fig 4.46 Loss and Tversky Performance for InceptionV3 + Added Layer

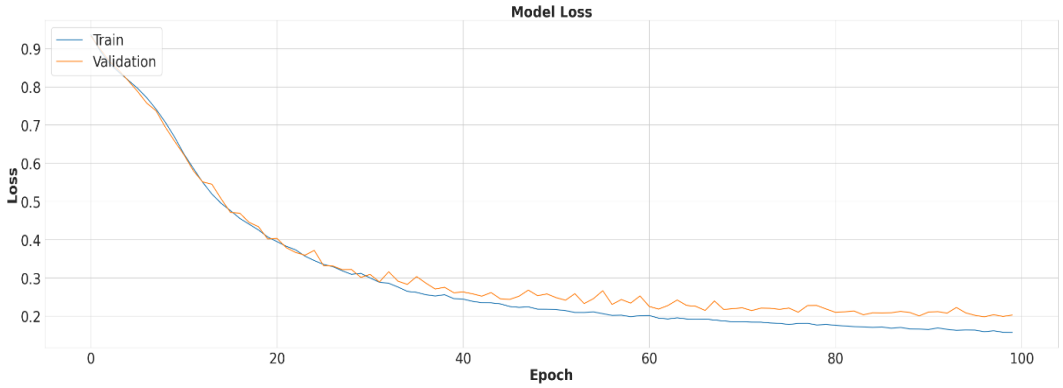

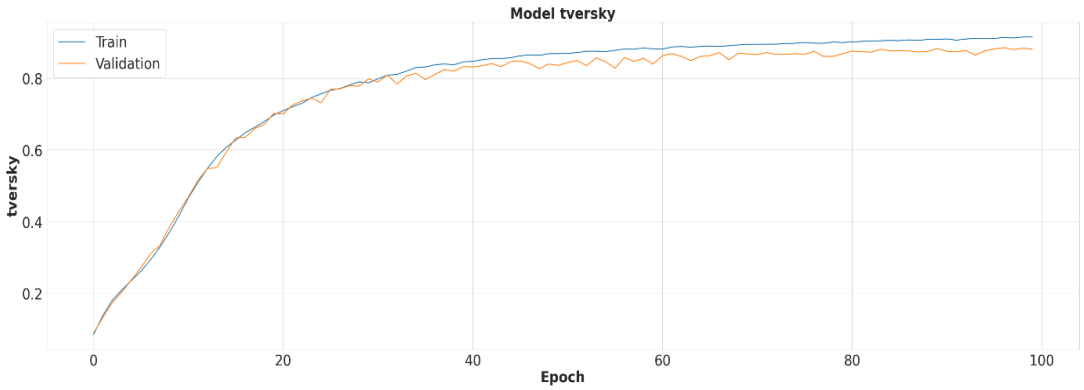

Fig 4.47 Loss and Tversky Performance for InceptionResNetV2 + Added Layer

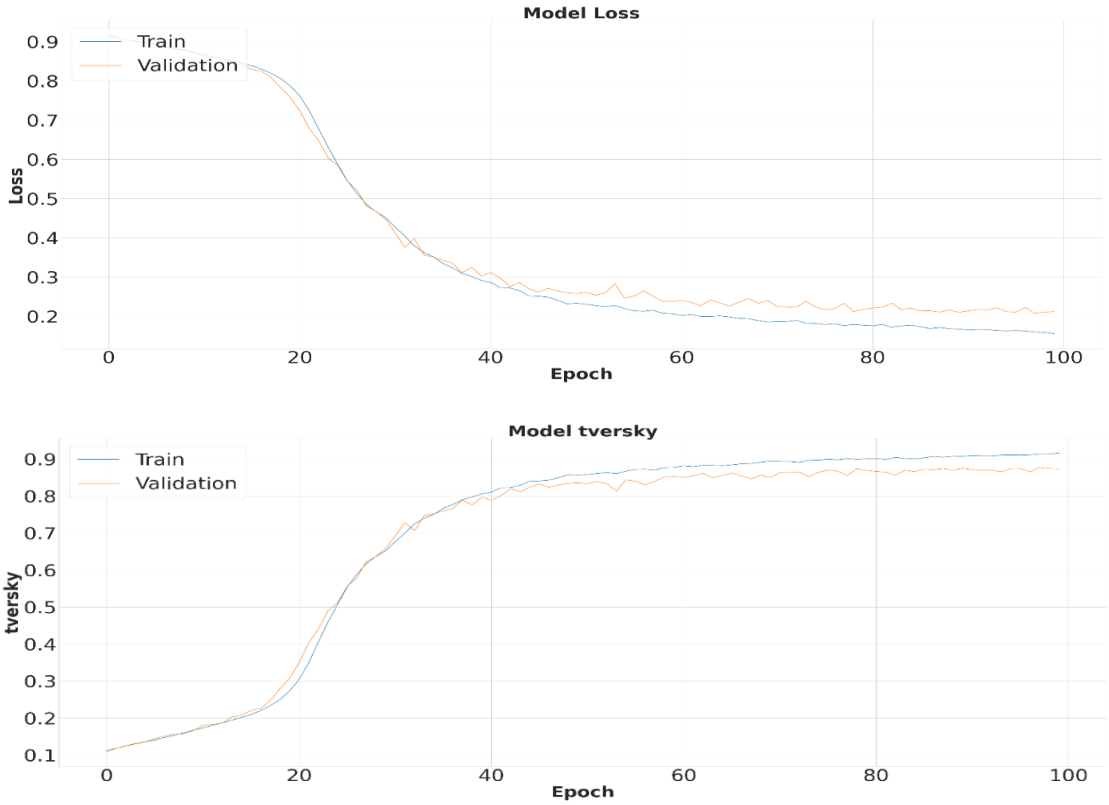

Fig 4.48 Loss and Tversky Performance for MobileNet + Added Layer

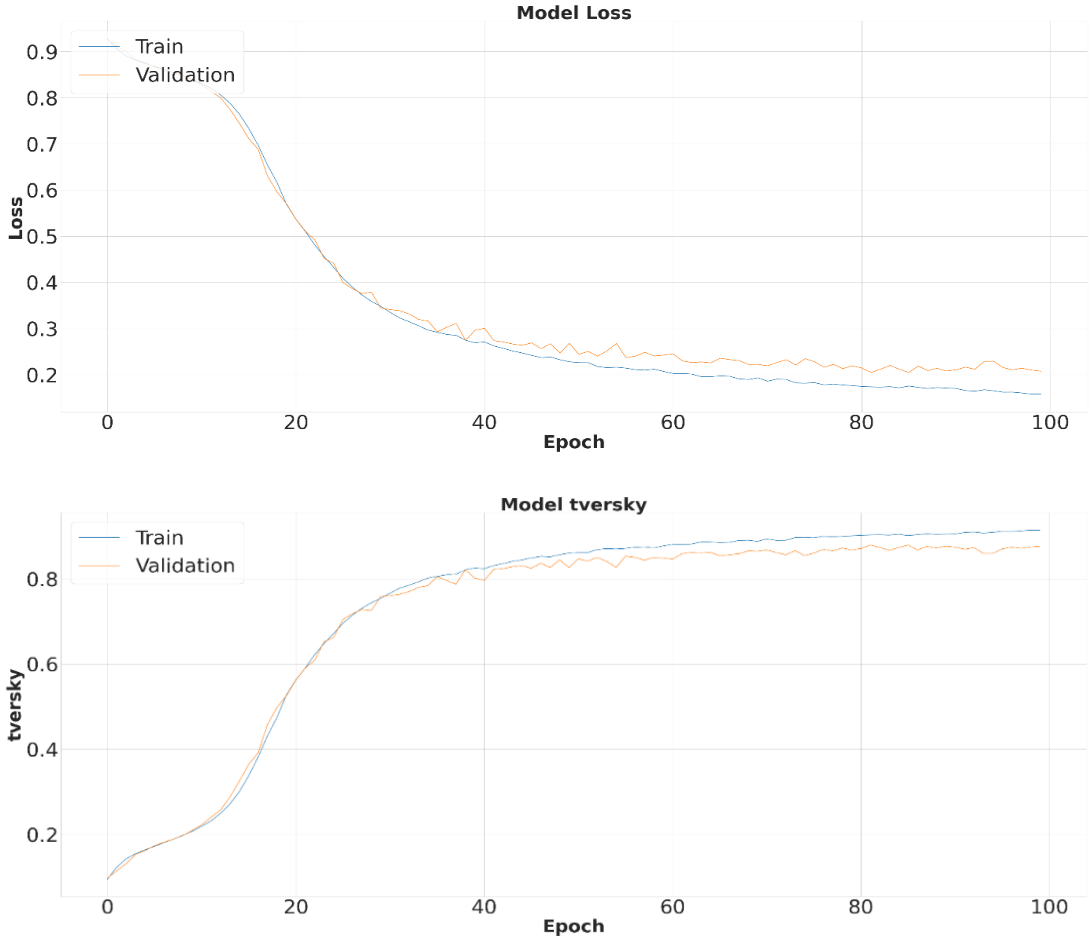

Fig 4.49 Loss and Tversky Performance for NASNetMobile + Added Layer

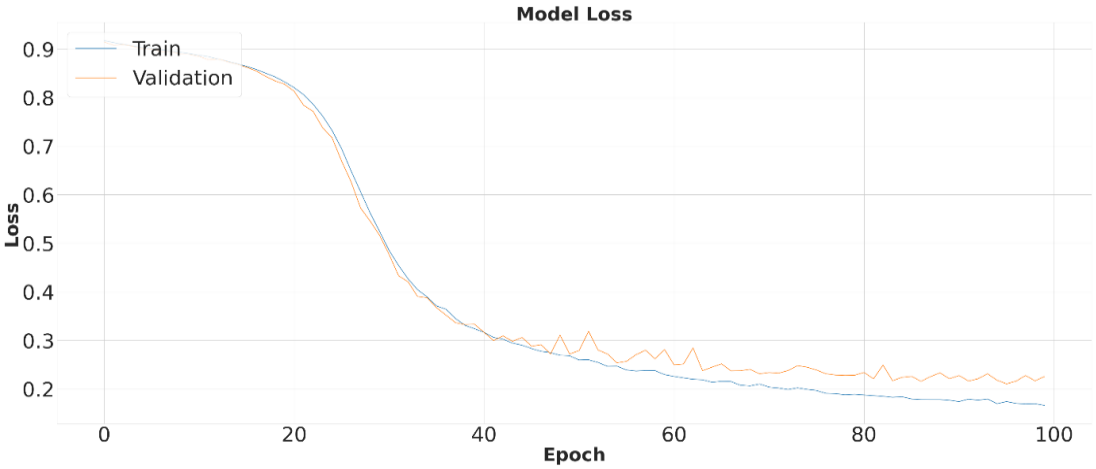

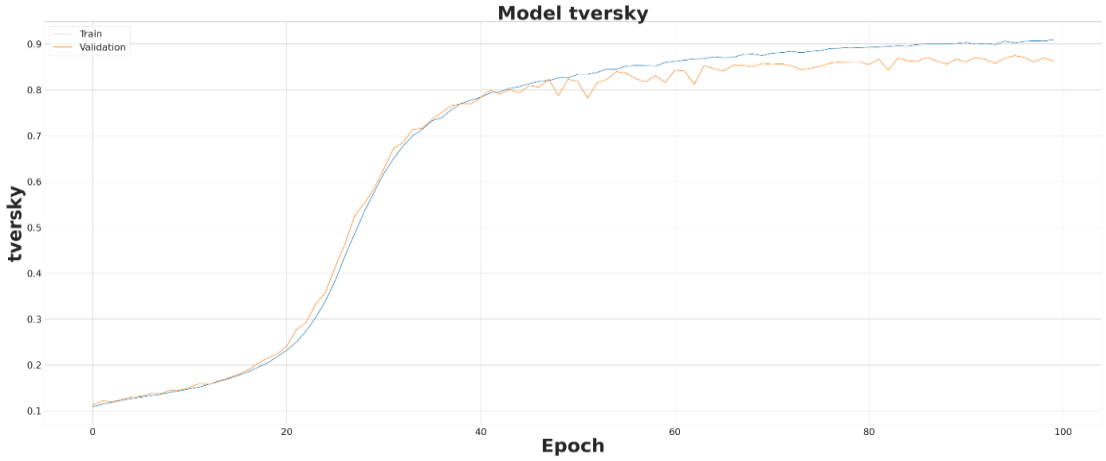

Fig 4.50 Loss and Tversky Performance for ResNet101 + Added Layer

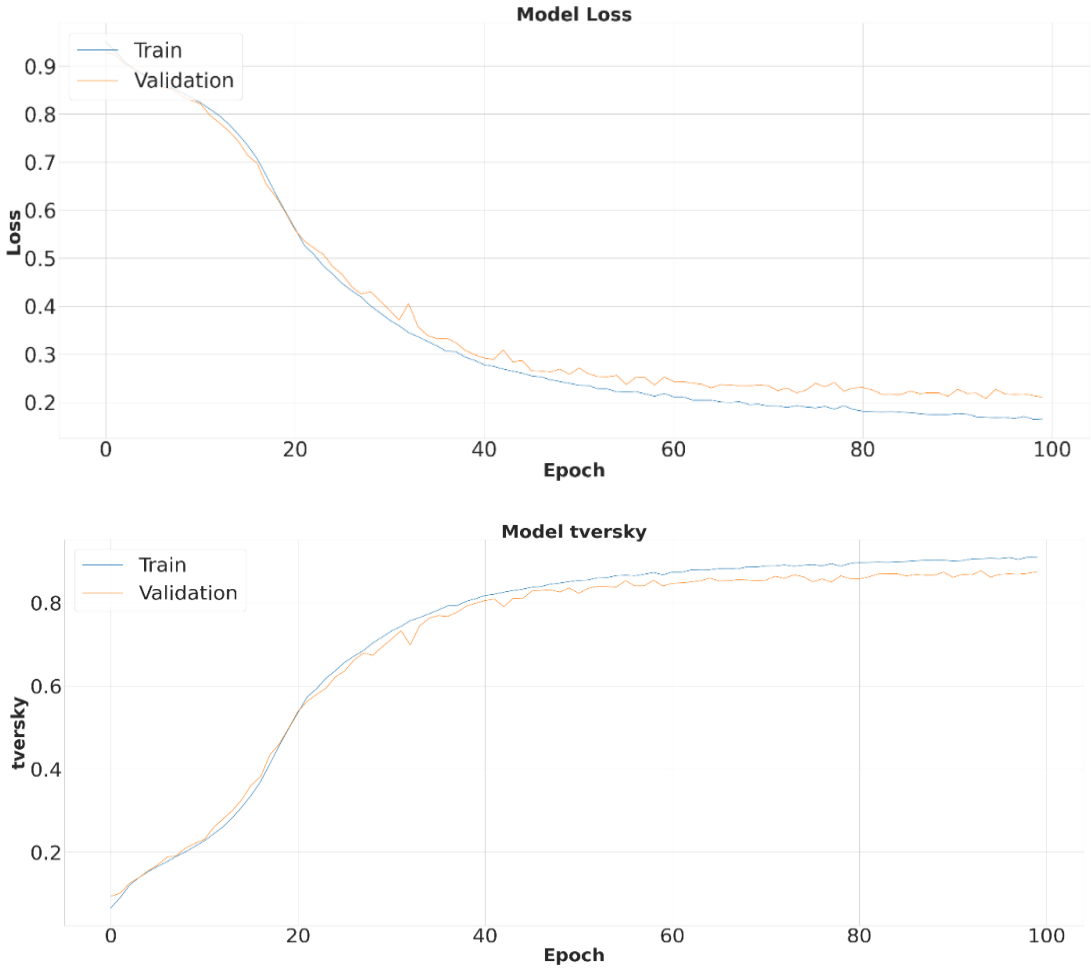

Fig 4.51 Loss and Tversky Performance for Xception + Added Layer

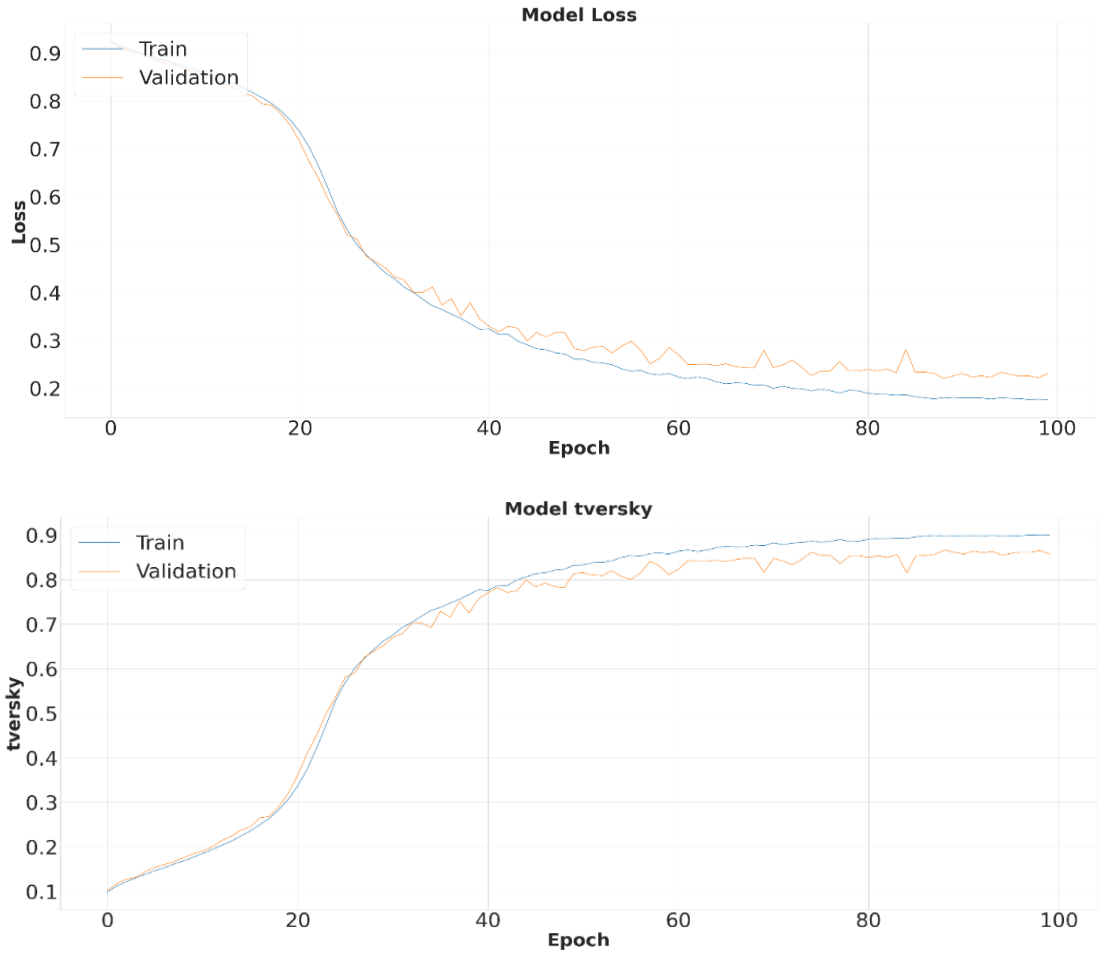

Fig 4.52 Loss and Tversky Performance for DenseNet201 + Added Layer

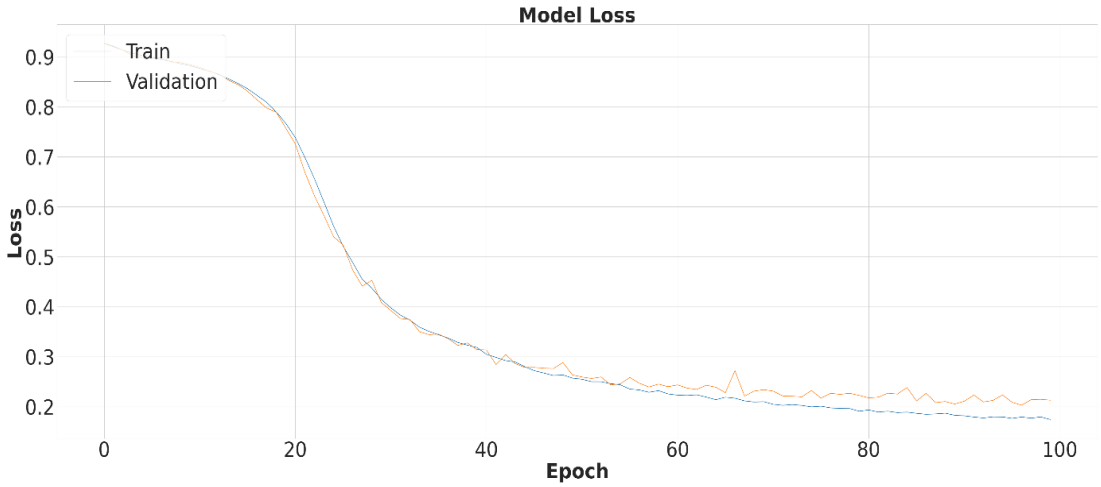

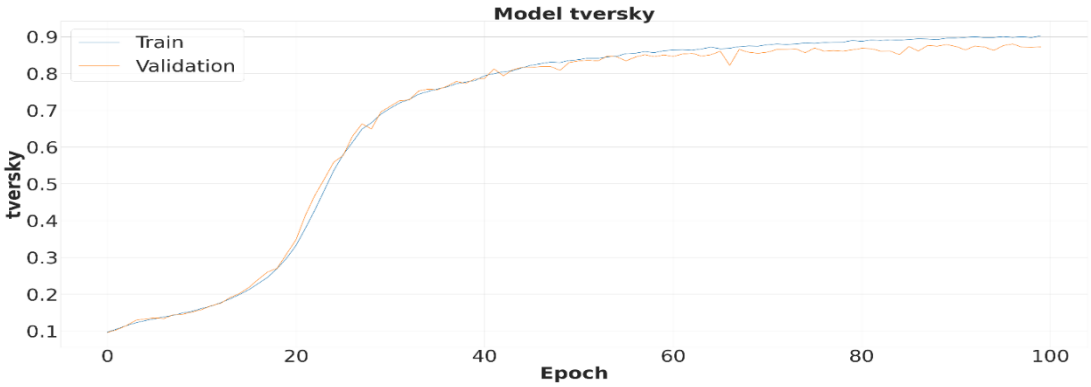

Fig 4.53 Loss and Tversky Performance for ResNet50 + Added Layer

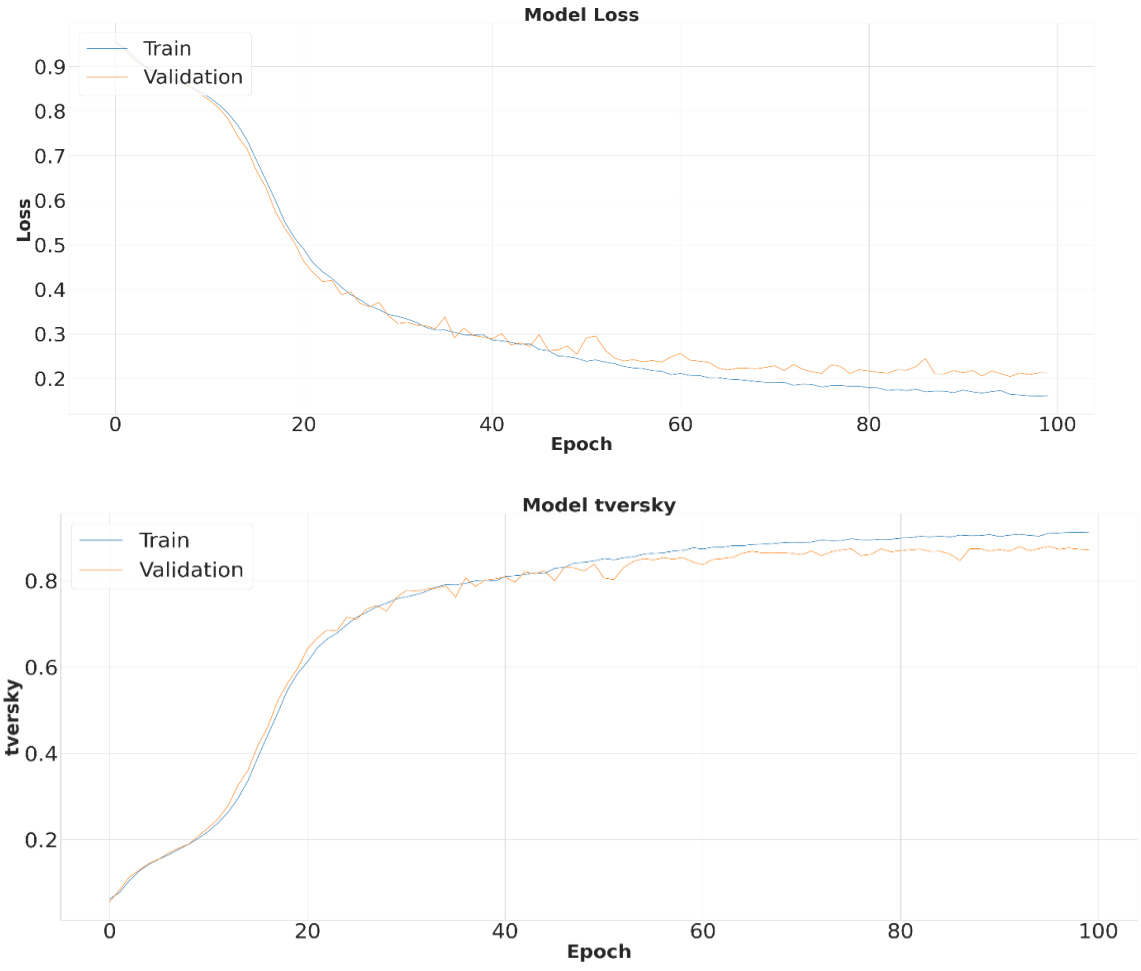

Fig 4.54 Loss and Tversky Performance for EfficientNetB7 + Added Layer

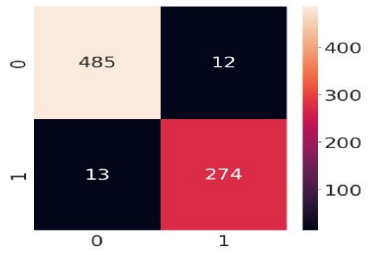

Confusion Matrix for InceptionV3 + Added Layer

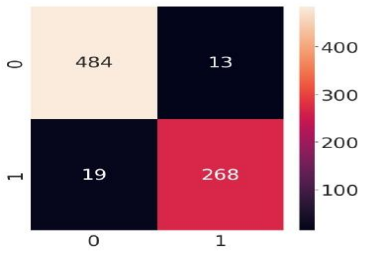

Confusion Matrix for InceptionResNetV2 + Added Layer

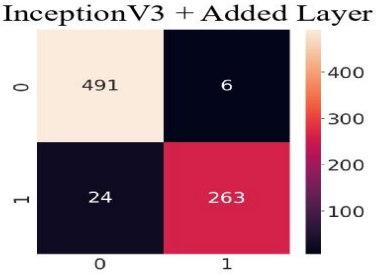

Confusion Matrix for MobileNet + Added Layer

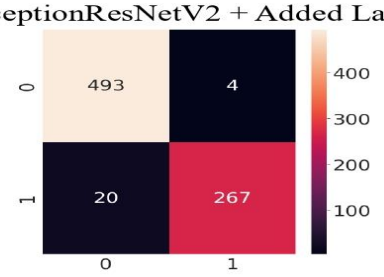

Confusion Matrix for NASNetMobile + Added Layer

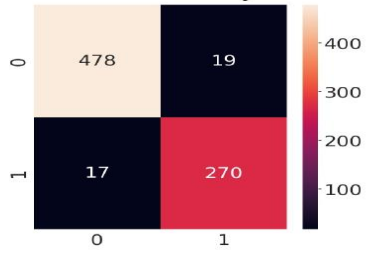

Confusion Matrix for ResNet101 + Added Layer

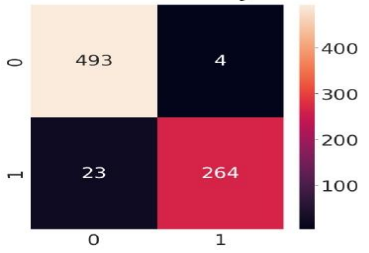

Confusion Matrix for Xception + Added Layer

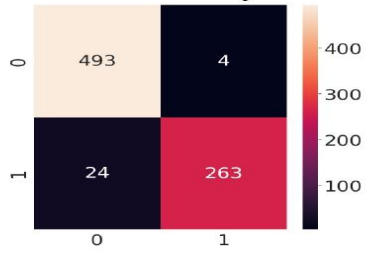

Confusion Matrix for DenseNet201 + Added Layer

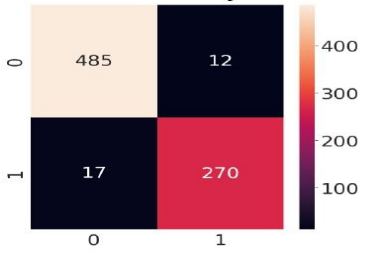

Confusion Matrix for ResNet50 + Added Layer

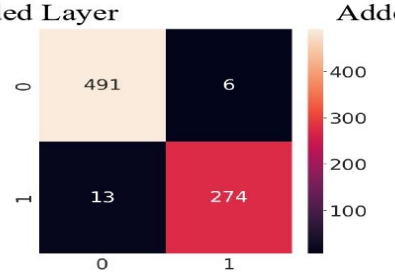

Confusion Matrix for EfficientNetB7 + Added Layer

Fig 4.55 Confusion Matrix for Classification Models

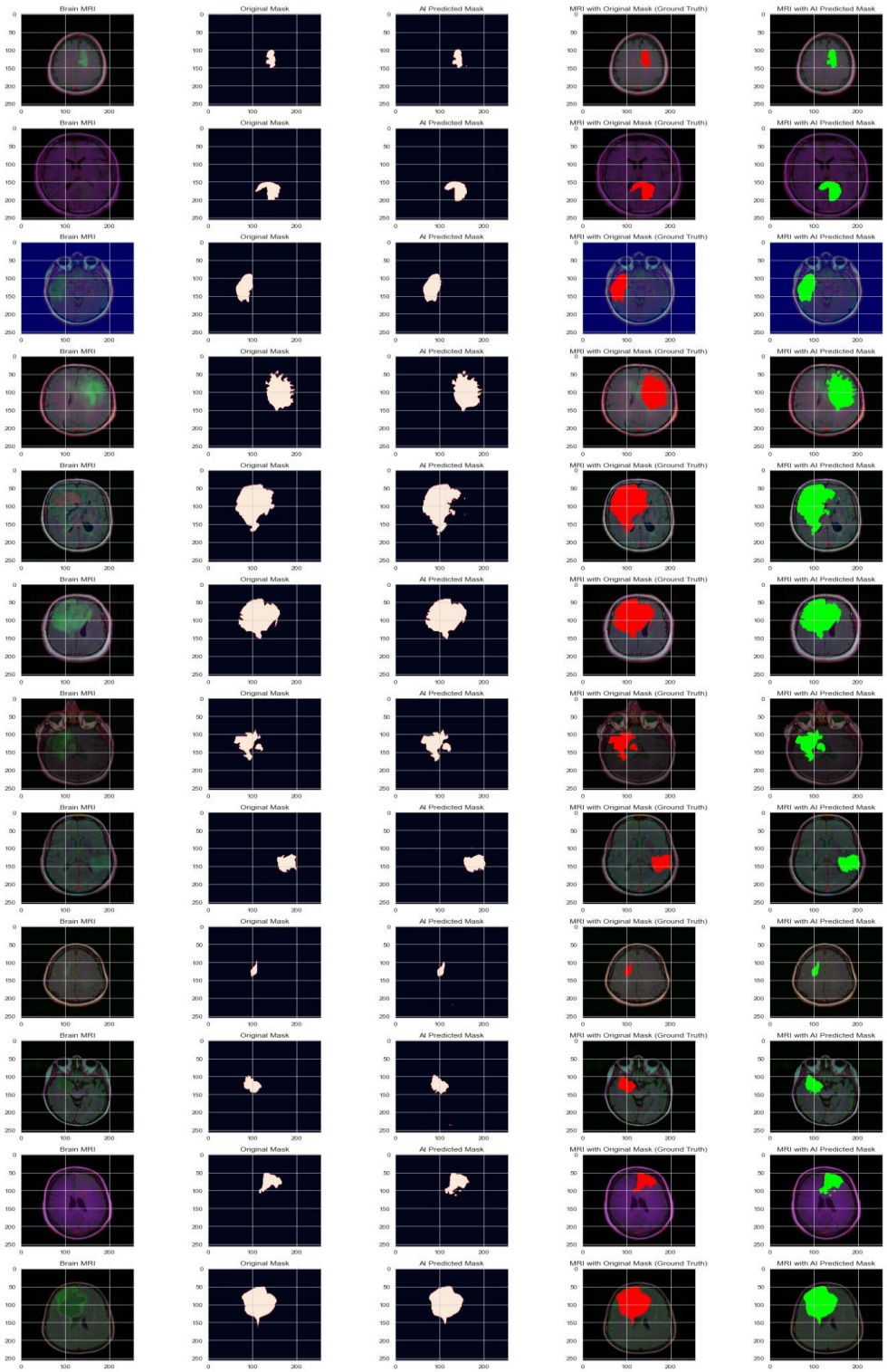

Fig 4.57 Localization of tumor and InceptionV3 + Added Layer Prediction

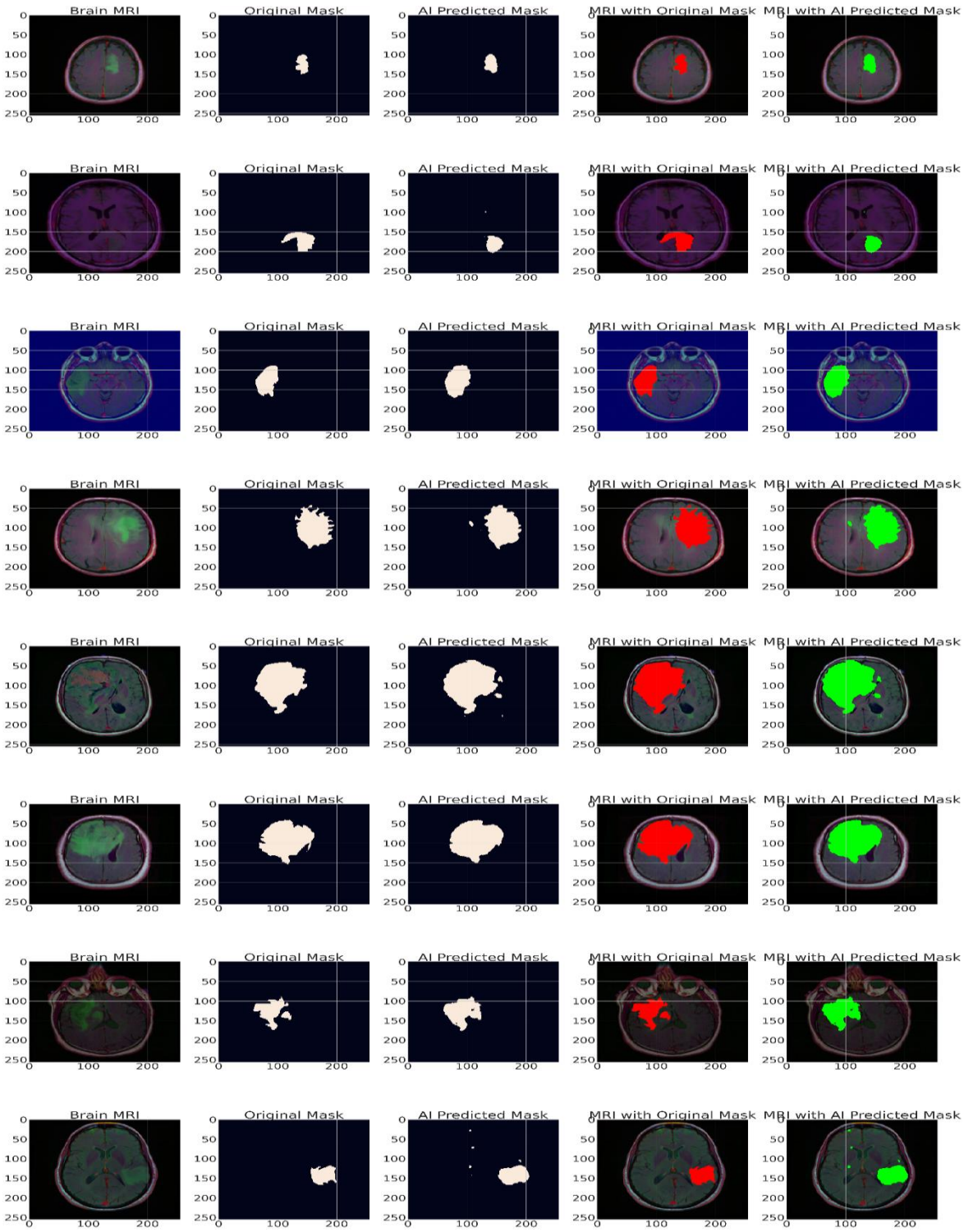

Fig 4.58 Localization of tumor and InceptionResNetV2 + Added Layer Prediction

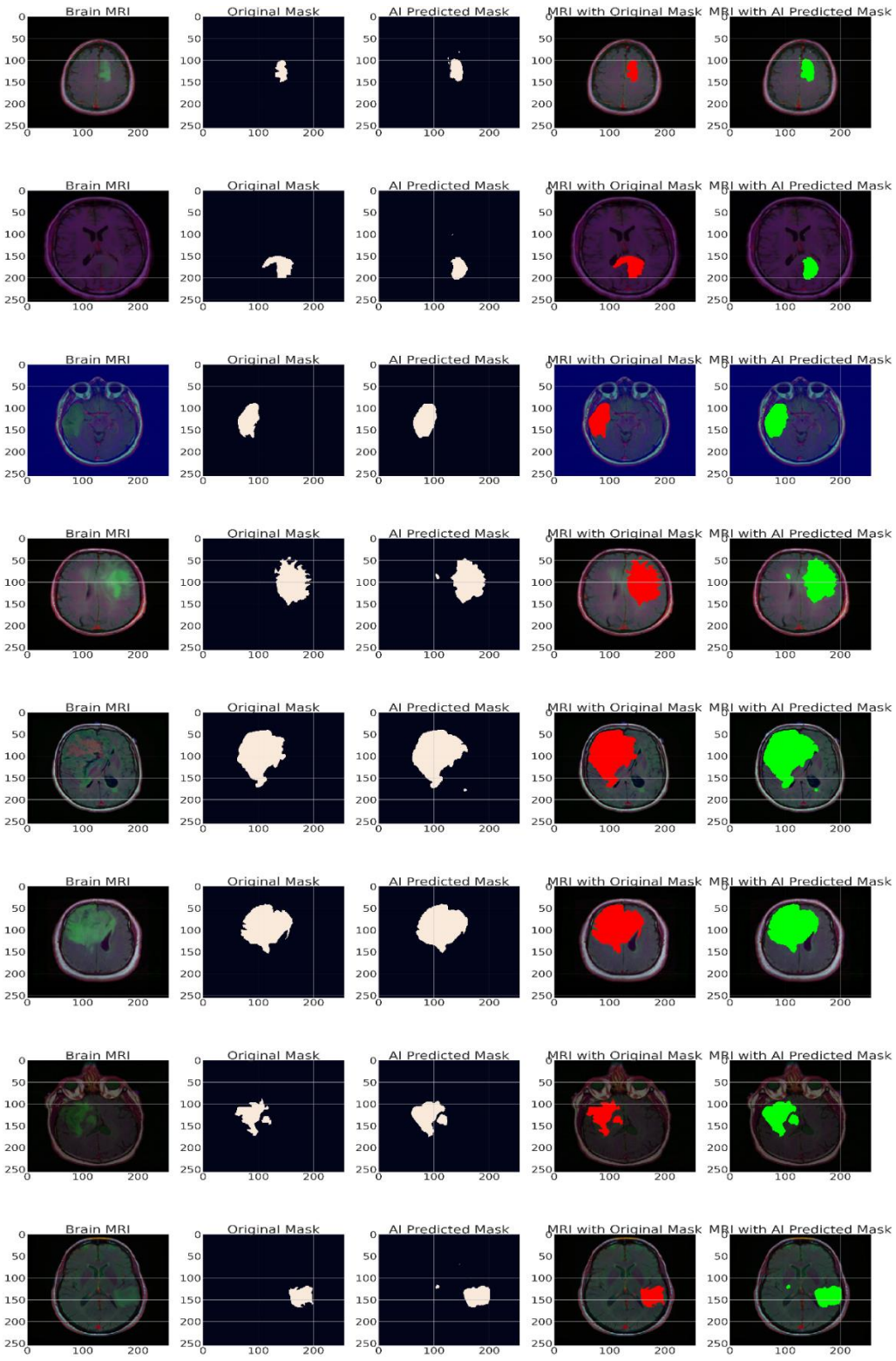

Fig 4.59 Localization of tumor and MobileNet + Added Layer Prediction

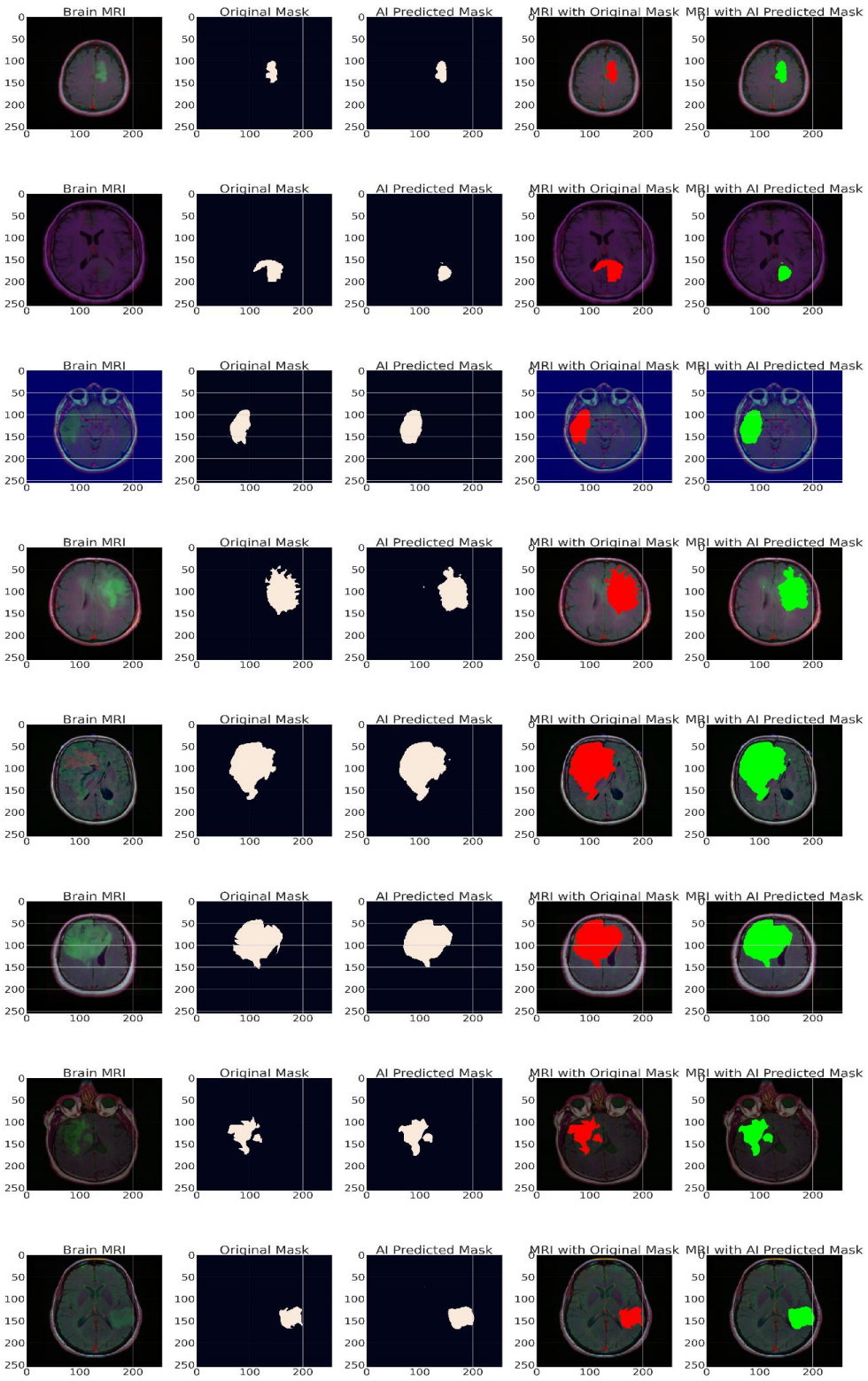

Fig 4.60 Localization of tumor and NASNetMobile + Added Layer Prediction

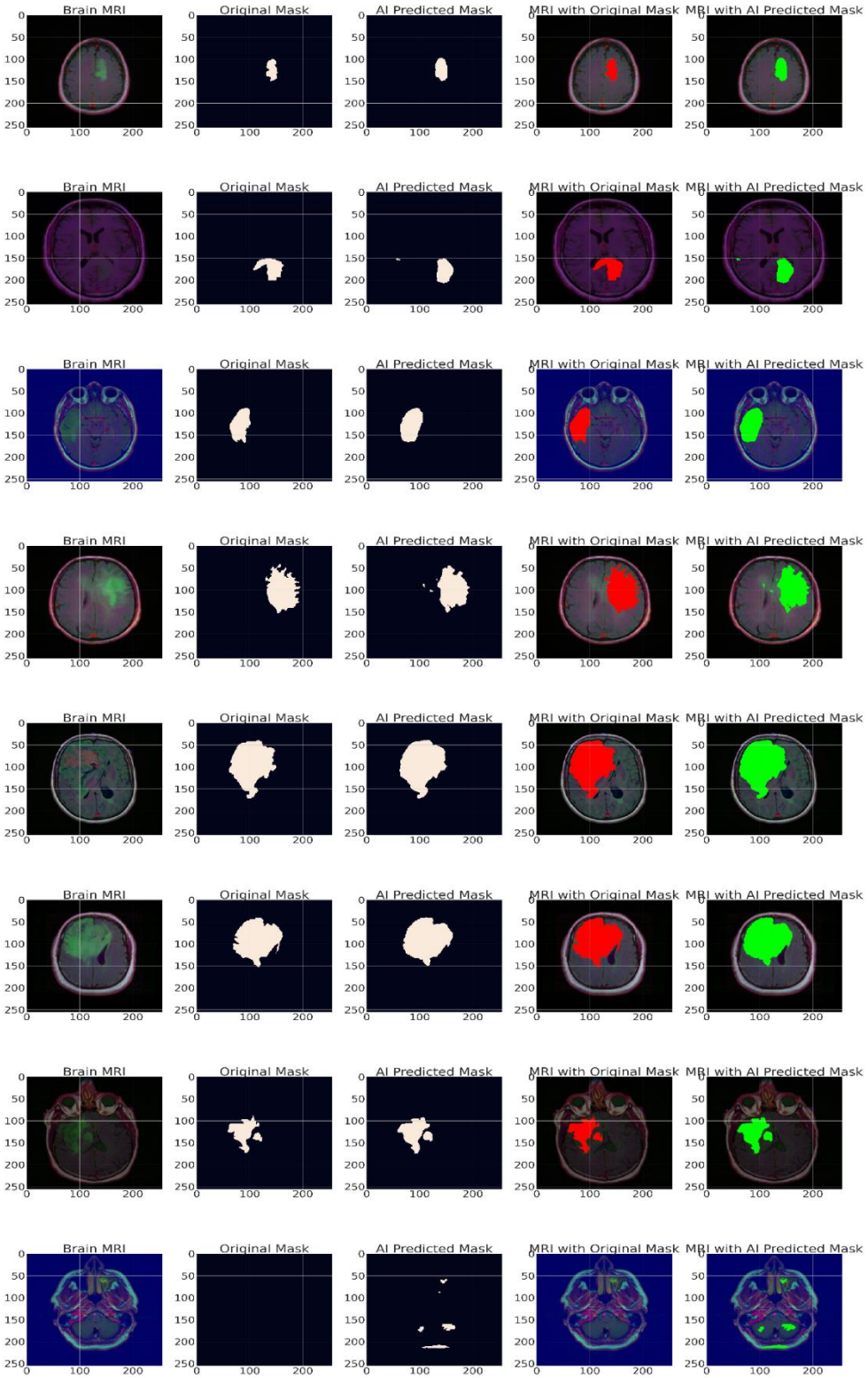

Fig 4.61 Localization of tumor and ResNet101 + Added Layer Prediction

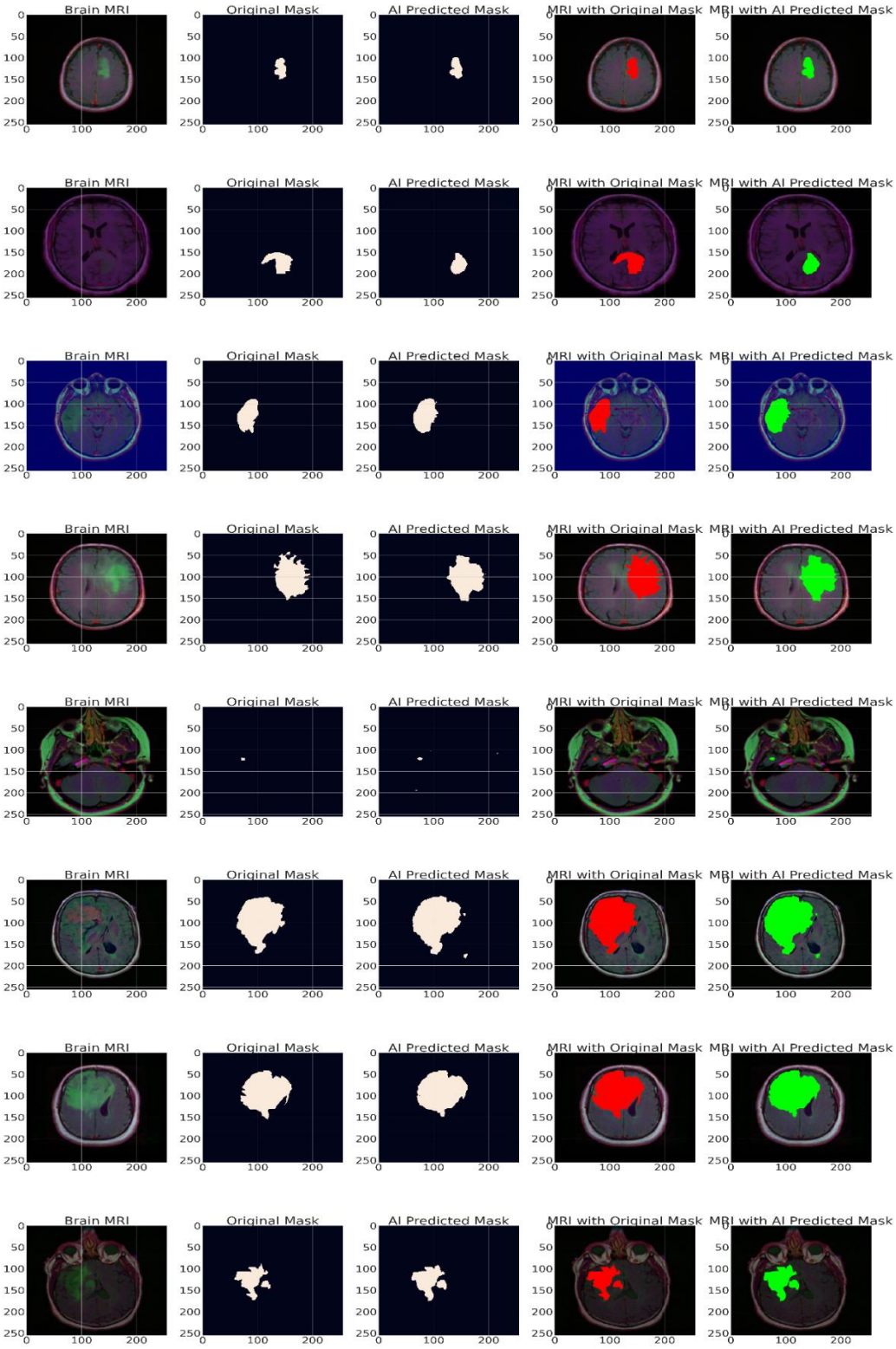

Fig 4.62 Localization of tumor and Xception + Added Layer Prediction

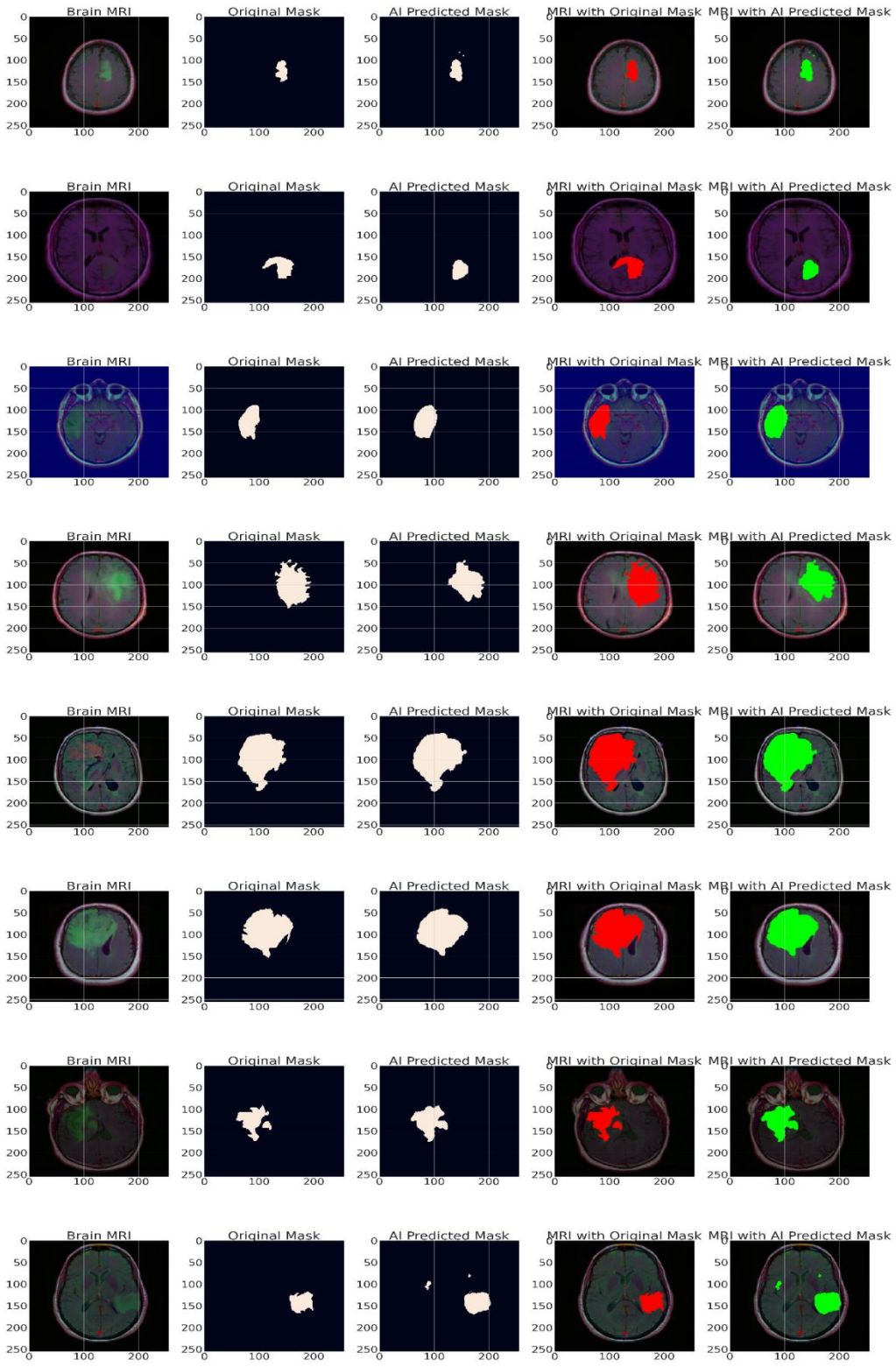

Fig 4.63 Localization of tumor and DenseNet201 + Added Layer Prediction

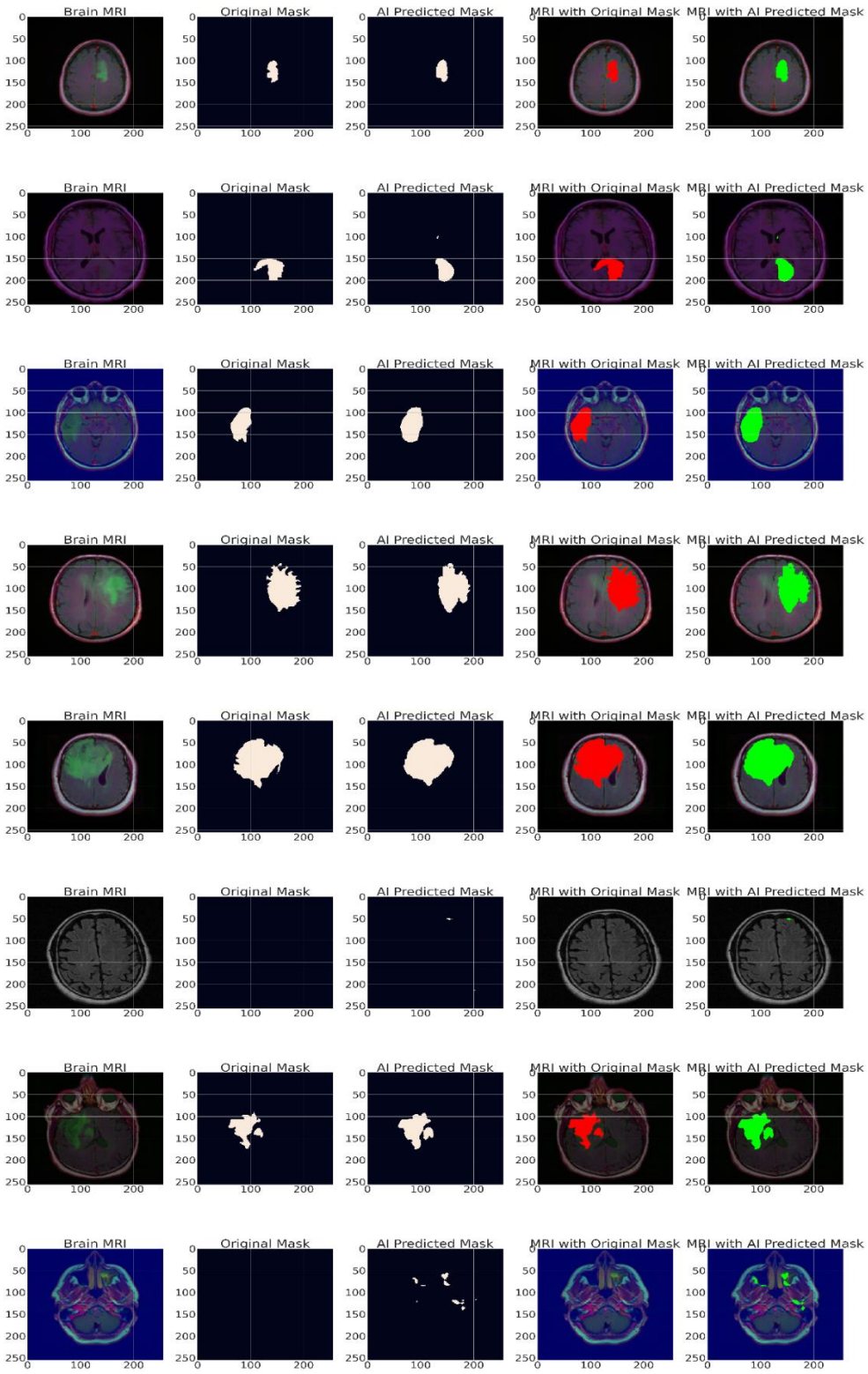

Fig 4.64 Localization of tumor and ResNet50 + Added Layer Prediction

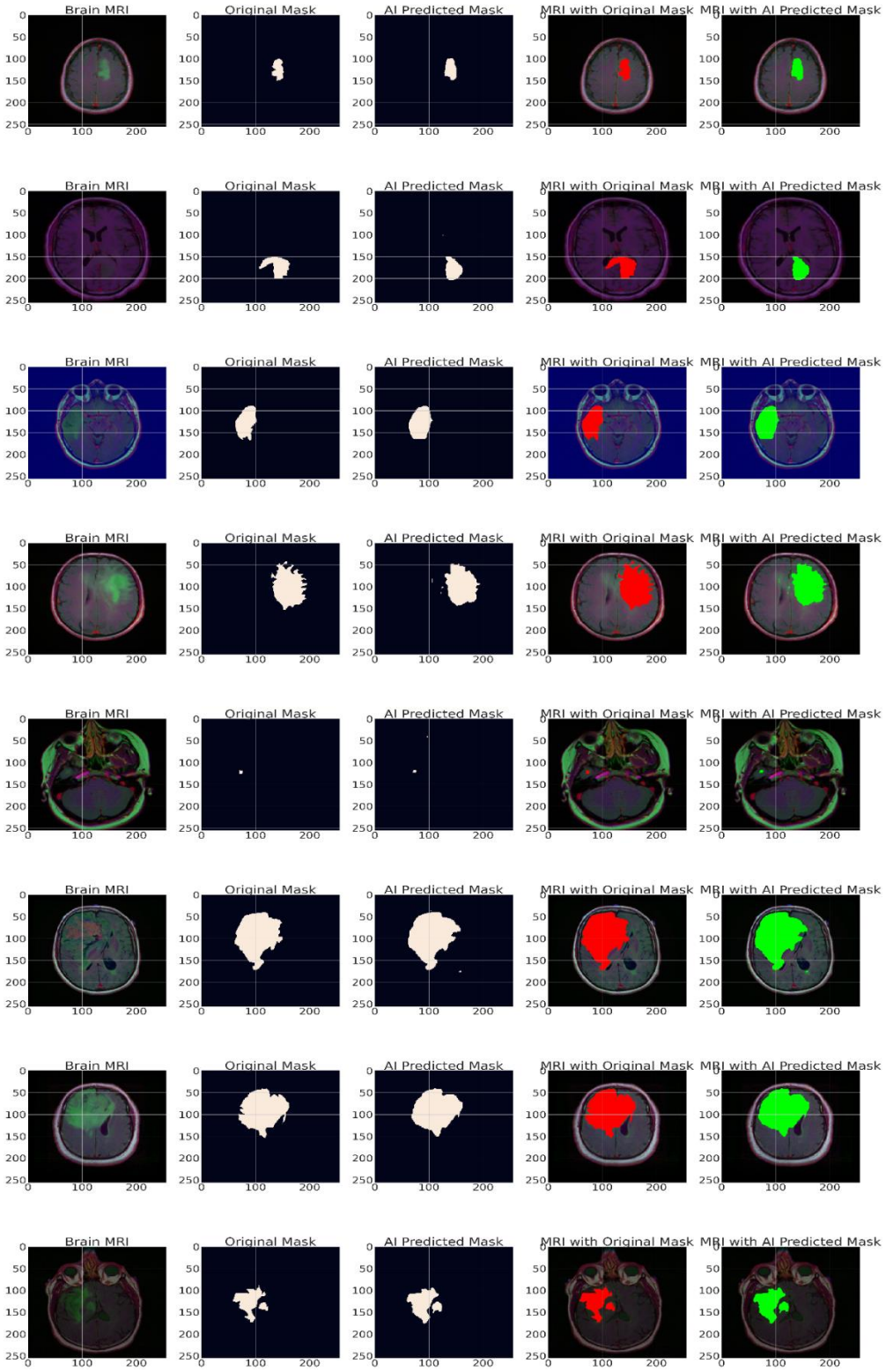

Fig 4.65 Localization of tumor and EfficientNetB7 + Added Layer Prediction

4.7 Discussion

The representation depicts the precise position of the tumour as well as the model's accurate forecasts regarding the tumor's existence or nonexistence. Subsequently, the performance of the suggested model is assessed and contrasted with other established techniques in the current body of research. The results indicate that when the customized EfficientNetV7 is used as the base layer and an additional layer is added with RESUNET, it outperforms traditional approaches, producing more accurate and clinically relevant images.

Table 4.7 Comparison with other state of art model

S. No	Ref No	Model Adapted	Accuracy
1	Ge et al., 2020	CNN-GAN	0.8653
2	Özyurt et al., 2019	CNN-SVM	0.9310
3	Sert et al., 2019	SISR-MFES-CNN	0.9500
4	Ghosh & Santosh, 2021	UNET with RESNeXt50	0.9320
5	Esmaeili et al., 2021	Densenet-121	0.9210
6	Esmaeili et al., 2021	GoogLeNet	0.8730
7	Esmaeili et al., 2021	MobileNet	0.8890
8	Kabir Anaraki et al., 2019	CNN + GA	0.9090
9	Rohilla & Jain, 2023	ResUNetmodel-based CNN	0.9677
10	S et al., 2022	Efficient Regularized CNN with Dimensionality Reduction Module	0.9670
11	Proposed Methodology	InceptionV3 + Added Layer	0.9681
12		InceptionResNetV2 + Added Layer	0.9600
13		MobileNet + Added Layer	0.9600
14		NASNetMobile + Added Layer	0.9700
15		ResNet101 + Added Layer	0.9500
16		Xception + Added Layer	0.9700
17		DenseNet201 + Added Layer	0.9600
18		ResNet50 + Added Layer	0.9630
19		**EfficientNetB7 + Added Layer**	**0.9800**

Our experimental findings provide several key insights into the proposed approach:

(i). The model performed exceptionally well on the provided dataset in accurately determining the presence or absence of a tumor.

(ii). Utilizing Deep Learning Model as the base layer with an additional layer using the RESUNET technique was highly effective in both localizing tumors and predicting their presence or absence.

(iii). The introduction of augmented data during training significantly improved classification performance on the testing set.

(iv). Large imbalances in training data between different classes should be avoided, as they can lead to noticeable variations in performance across individual classes.

(v). When compared to various state-of-the-art methods, our suggested approach achieved performance that was on par with fully supervised approaches, indicating its competitiveness and effectiveness.

The combination of Deep Learning Models with added layers, including Dense Layer, Flatten Layer, Dropout Layer, and Activation Layer, in conjunction with the RESUNET architecture can be highly effective for various tasks. However, there are some limitations to be aware of:

- **Complexity and Resource Requirements:** Adding extra layers and complexity to a model can significantly increase its computational and memory requirements. This may limit its feasibility for deployment on resource-constrained devices or in situations where computational resources are limited.
- **Overfitting Risk:** With the introduction of additional layers, there is a risk of overfitting the model to the training data, especially if the dataset is not large enough or if the regularization provided by the Dropout Layer is insufficient. Careful hyperparameter tuning and the use of a diverse and representative dataset are essential to mitigate this risk.

- **Training Time:** More complex models with added layers typically require longer training times. This can be a limitation when you need to quickly train and deploy a model.
- **Interpretability:** As models become more complex, it can be challenging to interpret and understand their decision-making processes. This is particularly important in applications where model interpretability is a critical factor.
- **Limited Generalization:** Although the addition of layers can improve the model's capacity to understand intricate patterns in the training data, it can also diminish its ability to generalise. Put simply, the model may become too tailored to the training data and exhibit worse performance when faced with unfamiliar data.
- **Data Requirements:** Highly complex models with added layers may require more extensive and diverse training data to perform optimally. In situations where collecting such data is challenging or expensive, this can be a limitation.
- **Hyperparameter Tuning:** Optimising the hyperparameters of the further layers, such as the neuron count in the Dense Layer, the dropout rate, and the selection of activation function, may need extensive testing and fine-tuning.
- **Model Size:** The addition of layers can increase the model's size, which might be a concern in scenarios where model size needs to be minimized for deployment, such as on mobile devices.

4.8 Conclusion

The deep learning model enriched with added layers, including Dense Layer, Flatten Layer, Dropout Layer, and Acivation Layer, in conjunction with the RESUNET architecture, brings about a significant and noteworthy conclusion. This model has demonstrated remarkable improvements in performance, particularly excelling in image segmentation, object detection, and tumor localization tasks. The additional layers have not only boosted accuracy but have also contributed to striking a delicate

balance between model complexity and its generalization capacity. The integration of Dropout Layers has proven to be an effective means of preventing overfitting, reinforcing the model's reliability and robustness. Despite its increased complexity, this model maintains efficiency and manageability in terms of computing resources, making it a versatile option for many applications without requiring excessive computer resources. Moreover, the use of data augmentation techniques during the training phase has significantly improved the model's capacity to produce precise predictions on testing data, highlighting the importance of data preparation. The success of this approach is particularly noteworthy, serving as evidence of its strong competitiveness and efficacy. When compared to other advanced techniques, it has produced similar results to fully supervised algorithms, indicating its usefulness in many and challenging machine learning problems.

CHAPTER 5

MRI BASED BRAIN TUMOR FEATURE EXTRACTION WITH OVERALL SURVIVAL PREDICTION USING DEEP LEARNING INSPIRED REPLICATOR NEURAL NETWORK

In general, predicting a patient's overall survival involves estimating the duration of their life following a given treatment while considering the current state of their tumor. This automated prediction of overall survival takes into account various tumor-related features, such as tumor status, clinical data, age, and gene expression that may be available. Collecting all this information can be somewhat challenging in the healthcare field. Fortunately, the BraTS training dataset offers valuable information like age, resection status, and survival duration to assist in making accurate overall survival predictions. According to the BraTS classification, a patient's survival outcome is categorized into three groups: long-term survivors, mid-term survivors, and short-term survivors.

The mean ages of individuals who survive for mid-term, short-term, and long-term durations are 59, 66 and 57, respectively. However, there is considerable age overlap observed within these groups. Efficient feature selection from MRI images is essential for training the model to make accurate predictions. This section showcases the characteristics derived from MRI scans and highlights the utilisation of a replicator neural network influenced by deep learning for the objective of predicting Overall Survival.

There are a number of important ways in which this study advances healthcare and imaging in medicine.

- The study focuses on the crucial matter of identifying and categorising brain tumours through the use of MRI images. This is highly significant in the

prompt identification and treatment of brain-related diseases. The study makes substantial progress in enhancing the precision and dependability of tumour diagnosis by utilising methods such as deep learning and the Replicator Neural Network.

- Going beyond tumor detection, the study takes a step further by incorporating overall survival prediction, a vital component in clinical decision-making. By leveraging deep learning methods, the research provides a more holistic and comprehensive approach to brain tumor diagnosis and patient care.
- A crucial stage in the processing of medical visuals, obtaining features from MRI exams is the subject of the work. Research aids in the creation of better diagnostic tools by creating and using sophisticated methods for feature extraction.
- The utilization of the Replicator Neural Network showcases innovation in deep learning. This novel approach has the potential to enhance the efficiency and effectiveness of neural networks, making it a valuable addition to the field of medical imaging and healthcare.

This investigate significantly contributes to the progression of medical imaging and healthcare by addressing critical challenges in brain tumor detection, overall survival prediction, and feature extraction using innovative deep learning techniques. It has the potential to bring about positive changes in the diagnosis and treatment of brain-related pathologies, ultimately benefitting patients and the medical community as a whole.

5.1 Specification of Image Dataset

In this intriguing study, we set out to assess the effectiveness of our innovative approach in extracting features and segmenting brain MRI scans using the BraTS2020 dataset. This treasure trove comprises 368 MRI scans, each a canvas of 240x240 dimensions with 155 intricate slices. Within this rich tapestry, we harnessed the power

of four separate forms of imaging: T1, T1C, T2, and FLAIR, as elegantly depicted in Fig 5.1.

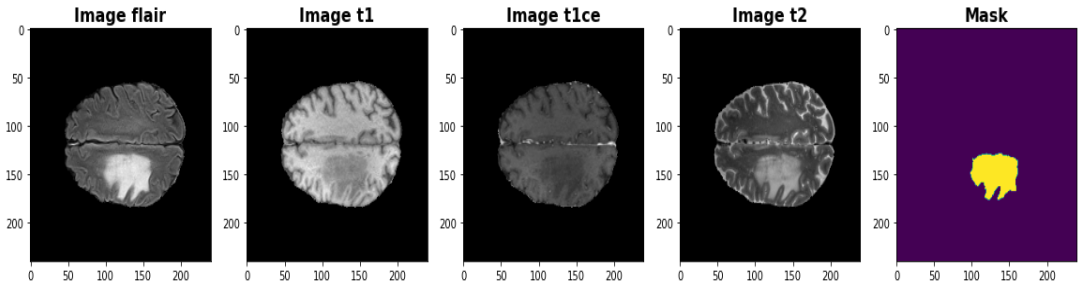

Fig 5.1 Visualization of imaging modalities: T1C (contrast enhanced T1-weighted), T1 (T1-weighted), FLAIR (Fluid Attenuation Inversion Recovery), T2 (T2-weighted).

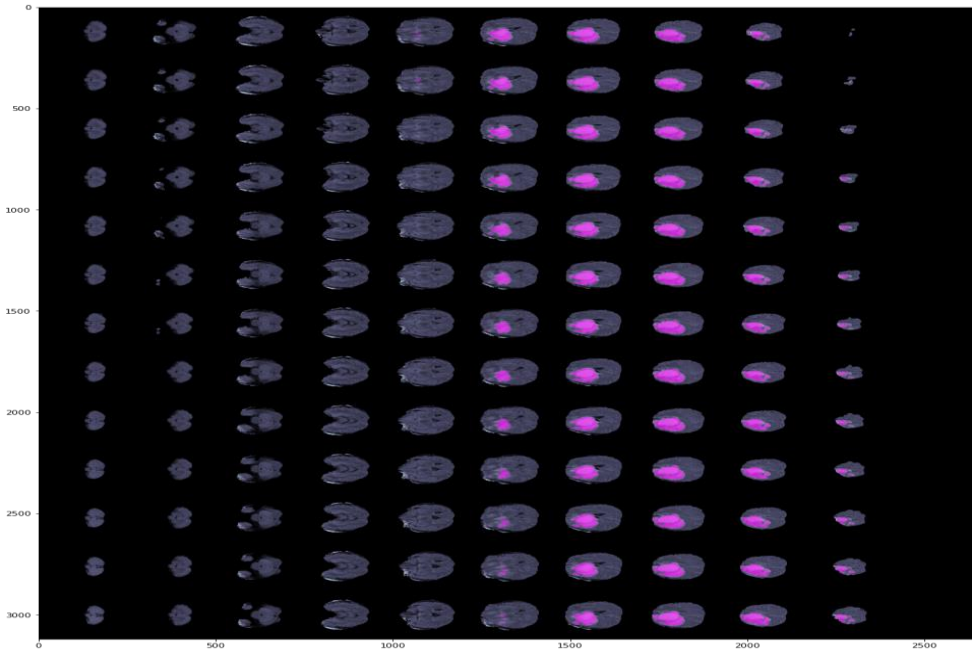

Fig 5.2 Visualization of MR image and mask

Our scientific journey was charted on a machine boasting an i7-6500U CPU, a chip running at a brisk 2.50 GHz, flanked by 16GB of RAM, and graced with the presence of an NVIDIA GEFORCE GTX. Each of these modalities bestowed us with a unique lens through which to unravel the mysteries of brain tumors. The T1 images unveiled the secrets of healthy tissues, while the T1C mode became our guide in tracing the contours of tumors. FLAIR images provided the clues to distinguish edema regions

from cerebrospinal fluid, and the trusty T2 images were our beacon for navigating the edema tumor regions.

With a deft touch, we included all these imaging modalities in our novel approach, giving them the care and attention, they deserved through preprocessing. These preprocessed images then assumed their roles as the artistic brushstrokes on the canvas of neural networks, contributing to a symphony of discovery and insight.

The visualization of MR images and their masks using unique image values, minimum and maximum values, and unique mask values is shown in figure 6. For the MR image dataset used in this study, one image had 1202 unique values, with minimum and maximum image values of 0 and 1. The number of unique mask values was given as (array ([0., 1.], dtype=float32), array ([8727379, 200621])).

5.2 Preprocessing

Improving MR image quality for human and artificial intelligence system interpretations is the primary goal of the pre-processing step. This transformative process not only elevates the visual appeal of MR images but also optimizes their utility by amplifying the signal-to-noise ratio, eliminating undesirable background elements and noise, smoothing out imperfections within regions, and preserving their defining edges.

In the context of the BRATS 2020 dataset, which houses a collection of 368 MR images in the nii format, practical considerations led us to work with a subset of 150 MR images for this experiment. These were thoughtfully partitioned into three segments for training, testing, and validation, corresponding to 75%, 13%, and 12% of the dataset, respectively.

Once these images underwent resizing and were introduced into our system, the next step involved their normalization. In order to ensure that the extraction of features goes smoothly, this normalisation step strengthens them. To achieve this, we harnessed the MinMax scaling technique, a method that ensures consistency among variables assessed at varying scales.

MinMax scaling, a widely embraced practice in data preparation, entails the transformation of input variables into a standardized range of [0,1], where 0 and 1 represent the minimum and

maximum values for each feature or variable. This operation adheres to the underlying principle of equitably adjusting variables to forestall biases during model fitting and learning functions. Equation 1 outlines the mathematical formulation for the min-max scaling process.

$$x_{scaled} = \frac{x - \min(x)}{\max(x) - \min(x)} \quad [5.1]$$

Fig 5.3 represents the distribution graph for training, testing and validation.

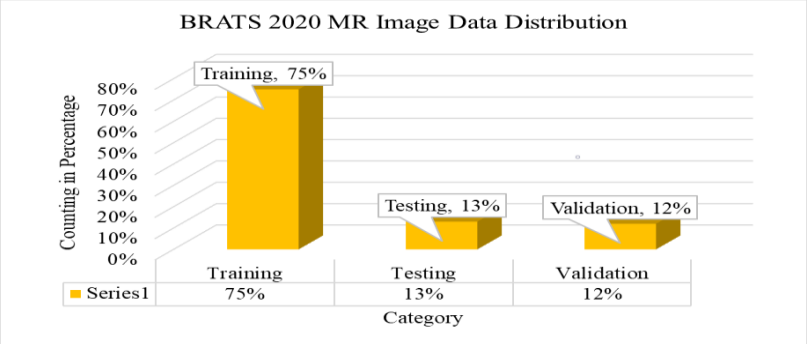

Fig 5.3 Distribution graph for BRATS 2020 Dataset

Pseudocode of class implementation for BRATS Dataset – Pre-processing for feature extraction process

Description: Here Dataset is a set of MR image that will used in the process of pre-processing

Initialization (instance of class, dataframe, phase, resize operation)

Description: Here the process of initialization will be acquired for pre-processing

Set instance of class

Set phase for dataset

Set Augmentation variable to initialize with calling the function for given phase

Set data_types for dataset images

Set resize variable for images

Length (instance of class)

Description: Here to find the shape in dataframe

Return the value of shape in dataframe

Fetch_Images(instance of the class , id for images)

Set id for the location of BRATS images

Set root_path to fatch the value

Set variable for images to load all the modalities

for data_type in class_instance.data_types

Set image_path as per given datatypes

Set variable img to load images from image_path

if class_instance.resize is true then

Update the img with new image size

Load value in img after the calling class_instance.normalize function with given img value as a pareameter

Append all the images

Create a stack for the images

Update the axis

if class_instance.phase not equal to the passed value then

Set variable for the mask_path using the .seg value of MR image

Set variable mask for the loading of segmented value

if class_instance.resize is true then

Update mask with resize value

Convert mask value from int to float and update mask variable

Update mask with 0 and 1 value

Call the function to update the mask label

Perform the operation of augmentation

Set img and mask for augmented value of image and mask

Return value of id, image and mask

Return id and image

Load_Images(class_instance, path of the file)

Description: This function to load all the images and convert into array form

Set data variable to load value of file path

Update data variable after converting into array

Return data value

Normalize_data(class_instance, data as array form)

Description: This function dedicated to normalize the data as per min and max value of

images

Set datamin for minimum value of the data

Return value of the expression [(data – datamin)/(max(data) - datamin]

Preprocess_label_mask(class_instance, mask as an array)

Description: Update mask value for the object of WT, TC and ET

Update mask value for Whole Tumor with the value of 0 and 1

Update mask value for Tumor Core with the value of 0 and 1

Update mask value for Enhanced Tumor with the value of 0 and 1

Create a stack for WT, TC and ET mask value

Update the axis for mask value

Return value of the mask

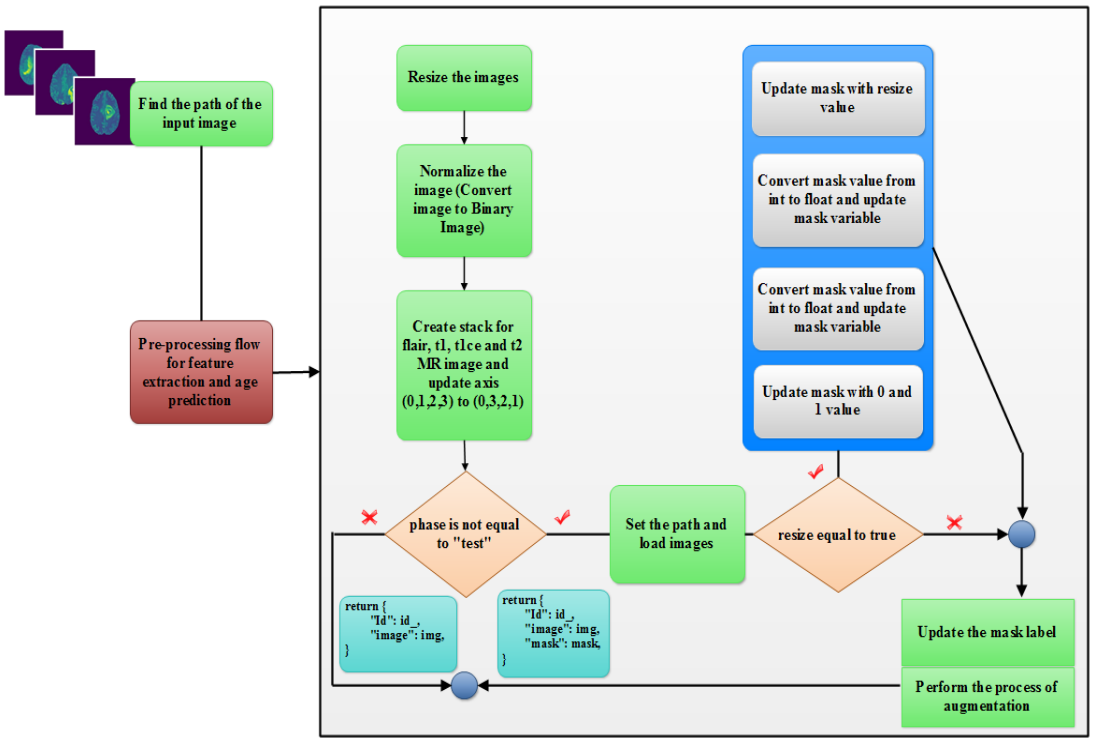

Fig 5.4 Work flow for Preprocessing

5.3 Network Architecture and Training Approach for Feature Extraction (3D Replicator Neural Network Methodology)

A Replicator Neural Network belongs to the family of feedforward neural networks that possesses the unique ability to reconstruct output based on the very input it receives. It follows a distinctive process wherein it initially reduces the dimensionality of the input data and subsequently generates the output based on this transformed representation. These networks find frequent application in the domain of unsupervised learning, where their prowess lies in unveiling concealed data relationships and rendering them in a more concise and understandable format.

One of the intriguing qualities of Replicator Neural Networks is their capability to reframe unsupervised learning challenges into supervised learning algorithms. By doing so, they become adept at discerning intricate patterns within datasets. The core operation of these networks involves transmitting the input through to the output. Simultaneously, an encoder network takes on the role of compressing the input into a more compact encoded form, while a decoder network is entrusted with the task of decoding this encoding to reconstruct the original input, as detailed in (Chen & Guo, 2023).

The encoding created by the encoder layer not only represents the information in a lower-dimensional form but also unveils intricate and complex connections between data points. The components of a Replicator Neural Network, as elucidated in Figure 5.5, are as follows:

- Encoder: The encoder is a part of the network that takes in data and uses it to generate a lower-dimensional encoding.
- Bottleneck: The encoding originates in the lower-dimensional hidden layer. It decides on the dimensional encoding of the input and reduces the number of nodes in the bottleneck layer.
- Decoder: The decoder takes the input data and uses it to recreate the original data using the encoded data.

Hyperparameters:

- Code Size: Signifies the number of intermediate layer nodes, where fewer nodes lead to more compression.
- Number of Layers: Shows the entire number of layers used by the encoder as well as the decoder network.
- Nodes per layer: a stacked encoding network, like the replicator neural network in the above picture, has a decreasing number of vertices per level in the encoder levels that follow the homogeneous decoder and an increasing number in the symmetric decoder.
- Loss Function: Cross entropy is commonly used if the input values are within the range [0, 1], otherwise should be used Mean Squared Error.

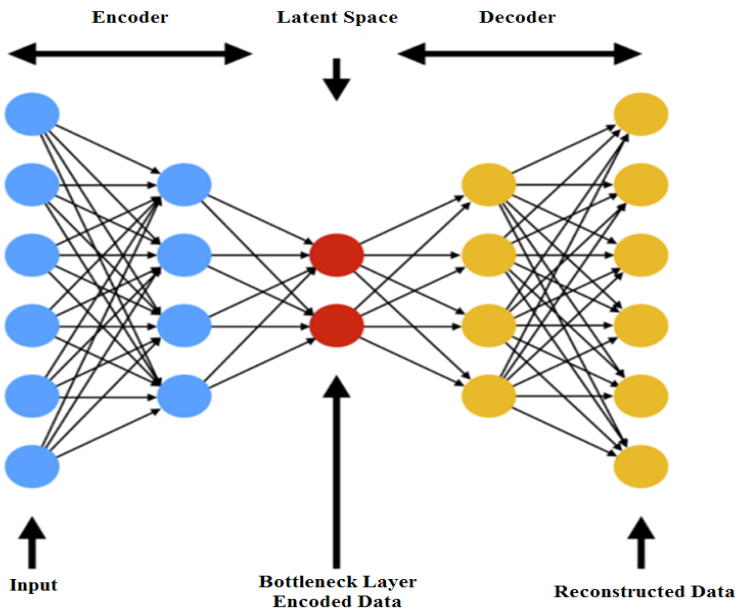

Fig 5.5 Component of Replicator Neural Network with Latent Space (Kay et al., 2022)

According to the following elements, replicator neural network is described: The spaces of decoded instructions **(X)** and encoded information **(Z)** are two sets. The majority of the time, **X** and **Z** are both Euclidean spaces, with $\mathbf{X}=\mathbb{R}^m$ and $\mathbf{Z}=\mathbb{R}^n$ for certain m and n.

There are two primary components of functions that have been parametrized: the encoder family $\boldsymbol{E_{\emptyset} : X \rightarrow Z}$, parametrized by $\emptyset$; and the decoder family $\boldsymbol{D_{\theta} : Z \rightarrow X}$; parametrized by θ.

We often write $\boldsymbol{z = E_{\emptyset}}$ for any value of $\boldsymbol{x \in X}$ and refer to it by many names, including the code, latent variable, latent representation, latent vector, etc. On the other hand, we often write $\boldsymbol{x' = D_{\theta}(z)}$ and correspond to this as the (decoded) message for any $\boldsymbol{z \in Z}$.

Typically, multilayer perception is used to design both the encoder and the decoder. As an illustration, the one-layer MLP encoder $\boldsymbol{E_{\emptyset}}$ **is**

$$\boldsymbol{E_{\emptyset}(x) = \sigma(W_x + b)} \qquad [5.2]$$

The term "weight" refers to a matrix represented by W, "bias" refers to a vector indicated by b, and "activation function," denoted by $\boldsymbol{\sigma}$.

5.3.1 Training a Replicator Neural Network

The training of proposed 3D replicator neural network consists of just a bundle of two factors on its own. Training needs an assignment in order to assess its quality. A benchmark probability distribution $\boldsymbol{\mu_{ref}}$ over $\boldsymbol{X}$ and a "reconstruction efficiency" function $\boldsymbol{d : X \times X \rightarrow [0, \infty]}$ are used to define a job, and $\boldsymbol{d(x, x')}$ is a measurement of how far **x'** deviates from **x**.

These enable us to construct the replicator neural network's loss function as

$$\boldsymbol{L(\theta, \emptyset) := \mathbf{E}_{x \sim \mu_{ref}}[d(x, D_{\theta}(E_{\emptyset}(x)))]} \qquad [5.3]$$

The presented replicator neural network for the assumed job $\boldsymbol{(\mu_{ref}, d)}$ is then $\boldsymbol{\arg\min_{\theta,\emptyset} L(\theta, \emptyset)}$. Any mathematical optimization approach can be used to find the suggested replicator neural network.

The two primary components of replicator neural network are an encoder that converts a communication to a code and a decoder that extracts the information from the code. The recovery quality function d defines "near to perfect" as the performance that an ideal replicator neural network may achieve in terms of restoration.

5.3.2 Interpretation

Figure 10 illustrates how the 3D Replicator Neural Network for feature extraction interprets the model; the model is displayed after input has undergone pre-processing and normalisation, and the encoder has three convolutional layers, three pooling layers, and one linear layer.

Step 1 - Initialization for encoding representation is like that

$$Convolutional\ Layer = \begin{cases} conv1 \rightarrow conv3d(4,16,3) \\ conv2 \rightarrow conv3d(16,32,3) \\ conv3 \rightarrow conv3d(32,96,3) \end{cases}$$

$$Pooling\ Layer = \begin{cases} pool1 \rightarrow MaxPool3d(kernel\_size = 2, stride = 2, return\_indices = True) \\ pool2 \rightarrow MaxPool3d(kernel\_size = 3, stride = 3, return\_indices = True) \\ pool3 \rightarrow MaxPool3d(kernel\_size = 2, stride = 2, return\_indices = True) \end{cases}$$

Step 2 - Initialization for decoding representation is like that

$$Deconvolutional\ Layer = \begin{cases} deconv1 \rightarrow ConvTranspose3d(96, 32, 2) \\ deconv2 \rightarrow ConvTranspose3d(32, 16, 3) \\ deconv3 \rightarrow ConvTranspose3d(16, 4, 3) \end{cases}$$

$$Unpooling\ Layer = \begin{cases} unpool1 \rightarrow\ MaxUnpool3d(kernel\_size = 2, stride = 2) \\ unpool2 \rightarrow\ MaxUnpool3d(kernel\_size = 3, stride = 3) \\ unpool3 \rightarrow\ MaxUnpool3d(kernel\_size = 2, stride = 2) \end{cases}$$

Step 3 – To perform the operation of Encoding the data frame:

$$conv1 \rightarrow pool1 \rightarrow conv2 \rightarrow pool2 \rightarrow conv3 \rightarrow pool3 \rightarrow Encoding\_linear$$

After the process of the above mention layers, the Replicator Neural Network 3D model returns the features that will be decoded by the next steps.

Step 4 – The layering structure for the decoding as per the return features using deconvolution and unpooling like that:

$$Decoding\_Linear \rightarrow unpool1 \rightarrow deconv1 \rightarrow unpool2 \rightarrow deconv2 \rightarrow unpool3 \rightarrow deconv3$$

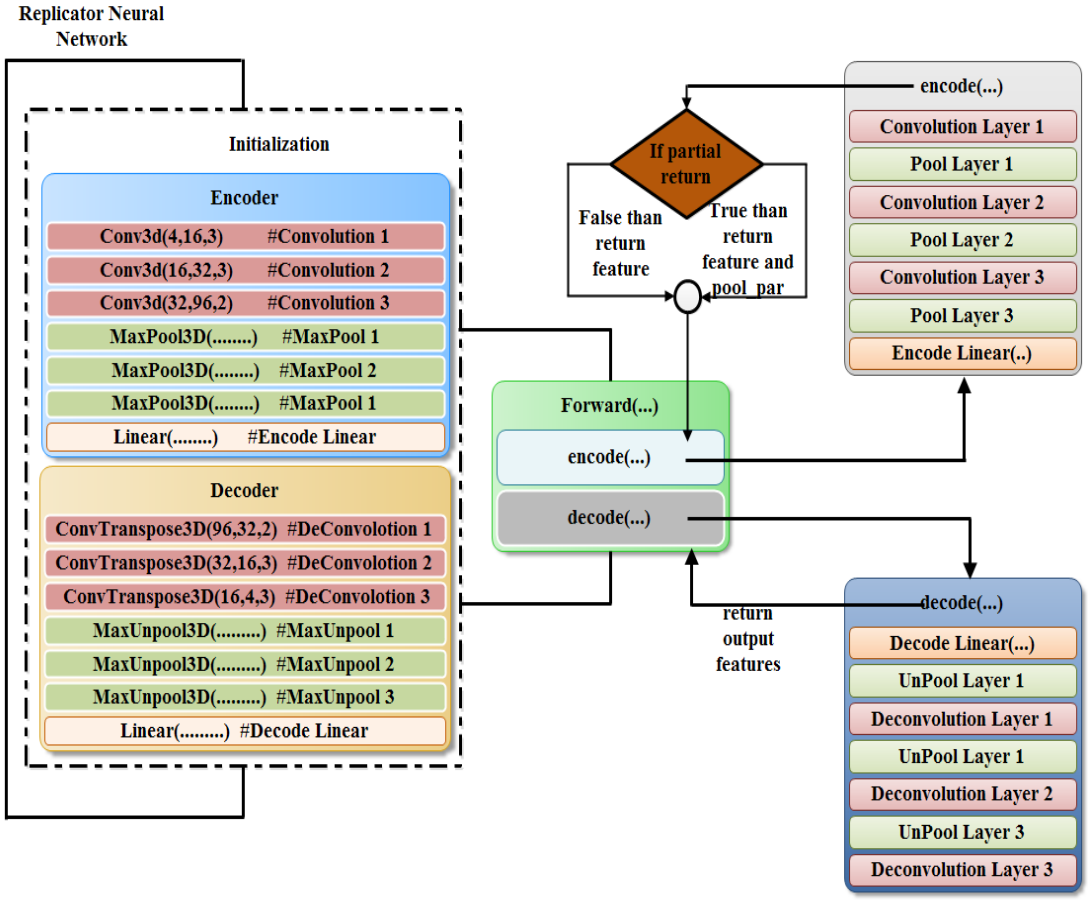

Fig 5.6. 3D Replicator Neural Network Working Flow

5.4 Measuring Parameter and Experimental Results

Feature extraction involves the process of acquiring additional, in-depth information from an image, encompassing attributes like its texture, shape, contrast, and color. Texture analysis holds a pivotal part in both learning systems and human visual interpretation. When we meticulously select and highlight significant features, it has the possible to considerably augment the precision of diagnostic systems. Observations and analyses of texture can be invaluable in the assessment of various tumor stages (tumor staging) and in aiding the diagnostic process. The formulae for pertinent statistical measures and the outcomes of our experiments are presented below.

Mean (M): Taking the total of every value for each pixel and calculating them by the total quantity of pixels in an object yields the object's mean.

$$M = \left(\frac{1}{m \times n}\right) \sum_{x=0}^{m-1} \sum_{y=0}^{n-1} f(x, y) \qquad [5.4]$$

Experimental result of mean for the BRATS 2020 dataset with t1 weighted, t1ce weighted, t2 weighted and flair is shown in figure 12.

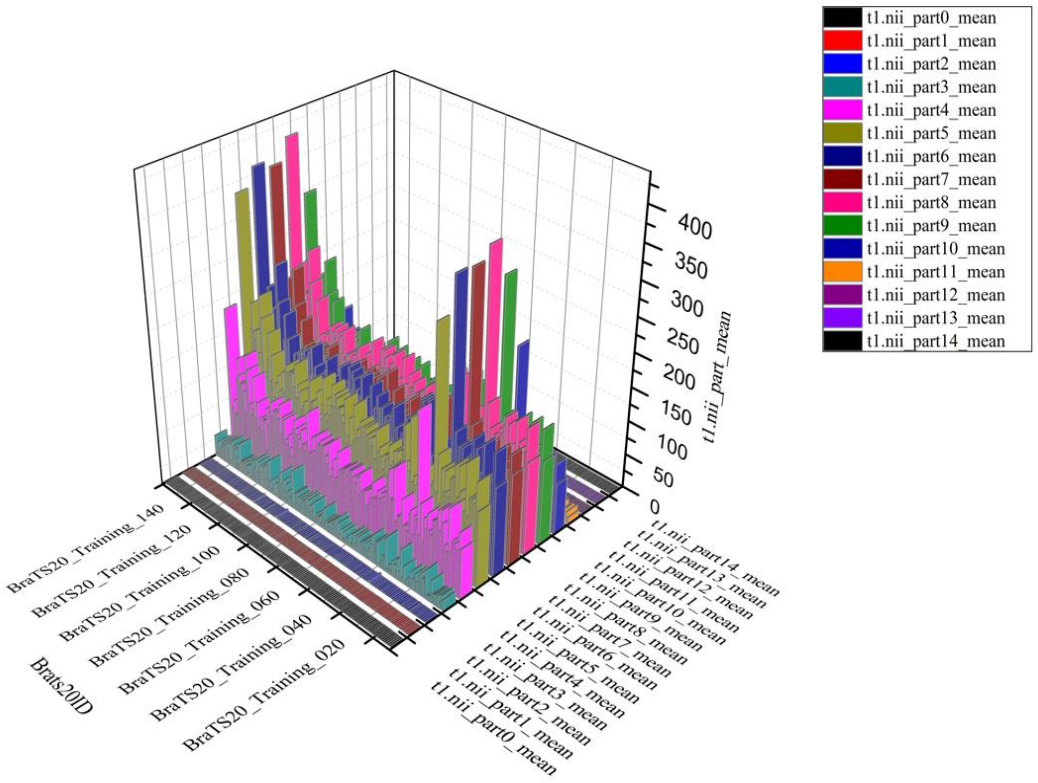

(a) t1 weighted values

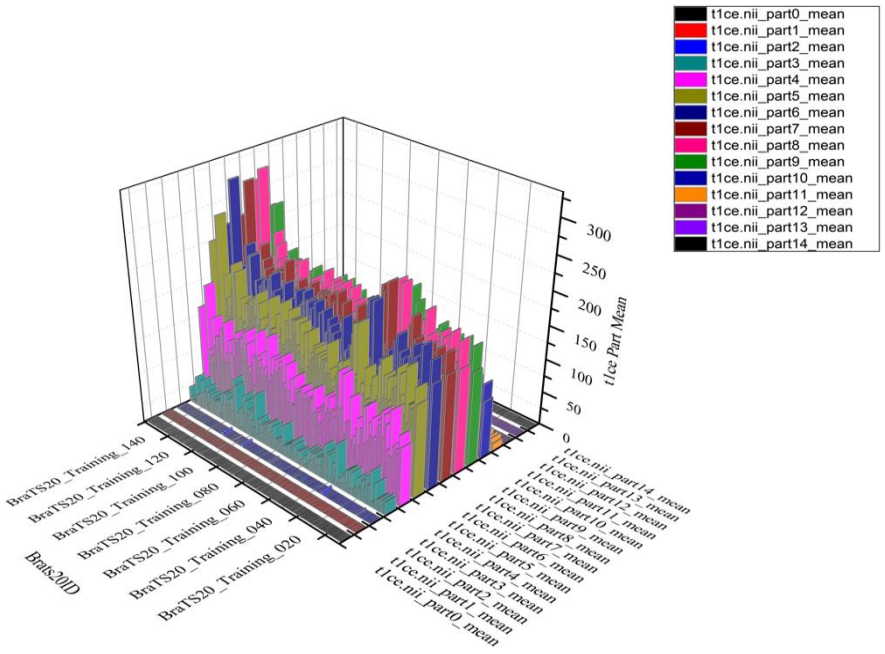

(b) t1ce weighted values

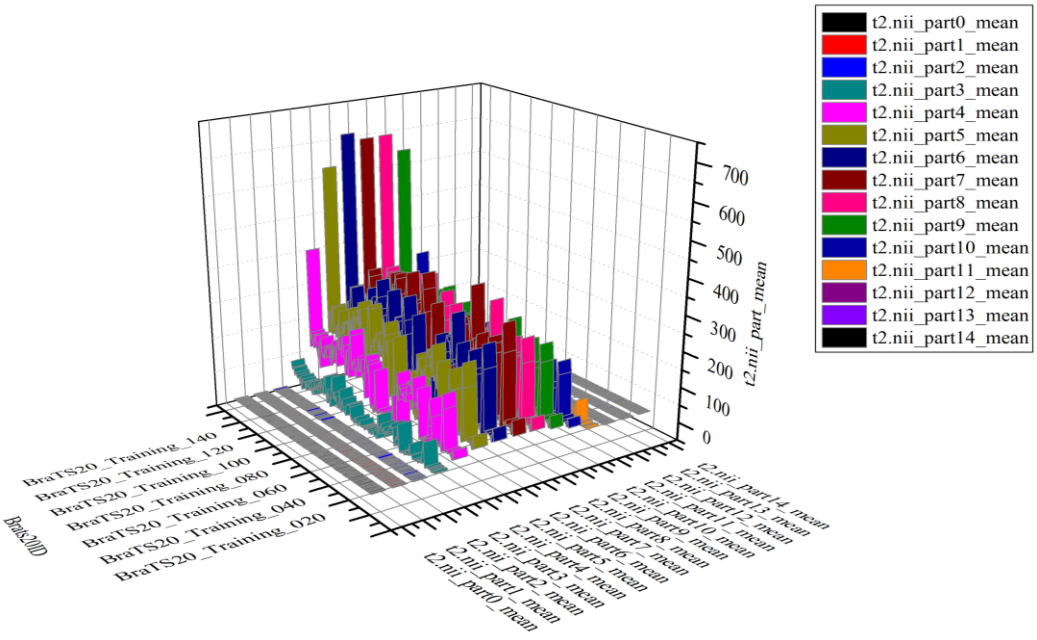

(c) t2 weighted values

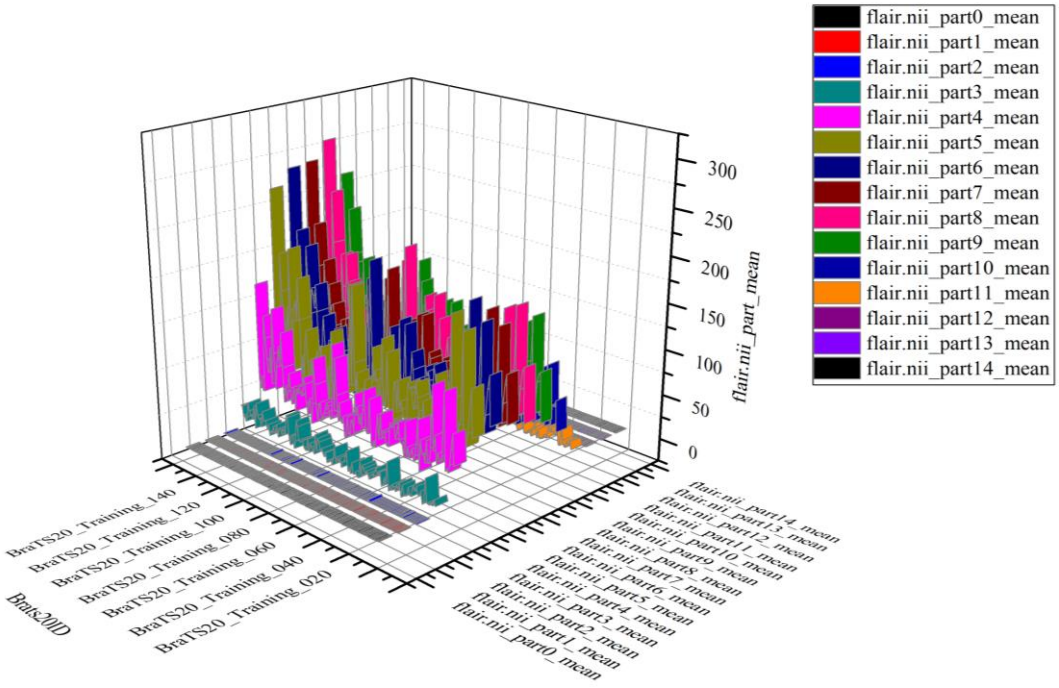

(d) flair values

Fig 5.7 Mean Value Experimental Result for BRATS2020 MRI Dataset

Skewness (S_{kn}): Skewness is a metric for symmetry or lack thereof. The definition of the skewness of an arbitrary variable X, represented as $S_{kn}(X)$, is the determination of the image's mean.

$$S_{kn}(X) = \left(\frac{1}{m \times n}\right)\frac{\sum(f(x,y) - M)^3}{SD^3} \quad [5.5]$$

Where SD is standard deviation and will be evaluated like that

$$SD(\sigma) = \sqrt{\left(\frac{1}{m \times n}\right)\sum_{x=0}^{m-1}\sum_{y=0}^{n-1}(f(x,y) - M)^2} \quad [5.6]$$

Experimental result of Skewness for the 2020 dataset of BRATS with t1 weighted, t1ce weighted, t2 weighted and flair is shown in fig 5.8.

Kutosis (K_{rt}): The Kurtosis parameter describes the probability distribution's form for a random variable. For the random identifier X, the Kurtosis is identified as K_{rt} (X) and it is defined as

$$K_{rt}(X) = \left(\frac{1}{m \times n}\right)\frac{\sum(f(x,y) - M)^4}{SD^4} \quad [5.7]$$

Experimental result of Kurtosis for the 2020 dataset of BRATS with t1 weighted, t1ce weighted, t2 weighted and flair is shown in fig 5.9.

Skewness Difference: The amount and direction of a distribution's asymmetry are shown by the skewness measure differences. Fig 5.10 shows the experimental result of skewness differences for the 2020 dataset of BRATS with t1 weighted, t1ce weighted, t2 weighted and flair.

Intensive Distance: When this happens, it means that the provided data value is higher than the mean value. Experiment results for the 2020 dataset of BRATS with t1 weighted, t1ce weighted, t2 weighted, and flair are shown in Figure 5.11.

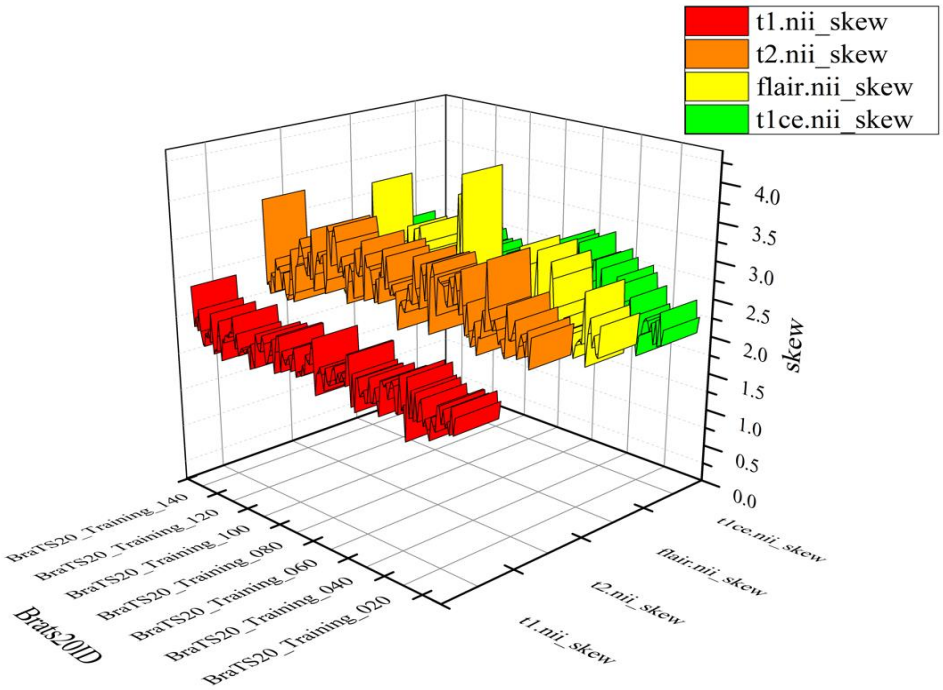

Fig 5.8 Skewness for t1 Weighted Values, t2 Weighted Value, t1ce Weighted Values, Flair Value

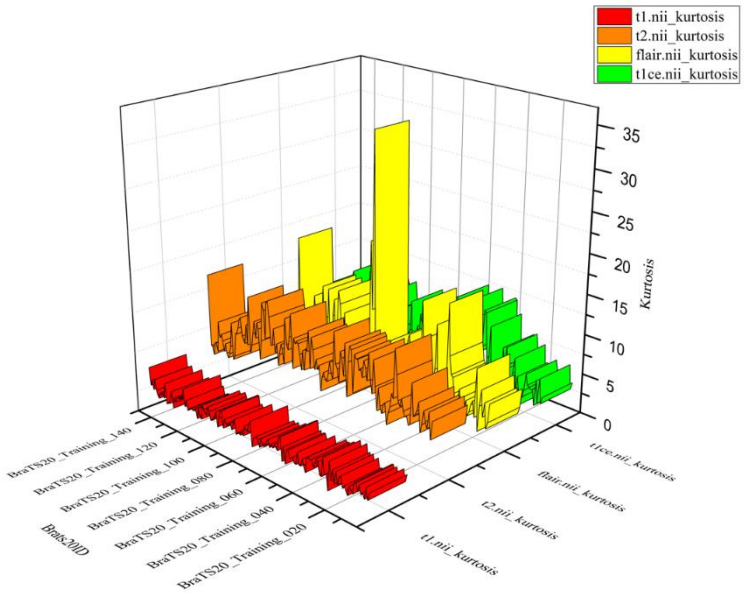

Fig 5.9 Kurtosis for t1 Weighted Values, t2 Weighted Value, t1ce Weighted Values, Flair Value

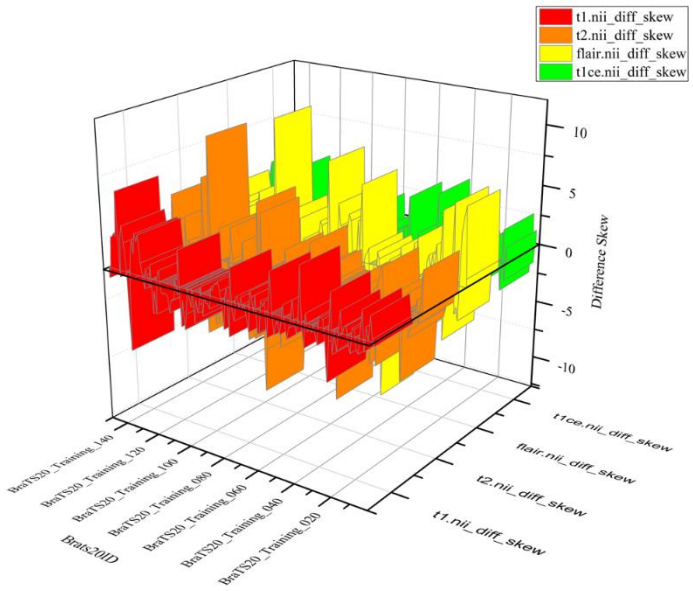

Fig 5.10 Skewness Difference for t1 Weighted Values, t2 Weighted Value, t1ce Weighted Values, Flair Value

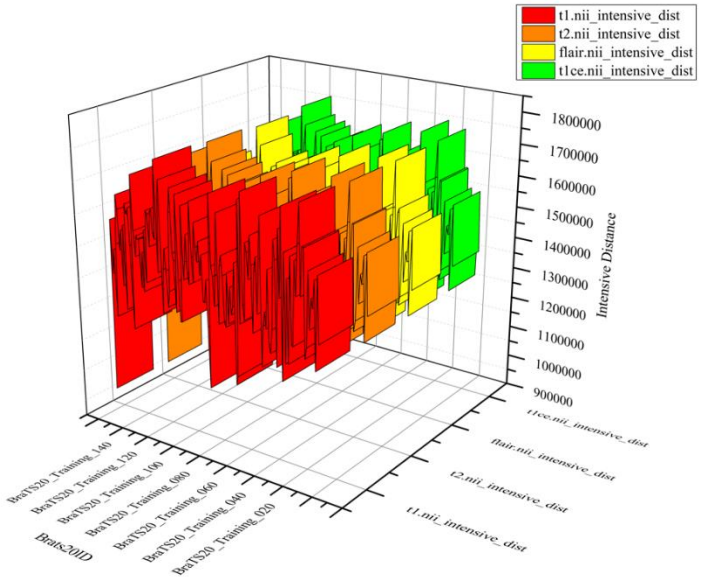

Fig 5.11 Intensive Distance for t1 Weighted Values, T2 Weighted Value, T1ce Weighted Values, Flair Value

Non-Intensive Distance: It is the condition in which the input value is less than the mean value. Fig 5.12 show the experimental result of non-intensive distribution for the BRATS 2020 data set with t1 weighted, t1ce weighted, t2 weighted and flair.

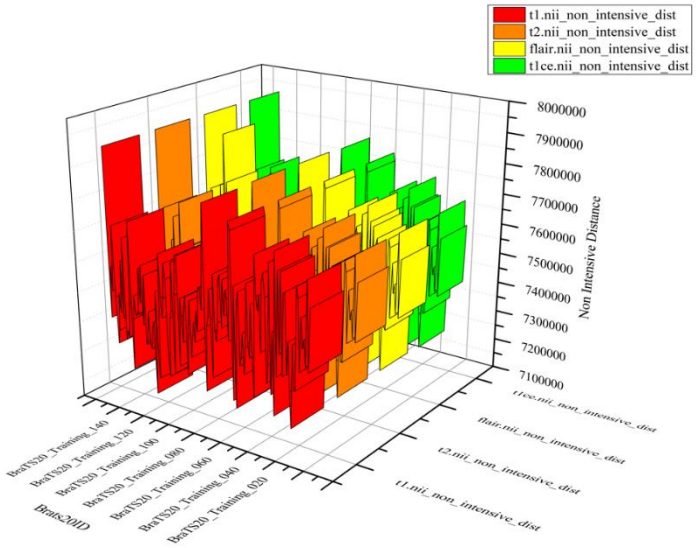

Fig 5.12 Non-Intensive Distance for t1 Weighted Values, t2 Weighted Value, t1ce Weighted Values, Flair Value

Intensive Skewness: It is the measurement of skewness for intensive distribution data. Fig 5.13 shows the experimental result of intensive skewness for the BRATS 2020 dataset with t1 weighted, t1ce weighted, t2 weighted and flair.

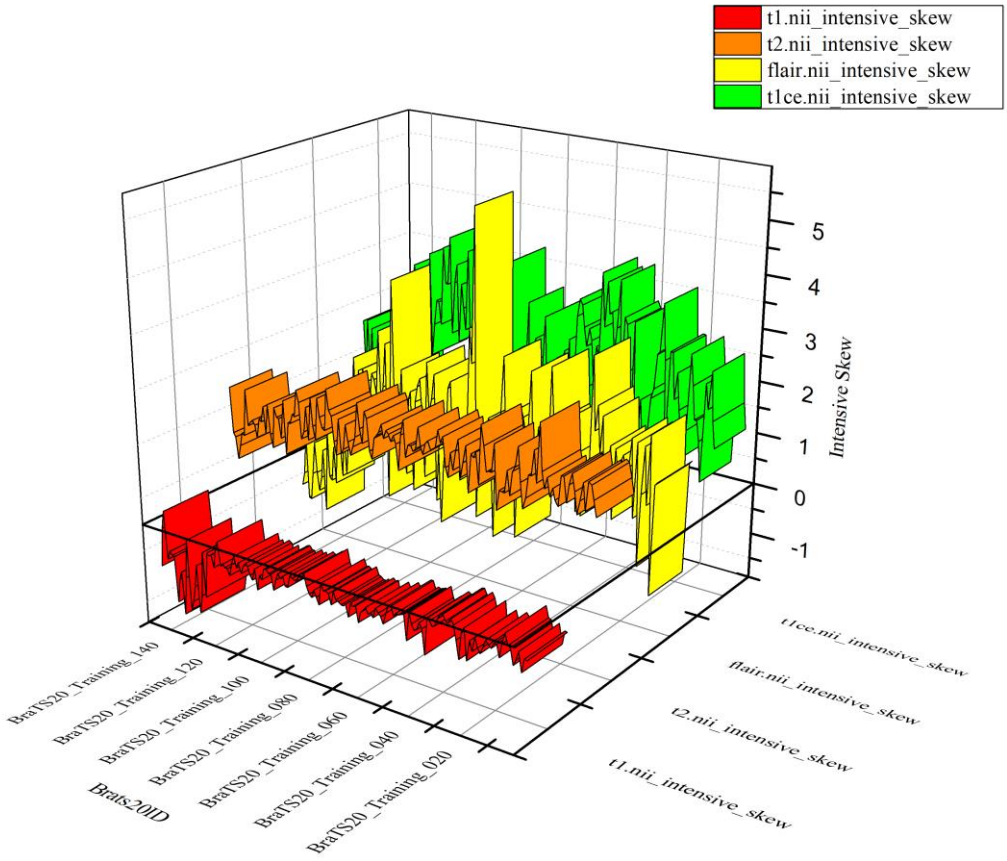

Fig 5.13 Intensive Skewness for t1 Weighted Values, t2 Weighted Value, t1ce Weighted Values, Flair Value

Non-Intensive Skewness: It is the measurement of skewness for non-intensive distribution data. Fig 5.14 shows the experimental result of non-intensive skewness for the BRATS 2020 dataset with t1 weighted, t1ce weighted, t2 weighted and flair.

Data Intensive Skewness Difference: It is the difference between data skewness and data intensive skewness. Fig 5.15 show the experimental result of Intensive Skewness Difference for the BRATS 2020 data set with t1 weighted, t1ce weighted, t2 weighted and flair.

Data Non-Intensive Skewness Difference: It is the difference between data skewness and non-intensive skewness. Fig 5.16 show the experimental result of data non intensive skewness Difference for the BRATS 2020 data set with t1 weighted, t1ce weighted, t2 weighted and flair.

Latent Feature: A set of objects is embedded within a multidimensional in a latent space, often referred to as a latent feature space or embedding space (fig 5.17). In the latent space, the items that are more similar to one another are placed closer to one another. Simply said, the latent space is a depiction of compressed data, where like data points are located near to one another. Latent space is helpful for discovering more straightforward visualisations for analysis as well as for learning data features.

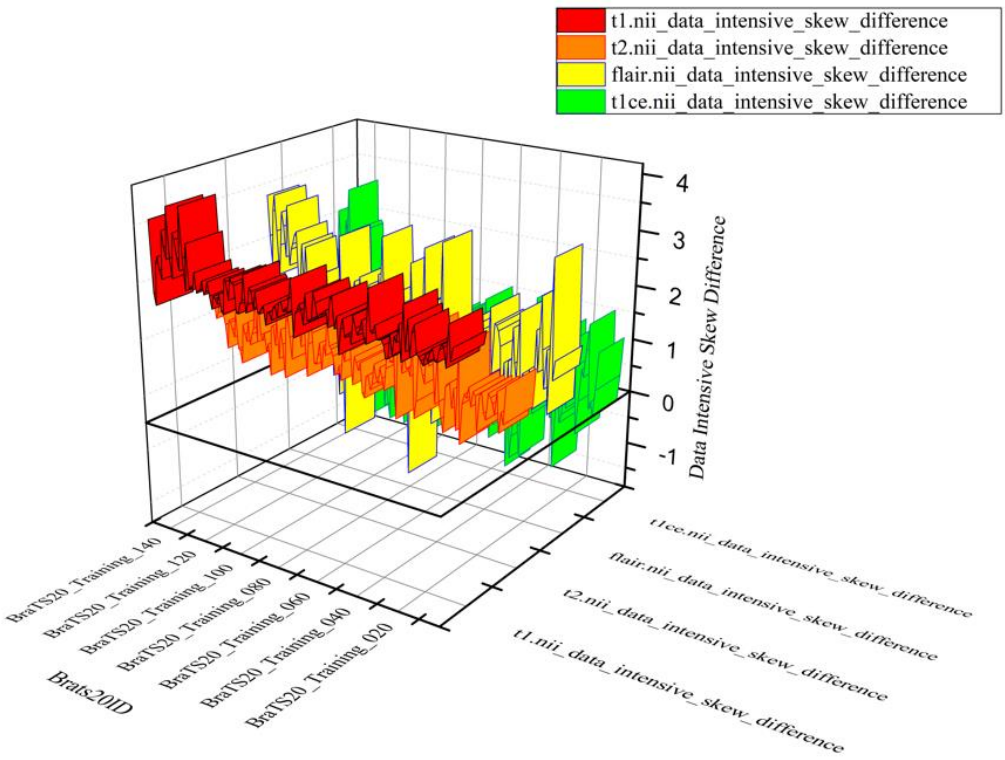

Fig 5.14 Data Non-Intensive Skewness for t1 Weighted Values, t2 Weighted Value, t1ce Weighted Values, Flair Value

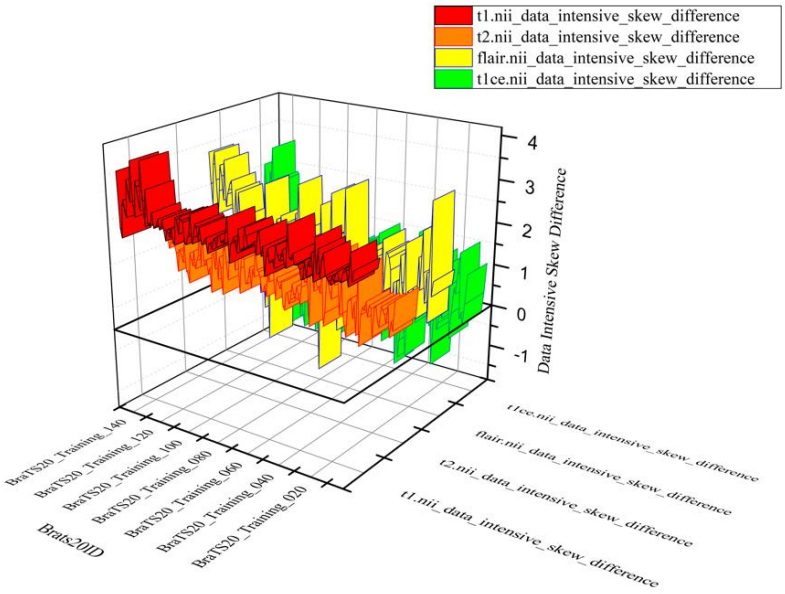

Fig 5.15 Data Intensive Skewness Difference for t1 Weighted Values, t2 Weighted Value, t1ce Weighted Values, Flair Value

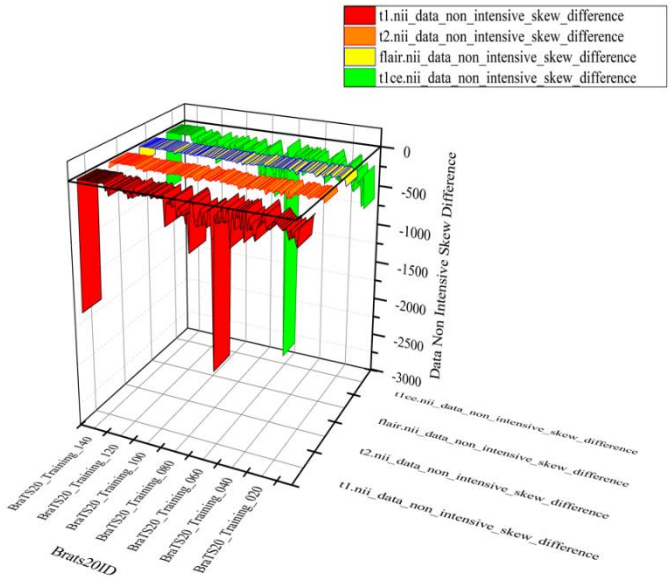

Fig 5.16 Data Non-Intensive Skew Difference for t1 Weighted Values, t2 Weighted Value, t1ce Weighted Values, Flair Value

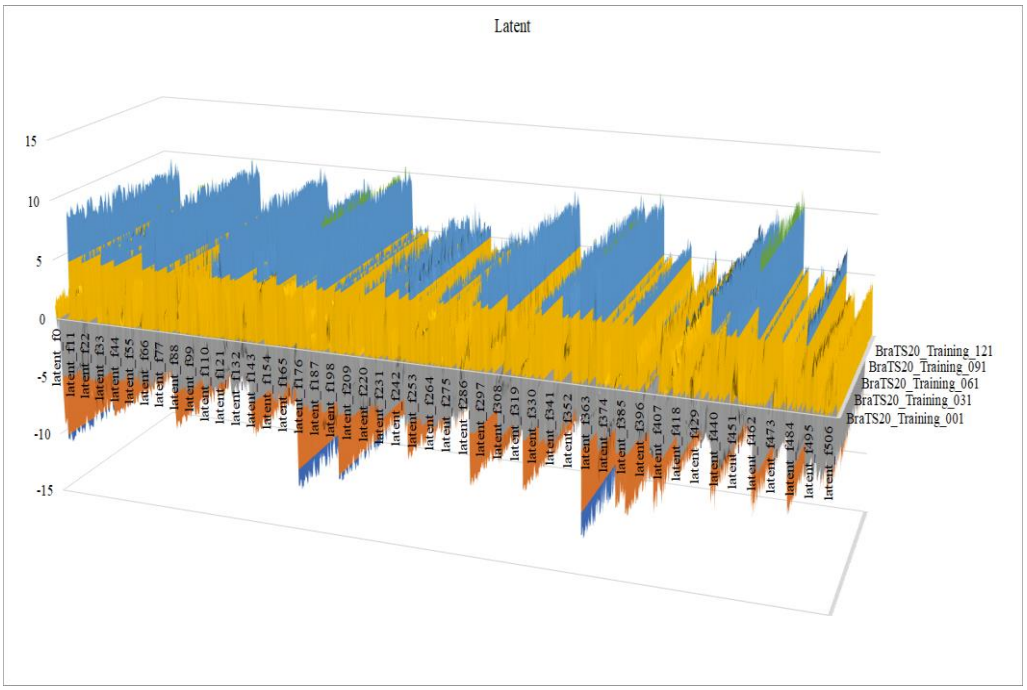

Fig 5.17 Latent Feature

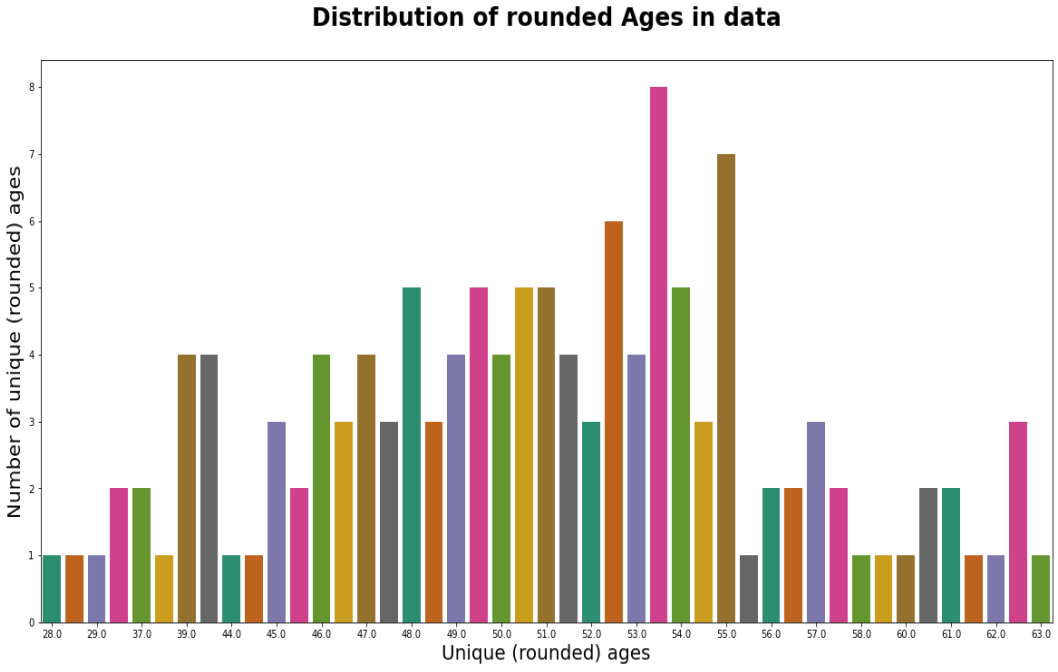

Fig 5.18 Distribution of Rounded Ages in BRATS2020

Brain tumour survival prediction is a complicated and multi-faceted process that necessitates a thorough assessment of several criteria, such as tumour type, location, stage, size, age, and patient's general health. Many criteria may be used to predict how long a patient with a brain tumour will live, including the tumor's histology, its level of malignancy, the amount of tissue removed, whether or not metastases are present, the patient's age, and their general health. The graph fig 5.18 and 5.19 is representing the distribution of rounded ages of data as given in BRATS 2020.

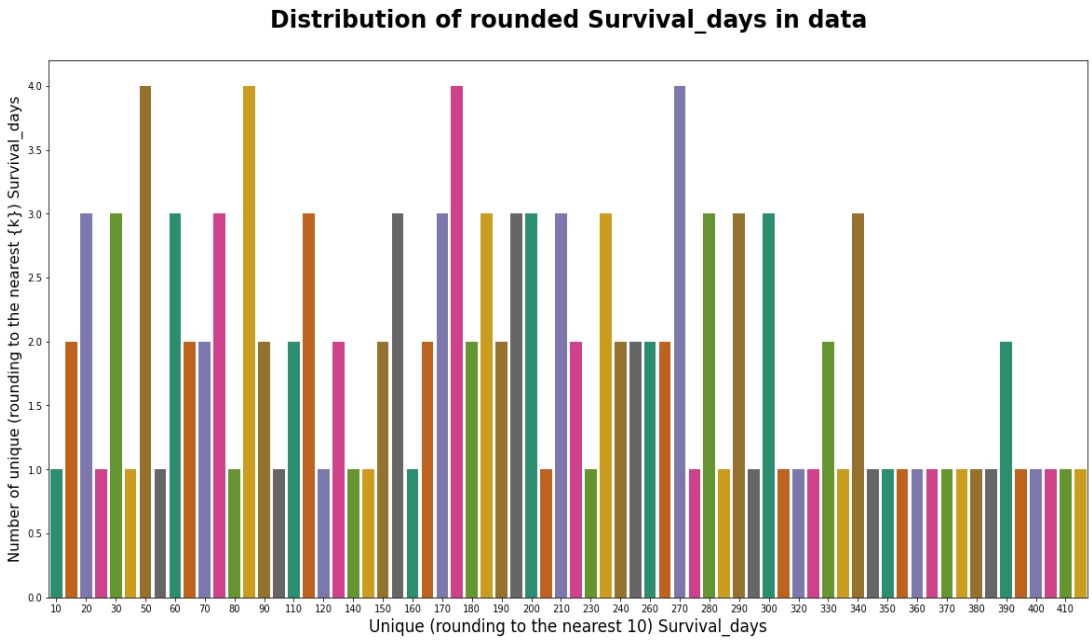

Fig 5.19 Distribution of Rounded Survival Days of Patient as given in BRATS 2020

The utilization of MRI-based brain tumor feature extraction with overall survival prediction through a deep learning-inspired Replicator Neural Network offers several notable advantages:

- **Early Detection:** By leveraging MRI data, this approach enables early and accurate detection of brain tumors, facilitating prompt medical intervention. Early detection often translates to improved patient outcomes.
- **Survival Prediction:** The integration of overall survival prediction is a crucial advancement. It equips medical practitioners with insights into a patient's prognosis, aiding in personalized treatment plans and enhancing patient care.

- **Advanced Imaging Analysis:** This method delves into the intricate details of MRI images, extracting essential features such as texture, shape, and color. This in-depth analysis provides a comprehensive understanding of the tumor's characteristics.
- **Enhanced Diagnostic Accuracy:** Through feature extraction and deep learning, the model enhances diagnostic accuracy, reducing the chances of misclassification and ensuring that medical decisions are based on robust data.
- **Reduced Subjectivity:** The use of a neural network minimizes the subjectivity in tumor diagnosis. It provides a standardized and objective assessment, reducing inter-observer variability.
- **Optimized Resource Allocation:** With survival predictions, medical resources can be allocated more efficiently. Patients with a lower survival prognosis can receive more intensive care, while others can benefit from a more conservative approach.
- **Interdisciplinary Approach:** The research bridges the fields of medical imaging, deep learning, and healthcare, fostering collaboration between these domains and potentially leading to innovative solutions.
- **Potential for Personalized Medicine:** The ability to predict overall survival allows for personalized treatment strategies, tailoring medical interventions to individual patient needs.
- **Research Advancement:** This research contributes to the evolving landscape of medical image analysis and deep learning, paving the way for future developments and breakthroughs in healthcare.

5.5 Conclusion

Overall survival prediction utilising a Replicator Neural Network influenced by deep learning and MRI-based brain tumour feature extraction is a huge step forward for medical imaging and patient care. This novel strategy has enormous potential for improving the detection and treatment of brain tumours in the future, thanks to its many advantages. This technology allows for the early and precise diagnosis of brain tumours through the rigorous examination of MRI data, enabling medical intervention to be initiated promptly. Furthermore, the integration of overall survival prediction empowers healthcare professionals with invaluable insights into patient prognosis,

enabling the tailoring of treatment plans to individual needs. The deep dive into MRI images, extracting crucial features like texture, shape, and color, provides a comprehensive understanding of tumor characteristics. This in-depth analysis significantly enhances diagnostic accuracy, reducing the risk of misclassification and ensuring that medical decisions are grounded in robust data. One of the most noteworthy advantages of this approach is the reduction of subjectivity in tumor diagnosis. The neural network provides a standardized and objective assessment, mitigating inter-observer variability in medical practice. Additionally, the incorporation of survival predictions optimizes the allocation of medical resources, ensuring that patients receive the most appropriate level of care based on their prognoses. This approach opens doors to personalized medicine, where treatment strategies can be tailored to individual patient needs. By bridging the fields of medical imaging, deep learning, and healthcare, this research encourages interdisciplinary collaboration and has the potential to inspire innovative solutions and future developments in the medical field. A major step forward that could change the game for brain tumour diagnosis and treatment is MRI-based feature extraction with overall survival prediction using a Replicator Neural Network influenced by deep learning. It might lead to better health outcomes for patients, lower healthcare expenditures, and new discoveries in the field of medicine. The future of healthcare is looking better and more optimistic thanks to this study.

CHAPTER 6

CONCLUSION AND FUTURE SCOPE

6.1 Conclusion

The research on "Survival Prediction in Glioblastoma Brain Tumor using Segmentation and Detection with Advanced Computational Techniques" represents a pivotal milestone in the domain of medical imaging, predictive healthcare, and the battle against one of the most aggressive and devastating forms of brain tumors, glioblastoma. This study amalgamates cutting-edge segmentation and detection techniques with advanced computational methods to offer a comprehensive approach to glioblastoma diagnosis, localization, and overall survival prediction.

The primary focus of this research is the development of an integrated framework that combines the strengths of image analysis, machine learning, and clinical data to enhance our understanding of glioblastoma and improve patient outcomes. By leveraging state-of-the-art computational techniques, this research has achieved notable success in the accurate segmentation and detection of glioblastoma tumors, enabling precise diagnosis and localization.

One of the most significant achievements of this research is the incorporation of survival prediction into the diagnostic process. The ability to forecast patient outcomes is transformative. It empowers healthcare professionals to make data-driven decisions, tailor treatments to individual patients, and allocate medical resources more efficiently. This is a pivotal step towards personalized medicine in the realm of glioblastoma treatment.

However, while this research marks a substantial advancement, it is essential to acknowledge its limitations. The predictive accuracy of survival outcomes, while promising, can be further refined through the inclusion of more extensive and diverse patient data. As medical imaging and machine learning technologies continue to

evolve, it is reasonable to expect that future iterations of this framework will yield even more accurate predictions.

6.2 Future Scope

The future scope of "Survival Prediction in Glioblastoma Brain Tumor using Segmentation and Detection with Advanced Computational Techniques" is both exciting and filled with opportunities for further advancements in the field of medical imaging, predictive healthcare, and the battle against glioblastoma. As we reflect on the achievements of this research, it becomes evident that there is much more to explore and develop in the quest for improved diagnosis, treatment, and survival prediction for glioblastoma patients.

One of the key avenues for future exploration is the expansion of the dataset. By incorporating a more extensive and diverse range of patient data, including various demographic factors, genetic information, and comprehensive treatment histories, the predictive power of the model can be significantly enhanced. The inclusion of such data can provide a more holistic understanding of the patient's condition and prognosis. In the realm of medical imaging, the integration of multiple imaging modalities, such as MRI, CT, and PET scans, holds great promise. Each modality offers unique insights into the tumor's characteristics, and the combination of these modalities can lead to more accurate and detailed segmentation and detection.

Genetic and molecular data represent another frontier of exploration. By incorporating genetic information, researchers can unveil the underlying genetic mutations and biomarkers associated with glioblastoma. This information can enable a more personalized approach to treatment, targeting the specific genetic drivers of the tumor.

Advancements in deep learning techniques continue to shape the landscape of medical image analysis. Researchers can explore state-of-the-art deep learning models, such as convolutional neural networks (CNNs) and recurrent neural networks (RNNs), to further refine the segmentation and detection processes, ultimately improving

accuracy and efficiency. Beyond prediction, future research can focus on treatment optimization. By integrating the predicted survival outcomes with treatment recommendations, the framework can assist healthcare professionals in tailoring treatment plans for each patient, potentially improving the effectiveness of therapies. The development of real-time predictive models that can adapt to changing patient conditions during the course of treatment is an exciting avenue for future research. Such models can provide dynamic recommendations based on evolving patient data, optimizing treatment strategies. The generalizability of the framework to other types of brain tumors and even various forms of cancer is a promising direction. The principles and techniques developed in this research can serve as a foundation for broader applications in the field of oncology.

Translating the research findings into clinical practice is a critical step on the horizon. Collaboration with healthcare institutions and clinicians can facilitate the integration of the developed framework into the healthcare system, where it can directly impact patient care and contribute to the advancement of glioblastoma treatment.

References

[1]. Abd El Kader I, Xu G, Shuai Z, et al. Brain Tumor Detection and Classification on MR Images by a Deep Wavelet Auto-Encoder Model. Diagnostics. 2021;11(9). doi:10.3390/diagnostics11091589

[2]. Abdelaziz Ismael, S. A., Mohammed, A., & Hefny, H. (2020). An enhanced deep learning approach for brain cancer MRI images classification using residual networks. Artificial Intelligence in Medicine, 102, 101779. https://doi.org/10.1016/j.artmed.2019.101779

[3]. Abd-Ellah, M. K., Awad, A. I., Khalaf, A. A. M., & Hamed, H. F. A. (2019). A review on brain tumor diagnosis from MRI images: Practical implications, key achievements, and lessons learned. Magnetic Resonance Imaging, 61(August 2018), 300–318. https://doi.org/10.1016/j.mri.2019.05.028

[4]. AboElenein NM, Piao S, Noor A, Ahmed PN. MIRAU-Net: An improved neural network based on U-Net for gliomas segmentation. Signal Process Image Commun. 2022;101:116553. doi:https://doi.org/10.1016/j.image.2021.116553

[5]. Ahuja S, Panigrahi BK, Gandhi TK. Enhanced performance of Dark-Nets for brain tumor classification and segmentation using colormap-based superpixel techniques. Mach Learn with Appl. 2022;7:100212. doi:https://doi.org/10.1016/j.mlwa.2021.100212

[6]. Akbar AS, Fatichah C, Suciati N. Single level UNet3D with multipath residual attention block for brain tumor segmentation. J King Saud Univ - Comput Inf Sci. 2022;34(6, Part B):3247-3258. doi:https://doi.org/10.1016/j.jksuci.2022.03.022

[7]. Alagarsamy, S., Kamatchi, K., Govindaraj, V., Zhang, Y. D., & Thiyagarajan, A. (2019). Multi-channeled MR brain image segmentation: A new automated approach combining BAT and clustering technique for better identification of heterogeneous tumors. Biocybernetics and Biomedical Engineering, 39(4), 1005–1035. https://doi.org/10.1016/j.bbe.2019.05.007

[8]. Alfonse, M., & Salem, A.-B. M. (2016). An Automatic Classification of Brain Tumors through MRI Using Support Vector Machine. Egyptian Computer Science Journal, 40(03), 1110–2586.

[9]. Aljunid, M. F., & Manjaiah, D. H. (2019). Data Management, Analytics and Innovation. In Proceedings of ICDMAI (Vol. 808). http://link.springer.com/10.1007/978-981-13-1402-5

[10]. Alnowami M, Taha E, Alsebaeai S, Muhammad Anwar S, Alhawsawi A. MR image normalization dilemma and the accuracy of brain tumor classification model. J Radiat Res Appl Sci. 2022;15(3):33-39. doi:https://doi.org/10.1016/j.jrras.2022.05.014

[11]. Alnowami, M., Taha, E., Alsebaeai, S., Muhammad Anwar, S., & Alhawsawi, A. (2022, September). MR image normalization dilemma and the accuracy of brain tumor classification model. Journal of Radiation Research and Applied Sciences, 15(3), 33–39. https://doi.org/10.1016/j.jrras.2022.05.014

[12]. Al-Saffar ZA, Yildirim T. A hybrid approach based on multiple Eigenvalues selection (MES) for the automated grading of a brain tumor using MRI. Comput Methods Programs Biomed. 2021;201:105945. doi:https://doi.org/10.1016/j.cmpb.2021.105945

[13]. Alzubaidi, L., Zhang, J., Humaidi, A. J., Al-Dujaili, A., Duan, Y., Al-Shamma, O., Santamaría, J., Fadhel, M. A., Al-Amidie, M., & Farhan, L. (2021, March 31). Review of deep learning: concepts, CNN architectures, challenges, applications, future directions. Journal of Big Data, 8(1). https://doi.org/10.1186/s40537-021-00444-8

[14]. Amin, J., Sharif, M., Gul, N., Raza, M., Anjum, M. A., Nisar, M. W., & Bukhari, S. A. C. (2020). Brain Tumor Detection by Using Stacked Autoencoders in Deep Learning. Journal of Medical Systems, 44(2). https://doi.org/10.1007/s10916-019-1483-2

[15]. Amin, J., Sharif, M., Gul, N., Yasmin, M., & Shad, S. A. (2020). Brain tumor classification based on DWT fusion of MRI sequences using convolutional

neural network. Pattern Recognition Letters, 129, 115–122. https://doi.org/10.1016/j.patrec.2019.11.016

[16]. Amin, J., Sharif, M., Yasmin, M., & Fernandes, S. L. (2017). A distinctive approach in brain tumor detection and classification using MRI. Pattern Recognition Letters, 0, 1–10. https://doi.org/10.1016/j.patrec.2017.10.036

[17]. Amin, J., Sharif, M., Yasmin, M., & Fernandes, S. L. (2017). A distinctive approach in brain tumor detection and classification using MRI. Pattern Recognition Letters, 0, 1–10. https://doi.org/10.1016/j.patrec.2017.10.036

[18]. Amin, J., Sharif, M., Yasmin, M., Saba, T., Anjum, M. A., & Fernandes, S. L. (2019). A New Approach for Brain Tumor Segmentation and Classification Based on Score Level Fusion Using Transfer Learning. Journal of Medical Systems, 43(11). https://doi.org/10.1007/s10916-019-1453-8

[19]. Arunkumar, N., Mohammed, M. A., Mostafa, S. A., Ibrahim, D. A., Rodrigues, J. J. P. C., & de Albuquerque, V. H. C. (2020). Fully automatic model-based segmentation and classification approach for MRI brain tumor using artificial neural networks. Concurrency Computation , 32(1), 1–9. https://doi.org/10.1002/cpe.4962

[20]. Badža MM, Barjaktarović MČ. Segmentation of Brain Tumors from MRI Images Using Convolutional Autoencoder. Appl Sci. 2021;11(9). doi:10.3390/app11094317

[21]. Badža, M. M., & Barjaktarović, M. C. (2020). Classification of brain tumors from mri images using a convolutional neural network. Applied Sciences (Switzerland), 10(6). https://doi.org/10.3390/app10061999

[22]. Baheti, B., Innani, S., Gajre, S., & Talbar, S. (2020, June). Eff-UNet: A Novel Architecture for Semantic Segmentation in Unstructured Environment. 2020 IEEE/CVF Conference on Computer Vision and Pattern Recognition Workshops (CVPRW). https://doi.org/10.1109/cvprw50498.2020.00187

[23]. Bakas, S., Akbari, H., Sotiras, A., Bilello, M., Rozycki, M., Kirby, J. S., Freymann, J. B., Farahani, K., & Davatzikos, C. (2017, September 5).

Advancing The Cancer Genome Atlas glioma MRI collections with expert segmentation labels and radiomic features. Scientific Data, 4(1). https://doi.org/10.1038/sdata.2017.117

[24]. Begum, S. S., & Lakshmi, D. R. (2020). Combining optimal wavelet statistical texture and recurrent neural network for tumour detection and classification over MRI. Multimedia Tools and Applications, 79(19–20), 14009–14030. https://doi.org/10.1007/s11042-020-08643-w

[25]. Ben naceur, M., Akil, M., Saouli, R., & Kachouri, R. (2020). Fully automatic brain tumor segmentation with deep learning-based selective attention using overlapping patches and multi-class weighted cross-entropy. Medical Image Analysis, 63, 101692. https://doi.org/10.1016/j.media.2020.101692

[26]. Berger A. How does it work? Positron emission tomography. BMJ. 2003 Jun 28;326(7404):1449. doi: 10.1136/bmj.326.7404.1449. PMID: 12829560; PMCID: PMC1126321.

[27]. Bidkar PS, Kumar R, Ghosh A. SegNet and Salp Water Optimization-driven Deep Belief Network for Segmentation and Classification of Brain Tumor. Gene Expr Patterns. 2022;45:119248. doi:https://doi.org/10.1016/j.gep.2022.119248

[28]. Bienkowski, M., Furtner, J., & Hainfellner, J. A. (2018). Clinical neuropathology of brain tumors. In Handbook of Clinical Neurology (Vol. 145). Elsevier B.V. https://doi.org/10.1016/B978-0-12-802395-2.00032-8

[29]. Biswas-Diener, R. (2020). The brain and nervous system. In R. Biswas-Diener & E. Diener (Eds), Noba textbook series: Psychology. Champaign, IL: DEF publishers. Retrieved from http://noba.to/4hzf8xv6

[30]. Biswas-Diener, R. (2020). The brain and nervous system. In R. Biswas-Diener & E. Diener (Eds), Noba textbook series: Psychology. Champaign, IL: DEF publishers. Retrieved from http://noba.to/4hzf8xv6

[31]. Bouguettaya, A., Yu, Q., Liu, X., Zhou, X., & Song, A. (2015, April). Efficient agglomerative hierarchical clustering. Expert Systems With

Applications, 42(5), 2785–2797. https://doi.org/10.1016/j.eswa.2014.09.054

[32]. Boustani, A., & El Bachari, E. (2019). MRI Brain Images Compression and Classification Using Different Classes of Neural Networks (pp. 122–134). https://doi.org/10.1007/978-3-030-32213-7_9

[33]. Bradley, J. D., Moughan, J., Graham, M. V., Byhardt, R., Govindan, R., Fowler, J., Purdy, J. A., Michalski, J. M., Gore, E., & Choy, H. (2010, June). A Phase I/II Radiation Dose Escalation Study With Concurrent Chemotherapy for Patients With Inoperable Stages I to III Non-Small-Cell Lung Cancer: Phase I Results of RTOG 0117. International Journal of Radiation Oncology*Biology*Physics, 77(2), 367–372. https://doi.org/10.1016/j.ijrobp.2009.04.029

[34]. Brain Anatomy and How the Brain Works. (2021, July 14). Johns Hopkins Medicine. https://www.hopkinsmedicine.org/health/conditions-and-diseases/anatomy-of-the-brain

[35]. Brain Basics: Know Your Brain. (n.d.). National Institute of Neurological Disorders and Stroke. https://www.ninds.nih.gov/health-information/public-education/brain-basics/brain-basics-know-your-brain

[36]. Brain Tumor - Statistics. (2023, May 31). Cancer.Net. https://www.cancer.net/cancer-types/brain-tumor/statistics

[37]. Brain Tumor - Statistics. (2023, May 31). Cancer.Net. https://www.cancer.net/cancer-types/brain-tumor/statistics

[38]. Broggio, S. J. a. J. (2019). Cancer survival in England - Office for National Statistics. www.ons.gov.uk. https://www.ons.gov.uk/peoplepopulationandcommunity/healthandsocialcare/conditionsanddiseases/bulletins/cancersurvivalinengland/stageatdiagnosisandchildhoodpatientsfollowedupto2018#10-year-predicted-survival-estimates

[39]. Chahal PK, Pandey S. A hybrid weighted fuzzy approach for brain tumor segmentation using MR images. Neural Comput Appl. Published online 2021. doi:10.1007/s00521-021-06010-w

[40]. Chattaraj, A., Das, A., & Bhattacharya, M. (2017). Mammographic image segmentation by marker controlled watershed algorithm. 2017 IEEE International Conference on Bioinformatics and Biomedicine (BIBM), 1000–1003.

[41]. Chattaraj, A., Das, A., & Bhattacharya, M. (2017, November). Mammographic image segmentation by marker controlled watershed algorithm. 2017 IEEE International Conference on Bioinformatics and Biomedicine (BIBM). https://doi.org/10.1109/bibm.2017.8217793

[42]. Chavent, M., Lechevallier, Y., & Briant, O. (2007, October). DIVCLUS-T: A monothetic divisive hierarchical clustering method. Computational Statistics & Data Analysis, 52(2), 687–701. https://doi.org/10.1016/j.csda.2007.03.013

[43]. Chawla R, Beram SM, Murthy CR, et al. Brain tumor recognition using an integrated bat algorithm with a convolutional neural network approach. Meas Sensors. 2022;24:100426. doi:https://doi.org/10.1016/j.measen.2022.100426

[44]. Chen B, Zhang L, Chen H, Liang K, Chen X. A novel extended Kalman filter with support vector machine based method for the automatic diagnosis and segmentation of brain tumors. Comput Methods Programs Biomed. 2021;200:105797. doi:https://doi.org/10.1016/j.cmpb.2020.105797

[45]. Chen W, Zhou W, Zhu L, Cao Y, Gu H, Yu B. MTDCNet: A 3D multi-threading dilated convolutional network for brain tumor automatic segmentation. J Biomed Inform. 2022;133:104173. doi:https://doi.org/10.1016/j.jbi.2022.104173

[46]. Chen, G., Li, Q., Shi, F., Rekik, I., & Pan, Z. (2020). RFDCR: Automated brain lesion segmentation using cascaded random forests with dense

conditional random fields. NeuroImage, 211, 116620. https://doi.org/10.1016/j.neuroimage.2020.116620

[47]. Chen, H., Qin, Z., Ding, Y., Tian, L., & Qin, Z. (2020). Brain tumor segmentation with deep convolutional symmetric neural network. Neurocomputing, 392(xxxx), 305–313. https://doi.org/10.1016/j.neucom.2019.01.111

[48]. Chen, S., & Guo, W. (2023, April 7). Auto-Encoders in Deep Learning—A Review with New Perspectives. Mathematics, 11(8), 1777. https://doi.org/10.3390/math11081777

[49]. Chintalapudi N, Battineni G, Goyal LM, Amenta F. 7 - Brain tumor classifications by gradient and XG boosting machine learning models. In: Roy S, Goyal LM, Balas VE, Agarwal B, Mittal M, eds. Predictive Modeling in Biomedical Data Mining and Analysis. Advanced Studies in Complex Systems: Theory and Applications. Academic Press; 2022:123-136. doi:https://doi.org/10.1016/B978-0-323-99864-2.00014-7

[50]. Chollet, F. (2017, July). Xception: Deep Learning with Depthwise Separable Convolutions. 2017 IEEE Conference on Computer Vision and Pattern Recognition (CVPR). https://doi.org/10.1109/cvpr.2017.195

[51]. Çinar, A., & Yildirim, M. (2020). Detection of tumors on brain MRI images using the hybrid convolutional neural network architecture. Medical Hypotheses, 139(February), 109684. https://doi.org/10.1016/j.mehy.2020.109684

[52]. Coslett, H. B., & Schwartz, M. F. (2018). The parietal lobe and language. Handbook of Clinical Neurology, 365–375. https://doi.org/10.1016/b978-0-444-63622-5.00018-8

[53]. Dandıl, E., Çakıroğlu, M., & Ekşi, Z. (2015). Computer-Aided Diagnosis of Malign and Benign Brain Tumors on MR Images. ICT Innovations 2014, 157–166. https://doi.org/10.1007/978-3-319-09879-1_16

[54]. Dang K, Vo T, Ngo L, Ha H. A Deep Learning Framework Integrating MRI Image Preprocessing Methods for Brain Tumor Segmentation and

Classification. IBRO Neurosci Reports. Published online 2022. doi:https://doi.org/10.1016/j.ibneur.2022.10.014

[55]. Deepa G, Mary GLR, Karthikeyan A, Rajalakshmi P, Hemavathi K, Dharanisri M. Detection of brain tumor using modified particle swarm optimization (MPSO) segmentation via haralick features extraction and subsequent classification by KNN algorithm. Mater Today Proc. 2022;56:1820-1826. doi:https://doi.org/10.1016/j.matpr.2021.10.475

[56]. Deepak, S., & Ameer, P. M. (2019). Brain tumor classification using deep CNN features via transfer learning. Computers in Biology and Medicine, 111(March), 103345. https://doi.org/10.1016/j.compbiomed.2019.103345

[57]. Deng, Z., Guo, Q., & Zhu, Z. (2019). Dynamic regulation of level set parameters using 3D convolutional neural network for liver tumor segmentation. Journal of Healthcare Engineering, 2019.

[58]. Deng, Z., Guo, Q., & Zhu, Z. (2019, February 24). Dynamic Regulation of Level Set Parameters Using 3D Convolutional Neural Network for Liver Tumor Segmentation. Journal of Healthcare Engineering, 2019, 1–17. https://doi.org/10.1155/2019/4321645

[59]. Díaz-Pernas FJ, Martínez-Zarzuela M, Antón-Rodríguez M, González-Ortega D. A Deep Learning Approach for Brain Tumor Classification and Segmentation Using a Multiscale Convolutional Neural Network. Healthcare. 2021;9(2). doi:10.3390/healthcare9020153

[60]. Domingues, R., Filippone, M., Michiardi, P., & Zouaoui, J. (2018). A comparative evaluation of outlier detection algorithms: Experiments and analyses. Pattern Recognition, 74, 406–421. https://doi.org/https://doi.org/10.1016/j.patcog.2017.09.037

[61]. Domingues, R., Filippone, M., Michiardi, P., & Zouaoui, J. (2018). A comparative evaluation of outlier detection algorithms: Experiments and analyses. Pattern Recognition, 74, 406–421. https://doi.org/https://doi.org/10.1016/j.patcog.2017.09.037

[62]. Domingues, R., Filippone, M., Michiardi, P., & Zouaoui, J. (2018). A comparative evaluation of outlier detection algorithms: Experiments and analyses. Pattern Recognition, 74, 406–421. https://doi.org/https://doi.org/10.1016/j.patcog.2017.09.037

[63]. Du Cancer, C. C. S. S. C. (n.d.). Cancer statistics at a glance. Canadian Cancer Society. https://cancer.ca/en/research/cancer-statistics/cancer-statistics-at-a-glance

[64]. Du, K. L., & Swamy, M. N. S. (2019). Neural Networks and Statistical Learning. https://doi.org/10.1007/978-1-4471-7452-3

[65]. ELAYARAJA, P., & SUGANTHI, M. (2014, November 27). Survey on Medical Image Segmentation Algorithms. IJARCCE, 8591–8593. https://doi.org/10.17148/ijarcce.2014.31153

[66]. Elazab, A., Anter, A. M., Bai, H., Hu, Q., Hussain, Z., Ni, D., Wang, T., & Lei, B. (2019). An optimized generic cerebral tumor growth modeling framework by coupling biomechanical and diffusive models with treatment effects. Applied Soft Computing Journal, 80, 617–627. https://doi.org/10.1016/j.asoc.2019.04.034

[67]. El-Sawy, A. A., El-Bakry, H. M., & Loey, M. (2016, October 18). CNN for Handwritten Arabic Digits Recognition Based on LeNet-5. Advances in Intelligent Systems and Computing. https://doi.org/10.1007/978-3-319-48308-5_54

[68]. Esmaeili, M., Vettukattil, R., Banitalebi, H., Krogh, N. R., & Geitung, J. T. (2021, November 16). Explainable Artificial Intelligence for Human-Machine Interaction in Brain Tumor Localization. Journal of Personalized Medicine, 11(11), 1213. https://doi.org/10.3390/jpm11111213

[69]. Feature Detectors - Sobel Edge Detector. (n.d.). https://homepages.inf.ed.ac.uk/rbf/HIPR2/sobel.htm#:~:text=The%20Sobel%20operator%20performs%20a,in%20an%20input%20grayscale%20image.

[70]. Fernandes, S. L., Tanik, U. J., Rajinikanth, V., & Karthik, K. A. (2019). A reliable framework for accurate brain image examination and treatment planning based on early diagnosis support for clinicians. Neural Computing and Applications, 5. https://doi.org/10.1007/s00521-019-04369-5

[71]. Fonov, V., Evans, A. C., Botteron, K., Almli, C. R., McKinstry, R. C., & Collins, D. L. (2011, January). Unbiased average age-appropriate atlases for pediatric studies. NeuroImage, 54(1), 313–327. https://doi.org/10.1016/j.neuroimage.2010.07.033

[72]. Fonov, V., Evans, A. C., Botteron, K., Almli, C. R., McKinstry, R. C., & Collins, D. L. (2011, January). Unbiased average age-appropriate atlases for pediatric studies. NeuroImage, 54(1), 313–327. https://doi.org/10.1016/j.neuroimage.2010.07.033

[73]. G, P., L, R., K, A., & Y, J. (2019, May 1). Predicting Source and Age of Brain Tumor Using Canny Edge Detection Algorithm and Threshold Technique. Asian Pacific Journal of Cancer Prevention, 20(5), 1409–1414. https://doi.org/10.31557/apjcp.2019.20.5.1409

[74]. G., J., & Inbarani H., H. (2016). Hybrid Tolerance Rough Set–Firefly based supervised feature selection for MRI brain tumor image classification. Applied Soft Computing Journal, 46, 639–651. https://doi.org/10.1016/j.asoc.2016.03.014

[75]. Ge, C., Gu, I. Y. H., Jakola, A. S., & Yang, J. (2020, July 29). Deep semi-supervised learning for brain tumor classification. BMC Medical Imaging, 20(1). https://doi.org/10.1186/s12880-020-00485-0

[76]. Ghassemi, N., Shoeibi, A., & Rouhani, M. (2020). Deep neural network with generative adversarial networks pre-training for brain tumor classification based on MR images. Biomedical Signal Processing and Control, 57, 101678. https://doi.org/10.1016/j.bspc.2019.101678

[77]. Ghosh S, Chaki A, Santosh KC. Improved U-Net architecture with VGG-16 for brain tumor segmentation. Phys Eng Sci Med. 2021;44(3):703-712. doi:10.1007/s13246-021-01019-w

[78]. Ghosh, S., & Santosh, K. (2021, June). Tumor Segmentation in Brain MRI: U-Nets versus Feature Pyramid Network. 2021 IEEE 34th International Symposium on Computer-Based Medical Systems (CBMS). https://doi.org/10.1109/cbms52027.2021.00013

[79]. Giammarco M Di, Martinelli F, Mercaldo F, Santone A. High Grade Brain Cancer Segmentation by means of Deep Learning. Procedia Comput Sci. 2022;207:1633-1640. doi:https://doi.org/10.1016/j.procs.2022.09.220

[80]. Gull S, Akbar S, Hassan SA, Rehman A, Sadad T. Automated Brain Tumor Segmentation and Classification Through MRI Images. In: Liatsis P, Hussain A, Mostafa SA, Al-Jumeily D, eds. Emerging Technology Trends in Internet of Things and Computing. Springer International Publishing; 2022:182-194.

[81]. Gupta, M., & Sasidhar, K. (2020, February). Non-invasive Brain Tumor Detection using Magnetic Resonance Imaging based Fractal Texture Features and Shape Measures. 2020 3rd International Conference on Emerging Technologies in Computer Engineering: Machine Learning and Internet of Things (ICETCE). https://doi.org/10.1109/icetce48199.2020.9091756

[82]. Gupta, N., & Khanna, P. (2017). A non-invasive and adaptive CAD system to detect brain tumor from T2-weighted MRIs using customized Otsu's thresholding with prominent features and supervised learning. Signal Processing: Image Communication, 59, 18–26. https://doi.org/https://doi.org/10.1016/j.image.2017.05.013

[83]. Gupta, N., & Khanna, P. (2017, November). A non-invasive and adaptive CAD system to detect brain tumor from T2-weighted MRIs using customized Otsu's thresholding with prominent features and supervised learning. Signal Processing: Image Communication, 59, 18–26. https://doi.org/10.1016/j.image.2017.05.013

[84]. Gupta, N., & Khanna, P. (2017, November). A non-invasive and adaptive CAD system to detect brain tumor from T2-weighted MRIs using

customized Otsu's thresholding with prominent features and supervised learning. Signal Processing: Image Communication, 59, 18–26. https://doi.org/10.1016/j.image.2017.05.013

[85]. H. Mohsen, E.-S. A. El-Dahshan, E.-S. M. El-Horbaty, and A.-B. M. Salem, 'Classification using deep learning neural networks for brain tumors', Futur. Comput. Informatics J., vol. 3, no. 1, pp. 68–71, 2018, doi: 10.1016/j.fcij.2017.12.001

[86]. Habib H, Amin R, Ahmed B, Hannan A. Hybrid algorithms for brain tumor segmentation, classification and feature extraction. J Ambient Intell Humaniz Comput. 2022;13(5):2763-2784. doi:10.1007/s12652-021-03544-8

[87]. Han, C., Rundo, L., Araki, R., Furukawa, Y., Mauri, G., Nakayama, H., & Hayashi, H. (2020). Infinite Brain MR Images: PGGAN-Based Data Augmentation for Tumor Detection. Smart Innovation, Systems and Technologies, 151, 291–303. https://doi.org/10.1007/978-981-13-8950-4_27

[88]. Harris L, M Das J. Stereotactic Radiosurgery. [Updated 2023 Jul 25]. In: StatPearls [Internet]. Treasure Island (FL): StatPearls Publishing; 2023 Jan-. Available from: https://www.ncbi.nlm.nih.gov/books/NBK542166/

[89]. He, K., Zhang, X., Ren, S., & Sun, J. (2016, June). Deep Residual Learning for Image Recognition. 2016 IEEE Conference on Computer Vision and Pattern Recognition (CVPR). https://doi.org/10.1109/cvpr.2016.90

[90]. Howard, A.G., Zhu, M., Chen, B., Kalenichenko, D., Wang, W., Weyand, T., Andreetto, M., & Adam, H. (2017). MobileNets: Efficient Convolutional Neural Networks for Mobile Vision Applications. ArXiv, abs/1704.04861.

[91]. Huang Z, Zhao Y, Liu Y, Song G. GCAUNet: A group cross-channel attention residual UNet for slice based brain tumor segmentation. Biomed Signal Process Control. 2021;70:102958. doi:https://doi.org/10.1016/j.bspc.2021.102958

[92]. Huang, G., Liu, Z., Van Der Maaten, L., & Weinberger, K. Q. (2017, July). Densely Connected Convolutional Networks. 2017 IEEE Conference on Computer Vision and Pattern Recognition (CVPR). https://doi.org/10.1109/cvpr.2017.243

[93]. Huang, G., Liu, Z., Van Der Maaten, L., & Weinberger, K. Q. (2017, July). Densely Connected Convolutional Networks. 2017 IEEE Conference on Computer Vision and Pattern Recognition (CVPR). https://doi.org/10.1109/cvpr.2017.243

[94]. Iandola, F. N., Han, S., Moskewicz, M. W., Ashraf, K., Dally, W. J., & Keutzer, K. (2016). SqueezeNet: AlexNet-level accuracy with 50x fewer parameters and< 0.5 MB model size. arXiv preprint arXiv:1602.07360.

[95]. Image classification - Random Forest. (n.d.). 9. Image Classification - Random Forest. https://pages.cms.hu-berlin.de/EOL/geo_rs/S09_Image_classification2.html

[96]. Image classification - Random Forest. (n.d.). 9. Image Classification - Random Forest. https://pages.cms.hu-berlin.de/EOL/geo_rs/S09_Image_classification2.html

[97]. Image Recognition with Mobilenet. (2022, July 7). GeeksforGeeks. https://www.geeksforgeeks.org/image-recognition-with-mobilenet/

[98]. Inception V4 and Inception ResNets. (2022, February 7). GeeksforGeeks. https://www.geeksforgeeks.org/inception-v4-and-inception-resnets/

[99]. Islam, R., Imran, S., Ashikuzzaman, M., & Khan, M. M. A. (2020). Detection and Classification of Brain Tumor Based on Multilevel Segmentation with Convolutional Neural Network. Journal of Biomedical Science and Engineering, 13(04), 45–53. https://doi.org/10.4236/jbise.2020.134004

[100]. Ito, R., Nakae, K., Hata, J., Okano, H., & Ishii, S. (2019). Semi-supervised deep learning of brain tissue segmentation. Neural Networks, 116, 25–34. https://doi.org/10.1016/j.neunet.2019.03.014

[101]. Jemimma TA, Raj YJV. Significant LOOP with clustering approach and optimization enabled deep learning classifier for the brain tumor segmentation and classification. Multimed Tools Appl. 2022;81(2):2365-2391. doi:10.1007/s11042-021-11591-8

[102]. Jemimma TA, Vetharaj YJ. Fractional probabilistic fuzzy clustering and optimization based brain tumor segmentation and classification. Multimed Tools Appl. 2022;81(13):17889-17918. doi:10.1007/s11042-022-11969-2

[103]. Joo B, Ahn SS, An C, et al. Fully automated radiomics-based machine learning models for multiclass classification of single brain tumors: Glioblastoma, lymphoma, and metastasis. J Neuroradiol. Published online 2022. doi:https://doi.org/10.1016/j.neurad.2022.11.001

[104]. Kabir Anaraki, A., Ayati, M., & Kazemi, F. (2019, January). Magnetic resonance imaging-based brain tumor grades classification and grading via convolutional neural networks and genetic algorithms. Biocybernetics and Biomedical Engineering, 39(1), 63–74. https://doi.org/10.1016/j.bbe.2018.10.004

[105]. Kalaiselvi, T., Padmapriya, S. T., Sriramakrishnan, P., & Somasundaram, K. (2020). Deriving tumor detection models using convolutional neural networks from MRI of human brain scans. International Journal of Information Technology (Singapore), 12(2), 403–408. https://doi.org/10.1007/s41870-020-00438-4

[106]. Kamnitsas, K., Ledig, C., Newcombe, V. F. J., Simpson, J. P., Kane, A. D., Menon, D. K., Rueckert, D., & Glocker, B. (2017). Efficient multi-scale 3D CNN with fully connected CRF for accurate brain lesion segmentation. Medical Image Analysis, 36, 61–78. https://doi.org/10.1016/j.media.2016.10.004

[107]. Kapila D, Bhagat N. Efficient feature selection technique for brain tumor classification utilizing hybrid fruit fly based abc and ann algorithm. Mater Today Proc. 2022;51:12-20. doi:https://doi.org/10.1016/j.matpr.2021.04.089

[108]. Karayegen G, Aksahin MF. Brain tumor prediction on MR images with semantic segmentation by using deep learning network and 3D imaging of tumor region. Biomed Signal Process Control. 2021;66:102458. doi:https://doi.org/10.1016/j.bspc.2021.102458

[109]. Kaur, S., & Singh, I. (2016, July 15). Comparison between Edge Detection Techniques. International Journal of Computer Applications, 145(15), 15–18. https://doi.org/10.5120/ijca2016910867

[110]. Kaur, T., Saini, B. S., & Gupta, S. (2018). An optimal spectroscopic feature fusion strategy for MR brain tumor classification using Fisher Criteria and Parameter-Free BAT optimization algorithm. Biocybernetics and Biomedical Engineering, 38(2), 409–424. https://doi.org/10.1016/j.bbe.2018.02.008

[111]. Kay, S., Kay, H., Mowbray, M., Lane, A., Mendoza, C., Martin, P., & Zhang, D. (2022, September 5). Integrating Autoencoder and Heteroscedastic Noise Neural Networks for the Batch Process Soft-Sensor Design. Industrial & Engineering Chemistry Research, 61(36), 13559–13569. https://doi.org/10.1021/acs.iecr.2c01789

[112]. Kaya, & Bilge. (2019, August 21). Deep Metric Learning: A Survey. Symmetry, 11(9), 1066. https://doi.org/10.3390/sym11091066

[113]. Ker, J., Wang, L., Rao, J., & Lim, T. (2018). Deep Learning Applications in Medical Image Analysis. IEEE Access, 6, 9375–9389. https://doi.org/10.1109/access.2017.2788044

[114]. Khairandish MO, Sharma M, Jain V, Chatterjee JM, Jhanjhi NZ. A Hybrid CNN-SVM Threshold Segmentation Approach for Tumor Detection and Classification of MRI Brain Images. IRBM. 2022;43(4):290-299. doi:https://doi.org/10.1016/j.irbm.2021.06.003

[115]. Koka, K., Verma, A., Dwarakanath, B. S., & Papineni, R. V. (2022, April). Technological Advancements in External Beam Radiation Therapy (EBRT): An Indispensable Tool for Cancer Treatment. Cancer Management

and Research, Volume 14, 1421–1429. https://doi.org/10.2147/cmar.s351744

[116]. Krizhevsky, A., Sutskever, I., & Hinton, G. E. (2017, May 24). ImageNet classification with deep convolutional neural networks. Communications of the ACM, 60(6), 84–90. https://doi.org/10.1145/3065386

[117]. Kumar, S., Vig, G., Varshney, S., & Bansal, P. (2020). Brain Tumor Detection Based on Multilevel 2D Histogram Image Segmentation Using DEWO Optimization Algorithm. International Journal of E-Health and Medical Communications (IJEHMC), 11(3), 71–85.

[118]. Kumar, S., Vig, G., Varshney, S., & Bansal, P. (2020, July 1). Brain Tumor Detection Based on Multilevel 2D Histogram Image Segmentation Using DEWO Optimization Algorithm. International Journal of E-Health and Medical Communications, 11(3), 71–85. https://doi.org/10.4018/ijehmc.2020070105

[119]. Kumar, V., & L., M. (2018, July 16). Deep Learning as a Frontier of Machine Learning: A Review. International Journal of Computer Applications, 182(1), 22–30. https://doi.org/10.5120/ijca2018917433

[120]. Kurup, R. V., Sowmya, V., & Soman, K. P. (2020). ICICCT 2019 – System Reliability, Quality Control, Safety, Maintenance and Management. In ICICCT 2019 – System Reliability, Quality Control, Safety, Maintenance and Management. Springer Singapore. https://doi.org/10.1007/978-981-13-8461-5

[121]. Lakshmi, S., & Sankaranarayanan, D. (2010, August 20). A study of Edge Detection Techniques for Segmentation Computing Approaches. International Journal of Computer Applications, CASCT(1), 35–41. https://doi.org/10.5120/993-25

[122]. LeCun, Y., Bengio, Y., & Hinton, G. (2015, May 27). Deep learning. Nature, 521(7553), 436–444. https://doi.org/10.1038/nature14539

[123]. Lefkovits, L., Lefkovits, S., & Vaida, M. F. (2015, March 1). An Atlas Based Performance Evaluation of Inhomogeneity Correcting Effects. MACRo 2015, 1(1), 79–90. https://doi.org/10.1515/macro-2015-0008

[124]. Li P, Wu W, Liu L, Michael Serry F, Wang J, Han H. Automatic brain tumor segmentation from Multiparametric MRI based on cascaded 3D U-Net and 3D U-Net++. Biomed Signal Process Control. 2022;78:103979. doi:https://doi.org/10.1016/j.bspc.2022.103979

[125]. Liew A, Lee CC, Lan BL, Tan M. CASPIANET++: A multidimensional Channel-Spatial Asymmetric attention network with Noisy Student Curriculum Learning paradigm for brain tumor segmentation. Comput Biol Med. 2021;136:104690. doi:https://doi.org/10.1016/j.compbiomed.2021.104690

[126]. Liu, D., Liu, Y., & Dong, L. (2019). G-ResNet: Improved ResNet for Brain Tumor Classification (pp. 535–545). https://doi.org/10.1007/978-3-030-36708-4_44

[127]. Loughan, A. R., Willis, K., Lanoye, A., Allen, D., Reid, M., Ravyts, S., Boutte, R., & Brechbeil, J. (2022). Psychosocial issues in cancer patients with neurological complications. Neurological Complications of Systemic Cancer and Antineoplastic Therapy, 611–634. https://doi.org/10.1016/b978-0-12-821976-8.00036-0

[128]. Louis, D. N., Perry, A., Reifenberger, G., von Deimling, A., Figarella-Branger, D., Cavenee, W. K., Ohgaki, H., Wiestler, O. D., Kleihues, P., & Ellison, D. W. (2016). The 2016 World Health Organization Classification of Tumors of the Central Nervous System: a summary. Acta Neuropathologica, 131(6), 803–820. https://doi.org/10.1007/s00401-016-1545-1

[129]. Louis, D. N., Perry, A., Reifenberger, G., von Deimling, A., Figarella-Branger, D., Cavenee, W. K., Ohgaki, H., Wiestler, O. D., Kleihues, P., & Ellison, D. W. (2016, May 9). The 2016 World Health Organization Classification of Tumors of the Central Nervous System: a summary. Acta

Neuropathologica, 131(6), 803–820. https://doi.org/10.1007/s00401-016-1545-1

[130]. M. Kachwalla, M. P. Shinde, R. Katare, A. Agrawal, V. M. Wadhai, and M. S. Jadhav, 'Classification of Brain MRI Images For Cancer Detection Using Deep Learning', vol. 3, no. 10, pp. 635–637, 2017, doi: 10.17148/IJARCCE.2018.7454

[131]. Maharjan, S., Alsadoon, A., Prasad, P. W. C., Al-Dalain, T., & Alsadoon, O. H. (2020). A novel enhanced softmax loss function for brain tumour detection using deep learning. Journal of Neuroscience Methods, 330, 108520. https://doi.org/10.1016/j.jneumeth.2019.108520

[132]. Maji D, Sigedar P, Singh M. Attention Res-UNet with Guided Decoder for semantic segmentation of brain tumors. Biomed Signal Process Control. 2022;71:103077. doi:https://doi.org/10.1016/j.bspc.2021.103077

[133]. Mark D'Esposito, Jordan H. Grafman, The Frontal Lobes, Academic Press, 2019, ISBN-0128043261, 9780128043264

[134]. Mark D'Esposito, Jordan H. Grafman, The Frontal Lobes, Academic Press, 2019, ISBN-0128043261, 9780128043264

[135]. Medeiros, F. A., Jammal, A. A., & Thompson, A. C. (2019, April). From Machine to Machine. Ophthalmology, 126(4), 513–521. https://doi.org/10.1016/j.ophtha.2018.12.033

[136]. Mekhmoukh, A., & Mokrani, K. (2015). Improved Fuzzy C-Means based Particle Swarm Optimization (PSO) initialization and outlier rejection with level set methods for MR brain image segmentation. Computer Methods and Programs in Biomedicine, 122(2), 266–281. https://doi.org/10.1016/j.cmpb.2015.08.001

[137]. Mittal, H., Pandey, A. C., Saraswat, M., Kumar, S., Pal, R., & Modwel, G. (2021, February 9). A comprehensive survey of image segmentation: clustering methods, performance parameters, and benchmark datasets. Multimedia Tools and Applications, 81(24), 35001–35026. https://doi.org/10.1007/s11042-021-10594-9

[138]. Mittal, H., Pandey, A.C., Saraswat, M. et al. A comprehensive survey of image segmentation: clustering methods, performance parameters, and benchmark datasets. Multimed Tools Appl 81, 35001–35026 (2022). https://doi.org/10.1007/s11042-021-10594-9

[139]. Mittal, M., Goyal, L. M., Kaur, S., Kaur, I., Verma, A., & Jude Hemanth, D. (2019). Deep learning based enhanced tumor segmentation approach for MR brain images. Applied Soft Computing Journal, 78, 346–354. https://doi.org/10.1016/j.asoc.2019.02.036

[140]. Mohan, G., & Subashini, M. M. (2018). MRI based medical image analysis: Survey on brain tumor grade classification. Biomedical Signal Processing and Control, 39, 139–161. https://doi.org/10.1016/j.bspc.2017.07.007

[141]. Mohsen, H., El-Dahshan, E.-S. A., El-Horbaty, E.-S. M., & Salem, A.-B. M. (2018). Classification using deep learning neural networks for brain tumors. Future Computing and Informatics Journal, 3(1), 68–71.

[142]. Muniasamy, A., & Alasiry, A. (2020, January 15). Deep Learning: The Impact on Future eLearning. International Journal of Emerging Technologies in Learning (IJET), 15(01), 188. https://doi.org/10.3991/ijet.v15i01.11435

[143]. Muthukrishnan, R., & Radha, M. (2011, December 31). Edge Detection Techniques For Image Segmentation. International Journal of Computer Science and Information Technology, 3(6), 259–267. https://doi.org/10.5121/ijcsit.2011.3620

[144]. Nair, L. R., Subramaniam, K., & Prasannavenkatesan, G. K. D. (2020). A review on multiple approaches to medical image retrieval system. In Advances in Intelligent Systems and Computing (Vol. 1125). https://doi.org/10.1007/978-981-15-2780-7_55

[145]. Narayanan, A., Rajasekaran, M. P., Zhang, Y., Govindaraj, V., & Thiyagarajan, A. (2019). Multi-channeled MR brain image segmentation: A novel double optimization approach combined with clustering technique

for tumor identification and tissue segmentation. Biocybernetics and Biomedical Engineering, 39(2), 350–381. https://doi.org/10.1016/j.bbe.2018.12.003

[146]. Naser, M. A., & Deen, M. J. (2020). Brain tumor segmentation and grading of lower-grade glioma using deep learning in MRI images. Computers in Biology and Medicine, 121, 103758. https://doi.org/10.1016/j.compbiomed.2020.103758

[147]. Nayak, D. R., Dash, R., & Majhi, B. (2020). Automated diagnosis of multi-class brain abnormalities using MRI images: A deep convolutional neural network based method. Pattern Recognition Letters, 138, 385–391. https://doi.org/10.1016/j.patrec.2020.04.018

[148]. Nazir M, Shakil S, Khurshid K, Role of Deep Learning in Brain Tumor Detection and Classification (2015 to 2020): A Review, Computerized Medical Imaging and Graphics (2021), doi: https://doi.org/10.1016/j.compmedimag.2021.101940

[149]. Neelima G, Chigurukota DR, Maram B, Girirajan B. Optimal DeepMRSeg based tumor segmentation with GAN for brain tumor classification. Biomed Signal Process Control. 2022;74:103537. doi:https://doi.org/10.1016/j.bspc.2022.103537

[150]. Özyurt, F., Sert, E., & Avcı, D. (2020). An expert system for brain tumor detection: Fuzzy C-means with super resolution and convolutional neural network with extreme learning machine. Medical Hypotheses, 134(October 2019). https://doi.org/10.1016/j.mehy.2019.109433

[151]. Özyurt, F., Sert, E., Avci, E., & Dogantekin, E. (2019, December). Brain tumor detection based on Convolutional Neural Network with neutrosophic expert maximum fuzzy sure entropy. Measurement, 147, 106830. https://doi.org/10.1016/j.measurement.2019.07.058

[152]. Pa, S. (2021, December 14). An Overview on MobileNet: An Efficient Mobile Vision CNN. Medium. https://medium.com/@godeep48/an-overview-on-mobilenet-an-efficient-mobile-vision-cnn-f301141db94d

[153]. Padding and Stride — Dive into Deep Learning 1.0.3 documentation. (n.d.). 7.3. Padding And Stride — Dive Into Deep Learning 1.0.3 Documentation. https://d2l.ai/chapter_convolutional-neural-networks/padding-and-strides.html

[154]. Padding and Stride — Dive into Deep Learning 1.0.3 documentation. (n.d.). 7.3. Padding And Stride — Dive Into Deep Learning 1.0.3 Documentation. https://d2l.ai/chapter_convolutional-neural-networks/padding-and-strides.html

[155]. Paoletti, M., Haut, J., Plaza, J., & Plaza, A. (2018, September 11). Deep&Dense Convolutional Neural Network for Hyperspectral Image Classification. Remote Sensing, 10(9), 1454. https://doi.org/10.3390/rs10091454

[156]. Pasquini, C. (2003, April). Near Infrared Spectroscopy: fundamentals, practical aspects and analytical applications. Journal of the Brazilian Chemical Society, 14(2), 198–219. https://doi.org/10.1590/s0103-50532003000200006

[157]. Pasquini, C. (2018, October). Near infrared spectroscopy: A mature analytical technique with new perspectives – A review. Analytica Chimica Acta, 1026, 8–36. https://doi.org/10.1016/j.aca.2018.04.004

[158]. Patel A, Biso GMNR, Fowler J B. Neuroanatomy, Temporal Lobe, StatPearls Publishing; 2020, https://www.ncbi.nlm.nih.gov/books/NBK519512/

[159]. Patel A, Biso GMNR, Fowler J B. Neuroanatomy, Temporal Lobe, StatPearls Publishing; 2020, https://www.ncbi.nlm.nih.gov/books/NBK519512/

[160]. Pereira, S., Pinto, A., Alves, V., & Silva, C. A. (2016, May). Brain Tumor Segmentation Using Convolutional Neural Networks in MRI Images. IEEE Transactions on Medical Imaging, 35(5), 1240–1251. https://doi.org/10.1109/tmi.2016.2538465

[161]. Perumal V, Narayanan V, Rajasekar SJS. 11 - Detection of Brain Tumor with Magnetic Resonance Imaging using Deep Learning Techniques. In: Chaki J, ed. Brain Tumor MRI Image Segmentation Using Deep Learning Techniques. Academic Press; 2022:183-196. doi:https://doi.org/10.1016/B978-0-323-91171-9.00014-4

[162]. Rai HM, Chatterjee K, Nayyar A. Automatic Segmentation and Classification of Brain Tumor from MR Images Using DWT-RBFNN. In: Dash S, Pani SK, Abraham A, Liang Y, eds. Advanced Soft Computing Techniques in Data Science, IoT and Cloud Computing. Springer International Publishing; 2021:215-243. doi:10.1007/978-3-030-75657-4_10

[163]. Rajasree R, Columbus CC, Shilaja C. Multiscale-based multimodal image classification of brain tumor using deep learning method. Neural Comput Appl. 2021;33(11):5543-5553. doi:10.1007/s00521-020-05332-5

[164]. Raju, A. R., Suresh, P., & Rao, R. R. (2018). Bayesian HCS-based multi-SVNN: A classification approach for brain tumor segmentation and classification using Bayesian fuzzy clustering. Biocybernetics and Biomedical Engineering, 38(3), 646–660. https://doi.org/10.1016/j.bbe.2018.05.001

[165]. Ramya P, Thanabal MS, Dharmaraja C. Brain tumor segmentation using cluster ensemble and deep super learner for classification of MRI. J Ambient Intell Humaniz Comput. 2021;12(10):9939-9952. doi:10.1007/s12652-021-03390-8

[166]. Ranjbarzadeh R, Bagherian Kasgari A, Jafarzadeh Ghoushchi S, Anari S, Naseri M, Bendechache M. Brain tumor segmentation based on deep learning and an attention mechanism using MRI multi-modalities brain images. Sci Rep. 2021;11(1):10930. doi:10.1038/s41598-021-90428-8

[167]. Rasool Reddy K, Dhuli R. Segmentation and classification of brain tumors from MRI images based on adaptive mechanisms and ELDP feature

descriptor. Biomed Signal Process Control. 2022;76:103704. doi:https://doi.org/10.1016/j.bspc.2022.103704

[168]. Ravikumar M, Shivaprasad BJ. Segmentation of Brain Tumor from MR Images Using SegX-Net an Hybrid Approach. In: Kaiser MS, Xie J, Rathore VS, eds. Information and Communication Technology for Competitive Strategies (ICTCS 2020). Springer Nature Singapore; 2021:1007-1015.

[169]. Read, G. L., & Innis, I. J. (2017, August). Electroencephalography (Eeg). The International Encyclopedia of Communication Research Methods, 1–18. https://doi.org/10.1002/9781118901731.iecrm0080

[170]. Reda, M., Suwwan, R., Alkafri, S., Rashed, Y., & Shanableh, T. (2022, July 26). AgroAId: A Mobile App System for Visual Classification of Plant Species and Diseases Using Deep Learning and TensorFlow Lite. Informatics, 9(3), 55. https://doi.org/10.3390/informatics9030055

[171]. Rehman A, Al Khalili Y. Neuroanatomy, Occipital Lobe. [Updated 2020 Jul 31]. In: StatPearls [Internet]. Treasure Island (FL): StatPearls Publishing; 2020 Jan-. Available from: https://www.ncbi.nlm.nih.gov/books/NBK544320/

[172]. Rehman A, Al Khalili Y. Neuroanatomy, Occipital Lobe. In: StatPearls. StatPearls Publishing, Treasure Island (FL); 2019.

[173]. Rohilla, S., & Jain, S. (2023, August 16). Detection of Brain Tumor Employing Residual Network-based OptimizedDeep Learning. Current Computer-Aided Drug Design, 20. https://doi.org/10.2174/1573409920666230816090626

[174]. S, S. P. K., C, A. K., & R, J. R. (2022, August 8). ERCNN-DRM: an efficient regularized convolutional neural network with a dimensionality reduction module for the classification of brain tumour in magnetic resonance images. Automatika, 64(1), 79–92. https://doi.org/10.1080/00051144.2022.2103771

[175]. Sachdeva, J., Kumar, V., Gupta, I., Khandelwal, N., & Ahuja, C. K. (2016). A package-SFERCB-"Segmentation, feature extraction, reduction and classification analysis by both SVM and ANN for brain tumors". Applied Soft Computing Journal, 47, 151–167. https://doi.org/10.1016/j.asoc.2016.05.020

[176]. Sahayam S, Nenavath R, Jayaraman U, Prakash S. Brain tumor segmentation using a hybrid multi resolution U-Net with residual dual attention and deep supervision on MR images. Biomed Signal Process Control. 2022;78:103939. doi:https://doi.org/10.1016/j.bspc.2022.103939

[177]. Sajja, V. R., & Kalluri, H. K. (2020). Brain Tumor Segmentation Using Fuzzy C-Means and Tumor Grade Classification Using SVM. In Smart Technologies in Data Science and Communication (pp. 197–204). Springer.

[178]. Sasank VVS, Venkateswarlu S. An automatic tumour growth prediction based segmentation using full resolution convolutional network for brain tumour. Biomed Signal Process Control. 2022;71:103090. doi:https://doi.org/10.1016/j.bspc.2021.103090

[179]. Saxena, A., Prasad, M., Gupta, A., Bharill, N., Patel, O. P., Tiwari, A., Er, M. J., Ding, W., & Lin, C. T. (2017, December). A review of clustering techniques and developments. Neurocomputing, 267, 664–681. https://doi.org/10.1016/j.neucom.2017.06.053

[180]. Scarapicchia, V., Brown, C., Mayo, C., & Gawryluk, J. R. (2017, August 18). Functional Magnetic Resonance Imaging and Functional Near-Infrared Spectroscopy: Insights from Combined Recording Studies. Frontiers in Human Neuroscience, 11. https://doi.org/10.3389/fnhum.2017.00419

[181]. Schenck, J. F. (2003). Magnetic resonance imaging of brain iron. Journal of the Neurological Sciences, 207(1–2), 99–102. https://doi.org/10.1016/S0022-510X(02)00431-8

[182]. Seetha, J., & Raja, S. S. (2018). Brain tumor classification using Convolutional Neural Networks. Biomedical and Pharmacology Journal, 11(3), 1457–1461. https://doi.org/10.13005/bpj/1511

[183]. Sert, E., Özyurt, F., & Doğantekin, A. (2019, December). A new approach for brain tumor diagnosis system: Single image super resolution based maximum fuzzy entropy segmentation and convolutional neural network. Medical Hypotheses, 133, 109413. https://doi.org/10.1016/j.mehy.2019.109413

[184]. Shafiq, M., & Gu, Z. (2022, September 7). Deep Residual Learning for Image Recognition: A Survey. Applied Sciences, 12(18), 8972. https://doi.org/10.3390/app12188972

[185]. Shahrokhi M, Asuncion RMD. Neurologic Exam. [Updated 2023 Jan 16]. In: StatPearls [Internet]. Treasure Island (FL): StatPearls Publishing; 2023 Jan-. Available from: https://www.ncbi.nlm.nih.gov/books/NBK557589/

[186]. Sharif, M. I., Li, J. P., Khan, M. A., & Saleem, M. A. (2020). Active deep neural network features selection for segmentation and recognition of brain tumors using MRI images. Pattern Recognition Letters, 129, 181–189. https://doi.org/10.1016/j.patrec.2019.11.019

[187]. Sharif, M. I., Li, J. P., Khan, M. A., & Saleem, M. A. (2020). Active deep neural network features selection for segmentation and recognition of brain tumors using MRI images. Pattern Recognition Letters, 129, 181–189. https://doi.org/10.1016/j.patrec.2019.11.019

[188]. Shehab LH, Fahmy OM, Gasser SM, El-Mahallawy MS. An efficient brain tumor image segmentation based on deep residual networks (ResNets). J King Saud Univ - Eng Sci. 2021;33(6):404-412. doi:https://doi.org/10.1016/j.jksues.2020.06.001

[189]. Shehab, L. H., Fahmy, O. M., Gasser, S. M., & El-Mahallawy, M. S. (2020). An efficient brain tumor image segmentation based on deep residual networks (ResNets). Journal of King Saud University - Engineering Sciences. https://doi.org/10.1016/j.jksues.2020.06.001

[190]. Shi, X., Lv, F., Seng, D., Zhang, J., Chen, J., & Xing, B. (2020, November 3). Visualizing and understanding graph convolutional network.

Multimedia Tools and Applications, 80(6), 8355–8375. https://doi.org/10.1007/s11042-020-09885-4

[191]. Simonyan, K., & Zisserman, A. (2014). Very deep convolutional networks for large-scale image recognition. arXiv preprint arXiv:1409.1556.

[192]. Siva Raja, P. M., & rani, A. V. (2020). Brain tumor classification using a hybrid deep autoencoder with Bayesian fuzzy clustering-based segmentation approach. Biocybernetics and Biomedical Engineering, 40(1), 440–453. https://doi.org/10.1016/j.bbe.2020.01.006

[193]. Skowronek, J. (2017). Current status of brachytherapy in cancer treatment – short overview. Journal of Contemporary Brachytherapy, 9(6), 581–589. https://doi.org/10.5114/jcb.2017.72607

[194]. Song, S., Zheng, Y., & He, Y. (2017). A review of Methods for Bias Correction in Medical Images. Biomedical Engineering Review, 3(1). https://doi.org/10.18103/bme.v3i1.1550

[195]. Song, S., Zheng, Y., & He, Y. (2017). A review of Methods for Bias Correction in Medical Images. Biomedical Engineering Review, 3(1). https://doi.org/10.18103/bme.v3i1.1550

[196]. Soufineyestani, M., Dowling, D., & Khan, A. (2020). Electroencephalography (EEG) Technology Applications and Available Devices. Applied Sciences, 10(21), 7453. MDPI AG. Retrieved from http://dx.doi.org/10.3390/app10217453

[197]. Srinivas, C., K. S., N. P., Zakariah, M., Alothaibi, Y. A., Shaukat, K., Partibane, B., & Awal, H. (2022, March 8). Deep Transfer Learning Approaches in Performance Analysis of Brain Tumor Classification Using MRI Images. Journal of Healthcare Engineering, 2022, 1–17. https://doi.org/10.1155/2022/3264367

[198]. Sun Y, Wang C. A computation-efficient CNN system for high-quality brain tumor segmentation. Biomed Signal Process Control. 2022;74:103475. doi:https://doi.org/10.1016/j.bspc.2021.103475

[199]. Sunsuhi GS, Albin Jose S. An Adaptive Eroded Deep Convolutional neural network for brain image segmentation and classification using Inception ResnetV2. Biomed Signal Process Control. 2022;78:103863. doi:https://doi.org/10.1016/j.bspc.2022.103863

[200]. Support Vector Machine (SVM) Explained. (n.d.). Support Vector Machine (SVM) Explained - MATLAB & Simulink. https://www.mathworks.com/discovery/support-vector-machine.html

[201]. Support Vector Machine (SVM) Explained. (n.d.). Support Vector Machine (SVM) Explained - MATLAB & Simulink. https://www.mathworks.com/discovery/support-vector-machine.html

[202]. Szegedy, C., Ioffe, S., Vanhoucke, V., & Alemi, A. (2017, February 12). Inception-v4, Inception-ResNet and the Impact of Residual Connections on Learning. Proceedings of the AAAI Conference on Artificial Intelligence, 31(1). https://doi.org/10.1609/aaai.v31i1.11231

[203]. Szegedy, C., Vanhoucke, V., Ioffe, S., Shlens, J., & Wojna, Z. (2016, June). Rethinking the Inception Architecture for Computer Vision. 2016 IEEE Conference on Computer Vision and Pattern Recognition (CVPR). https://doi.org/10.1109/cvpr.2016.308

[204]. Szegedy, C., Wei Liu, Yangqing Jia, Sermanet, P., Reed, S., Anguelov, D., Erhan, D., Vanhoucke, V., & Rabinovich, A. (2015, June). Going deeper with convolutions. 2015 IEEE Conference on Computer Vision and Pattern Recognition (CVPR). https://doi.org/10.1109/cvpr.2015.7298594

[205]. Talo, M., Baloglu, U. B., Yıldırım, Ö., & Rajendra Acharya, U. (2019). Application of deep transfer learning for automated brain abnormality classification using MR images. Cognitive Systems Research, 54, 176–188. https://doi.org/10.1016/j.cogsys.2018.12.007

[206]. Tan, M., & Le, Q. (2019, May). Efficientnet: Rethinking model scaling for convolutional neural networks. In International conference on machine learning (pp. 6105-6114). PMLR.

[207]. Taye, M. M. (2023, March 6). Theoretical Understanding of Convolutional Neural Network: Concepts, Architectures, Applications, Future Directions. Computation, 11(3), 52. https://doi.org/10.3390/computation11030052

[208]. Taye, M. M. (2023, March 6). Theoretical Understanding of Convolutional Neural Network: Concepts, Architectures, Applications, Future Directions. Computation, 11(3), 52. https://doi.org/10.3390/computation11030052

[209]. Thaha, M. M., Kumar, K. P. M., Murugan, B. S., Dhanasekeran, S., Vijayakarthick, P., & Selvi, A. S. (2019). Brain Tumor Segmentation Using Convolutional Neural Networks in MRI Images. Journal of Medical Systems, 43(9). https://doi.org/10.1007/s10916-019-1416-0

[210]. Thakur SP, Doshi J, Pati S, Ha SM, Sako C, Talbar S, Kulkarni U, Davatzikos C, Erus G, Bakas S. Skull-Stripping of Glioblastoma MRI Scans Using 3D Deep Learning. Brainlesion. 2019 Oct;11992:57-68. doi: 10.1007/978-3-030-46640-4_6. Epub 2020 May 19. PMID: 32577629; PMCID: PMC7311100.

[211]. Thakur SP, Doshi J, Pati S, Ha SM, Sako C, Talbar S, Kulkarni U, Davatzikos C, Erus G, Bakas S. Skull-Stripping of Glioblastoma MRI Scans Using 3D Deep Learning. Brainlesion. 2019 Oct;11992:57-68. doi: 10.1007/978-3-030-46640-4_6. Epub 2020 May 19. PMID: 32577629; PMCID: PMC7311100.

[212]. Tiwari, A., Srivastava, S., & Pant, M. (2020). Brain tumor segmentation and classification from magnetic resonance images: Review of selected methods from 2014 to 2019. Pattern Recognition Letters, 131, 244–260. https://doi.org/10.1016/j.patrec.2019.11.020

[213]. Tiwari, A., Srivastava, S., & Pant, M. (2020). Brain tumor segmentation and classification from magnetic resonance images: Review of selected methods from 2014 to 2019. Pattern Recognition Letters, 131, 244–260. https://doi.org/10.1016/j.patrec.2019.11.020

[214]. Tiwari, A., Srivastava, S., & Pant, M. (2020, March). Brain tumor segmentation and classification from magnetic resonance images: Review

of selected methods from 2014 to 2019. Pattern Recognition Letters, 131, 244–260. https://doi.org/10.1016/j.patrec.2019.11.020

[215]. Toğaçar, M., Cömert, Z., & Ergen, B. (2020). Classification of brain MRI using hyper column technique with convolutional neural network and feature selection method. Expert Systems with Applications, 149. https://doi.org/10.1016/j.eswa.2020.113274

[216]. Toğaçar, M., Ergen, B., & Cömert, Z. (2020). BrainMRNet: Brain tumor detection using magnetic resonance images with a novel convolutional neural network model. Medical Hypotheses, 134, 109531. https://doi.org/10.1016/j.mehy.2019.109531

[217]. Tustison, N. J., Avants, B. B., Cook, P. A., Yuanjie Zheng, Egan, A., Yushkevich, P. A., & Gee, J. C. (2010, June). N4ITK: Improved N3 Bias Correction. IEEE Transactions on Medical Imaging, 29(6), 1310–1320. https://doi.org/10.1109/tmi.2010.204690

[218]. Vaibhavi, P., & Rupal, K. (2018). Brain Tumor Segmentation Using K-means–FCM Hybrid Technique. Advances in Intelligent Systems and Computing, 341–352. https://doi.org/10.1007/978-981-10-7386-1_30

[219]. Vaibhavi, P., & Rupal, K. (2018). Brain Tumor Segmentation Using K-means--FCM Hybrid Technique. In Ambient Communications and Computer Systems (pp. 341–352). Springer.

[220]. Vankdothu R, Hameed MA. Brain tumor segmentation of MR images using SVM and fuzzy classifier in machine learning. Meas Sensors. 2022;24:100440. doi:https://doi.org/10.1016/j.measen.2022.100440

[221]. Vishnuvarthanan, A., Rajasekaran, M. P., Govindaraj, V., Zhang, Y., & Thiyagarajan, A. (2017). An automated hybrid approach using clustering and nature inspired optimization technique for improved tumor and tissue segmentation in magnetic resonance brain images. Applied Soft Computing Journal, 57, 399–426. https://doi.org/10.1016/j.asoc.2017.04.023

[222]. Vishnuvarthanan, G., Rajasekaran, M. P., Vishnuvarthanan, N. A., Prasath, T. A., & Kannan, M. (2017). Tumor detection in T1, T2, FLAIR and MPR

brain images using a combination of optimization and fuzzy clustering improved by seed-based region growing algorithm. International Journal of Imaging Systems and Technology, 27(1), 33–45.

[223]. Vishnuvarthanan, G., Rajasekaran, M. P., Vishnuvarthanan, N. A., Prasath, T. A., & Kannan, M. (2017). Tumor detection in T1, T2, FLAIR and MPR brain images using a combination of optimization and fuzzy clustering improved by seed-based region growing algorithm. International Journal of Imaging Systems and Technology, 27(1), 33–45.

[224]. Vishnuvarthanan, G., Rajasekaran, M. P., Vishnuvarthanan, N. A., Prasath, T. A., & Kannan, M. (2017, March). Tumor detection in T1, T2, FLAIR and MPR brain images using a combination of optimization and fuzzy clustering improved by seed-based region growing algorithm. International Journal of Imaging Systems and Technology, 27(1), 33–45. https://doi.org/10.1002/ima.22208

[225]. Visser, M., Petr, J., Müller, D. M. J., Eijgelaar, R. S., Hendriks, E. J., Witte, M., Barkhof, F., van Herk, M., Mutsaerts, H. J. M. M., Vrenken, H., de Munck, J. C., & De Witt Hamer, P. C. (2020, June 5). Accurate MR Image Registration to Anatomical Reference Space for Diffuse Glioma. Frontiers in Neuroscience, 14. https://doi.org/10.3389/fnins.2020.00585

[226]. Wadhwa, A., Bhardwaj, A., & Singh Verma, V. (2019). A review on brain tumor segmentation of MRI images. Magnetic Resonance Imaging, 61(January), 247–259. https://doi.org/10.1016/j.mri.2019.05.043

[227]. Waghmare VK, Kolekar MH. Brain Tumor Classification Using Deep Learning. In: Chakraborty C, Banerjee A, Kolekar MH, Garg L, Chakraborty B, eds. Internet of Things for Healthcare Technologies. Springer Singapore; 2021:155-175. doi:10.1007/978-981-15-4112-4_8

[228]. Walsh J, Othmani A, Jain M, Dev S. Using U-Net network for efficient brain tumor segmentation in MRI images. Healthc Anal. 2022;2:100098. doi:https://doi.org/10.1016/j.health.2022.100098

[229]. WAN, Z., YIN, T., CHEN, H., & LI, D. (2016, March 31). Surgical treatment of a retroperitoneal benign tumor surrounding important blood vessels by fractionated resection: A case report and review of the literature. Oncology Letters, 11(5), 3259–3264. https://doi.org/10.3892/ol.2016.4395

[230]. Wang J, Gao J, Ren J, et al. DFP-ResUNet:Convolutional Neural Network with a Dilated Convolutional Feature Pyramid for Multimodal Brain Tumor Segmentation. Comput Methods Programs Biomed. 2021;208:106208. doi:https://doi.org/10.1016/j.cmpb.2021.106208

[231]. Wang Y, Ji Y, Xiao H. A data augmentation method for fully automatic brain tumor segmentation. Comput Biol Med. 2022;149:106039. doi:https://doi.org/10.1016/j.compbiomed.2022.106039

[232]. Wang YL, Zhao ZJ, Hu SY, Chang FL. CLCU-Net: Cross-level connected U-shaped network with selective feature aggregation attention module for brain tumor segmentation. Comput Methods Programs Biomed. 2021;207:106154. doi:https://doi.org/10.1016/j.cmpb.2021.106154

[233]. Wong, K. K., Rostomily, R., & Wong, S. T. C. (2019). Prognostic gene discovery in glioblastoma patients using deep learning. Cancers, 11(1), 1–15. https://doi.org/10.3390/cancers11010053

[234]. Wu, T. C., Wang, X., Li, L., Bu, Y., & Umulis, D. M. (2021, May 10). Automatic wavelet-based 3D nuclei segmentation and analysis for multicellular embryo quantification. Scientific Reports, 11(1). https://doi.org/10.1038/s41598-021-88966-2

[235]. Wu, T. C., Wang, X., Li, L., Bu, Y., & Umulis, D. M. (2021, May 10). Automatic wavelet-based 3D nuclei segmentation and analysis for multicellular embryo quantification. Scientific Reports, 11(1). https://doi.org/10.1038/s41598-021-88966-2

[236]. XCeption Model and Depthwise Separable Convolutions. (2019, March 20). https://maelfabien.github.io/deeplearning/xception/#i-what-is-an-xception-network

[237]. Xue G, Chen C, Lu ZL, Dong Q. Brain Imaging Techniques and Their Applications in Decision-Making Research. Xin Li Xue Bao. 2010 Feb 3;42(1):120-137. doi: 10.3724/SP.J.1041.2010.00120. PMID: 20376329; PMCID: PMC2849100.

[238]. Yiming, C., Qin, G., Zhao, R., Liang, Y., & Sun, M. (2019). ConvCaps: Multi-input Capsule Network for Brain Tumor Classification (pp. 524–534). https://doi.org/10.1007/978-3-030-36708-4_43

[239]. Yogamangalam, R. & Karthikeyan, B.. (2013). Segmentation techniques comparison in image processing. International Journal of Engineering and Technology. 5. 307-313.

[240]. Younger, D. S. (2023). Adult and childhood vasculitis. Motor System Disorders, Part I: Normal Physiology and Function and Neuromuscular Disorders, 653–705. https://doi.org/10.1016/b978-0-323-98818-6.00008-x

[241]. Zagoruyko, S., & Komodakis, N. (2016). Wide residual networks. arXiv preprint arXiv:1605.07146.

[242]. Zhang D, Huang G, Zhang Q, Han J, Han J, Yu Y. Cross-modality deep feature learning for brain tumor segmentation. Pattern Recognit. 2021;110:107562. doi:https://doi.org/10.1016/j.patcog.2020.107562

[243]. Zhang Y, Liu X, Wa S, Liu Y, Kang J, Lv C. GenU-Net++: An Automatic Intracranial Brain Tumors Segmentation Algorithm on 3D Image Series with High Performance. Symmetry (Basel). 2021;13(12). doi:10.3390/sym13122395

[244]. Zhang Y, Lu Y, Chen W, Chang Y, Gu H, Yu B. MSMANet: A multi-scale mesh aggregation network for brain tumor segmentation. Appl Soft Comput. 2021;110:107733. doi:https://doi.org/10.1016/j.asoc.2021.107733

[245]. Zhang, Q., Zhang, M., Chen, T., Sun, Z., Ma, Y., & Yu, B. (2019, January). Recent advances in convolutional neural network acceleration. Neurocomputing, 323, 37–51. https://doi.org/10.1016/j.neucom.2018.09.038

[246]. Zhao, X., Wu, Y., Song, G., Li, Z., Zhang, Y., & Fan, Y. (2018). A deep learning model integrating FCNNs and CRFs for brain tumor segmentation. Medical Image Analysis, 43, 98–111. https://doi.org/10.1016/j.media.2017.10.002

[247]. Zhou X, Li X, Hu K, Zhang Y, Chen Z, Gao X. ERV-Net: An efficient 3D residual neural network for brain tumor segmentation. Expert Syst Appl. 2021;170:114566. doi:https://doi.org/10.1016/j.eswa.2021.114566

[248]. Zhou, Y., Li, Z., Zhu, H., Chen, C., Gao, M., Xu, K., & Xu, J. (2019). Holistic Brain Tumor Screening and Classification Based on DenseNet and Recurrent Neural Network (pp. 208–217). https://doi.org/10.1007/978-3-030-11723-8_21